CLEAR, AQUEOUS TOPICAL NANOMICELLE FORMULATION FOR DIABETIC MACULA EDEMA

A DISSERTATION IN
Pharmaceutical Sciences
and
Chemistry

Presented to the Faculty of University
of Missouri - Kansas City in partial fulfillment of
the requirements for the degree

DOCTOR OF PHILOSOPHY

By

HOANG MY TRINH

B. Pharm. Ho Chi Minh City University of Medicine and Pharmacy, Vietnam, 2008
Kansas City, Missouri
2018

CLEAR, AQUEOUS TOPICAL NANOMICELLE FORMULATION FOR DIABETIC MACULA EDEMA

Hoang M. Trinh, Candidate for the Doctor of Philosophy Degree

University of Missouri-Kansas City, 2018.

ABSTRACT

The objective of this study was to develop a clear aqueous mixed nanomicellar formulation (NMF) of hydrophobic drugs for diabetic macula edema. The hydrophobic drugs include triamcinolone acetonide (TA), fluocinolonce acetonide (FA) and triamcinolone (T1) were encapsulated with a combination of nonionic surfactant hydrogenated castor oil (HCO) and octoxynol-40 (Oc-40).

A design of experiment (DOE) with JMP software was performed to optimize the formulation to delineate the effects of drug-polymer interactions. In this study, the amount of polymers HCO and OC-40 as independent variables. All formulations were prepared following solvent evaporation and film rehydration method, characterized with size, polydispersity, shape, morphology, clarity/ appearance and cytotoxicity on human corneal and retinal cell lines.

A specific blend of HCO and Oc-40 at a particular wt% ratio which produced highest desirability generated by JMP software. The optimized formulations were characterized with all standard and safe and potentially suitable for ocular eye drop for future study.

APPROVAL PAGE

The faculties listed below, appointed by the Dean of the School of Graduate Studies have examined a dissertation titled “Clear, Aqueous Topical Nanomicelle Formulation For Diabetic Macula Edema.” presented by Hoang My Trinh, candidate for the Doctor of Philosophy degree and certify that in their opinion it is worthy of acceptance.

Supervisory Committee

Ashim K. Mitra, Ph.D., Committee Chair
Department of Pharmaceutical Sciences

Kun Cheng, Ph.D.
Department of Pharmaceutical Sciences

Chi Lee, Ph.D.
Department of Pharmaceutical Sciences

J. David Van Horn, Ph.D.
Department of Chemistry

Russell B. Melchert, Ph.D., R.Ph
Department of Pharmacology & Toxicology

TABLE OF CONTENTS

ABSTRACT iii

LIST OF ILLUSTRATIONS xii

LIST OF TABLES xvi

ACKNOWLEDGEMENTS xviii

1. INTRODUCTION 1

1.1 Overview 1

1.2 Statement of Problem and Hypothesis 2

1.3 Objectives 5

2. OCULAR ANATOMY & DRUG DELIVER 6

2.1 Ocular Anatomy 6

2.1.1 Anterior Segment 7

2.1.2 Posterior Segment 12

2.2 Barriers To Ocular Drug Delivery (ODD) 16

2.2.1 Anterior Segment Static Barriers 17

2.2.2 Anterior Segment Dynamic Barriers 20

2.2.3 Posterior Segment Static Barriers 21

2.2.4 Posterior Segment Dynamic Barriers 22

2.3 Routes of Ocular Administration 22

2.3.1 Topical Route 24

2.3.2 Systemic Route 28

2.3.3 Intraocular Injection 28

2.3.4 Periocular Injection 30

3 DIABETIC MACULA EDEMA (DME) 33

3.1 Physiology of DME 35

3.1.2 Macro-vascular Factors 35

3.1.2 Micro-vascular Factors 36

3.2 Existing Treatment for DME 38

3.2.1 Laser Photocoagulation 38

3.2.2 Vitrectomy 39

3.2.3 Intravitreal Anti-VEGF Therapy 40

3.3 Emerging Formulations for Treatment of Diabetic Macular Edema 44

4 MICELLE APPLICATION FOR DRUG DELIVERY 55

4.1 Nanomicelle Preparations 56

4.2 Application of Nanomicelles in Drug Delivery 58

4.2.1 Solubilize Poor Water-Soluble Drugs 59

4.2.2 Targeted Nanomicelles 59

4.2.3 Stimuli Responsive Nanomicelles 60

4.2.4 Multifunctional Nanomicelle Carrier 62

4.3 Conclusion 62

5 PREPARATION AND OPTIMIZATION OF TRIAMCINOLONE ACETONIDE-LOADED NANOMICELLES 64

5.1 Rationale 64

5.2 Materials 67

5.3 Methods.....67

5.3.1 Film-Hydration Method for Nanomicelle Preparation 67

5.3.2 Drug Concentration Determination Using High Performance Liquid Chromatography (HPLC).....68

5.3.3 Exploratory Model (Design of Experiments (DOE)) 68

5.3.4 Entrapment Efficiency (EE) and Loading Efficiency (LE) 70

5.3.5 Determination of Critical Micellar Concentration (CMC) 71

5.3.6 Micelle Size, Polydispersity and Surface Potential Charge.....71

5.3.7 Morphology Transmission Electron Microscopy (TEM) 71

5.3.8 Light Transmittance.....72

5.3.9 Dilution Effect 72

5.3.10 Powder X-Ray Diffraction (XRD).....72

5.3.11 ^{1}H-NMR Spectroscopy of Nanomicelles.....72

5.3.12 Osmolality and pH.....73

5.3.13 Viscosity 73

5.3.14 Cell Culture.....73

5.3.15 In vitro Cytotoxicity.....74

5.3.16 In Vitro Drug Release Study.....75

5.4 Results & Discussion:.....75

5.4.1 Exploratory Model (design of experiments (DOE)).....75

5.4.2 Entrapment Efficiency and Loading Efficiency 83

5.4.3 Micellar Size, Polydispersity Index (PDI), Zeta Potential.....87

5.4.4 Morphology TEM 88

5.4.5 Optical Clarity/Appearance 88

5.4.6 Critical Micellar Concentration (CMC) 90

5.4.7 Viscosity 90

5.4.8 Dilution Effect 90

5.4.9 Osmolality and pH 91

5.4.10 ^{1}H NMR Characterization 92

5.4.11 Powder XRD Analysis of Blank NMF and TA NMF 95

5.4.12 In Vitro Cytotoxicity 96

5.4.13 In Vitro Drug Release Study 99

5.5 Conclusion 100

6 PREPARATION AND OPTIMIZATION DEVELOPMENT OF FLUOCINOLONE ACETONIDE-LOADED NANOMICELLES 102

6.1 Rationale: 102

6.2 Materials 106

6.3 Methods 106

6.3.1 High performance liquid chromatography (HPLC) analysis 106

6.3.2 Experimental Design 106

6.3.3 Nanomicelle Preparation 109

6.3.4 Solubility 110

6.3.5 Mixed Nanomicellar Size, Polydispersity Index (PDI), and Surface Potential 110

6.3.6 Light Transmittance 110
6.3.7 Viscosity 111
6.3.8 Dilution Effect 111
6.3.9 ^{1}H NMR Characterization 111
6.3.10 In vitro Drug Release Study 112
6.3.11 Osmolality and pH 112
6.3.12 Powder X-ray Diffraction (XRD) 113
6.3.13 Cell Culture 113
6.3.14 In vitro Cytotoxicity 113
6.3.15 Statistical Analysis 114
6.4 Results and Discussion 115
6.4.1 HPLC to Quantity the Amount of FA in Solution: 115
6.4.2 Experiment Design and FA Solubility 116
6.4.3 Micellar Size, Polydispersity Index (PDI) and Surface Potential 126
6.4.4 Optical Clarity/Appearance 129
6.4.5 Powder XRD Analysis of Blank Micelle and FA NMF 132
6.4.6 Viscosity 133
6.4.7 Dilution Effect 134
6.4.8 Osmolality and pH 135
6.4.9 ^{1}H NMR Characterization 135
6.4.10 In vitro Cytotoxicity 137

6.4.11 In Vitro Drug Release 140

6.5 Conclusion 141

7 APPLICATION OF MATHEMATICAL ENGINEERING STEEPEST ASCENT METHOD TO OPTIMIZE TOPICAL OCULAR NANOMICELLAR FORMULATION 143

7.1 Rationale 143

7.2 Methods 147

7.2.1 Nanomicelle Preparation 147

7.2.2 Solubility Determination using HPLC 147

7.2.3 Design of Experiment (DOE) 147

7.2.4 Steepest Ascent 149

7.2.5 Micellar Size, Polydispersity Index and Surface Potential 152

7.2.6 Viscosity 152

7.2.7 Dilution Effect 152

7.2.8 Optical Clarity/ Appearance 152

7.2.9 Osmolality and pH 152

7.2.10 ^{1}H-NMR Spectroscopy of Blank NMF and T1 NMF 152

7.2.11 In Vitro Cytotoxicity 152

7.3 Results & discussion 152

7.3.1 HPLC Analysis: 152

7.3.2 Design of Experiment (DOE1) and T1 Solubility 153

7.3.3 Steepest Ascent Steps and T1 Solubility 158

7.3.4 Design of Experiment (DOE2) and T1 Solubility 165

7.3.5 Micellar Size, Polydispersity Index (PDI) and Surface Potential 170

7.3.6 Optical Clarity/Appearance 172

7.3.7 Viscosity 173

7.3.8 Dilution Effect 174

7.3.9 Osmolality and pH 175

7.3.10 ^{1}H NMR Characterization 176

7.3.11 In vitro Cytotoxicity 177

7.4 Conclusion 179

8 SUMMARY AND RECOMMENDATIONS 181

8.1 Summary 181

8.2 Recommendations 185

APPENDIX 187

REFERENCES 192

VITA 215

LIST OF ILLUSTRATIONS

Figure 2-1: Anatomy of the Eye. 7

Figure 2-2: Corneal Layers of the Eye. (A) Histological Corneal Images; (1) Corneal Epithelium, (2) Bowman's Layer, (3) Stroma, (4) Descemet's Membrane and (5) Endothelium. (B) And (C) Diagrammatic Expanded Corneal Layers. *Reproduced with the Permission.....8

Figure 2-3: Histology of the Choroid. A. Schematic of the Layers of the Choroid. Reproduced with Permission from Remington, LA. Clinical Anatomy of the Visual System. B. Semithin Resin Section of the Outer Retina and Choroid in the Primate Eye. RPE: Retina Pigment Epithelium; CC, Choriocappilaries; SL, Sattler's Layer; HL, Haller's Layer. Reproduced with Permission from Forrester Et Al., 2002. The Eye: Basic Science in Practice.....14

Figure 2- 4: Biological Ocular Barriers in The Eye (A) Tear Film Barrier; (B) Corneal Barrier; (C) Vitreous Barrier; (D) Blood–Retinal Barrier And (E) Blood–Aqueous Barrier 17

Figure 2-5: Schematic Representation of Local Routes for Ocular Drug Delivery.....23

Figure 3- 1: Diabetic Macular Edema (DME) At Disease State; (A) Structure of Human Eye; (B) Expanded Representation of Macula Region for Normal Eye; (C) Expanded Representation of Macula Region for DME; (D) Optical Coherence Tomography (OCT) Image for DME.....33

Figure 3- 2: Treatment Strategies of Diabetic Macular Edema (DME).....40

Figure 4- 1: Schematic drawing image of (a). Polymeric micelle (b). Micelle conjugated with a targeting ligands (c). Micelle incorporating with contrast agents or imaging moieties (d). Stimuli-sensitive polymeric micelles (thermo/pH/

light/ultrasound-sensitive) (e). Multifunctional micelles with targeting ligands, contras agents or imaging moieties, therapeutic drugs.....63
Figure 5-1: Schematic drawing image of TA-loaded NMF. Reproduce with Permission.....66
Figure 5-2: Cytotoxicity Studies Conducted on HCEC Cells. Cells Treated with Blank and Loaded TA NMFs Solutions for 1h.....77
Figure 5-3: Summary of Variable Effects on Entrapment Efficiency (EE).....78
Figure 5-4: Summary of Variable Effects on Loading Efficiency (LE).....79
Figure 5-5: Summary of Variable Effects on Critical Micellar Concentration (CMC) 80
Figure 5-6: Prediction Profiler for Optimized TA NMF 82
Figure 5-7: Size Distribution of NMF Formulations (A) Blank NMF (B) Optimized TA Loaded NMF.....87
Figure 5-8: (A) Real-Time Scanning Transmission Electron Microscope (STEM) Image of Triamcinolone Acetonide-Loaded Nanomicelles (X147,000). Scale Bar 100 nm. (B) Image Showing Visual Appearance of 0.1% Triamcinolone Acetonide Loaded Nanomicelles on the Left Side in Comparison to Water on the Right Side ...88
Figure 5-9: Light Transmittance of Formulations (Blank, TA NMF) 89
Figure 5-11: Qualitative ^{1}H NMR Studies (A) ^{1}H NMR Spectrum for TA Pure Drug in $CDCl_3$; (B) ^{1}H NMR Spectrum For Placebo Polymer Micelles in $CDCl_3$; (C) ^{1}H NMR Spectrum for TA Nanomicelles in D_2O; (D) ^{1}H NMR Spectrum For TA Micelles in $CDCl_3$.....92
Figure 5-12: XRD Pattern of TA Raw, TA NMF and Polymers HCO-60, OC-40 96
Figure 5-13: Cytotoxicity Studies (LDH Assay) Conducted on D407 and HCEC Cells. Cells Treated with NMF for 1h.....98

Figure 5-14: Cytotoxicity Studies (WST Assay) Conducted on D407 and HCEC Cells. Cells Treated with NMF for 1h 98
Figure 5-15: In Vitro Releases Profile of TA from Nanomicelles and Ethanolic TA Solution under Sink Conditions At 37 ˚C 100
Figure 6- 1: Illuvien® Intravitreal Implant 103
Figure 6- 2: FA HPLC Standard Curve 115
Figure 6- 3: Statistical Summary of DOE1: Parameter Estimates, Summary of Fit, ANOVA, Effect Summary, Effect Tests 117
Figure 6- 4: Actual by Predicted Plot DOE1 FA NMF 118
Figure 6- 5: DOE1 Response Surface Curve of FA Solubility 119
Figure 6- 6: DOE1 Prediction Profiler FA NMF 119
Figure 6- 7: Statistical Summary of DOE2 FA NMF 123
Figure 6- 8: DOE2 Actual By Predicted Plot 124
Figure 6- 9: DOE2 Response Surface of FA Solubility 125
Figure 6- 10: DOE2 Prediction Profiler 125
Figure 6- 11: Size of Blank NMF and FA NMF 127
Figure 6- 12: Visual Appearance of FA-Loaded NMF on the Right in Comparison to Water on the Left 130
Figure 6- 13: Power X-Ray Diffraction (XRD) Pattern for Freeze Dried FA NMF, Blank NMF, FA Raw, OC-40 Raw and HCO-40 Raw 133
Figure 6- 14: Qualitative ^{1}H NMR Studies, ^{1}H NMR Spectrum for FA Nanomicelles in D_2O 137
Figure 6- 15: MTT Cytotoxicity of FA-Loaded NMFs on HCEC and D407 138
Figure 6- 16: MTT Cytotoxicity of Optimal NMFs on HCEC and D407 139
Figure 6- 17: LDH Cytotoxicity of Optimal NMFs on HCEC and D407 140

Figure 6- 18: Release Study of FA-Loaded NMF 141

Figure 7- 1: HPLC Triamcinolone Standard Curve 153

Figure 7- 2: Actual by Predicted Plot DOE1 of T1 NMF 155

Figure 7- 3: Statistical Summary of DOE1 of T1 NMF Optimization 156

Figure 7- 4: Prediction Profiler of T1 DOE1 156

Figure 7- 5: Surface Response of T1 DOE1 157

Figure 7- 6: Path of Steepest Ascent 158

Figure 7- 7: DOE2 JMP 165

Figure 7- 8: Actual By Predicted Plot for DOE2 T1 NMF 167

Figure 7- 9: Statistical Parameter of DOE2 T1 NMF 168

Figure 7- 10: Prediction Profiler of DOE2 T1 NMF 169

Figure 7- 11: Surface Response T1 DOE2 170

Figure 7- 12: Size distribution of T1 NMF1 to T1 NMF8 171

Figure 7- 13: Size Distribution of Optimized T1 NMF 171

Figure 7-14: Clarity of T1 NMF Compared with Water 173

Figure 7-15: Proton NMR of T1 Optimized NMF in D_2O 177

Figure 7- 16: MTT Cytotoxicity of Blank and T1 Optimized NMF on ARPE-19 178

Figure 7- 17: LDH Cytotoxicity of Blank and T1 NMF on ARPE-19 179

LIST OF TABLES

Table 3- 1: Current Therapeutic Drugs for DME 54

Table 5- 1: Details Design of Experimental (DOE) Coded and Uncoded Runs 70

Table 5- 2: Summary of Uncoded Design and Corresponding EE, LE, CMC, Size, PDI, Zeta Potential and % Light Transmittance 84

Table 5- 3: Characterization of Optimized TA NMF 86

Table 5- 4: Effect of Dilution on Nanomicellar Size and PDI of Optimized TA Loaded NMF.....91

Table 6- 1: Preliminary Data for FA Nanomicellar Formulations 105

Table 6- 4: Design of Experimental (DOE) Coded, Uncoded Runs and Solubility of Fluocinolone Acetonide for DOE2 (Micelles Preparation Method 2).....121

Table 6- 5: Summary of Size, PDI for DOE1 and DOE2 FA-Loaded Nanomicelle Formulations 128

Table 6- 6: Summary of Size, PDI for DOE1 Blank Nanomicellar Formulations 129

Table 6- 7: Characterizations of Optimal DOE1 and DOE2 FA NMFs.....131

Table 6- 8: Effect of Dilution on Nanomicelles Size and PDI of Optimal FA NMF 135

Table 7- 1: Design of Experiment (DOE) 1 Runs Coded, Uncoded Designs.....154

Table 7- 2: Coded and Uncoded Levels of Factors X1 And X2.....159

Table 7- 3: Steepest Ascent Calculations for Coded, Uncoded Variables and Predicted Response Value.....163

Table 7- 4: DOE2 Runs and Solubility.....166

Table 7- 5: Characterizations of Optimized T1 NMF.....172

Table 7- 6: Viscosity of Blank NMF Vs T1 NMF.....174

Table 7- 7: Dilution Effect of Optimized T1 NMF.....175

Table 7- 8: Osmolality ond pH of Blank and T1 Optimized NMF.....176

ACKNOWLEDGEMENTS

I would like to express my immense gratitude towards my mentor Dr. Ashim K. Mitra for his exceptional support and motivation during my graduate studies. His guidance was critical in solving a number of scientific challenges. I deeply appreciate him for encouragement and believing in me that helped me to develop critical thinking as a scientist. I would also like to extend my gratitude to members of my supervisory committee Drs. Kun Cheng, Chi Lee, Russell B. Melchert, and J. David Van Horn for their constant support, discussions on my research and valuable critics on my dissertation. It is my honor to have such extraordinary scientists and researchers as a part of my supervisory committee. I am greatly thankful to Dr. Dhananjay Pal for his endless support in the laboratory with scientific discussions or personal life. He encouraged me at my difficult time, without his encourage I could not make it through this PhD. I would also like to extend my appreciation to Mrs. Ranjana Mitra for her support during my PhD at UMKC.

I am greatly thankful to Ashutosh Barve, Dr. Harika Vemula, Mary Joseph, Abhirup Mandal, Dr. Kishore Cholkar, Dr. Xiaoyan Yang, Dr. Zhiying Wang, Dr. Aswani Dutt Vadlapudi, Dr. Divya Teja Vavilala, and Dr. Animikh Ray for their timely help, their valuable suggestions on my research projects and creating such a cheerful environment in the lab throughout my studies. I thankful to my junior Nitish, Meshal. I am especially thankful to my special friend Duc Le for unlimited support, suggestion, advice, cheer up and sharing love through the journey of my PhD.

I sincerely appreciate constant support of Joyce Johnson, Sharon Self, Ashley Ismert, Tamica Lige, Shana Eisentrager and Nancy Bahner in administrative assistance throughout my stay at UMKC. I appreciate support from Nancy Hoover from School of Graduate Studies and National Institute of Health for financial support. I would also

like to thank Dr. James B. Murowchick (School of Geological Sciences) for helping in XRD analysis.

My special gratitude towards my parents Thanh Trinh and Phan Huynh for bringing me to this world. Without their endless love, support, I could never be a person who I am. They always there for me and I never could ask for what they have given me. I also thankful to sisters Anh Trinh, Dung Trinh, brothers Thai Trinh, Lam Pham, nieces Betty Trinh, Kim Trinh and nephews Quy Pham, Nathan Pham for their endless support and love. They have spent time with me and cheer me up for last five years. At last, I would like to thank the Trinh and Goetz's family for sharing happiness, great entertainment, and encouragement. Special, I love to thank you to my coming son-Thien Duc Westin for motivation and giving me all positive energies to complete my PhD.

Dedicated to My Family

CHAPTER 1

1. INTRODUCTION

1.1 Overview

The eyes are the most complex and specialized sensory organ that allow human connection to the environment. The external light or images enter the eye through the clear cornea, pass the pupil, and iris, is focused by the lens and collected on the retina. The retina, containing photoreceptor rods, cones and retinal ganglion cells, is responsible for capturing and processing all the light rays into light impulses. Those signals are transmitted to the brain through the optic nerve; the brain interprets and produces the image as we see. Therefore, the eyes are highly protected.

The macula, a yellow spot near the center of retina where there is a maximum amount of rod cells and cone cells are present, provides the best sharp, central vision and fine details. Throughout the years and special disease conditions, the macula region is degenerated and leads to vision loss. Diabetic macular edema (DME), Age-related macular degeneration (AMD), glaucoma, proliferative vitreoretinopathy (PVR), and diabetic vitreoretinopathies are some of the common posterior eye diseases that may cause vision loss if not treated. There are different types of macular degeneration including dry AMD (approximately 85-90%), wet AMD (10-15%), also Stargardt disease, a form of macular degeneration found in young people.

Diabetes is the metabolic disease where the patients have high blood glucose and have to control, if not can lead to other conditions. People with diabetes will develop diabetic eye diseases including diabetic retinopathy (DR), diabetic macular edema (DME), cataract, and glaucoma. DR is a disease that the blood vessels in the retina damage; DME

is the consequence of DR where the vessels leak and the fluid accumulated in the macula. There are two forms of DME: focal DME and diffuse DME. Focal DME is caused by abnormal of blood vessel in the eye while diffuse DME is caused by swelling/widening of retinal capillaries. DME leads to blurry vision, floaters, double vision, and eventually blindness if untreated. The current treatments of DME are anti- vascular endothelial growth factor (VEGF), Focal/grid macular laser surgery, and glucocorticoids or combination.

Glucocorticoids have anti-inflammatory, anti-angiogenic and anti-permeability properties and have been shown to inhibit VEGF, growth factors and other cytokines. Even glucocorticoids have been used for many years for DME and many patients show the benefits from treatment with glucocorticoids, the US Food and Drug Administration (FDA) only approved fluocinolone acetonide intravitreal implant (ILUVIEN®) 0.19 mg for DME. Triamcinolone acetonide and Dexamethasone have been used as off-label.

1.2 Statement of Problem and Hypothesis

The current route of administration of corticoids in treatment of DME is intravitreal injection, which associates with retinal detachment, endophthalmitis, cataract and elevated intraocular pressure [1, 2] [3] [4].

Topical administration is the most noninvasive, patient compliant route. However, less than 5% drug reaches the back of the eye following the topical eye drop. There are many ocular barriers for ocular drug delivery including anterior and posterior barriers, static and dynamic barriers. There is extremely challenging task for drug delivery to intermediate and posterior segment via topical drops[5, 6]. The topical administration has typical volume around 30-40 µL and wash out via nasolacrimal drainage and tear refluxing. In order to avoid the drug loss and achieve the drug therapeutic level, higher concentration

of drug in aqueous solution is required. However, steroids such as fluocinolone acetonide, triamcinolone acetonide, and triamcinolone are highly hydrophobic, poorly water-soluble and cannot dissolve in water at high concentration. Steroids also have sub-optimal physico-chemical properties, and poor ocular membrane permeability. Topical drops of steroids are well tolerated but drug levels achieved in intermediate and posterior ocular segments are often subtherapeutic [7, 8].

Nanomicelles and liposomes are nanocarriers which have been used to enhance the solubility of hydrophobic drugs in aqueous medium[9-12]. Nanomicelles have small size range from 10 – 100 nm. Nanomicelles can be prepared from the amphiphilic polymeric system and encapsulate the hydrophobic drugs. The hydrophobic core can solubilize the hydrophobic drugs – steroids while the hydrophilic corona aids in the development of clear, aqueous solution. This novel nanomicellar strategy may (i) improve drug solubility ii) improve drug uptake and cell permeability, (iii) allow for non-invasive delivery of hydrophobic drugs to posterior ocular tissues and (iv) improve patient acceptability and compliance due to its noninvasive, nonirritating clear and aqueous system. Based on the particle size, the transportation across the dynamic and static barriers is different[13]. Recently, Inokuchi *et al.* have demonstrated that following topical administration the liposome size of ~110 nm has higher coumarin-6 accumulation in posterior segment[14]. Mixed micelle formulation of rapamycin and cyclosporine from our laboratory also resulted in significantly higher concentrations in the intraocular tissues [15, 16]. Nanomicelles may primarily follow non-corneal pathway such as conjunctival-scleral rather than uveo-sclera pathway after topical administration to reach the retina. It is theorized that the hydrophilic surface of nanomicelle will help it follow transcleral pathway and achieve the

higher concentration in the posterior segment. Therefore, nanomicelle has been become the promising drug delivery system for intraocular tissue following topical administration.

Rationale for Using Statistical Design of Experiments (DOE)

Design of Experiment (DOE) is a systematic method to determine the relationship between factors affecting a process and the output of that process. DOE helps the scientists learn the pattern of interactions among independent factors and their effects on dependent factors. This method can reduce a number of experiments for optimization. This process saves a lot of time and cost. Recently, design of experiment (DOE) has been widely utilized to optimize formulation. DOE is a structured powerful approach for conducting experiments to identify and explain the influence of individual factors and their interactions on response variables. In this project, DOE is used to identify the effect of two different polymers that may enhance the entrapment efficiency and loading efficiency, the interaction among factors (polymer-drug and polymer-polymer) may enhance or lower drug loading in nanomicelles. Based on information from the model, we will optimize and modify nanomicelle components to achieve higher aqueous solubility for steroids.

Rationale for Using Fluocinolone Acetonide (FA), Triamcinolone Acetonide (TA) and Triamcinolone (T1)

FA, TA and T1 are synthetic glucocorticoid, possessing anti-inflammatory and anti-angiogenic properties [17], not only regulate the expression of VEGF but also inhibit pro-inflammatory genes. Even only FA is a FDA approved drug for DME as intravitreal implant but TA and T1 have been used for many years and showed benefit effect on DME patients [18] [19] [20]. FA and TA have same vitreous elimination half-life of the solubilize fraction, short ranging from 2 to 3h [21].

In the present study, two amphiphilic polymers namely; hydrogenated castor oil (HCO) and octoxynol-40 (Oc-40) are selected. Both HCO and Oc-40 are safe and approved by FDA for human use. Amphiphilic nature of HCO and Oc-40 consist of hydrophobic core and hydrophilic corona allowing spontaneous formation of spherical nanomicelles in aqueous solution. Hydrophobic FA, TA and T1 may partition into hydrophobic core of nanomicellar structure whereas the corona is comprised of hydrophilic groups which extend towards surrounding aqueous environment in a manner to stabilize the inner hydrophobic core.

1.3 Objectives

The objective of current study is:

- To develop and optimize aqueous FA, TA and T1 loaded nanomicellar formulation (NMF) utilizing statistical design of experiment (DOE). The ratio of the combination HCO and Oc-40 was optimized with JMP 13.0 software. Standard least square fit analysis was carried out to identify the optimal NMF which generates the highest desirability
- To prepare nanomicelle encapsulating FA, TA and T1 using film hydration method
- To characterize the FA, TA and T1 loaded NMF for their size, polydispersity (PDI), shape, surface morphology, EE, LE, CMC, optical clarity, viscosity, dilution effect, osmolality, pH, proton NMR, powder XRD and *in vitro* drug release study.
- To evaluate for *in vitro* cytotoxicity on human corneal epithelial cells (HCEC) and human retinal pigment epithelial cells (D407 cells).

CHAPTER 2

2. OCULAR ANATOMY & DRUG DELIVER

2.1 Ocular Anatomy

The human eye is a complex sensory organ with multiple anatomic components; its sole purpose is to send external visual, photoreception, i.e. light signals, through the optic nerve to be interpreted by the occipital lobe of the cerebrum. As many of the specialized organs of the body, the eyes have full external protection through housing of the bony components of the skull. The orbital bones consist of a confluence of seven facial bones. These facial bones are arranged in superior, medial, lateral and inferior portions[22]. These portions are orbital surface of the frontal bone, orbital surface of the lesser wing of the sphenoid, orbital plate of the ethmoid bone, orbital process of the palatine bone, lacrimal bone, orbital surface of the greater wing of the sphenoid, orbital surface of the zygomatic bone and the orbital surface of the maxilla[23].

Moving internally from the facial bones of the orbit, surrounding the eye, one will find a multitude of muscles, glands, ligaments and fatty tissues. The eye is connected to six muscles, which control the various movements; i.e., superior rectus muscle, inferior rectus muscle, medial rectus muscle, lateral rectus muscles, superior oblique muscle and inferior oblique muscle[24]. One additional muscle, the levator palpebral superioris muscles, not in direct contact with the eye controls the movement of the upper eyelid. The movements of the muscles of the eye are controlled by a combination of cranial nerves III, IV and VI. The eye, or Oculus Bulbi, can be anatomically subdivided into anterior and posterior segments (Figure 2-1). The anterior segment is compartmentalized into the cornea, conjunctiva, aqueous humor, iris, ciliary body, pupil (aperture space) and lens. The

posterior segment is occupied with anatomic structures of the sclera, choroid, Brush's membrane, retinal pigment epithelium (RPE), neural retina and vitreous humor. A brief description of these ocular tissues is provided in following section.

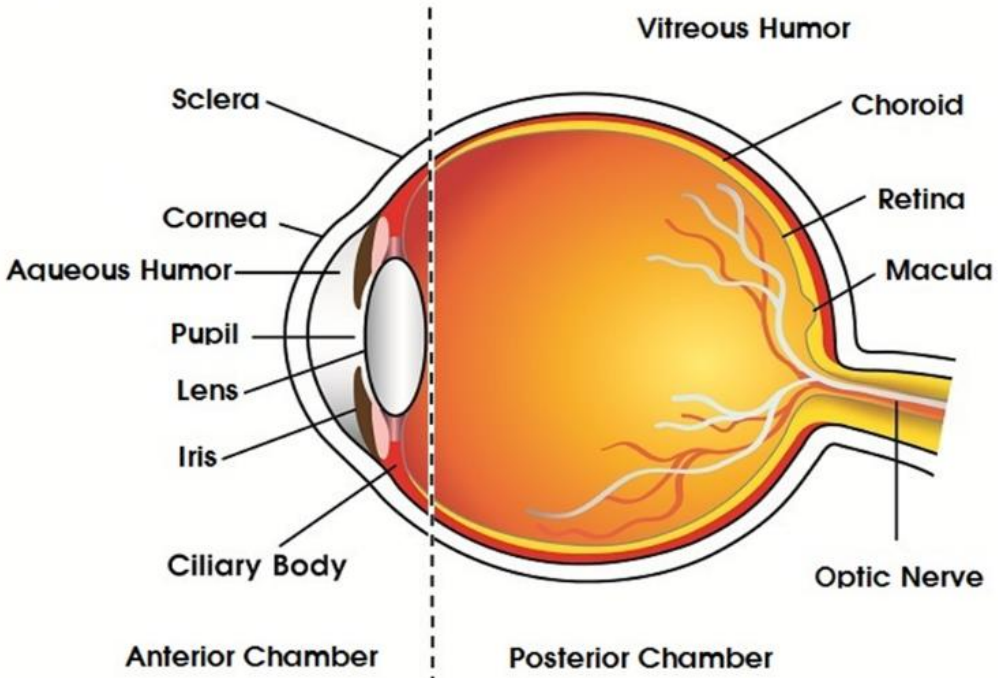

Figure 2-1: Anatomy of the Eye.

2.1.1 *Anterior Segment*

Cornea: The most superficial convex structure of the eye. The cornea is a multilayered transparent membrane composed of five layers (Fig. 2-2). The transparent nature of the cornea is imparted due to its arrangement of cells, collagen and absence of vasculature [25]. There are five layers which compose the cornea; (1) corneal epithelium, (2) Bowman's membrane, (3) stroma, (4) Descement's membrane and (5) endothelium (Figure

2-2). Another novel pre-Descemet's layer of cornea, called Dual's layer, has just been discovered recently and under debated [26]. These layers can be subdivided into three cellular (corneal epithelium, stroma and endothelium) and two interface layers (Bowman's membrane and Descemet's membrane)[27]. One addition to the corneal layers would include the external surface tear film. The tear film layer is produced by a combination of secretions from goblet cells, lacrimal gland, meibomian glands as well as Moll and Zeis glands that are found within the eyelids [25]. The cornea continues to increase in thickness as it moves peripherally, reaching a confluence with the sclera and conjunctiva. The junction of the cornea and sclera is referred to as the limbus.

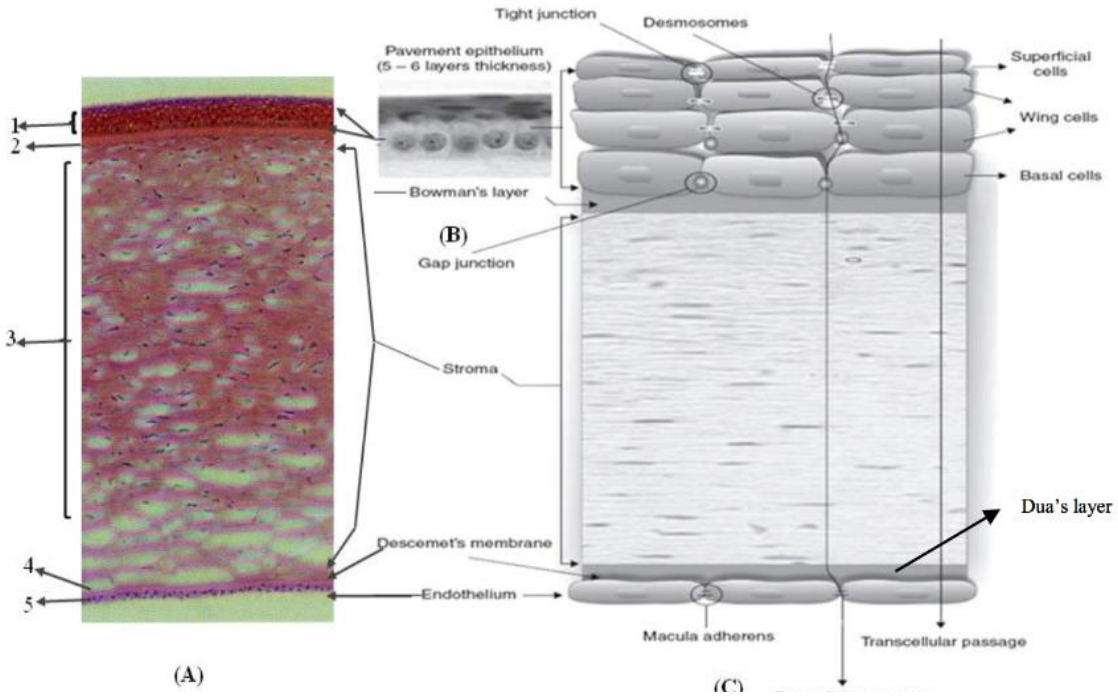

Figure 2-2: Corneal Layers of the Eye. (A) Histological Corneal Images; (1) Corneal Epithelium, (2) Bowman's Layer, (3) Stroma, (4) Descemet's Membrane and (5) Endothelium. (B) And (C) Diagrammatic Expanded Corneal Layers. *Reproduced with the Permission

The corneal epithelium is approximately four to six cell layers thick of a non-keratinized stratified squamous epithelium. Corneal epithelial cells have been noted to be replaced every seven to ten days. As such, two locations can be focused on for replacement, one being the limbus region which has been noted to be a location of increased vascularity and pluripotent stem cells in the anterior segment of the eye [28]. The single columnar basal layer of the corneal epithelium has shown mitosis capability for replacement of the wing and superficial cells [29]. The superficial cells present surface microvilli, with the addition of the tear film smooth's the surface irregularities and improves the optic properties of the cornea [27]. The corneal epithelial cells maintain the presence of tight junctional complexes preventing fluid movement within the intracellular spaces, as well as hemidesmosomal attachment to the basement membrane just coronal to Bowman's layer. Bowman's layer is a false membrane devoid of cellular content. The layer is composed of type I collagen and is approximately 15 µm in thickness, and aids in the shape maintenance of the cornea [27.] The corneal stroma comprises the largest portion of the cornea, contributing approximately 80 – 85% of corneal thickness [27.] The unique extracellular matrix of the stroma, consisting of bundles of collagen fibrils, are arranged in larger paralleling bundles called lamellae. The arrangement of the lamellae is key to reduction of anterior light scattering, while simultaneously aiding in the transparency and strength of the cornea [27]. Descemet's membrane, the second and most posterior of the corneal interface layer develops from secretions of endothelial cells. Electron microscopic views shows two distinct portion based on the time of formation, a banded and unbanded appearance, with the unbanded amorphous structure forming post birth, the total thickness approximate 10µm [27].

Corneal endothelium is the final posterior layer of the cornea. Viewed as a single cell layer thick, with tight cell adherence, maintaining direct contact with the aqueous humor. A high concentration of Na+, K+-ATPase pumps can be found in the lateral membranes of the corneal endothelial cells [30]. Additional function of endothelial cells is to help maintain the stroma at a relatively dehydrated state, approximately 78% water content, as they are in direct contact with the aqueous human [31]. This function is another aid in the maintenance of corneal transparency.

Iris: The pigmented aperture, which controls the size of the pupil, and thus the amount of light entering the eye. It consists of pigmented epithelial cells, circular muscles and dilator muscles. These muscles help constriction or miosis of the pupil by the action of cholinergic nerves. The dilator muscles are responsible for dilation of the pupils upon sympathetic stimulation [32]. The iris can be divided into four layers. (1) Anterior border layer, consisting of mainly fibroblast and pigmented melanocytes, large pits or holes termed crypts of Fuchs can be noted in this layer as well. (2) Stroma layer containing collagen fibers, blood vessels and nerve fibers. Within the deep stroma layer, the sphincter pupillae muscle is arranged around the pupillary margin. (3) The anterior epithelium containing myoepithelial cells of the dilator pupillae muscle, with the muscle fibers arranging themselves in a radial pattern, opposite the sphincter muscle orientation. (4) The fourth and final layer of the iris is the posterior pigmented epithelium, made up of highly pigmented columnar cells with the main physiologic function of light absorption within the iris.

Ciliary Body: The ciliary body is designed to regulate three major functions within the eye; (1) aqueous humor secretion, (2) control the shape of the lens and (3) help maintain

intra-ocular pressure and equilibrium of aqueous humor volume of the anterior chamber through drainage. The ciliary body is composed of the ciliary process and the muscle [33]. The ciliary muscle is attached to and controls suspensory ligaments known as zonules. The zonules is also attached the lens of the eye. Ciliary muscles have fibrous bundles and are highly flexible. Contraction of the ciliary muscles controls the shape, or accommodation of the lens, allowing images of various distances to be brought into focus.

Conjunctiva: A protective tissue of the eye that can be divided into three segments based on anatomical position, i.e., (1) fornical conjunctiva, (2) bulbar conjunctiva and (3) palpebral conjunctiva. These tissues are found lining the inner portions of the upper and lower eyelids. Conjunctiva tissues contain high vascularity, lymphoid tissue, mucous secreting cells and are highly innervated. It is made of non-keratinized stratified columnar epithelial cells that produce mucus and tears allowing the eyes stay lubricated.

Aqueous Humor: A transparent fluid produced from plasma by the ciliary body cells in the posterior chamber behind the iris, the aqueous humor occupies both chambers of the anterior cavity, the space posterior to the cornea and anterior to the lens [34]. The formation of aqueous humor is a three-component mechanism; diffusion, ultrafiltration and active secretion, which simultaneously controls the composition of the fluid [34, 35]. Production and drainage of aqueous humor are symbiotic to ensure equilibrium can be maintained [34]. The aqueous humor helps to provide needed nutrients, oxygen, and waste clearing to the avascular tissues of the cornea and lens [35]. Drainage of aqueous human assumes a posterior- anterior flow from the ciliary body anterior towards and drained into Schlemm's canal. Reports of approximately 5-10% of aqueous human can follow the uveo-

scleral pathway [36], [37]. The drained aqueous humor will collect and mix with the venous blood circulation [38].

Lens: The posterior anatomic boundary for the anterior segment of the eye is the lens. The lens, like cornea is an avascular tissue composed of multiple layers. Simplistically, the lens is a biconvex structure which can be divided into three layers, i.e., the capsule of the lens, the cortex and the nucleus of the lens. As the lens is the anatomic boundary for the anterior and posterior segments of the eye, aqueous humor is found on the anterior aspect of the lens, while vitreous humor is in contact with its posterior aspect[39]. The iris circumferentially overlaps the anterior portion of the lens forming the central open space into the lens referred to as the pupil. Posterior to the iris is the ciliary process with its zonular fiber extension which attach to the capsule of the lens, at its mid-junction or equator. With constriction or relaxation of the ciliary muscles lens accommodation can occur, allowing for object focusing. It has been noted that the capsule of the lens can take part in passive exchange and simple diffuse of metabolic substrates and waste with relation to their specific charge and molecular size[40-42]. The largest structural component of the lens is the cortex. The cells within the cortex can be found to be tightly packed with cellular components and a nucleus, as these cells age the nucleus and cellular content are lost leading adding in the transparency of the lens[43, 44]. As the cells age they continue their migration towards the center of the lens, which forms a thick and dense center known as the nucleus of the lens [45].

2.1.2 *Posterior Segment*

Sclera: The sclera is the largest portion of the globe, approximately 80%, and the cornea being the second largest component [46]. The sclera can be found to span from its

anterior junction of the cornea, the limbus, below the conjunctiva, to the posterior region known as the Lamina cribrosa of the sclera where the optic nerve exits. Sclera is composed of collagen fiber network with elastic fiber and dispersed melanocytes and the thickness increases from 0.5 to 1 mm moving toward the optic nerve [47]. This network is arranged in a disordered fashion, along with higher water content, causes light scattering, giving the sclera its classic white or opaque appearance. Sclera is highly porous tissue allowing the transport of water and others. The permeability of hydrophilic molecules is higher than hydrophobic one. The smaller molecule weight has higher permeability[48].

Choroid: The choroid layer can be found in between two layers, medial to the sclera and lateral to the retinal pigment epithelium (RPE). The choroid layer is highly vascularized. The main function of the choroid layer is retinal supply of oxygen and nutrients [49]. Additional role of the choroid layer deals specifically with aqueous humor drainage through the uveoscleral pathway of the anterior chamber, which can account for up to 35% [49]. Choroid layer blood flow through vasomotor control can also alter the intraocular pressure (IOP) [49]. The choroid can be subdivided into three layers; i.e., (1) suprachoroid, (2) vascular layers and (3) Bruch's membrane [49, 50] (Fig. 2-3). The arrangement places suprachoroid layer being most lateral in close approximation with the sclera, with each following layer moving more medial towards the RPE. It has been noted that the vascular layer can be separated into two layers, Haller's and Sattler's [49]. Haller's, Sattler's and choriocapillaries represent various vessel sizes, and positions within the vascular layer. (Figure 2-3). Bruch's membrane serves as the separating layer of choroid

from the RPE, with the basement membrane of the choriocapillaries endothelial cells forming its external layer of Bruch's membrane[49, 51, 52].

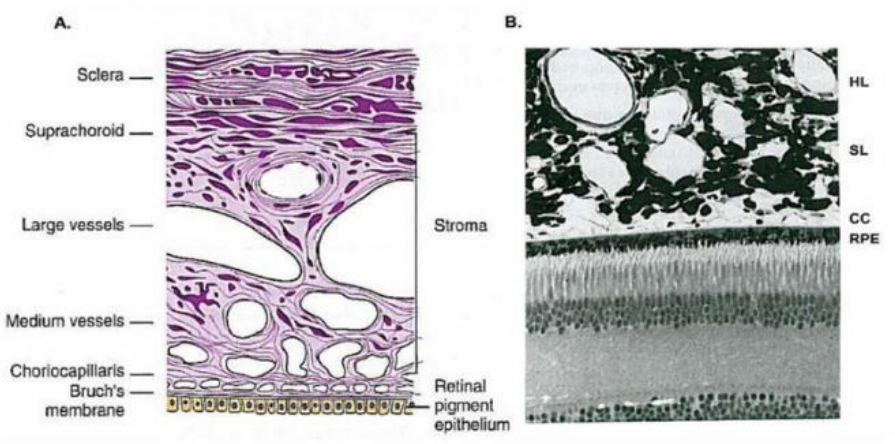

Figure 2-3: Histology of the Choroid. A. Schematic of the Layers of the Choroid. Reproduced with Permission from Remington, LA. Clinical Anatomy of the Visual System. B. Semithin Resin Section of the Outer Retina and Choroid in the Primate Eye. RPE: Retina Pigment Epithelium; CC, Choriocappilaries; SL, Sattler's Layer; HL, Haller's Layer. Reproduced with Permission from Forrester Et Al., 2002. The Eye: Basic Science in Practice

Retina: It is a light sensitive tissue made of two major layers i.e. Retinal Pigment Epithelium (RPE) and neurosensory retina. Retinal Pigment Epithelium (RPE) is directly in contact with the light sensing neural cells rods and cones. These cells are further associated with bipolar and ganglionic cells. The optic nerve is linked with the ganglionic cells, which are further coupled to amacrine cells. RPE functions as a nutrient source to the retina via the choroid. It forms a tight junction flanked by the choroid and retina. RPE cells also aid in the elimination of damaged photoreceptors via phagocytosis. A single cuboidal cell layer providing maintenance and survival to the retinal photoreceptor cells above, while regulating the choroidal capillaries of the choroidal layer below [53]. RPE undertakes a multitude of tasks, i.e. it forms the blood-retinal barrier (BRB), which plays an import role as a static posterior barrier to ocular drug delivery, transportation and clearance of

nutrients and waste products, production of growth factors, storage of retinoids and protection from free radicals [53].

The neural retina is a multilayered structure, consisting of the neurosensory retina and the RPE. Inner part of the neurosensory retina mainly obtains its blood supply from the retinal artery, whereas the outer portions fulfill their nutritional requirements by the choriocapillaries [51]. The two main photoreceptor cells found within this area are the rod and cone cells. The neural retina is found spanning from the Ora serrate anterior, ending at the optic nerve posterior. The multilayered neural retina forms the most internal layer of the eye. It can be subdivided into the posterior pole, or anatomic macula, and the peripheral retina, which makes of the remaining surfaces. Special anatomic areas have been of note, i.e. macula, fovea centralis and optic disk. Within the posterior pole, the fovea centralis is found to house the highest concentration of cone photoreceptor cells, thus the macula/fovea centralis is an area of heightened visual light detection [54]. The photoreceptor rod and cone cells can be found approximating the RPE cell layers, which are connected via inter-neurons called bipolar and ganglion cells which transmit electrical signals transformed form light energy to the brain for visual interpretation of images [55].

Vitreous Humor: It is a transparent matrix of hydrophilic gel with an approximate water concentration of 98%, which occupies the posterior segment, equaling around two thirds of the intraocular volume of the eye [56]. The vitreous human can be found attach anterior to the ora serrate of the retina and posteriorly around the optic nerve, allowing for compartmentalization and stabilization of the vitreous human against the retina. The vitreous made of collagen fibrils and hyaluronic acid. However, cortical region contains dispersed hyalocytes. The pH is around 7.5 [57].

2.2 Barriers To Ocular Drug Delivery (ODD)

The eyes are the most highly protected organ which have many barriers for drug delivery. Ocular diseases and other acute or chronic conditions of the eye, like other parts of the body, may require treatment in the form of medications and or invasive surgeries. As with any drug delivery, the goal is always to deliver the drug in the lowest effective bioavailable dose to the specific intended target tissue, while reducing or eliminating local or systemic collateral damage. Focusing on conditions that require ophthalmic drugs treatment protocols, one must understand the various forms and routes of administration to appreciate the barriers which will be encountered during delivery. The most common route of ophthalmic drug delivery is topical application, with various solutions, ointments and suspensions. Additional routes of ocular drug delivery have been developed to help overcome these various drug barriers. Although, more invasive in nature, and not without limitations, these routes include, i.e. intravenous administration, ocular injections to anatomic sites such as; intravitreal, subconjunctival, periocular, and even ocular implants.

Ocular drug barriers can be classified based on anatomic location, and their static or dynamic nature (Fig. 2-4). For those reasons two barrier segments exist; anterior and posterior segment barriers, with each segment containing both static and dynamic barrier forms. Static barriers of the anterior segment consist of; the cornea, conjunctiva, blood aqueous barrier (BAB) and efflux pumps on the cell surface. The dynamic barriers of the anterior segment include; tear drainage, conjunctival lymph and blood flow and aqueous humor. The posterior static barriers are; the sclera, Bruch's membrane, blood retinal barrier (BRB) and efflux pumps. The dynamic barrier of the posterior segment is the choroidal blood and lymph circulation.

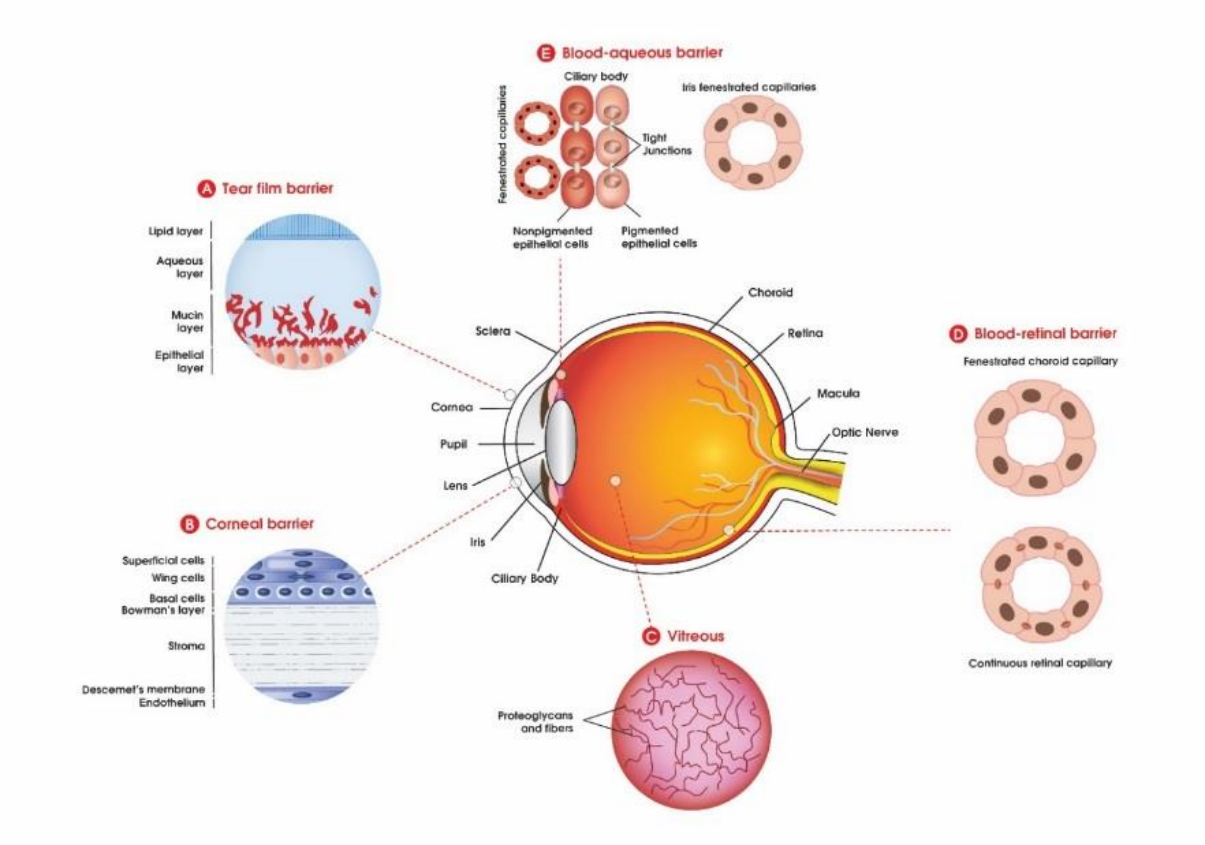

Figure 2- 4: Biological Ocular Barriers in The Eye (A) Tear Film Barrier; (B) Corneal Barrier; (C) Vitreous Barrier; (D) Blood–Retinal Barrier And (E) Blood–Aqueous Barrier

2.2.1 Anterior Segment Static Barriers

Cornea: The cornea acts as a physical barrier to topically applied drugs, in part due its structural nature. Consisting of five layers, the superficial epithelial layer presents with tight intracellular junctions, formed by cell adhesion proteins, occludins, which aid in preventing intracellular fluid and substance movement, along with hemidesmosomal attachment to the basement membrane, prevents deeper penetration into the ocular tissues. Additionally, the cornea is confluent with the sclera and conjunctiva. Therefore, topically administered drugs can contact and interact with these tissues. It should be noted that the conjunctiva has shown the highest permeability of these tissues, due to its large epithelial

pore size and increased paracellular space, of approximately 230 times more than the cornea [58]. Overall the conjunctiva can be two times as permeable as the sclera, which when compared with the cornea, the sclera shows a ten times higher permeability. Drugs can cross cell membranes by various routes; i.e. paracellular (movement through the intracellular space), transcellular (movement through the cell membrane, both the apical and basolateral cell membrane), active (movement across the cell membrane from an area of lower to higher concentration, enzyme and energy required), carrier-mediated (cell membrane transport via a carrier protein, can be active or passive forms) and receptor-mediated transport (endocytosis with specific vesicle and cell membrane receptors) [58]. The corneal epithelial occludins tight junctions prevent polar molecules from crossing by paracellular routes. Where, transcellular movement of lipophilic drugs have proven more effective, due to the high lipophilic nature of the corneal epithelial membrane layer, which accounts for approximately 90% of the corneal cell volume [5]. Both Bowman's and Descemet's membranes play no virtual role in limiting drug moment through the cornea. Whereas the stroma layer, being hydrophilic in nature, serves to limit the movement of lipid-soluble drugs. The final barrier of the cornea before reaching the aqueous humor is the corneal endothelium. It has shown the presence of leaky tight junctions that may allow movement of macromolecules through, and into the aqueous humor [59]. Of the noted mechanisms of drug movement through cell membranes, diffusion of drugs across corneal layers has proven to be the predominant role in reaching the aqueous humor. It has been noted that the two most important molecular properties effecting corneal epithelial permeability are ionization and pH of the drug molecules, with little impact imparted with regards to molecular size.

Conjunctiva: Although shown to exhibit a higher permeability than the cornea and sclera, it does not present without its own barriers. Due to the conjunctival epithelial surface layer, with the presence of tight junctions, once again, paracellular absorption is highly restricted. As with the cornea, the conjunctiva must also compete with the tear film production and nasolacrimal duct drainage of topically administered drugs. Mucin present in the tear film forms a hydrophilic layer coating the cornea and conjunctiva. With the tear films rapid rate of turnover and clearance, approximately every 2-3 minutes, most topically applied drugs can be cleared within 15-30 seconds [5]. Accounting for epithelial paracellular permeability issues and limited surface exposure time, topical drug administration can lead to as little as 5% of the administered drug reaching the intended intraocular tissues [60]. Additional barriers that face the conjunctiva is the lymphatic and capillary blood flow which will be discussed in greater detail in the anterior dynamic barrier segment.

Blood Aqueous Barrier: The blood aqueous barrier (BAB) in combination with the blood retinal barrier (BRB) make up the blood ocular barrier (BOB). The BOB as a whole plays a vital role as a major barrier for the entry and elimination of systemically administered drugs. The focus of this section will be the BAB. Anatomically the BAB constitutes in the posterior chamber of the anterior segment of the eye. It is comprised of two structures; the iris/ciliary blood vessel endothelium and the nonpigmented ciliary epithelium [5]. Again, cellular tight junctions play a role in controlling drug moment into deeper or posterior portions of the eye. Unlike the cellular tight junctions, the capillaries of the ciliary process may allow for passage of molecules. It was noted that dextrans up to 150kDa in size were able to cross the BAB [61]. The cilary capillaries control plasma protein entry with the aqueous humor. Although, drug molecules which may reach the aqueous

humor via ciliary capillaries are eliminated through the iris blood vessels, draining into the systemic circulation.

Efflux Pumps: Resistance and decreased drug bioavailability may be due to so called efflux pumps. Ocular drug efflux pumps belong to the superfamily known as adenosine triphosphate binding cassette (ABC) [58]. Two efflux pumps, i.e. permeability glycoprotein (P-gp) and multidrug resistance protein (MRP) have been of note in ocular drug barriers [5]. Lipophilic molecules have been shown be effluxed by the P-gp with some affinity [5]. P-gp efflux pumps have been identified on the ocular tissues of the cornea, conjunctiva and RPE, while MRP efflux pumps have been noted on the cornea, specifically MRP2 and MRP5 [62-65]. Active presence and function of efflux pumps will reduce the bioavailability by the reduction of the target cells intracellular drug concentrations.

2.2.2 Anterior Segment Dynamic Barriers

Tear Drainage: Drainage of precorneal fluid occurs through the nasolacrimal duct. The medial canthus of the eye contains the superior and inferior punctum which attach to the lacrimal canaliculi that converge into the nasolacrimal duct. The nasolacrimal duct drains into the inferior meatus of the nasal cavity. Most topically administered ocular drugs are absorbed into the corneal tissues by diffusion, although such factors as tear film drug dilution and drainage reduces the drug concentration gradient required for corneal diffusion. Approximately 7-10 µL can be held within the precorneal pocket of the eye, with the topical drug application volume exceeding the precorneal pocket volume, loss can occur with application spillage [66].

Conjunctival Lymph and Blood Flow: The conjunctiva is an anterior segment tissue comprised of high vascularity and lymphatic drainage. These factors help in

protection of the eye from the external environment. The protective nature also lends itself to a dynamic barrier for ocular drug delivery. The lymphatic and capillary blood flow expels a percentage of topically applied drugs which are transported from the surface of the eye to the lymphatic and systemic circulation. What remains is a reduced concentration and bioavailability of the applied drug to act on the cornea, sclera and conjunctiva.

Aqueous Humor: The aqueous humor itself does not activity seek out elimination of ocular drugs that may have diffused through the anterior segment tissues, but rather a physiological nature of the aqueous humor flow becomes the dynamic barrier. As the aqueous human is secreted into the posterior chamber of the anterior segment by the ciliary body, the aqueous humor flow moves anteriorly, opposing the posterior movement of the ocular drugs [58]. The drugs are carried and drained with the aqueous humor trabecular meshwork and the canal of Schlemm into the venous circulation.

2.2.3 Posterior Segment Static Barriers

Sclera: It is composed of hydrated collagen fibers with various thicknesse. The sclera is a static protective barrier for the posterior ocular tissues. Permeability of drugs across the sclera depends highly on lipophilicity and molecular size. A drop in sclera permeability can be noted when the lipophilicity and molecular weight of a drug increases, and can possible become trapped within the scleral pores [58]. As stated, the thickness of the sclera changes, with the greatest thickness noted in the posterior segment approximating the optic nerve, for this anatomic reason alone permeability of molecules is greatly reduced.

Bruch's Membrane: Situated between the choriocapillaries of choroid and the retinal pigment epithelium. The main function in a healthy state is to provide nutrient and metabolic waste exchange between the RPE/retina and choroidal blood vasculature [67]. Age

and disease related changes can lead to increased thickness of Bruch's membrane, this could cause a decrease in permeability from the outer sclera through and into the retinal tissues. Drugs could be trapped within the choroidal vasculature and be removed into systemic circulation before reaching Bruch's membrane and transported into the posterior retinal tissues.

Blood Retinal Barrier: The blood retinal barrier is composed of two layers, inner and outer BRB, with the RPE cells tight junctions forming the outer BRB layer and the inner layer formed from the endothelial cells of the retinal capillaries. This is one of the main barriers for ocular delivery. Astrocytes and Muller cells support the tight junctions, which allow great control of passive drug diffusion. Diffusion from choroid through the RPE outer layer of BRB allows lipophilic, CO_2 and O_2 molecules free movement into the retinal tissues, although do to these tight junctions transport of other molecules require energy mediated receptors.

2.2.4 Posterior Segment Dynamic Barriers

Choroidal Blood and Lymph Circulation: Highly vascularized and containing lymphatics makes this a significant dynamic barrier. Drainage of lipophilic drugs into the choroidal and lymphatic circulation preventing entry into the inner ocular tissue as these drugs are moved eventually into systemic circulation8. Hydrophilic drugs have shown the ability to have a lower potential to be eliminated or blocked by this barrier[68, 69].

2.3 Routes of Ocular Administration

Medications delivered to the eye can be divided into three groups; topical (drops, emulsions, suspensions, ointment and gels), systemic (oral or intravenous) and intra-ocular injection/implants following periocular (subconjunctival, subtenon, retrobulbar, and

posterior juxtascleral), and intravitreal route **(Fig. 2-5**). The most frequently used and suggested pathways for treating diseases of the eye based on anterior & posterior chamber location are; topical drops and intra-ocular injections/devices (implants), respectively. In the following sections these pathways for medication delivery will be discussed. Four routes of delivery can be used for medication distribution to the eye; topical, systemic, intraocular and periocular (including subconjunctival, Sub-Tenon's, retrobulbar and peribulbar) [70]. Fig. 2-5 depicts the multiple pathways of medication delivery to the eye.

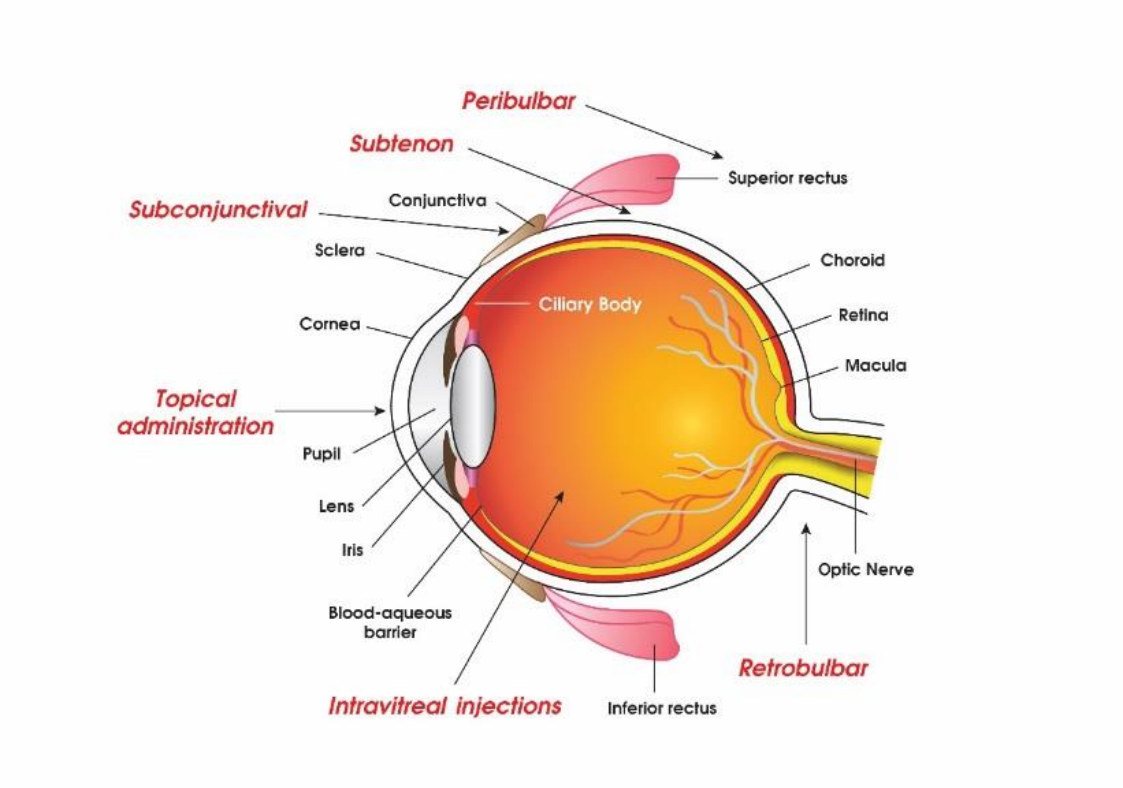

Figure 2-5: Schematic Representation of Local Routes for Ocular Drug Delivery

2.3.1 Topical Route

Alternative forms of topical ocular drops are; solutions, emulsions and suspensions. These can contain; water, active pharmaceuticals, excipients and preservatives. Multiple positives can be obtained from topical ocular drop delivery, such as; easy to use by patient, less invasive, reduced cost and by its ability to avoid first pass metabolism, medications can be selectively delivered to the anterior tissues of the eye. With these noted advantages, topical ocular drop will be the first choice with regards to treatment of diseases of the anterior eye. However, there are many limitations or barriers such as precorneal and corneal barriers. Therefore, a low fraction of medication reaches into ocular structures by topical route. Absorption of topically delivered medications to the eye is allowed by corneal and non-corneal, also referred to as trans-scleral pathway[71]. Although, corneal absorption is limited in part by its anatomic configuration, consisting of its main barrier, the corneal stroma, which is hydrophilic in nature, as well as tight junctions and lastly the epithelium of the cornea. Exceptions can be seen when active disease processes are occurring. During glaucoma and inflammatory events, back of eye tissues (choroid, iris and retina), can achieve a higher concentration of drug delivery[72].

Eye drops containers are designed to release a specific volume with each delivery for single or multiple deliveries. The medication solution is contained within glass or LDP plastic carriers. Topical drug carries have a solution volume range from 25.1 µL to 70 µL with an average drop size of 39 µL[73, 74]. The eye of a healthy adult can produce 7-9 µL of tear volume, at a generating rate of 0.5-2.2 µL/min. The ocular cul-de-sac, or lower conjunctival sac, marks the anatomic location for proper administration of topical eye medication solution [75]. Two distinct physiologic events follow the administration of topical

eye medication solutions: (1). Increase in tear volume productions and (2). Rapid reflex blinking. Following the proper unit dose delivery of topical medications only approximately 50% of the solution remains in the lower conjunctival sac, the remaining 50% is lost by two routes; directly spillage out of the eye onto the cheek and drainage within the middle meatus by means of the naso-lacrimal duct. Of the approximate 50% that remains in the lower conjunctival sac, a small portion, only 1 to 7% of drug is capable of reaching the aqueous humor of the eye. The reduced percentage of ocular drug delivery is predicated by two main barriers; static and dynamic. Static barriers are formed by anatomic building blocks of the eye, corneal and conjunctival tight junctions. A further complication in the insufficiency of topical drug delivery can be seen as a a true physical loss of solution during the eye delivery process. It can be occurred primarily in the elderly or other populations with decreased manual dexterity. This is even more important when the third-party payers can only provide a 30-day supply, and most of the solution is lost by drainage. To combat this issue and help reduce physical solution loss, topical application holders have been designed. The goal of the holders is to increase solution delivery into the lower conjunctival sac by; preventing eye lid closure and blinking, while directing the gaze of the eye to a proper position for the medication drop delivery.

Due to its high local concentration of capillary beds and the ability of the capillary blood flow to remove and reduce the concentration of medications to intended targets, the corneal route remains major absorptive pathway in comparison to non-corneal route, constructed by the conjunctiva and sclera, which acts as a minor absorptive pathway [76]. Anatomically compared, the epithelium of the conjunctiva offers less barrier activity than can be found in the epithelium of the cornea. Given the high permeability nature of the

sclera, compared to the cornea, by means of its poor vascularity and reduced penetration barriers to high molecular weight molecules, topically delivered medications reaching the sclera are afforded increased ocular access[72, 76]. Therefore, the sclera can be a main route of medication delivery to the eye, once absorbed by the conjunctival tissues. However, drainage loss through blood vessels of the conjunctiva can greatly affect the conjunctival/scleral pathway. Nevertheless, it should be noted that the conjunctival epithelium is the most viable route for ocular delivery of peptides oligonucleotides[77]. It is much harder to deliver drugs to the posterior segment because of membrane barriers. These barriers, in conjunction with nasolacrimal drainage of administered drops, drug metabolism, protein binding, lens barrier and long diffusional path lengths result in poor drug delivery to the retina following topical administration [78]. Moreover, the passage of drugs from the anterior segment to the posterior segment does not appear to be an efficient strategy because of the continuous drainage of the aqueous humor (i.e. a turnover of 2-3 mL/min). Thus, locally used ophthalmic therapies failed to provide an efficient pharmacological effect in the posterior segment (e.g. retina and vitreous) [76]. Many efforts have been directed towards enhancing the corneal permeability of the drug following topical administration. The application of high concentrations of penetration enhancer to increase the bioavailability may cause mucosal irritation and corneal abrasion, leading to toxicological complications.

The volume of the solution that can be instilled in the precorneal area is also limited. The eyelid and the conjunctival sac can take up a limited amount of the instilled solution. The volume that the precorneal area can accommodate is ~50 µL. When instilled volume is more than 50 µL, the excess solution is removed from the precorneal area via

nasolacrimal duct and the amount of drug in that volume of fluid is lost. Both in the nasolacrimal duct and in the nasopharynx, the drug can be absorbed systemically through the mucosa, avoiding pre-systemic hepatic first-pass metabolism[79-81]. Moreover, when the volume is more than the maximum volume, the reflux blinking and tearing remove the excess volume. The normal tear volume is restored within 2-3 min and the excess volume is lost within 20-30 sec by precorneal factors[82, 83]. The higher the volume of drop instilled, the more rapidly it will be lost via nasolacrimal duct system[80, 81, 84]. As the instilled volume is increased, more amount of drug is removed through nasolacrimal duct. When the instilled volume is very low, it may be diluted in the tear fluid, decreasing drug effect. 0.5% tropicamide, at drop volume of 5 µL produced less mydriasis than the one with 16 µL [85].

In summary, pathways of absorption of drug into the eye following topical instillation include: (a) corneal pathway, drugs transport through the cornea via passive diffusion. molecule must possess a balanced lipophilicity and hydrophilicity to have higher permeability. The drug transported across the cornea enters the aqueous humor, which is eliminated due to high aqueous humor turnover. Moreover, less is known to be permeable to drugs; (b) trans-corneal pathway, the conjunctiva and sclera are more permeable tissues compared to the cornea. once the drug crosses the sclera and enters the intraocular tissues, it may distribute in the surrounding tissues by diffusion. Drug absorption is limited to 5% at best following topical application due to precorneal and corneal barriers. Nonetheless, it is most patient compliant route. As ocular barriers and the physicochemical properties of drug molecules govern drug availability in the anterior and posterior segment. Studies should be directed to overcome these barriers by novel routes of administration and/or altering the properties of drug molecules [70].

2.3.2 Systemic Route

Drugs administered systemically (e.g. through the oral or intravenous route) also have poor access to the aqueous humor and the vitreous [72]. Ocular bioavailability of systemically administered drugs depends on the drug concentration gradient between serum and ocular tissues and as well as blood-ocular barrier (BOB) characteristics. The limitations of this route for drug delivery are poor ocular bioavailability due to BOB and systemic toxicity.

2.3.3 Intraocular Injection

Intraocular injections could be either intravitreal or intracameral. Injections that directs into the vitreous humor of the eye could be referred to as intravitreal injection, while injections into aqueous humor could be referred to as intracameral injection.

Intracameral Injection:

Intracameral delivery is intended to place the drug solution directly into the anterior segment of the eye. Although, intracameral injection has been extensively explored to improve delivery of biopharmaceuticals to both the anterior as well as posterior segments of the eye, it has not been possible to achieve therapeutic drug concentrations in the posterior segment of the eye following intracameral administration. Up to 100 µL volume in human can be injected in this route. However, repeated injections to maintain therapeutic concentrations over prolonged time period and low degradation of polymers may obstruct the aqueous flow, thereby elevating intraocular pressure and inducing risk of ocular infection[71, 78].

Intravitreal Injection:

During past two decades intravitreal injection is the main modality for delivering biopharmaceuticals to the posterior segment of the eye. It is an invasive procedure using a 30-gauge needle that involves injection of a drug solution and/or suspension into the vitreous cavity in the center of the eye after penetrating through all layers of the ocular globe. The vitreous cavity can generally accommodate a volume of 20–100 µL drug solution/suspension without resentfully altering the visual axis. However, various common complications including endophthalmitis, intraocular inflammation, retinal detachment, intraocular pressure elevation or glaucoma, ocular hemorrhage, floaters and cataract after intravitreal injections may lead to permanent vision loss if untreated[86]. Currently most of the biopharmaceuticals including pegaptanib sodium, ranibizumab, aflibercept and bevacizumab indicated for neovascular or wet AMD are given as intravitreal injections. A comparative pharmacokinetic analysis revealed concentration (Cmax) of bevacizumab in retina/ choroid after an intravitreal injection (1.25 mg/0.05 mL) to be approximately 317-fold higher than a subconjunctival injection at 1 week in rabbits [87]. Intravitreal injection of Avastin® generated significant bevacizumab concentrations in the retina, the retinal pigment epithelium, the choroid and particularly the photoreceptor outer segments in cynomolgus monkey [88]. Although, biopharmaceutical drugs due to their large molecular weight tend to prevent immediate elimination from the vitreous unlike small molecules, their vitreous half-lives of just few days to weeks may not be sufficient to achieve long-term therapeutic effect. Therefore, novel delivery methods and/or long-term controlled release formulations for protein and peptide-based biopharmaceuticals are warranted in order to significantly reduce complications caused by repeated injections.

2.3.4 Periocular Injection

The periocular region is the region surrounding the eye. Among existing routes, it is the most efficient and least painful route of drug delivery. Periocular injection is used when eye drops alone are not effective enough for treatment of eye inflammation and additional help is required. The drug is usually injected in close proximity to sclera in the posterior segment. Drugs delivered by this route can reach to the sclera, choroid, vitreous, retinal pigment epithelium, and neural retina. Peribulbar, retrobulbar, subconjunctival and Sub-Tenon's injections are frequently used approaches offered by periocular route for drug delivery in to the eye. Time to reach drug virtual level depends on available drug concentration and the intermittent barrier layers between target site and site of drug administration[70, 78]. Lack of efficacy, convenience and safety are few drawbacks of periocular route due to which it is yet not considered as a first line treatment and still serve as an additive to topical drug therapy [89].

Subconjunctival Injection:

Periocular delivery is frequently achieved through an injection into the subconjunctival area, i.e. the space underneath the conjunctiva. An injection rooted into the bulbar conjunctiva and superficial to the sclera may provide a way to directly deliver therapeutics into the subconjunctival space. Subconjunctival routes can be used for sustained delivery since a depot can be formed in the space that can expand and accommodate up to 500 µL volume. However, drugs injected into the subconjunctival space are often rapidly cleared via conjunctival blood and lymphatic flow. In addition, pore diameter and intracellular spaces of scleral fiber matrix regulate drug permeation to a large extent. Subconjunctival injection of bevacizumab can provide longer *in vivo* t1/2 in the

iris/ciliary body and retina/ choroid relative to intravitreal injection. It may be attributed to binding with negatively charged scleral proteoglycans [87]. In another *in vivo* study, high bevacizumab concentration was detected in the whole cornea post 24 h subcutaneous injection which remained almost unchanged in all layers of stroma over the next 14 days [90]. Various drug delivery technologies including microparticles/nanoparticles may be combined with physical techniques such as ultrasound and iontophoresis to achieve therapeutic concentrations of protein and peptide-based biopharmaceuticals following periocular administration[91, 92] .

Sub-Tenon's Injection:

The sub-tenon route is widely utilized for administering anesthetics during ocular surgery. It involves the injection of drug into a fibrous membrane, called tenon's capsule which along with the sclera binds the sub-tenon space. Although upto 4 ml of drug formulation could be injected through this route, administration complications including pain, chemosis, subconjunctival hemorrhage, retrobulbar and/or orbital hemorrhage, optic nerve damage, retinal ischemia, orbital swelling and rectus muscle dysfunction limit its use for the delivery of protein and peptide-based biopharmaceuticals [93]. In patients with clinically significant macular edema, sub tenon's injection of bevacizumab (2.5 mg in 0.1 mm volume) resulted in significant short-term visual improvement in eyes [94]. Thus, subtenon's injection may serve as an alternative to intravitreal injection for ocular delivery of biopharmaceuticals

Retrobulbar Injection:

Retrobulbar injections are used for administration of anesthetic agents or for corticosteroid therapy through the lower eyelid into muscles around the eye for the

treatment of posterior inflammation [71]. Because this route provides higher local concentration, it's utilized for anesthesia or akinesia and has little or no influence on intraocular pressure [78]. Therefore, it's selected if the drugs need to be in direct contact with posterior macular segment. The drugs are delivered into retrobulbar space within the muscle cone through a special 23-gauge sharp 1.5-inch needle with a rounded tip and a 100 bend. The needle is administered in the region between the lateral rectus and the inferior muscles and it directed to the apex of orbit allow the penetration to posterior segment until the orbital septum resists or intermuscular septum resists. This routes can take up to 2-3 mL of solution into the retrobulbar space [95]. This routes may cause the penetration through sclera therefore increase the movement of drug into vitreous and retina [72].

Peribulbar Injection:

Peribulbar injection is directly injected to the inferior lateral region of the orbit with 26-gauge half-inch disposable needle [96]. This can be sub-divided based on the depth of needle including; peri-ocular (anterior, superficial), circum-ocular (sub-tenon's, episcleral); peri-conal (posterior, deep) and epical (ultra deep) [97]. This route has been used to lower the risk of injury to intraorbital compared to retrobulbar injection during cataract surgery [98]. Considering both left and right sites, up to 8-10 mL of solution can be injected safely by this route [99]. However, it has less effective in anesthetizing the globe than retrobulbar injection. Even though both retrobulbar and peribulbar are used in analgesia, control of IOP post-operator analgesia, complication of orbital hemorrhage, brainstem anesthesia, artery occlusion, optic nerve trauma and apoptosis [70].

CHAPTER 3

3 DIABETIC MACULA EDEMA (DME)

Diabetic macular edema (DME) is a chronic back-of-the-eye disease that may lead to vision loss. DME causes retina thickening due to accumulation of fluid in the center of macula (Fig. 3-1)[100]. Chronic diseases such as diabetes, non-proliferative and proliferative diabetic retinopathy are notorious factors in developing DME[101]. The exact mechanism by which diabetes leads to retinopathy (DR) is not well-delineated. However, several theories have been postulated in the literature. DR may develop due to excessive growth of leaky

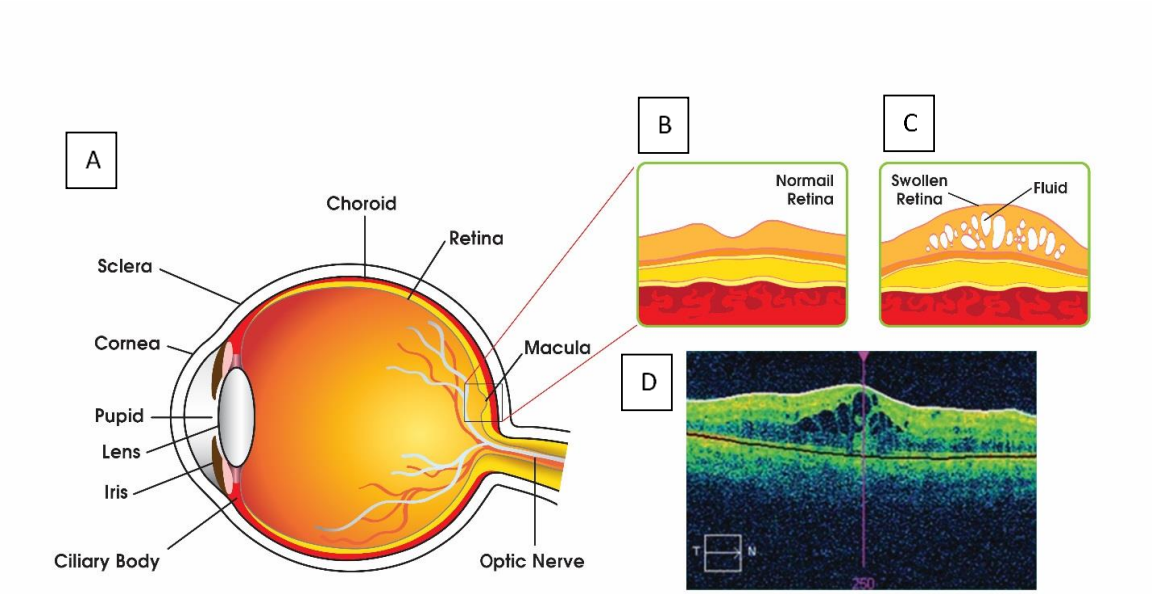

Figure 3-1: Diabetic Macular Edema (DME) at Disease State; (A) Structure of Human Eye; (B) Expanded Representation of Macula Region for Normal Eye; (C) Expanded Representation of Macula Region for DME; (D) Optical Coherence Tomography (OCT) Image for DME. *Reproduce with Permission.

vascularization in the retina. According to the National Eye Institute (NEI), DR progresses in four stages [102].

In brief, mild non-proliferative retinopathy is the initial first stage where tiny abnormal blood vessels or micro aneurysms develop. Such blood vessels appear as balloon-like swelling in the retina. With disease progress, in stage 2, moderate non-proliferative retinopathy develops with blood vessels supply nutrition to retina blocked. Severe non-proliferative retinopathy is known as stage 3. It is diagnosed with blockage of capillary vessels depriving blood flow in the retina. Under such conditions retina is deprived of oxygen and nutrients. Moreover, several cellular signals (particularly HIF-α) are triggered that cause development of new vasculature to compensate oxygen and nutrient supply. Proliferative retinopathy is termed as the final stage or the advanced stage of DR. The new abnormal blood vessels developed are fragile, and leaky. Such development is termed as neovascularization. Several factors can add to severity of DME depending on degree of DR, length of time subject suffering with diabetes, type of diabetes, hypertension, fluid retention, hypoalbuminemia, in body fluids, and hyperlipidemia in the blood. Advent of microscopic techniques such as fundus contact lens bio-microscopy or funduscopic examination are proven to aid in DME diagnosis. DME can be diagnosed with ocular clinical conditions such as retinal thickening within 500 μm and/or hard exudates within 500 μm or in one disk diameter in the center of macula [103].

Pathogenesis of DME is not clearly delineated in the literature. However, DME is a complex multifactorial ocular disease [104]. In the eye, blood retinal barrier (BRB) is an essential structure that regulates normal visual function. Such a physiologic barrier also regulates fluid movement in and out of retina [105]. BRB is comprised of inner and outer

BRB [106]. The inner BRB is composed of tight junctions between retinal capillary endothelial cells while the outer BRB tight junctions exist between retinal pigment epithelial cells [105]. The breakdown of inner BRB results in vasogenic edema, neural tissue impairment and ultimately vision loss, if not treated [107]. Disruption of BRB is a common factor for DME development[108, 109].

3.1 Physiology of DME

Many macro and microvascular factors along with various pathways are involved in retinal thickening, disruption of BRB and loss of pericytes [110].

3.1.2 Macro-vascular Factors

Starling's law and macular edema: According to the Starling's law, hydrostatic blood and osmotic pressures of tissue fluid are responsible for vasogenic edema. It appears maintenance of the gradients between two forces involving fluid movement between inner and outer retinal layers is crucial to prevent DME [107]. This law has explained that water accumulation is caused by decreasing osmotic pressure gradient between vessel and tissue. Current strategies for DME such as vitrectomy, laser, anti-VEGF or steroid administration have reversed osmotic pressure gradient and vascular permeability to prevent water accumulation.

Oxygen tension: In diabetes patients, the level of oxygen is reduced in retina region. Consequently hypoxia induces VEGF expression [111, 112] resulting in enhanced vascular permeability. Increasing in oxygen tension causes compensatory vasoconstriction of the retinal vessels which reduces hydrostatic pressure, resulting in macula edema[110, 113, 114]. Stefansson et al has explained why vitrectomy and photocoagulation have effects on DME

and other neovascularization retinopathies based on ocular oxygen tension improvement [115].

Shear stress: The damage of endothelial cells and endothelial decoupling caused by shear stress over time can lead to alterative fluid flow in edema. Increase in shear stress also elevates nitric oxide production, which can result in vasodilatation and increase hydrostatic pressure [116].

3.1.2 Micro-vascular Factors

Endothelial dysfunction and vascular damage due to hyperglycemia: Endothelial cells play very important role in maintaining the structure, vascular tone and prevention of platelet and leucocyte adhesion onto vessel wall. These cells are responsible for production of vasoconstriction and vasodilatation mediators and various inflammatory mediators such as intracellular adhesion molecule (ICAM), leucocyte adhesion molecule (LAM), and vascular cell adhesion molecule (VCAM)[117-119]. While endothelial progenitor cells play a role in repair of damaged vessels, number of these cells are reduced in hyperglycemic conditions[120, 121].

Blood–retinal barrier (BRB): Since endothelial cells play important roles in maintaining the integrity of BRB the damage to endothelial cells disrupts the integrity and enhances vascular permeability. This increased permeability leads to accumulation of extracellular fluids, and also it increases the oncotic pressure due to influx of protein from blood vessels to inner retina[122, 123].

Growth factors: Growth factors regulate angiogenesis by stimulating endothelial cell proliferation, migration, and survival. These factors have influence in many ocular diseases such as DME, DR and neo-vascular age-related macular degeneration[124-126].

Growth factors including vascular endothelial growth factor (VEGF), placental growth factor (PlGF), and hepatocyte growth factor (HGF) are responsible for increased vascular permeability. VEGF is the most promoted factor for endothelial cell migration, proliferation and survival.

Inflammation: Inflammation plays crucial role in DME pathogenesis. Leucocytes naturally adhere to vascular endothelium (leukostasis) and have ability to create poisonous superoxide radicals and enzymes[127]. Leukostasis initiates rapid vascular permeability and impair endothelial cells by producing enzymes, cytokine and free radicals[128, 129]. Also, inflammation stimulates the occludin phosphorylation which regulates tight junction and barrier function this resulting in the breakdown of BRB[130-132].

Oxidative stress: Diabetes can cause oxidative stress leading to elevated levels of nitric oxide (NO), superoxide, and peroxynitrite development and VEGF expression, which may alter vascular permeability and BRB breakdown[133-135].

Other factors include matrix metallo proteinases (MMP), protein kinase C, carbonic anhydrase, and angiotensin-II that have direct or indirect role in enhancing vascular permeability that results in DME [136-139]. Moreover, several pivotal pathways have been implicated in DME such as angiogenesis, inflammatory and oxidative stress pathways[110, 140]. Chronic hypertension and hyperglycemia cause blood vessels to become more porous allowing fluids, lipids and erythrocytes to escape. Such leakage and accumulation causes vascular basement membrane thickening, free radical formation, non-enzymatic glycosylation and pericyte death [141]. Moreover, increased vascular permeability and capillary dropout causes inadequate blood flow to retina.

3.2 Existing Treatment for DME

Fig. 3.2 shows the current treatment strategies for DME and the following section describes in detail.

3.2.1 *Laser Photocoagulation*:

Despite the fact that anti-VEGF (bevacizumab, ranibizumab and pegaptanib) and VEGF trap (aflibercept) have emerged as treatment options for back-of-the-eye diseases, laser (focal or/and grid) photocoagulation surfaced as another treatment option for diabetic macular edema (DME) [142]. A recent study was conducted on non-center involved (CI) DME subjects treated with focal laser photocoagulation. In this study, twenty-nine eyes with non-CI received focal laser coagulation and twenty eyes received no treatment serving as control. Photocoagulation treated eyes demonstrated a five letter gain in visual acuity in 21% subjects relative to 5% of control eyes [143]. Interestingly, this study indicated a decrease in inner and outer zone, central subfield thickness and reduction in total macula volume relative to control group [143].

Modern laser technologies and applications that have been used to treat DME. Such laser technologies include pattern scan laser photocoagulator (PASCAL) (OptiMedica Corp, Santa Clara, CA) and NAVILAS (OD-OS Teltow, Inc. Germany). The laser beam delivery systems have short pulse duration that reduces heat thereby minimizes thermal damage at the site of application leading to patient compliance[144, 145]. Other techniques such as subthreshold diode micro-pulse, navigated laser photocoagulation, pan retina photocoagulation and conventional single-spot laser techniques have been demonstrated to be more effective and safer relative to conventional laser photocoagulation [144].

Although laser photocoagulation has advantages, the associated drawbacks lessen enthusiasm, clinical application and patient compliance. Drawbacks include destruction of photoreceptors due to laser photocoagulation, retinal scar formation and impedance of visual prognosis[146]. However, laser photocoagulation may be beneficial in DME subjects who do not respond to drug treatments [147]. Recently, a combination of intravitreal drug administration with laser photocoagulation has been investigated. Such treatment appears to be promising[148, 149]. However, several studies may be required to establish the clinical gain with a combination approach and beneficial effects overweigh the side effects.

3.2.2 *Vitrectomy*:

Vitreous plays an important role in progression of DME. Studies demonstrated that improvement in vision for DME subjects may be achieved with induction of posterior vitreous detachment, pars plana vitrectomy (PPV), removal of internal limiting membrane (ILM) or taut posterior cortex[150-154]. However, the exact mechanism for vision restoration in DME subjects with vitrectomy is yet to be delineated. Recent studies suggest that exclusion of vitreous gel may reduce the concentration of DME-promoting factors, alter vascular permeability and enhance retinal oxygen supply[155]. Vitrectomy may also improve vasoconstriction by lowering tissue pressure and elevating hydrostatic pressure gradient between the vascular and tissue compartments [115]. Moreover, vitrectomy improves vaso-permeability of the retinal endothelial cells and restores visual acuity. In a cohort study of vitrectomy outcomes in DME subjects, 87 eyes were evaluated for visual acuity 20/63-20/400 including 54% internal limiting membrane peeling, 61% epiretinal membrane peeling, and 40% panretinal photocoagulation[155]. Vitrectomy significantly reduced retinal thickness and improved visual acuity. However, vitrectomy is associated with side effects

such as elevated intraocular pressure (IOP), vitreal hemorrhage, endophthalmitis, retinal detachment, induction of iris neovascularization and cataract formation[156]. Several randomized, controlled trials were conducted to investigate the side effects of vitrectomy on DME[157-161]. Such studies compared vitrectomy with laser, intravitreal steroid injection, and combinations. Vitrectomy may be applicable in DME subjects demonstrating epiretinal membrane and/or vitreomacular traction[162].

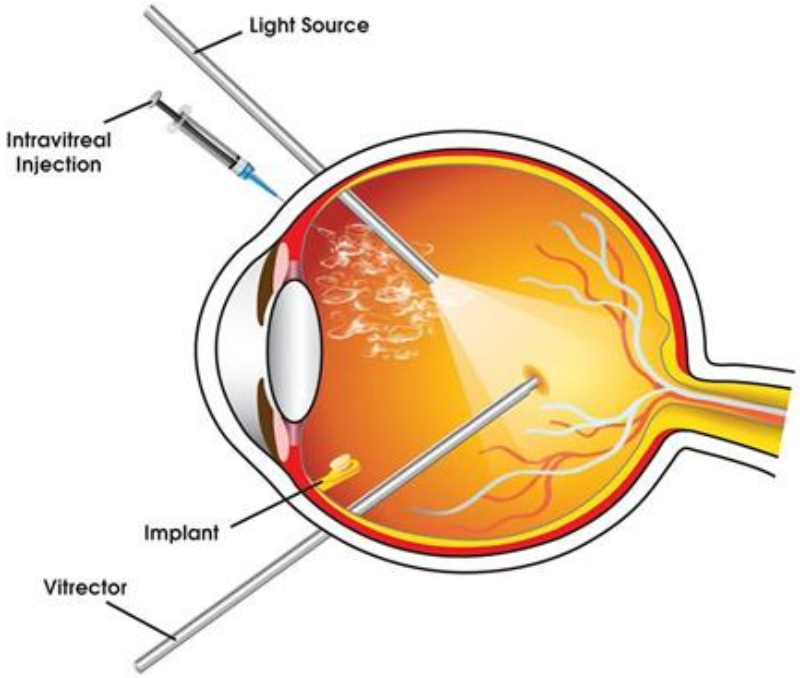

Figure 3-2: Treatment Strategies of Diabetic Macular Edema (DME). Reproduce with Permission

3.2.3 Intravitreal Anti-VEGF Therapy

Macromolecular Therapy:

Vascular endothelial growth factor (VEGF) plays an important role in retinal vascular permeability, breakdown of BRB and formation of macular edema. The current gold standard therapy for DME treatment is administering anti-VEGF agents[163-165]. VEGF inhibitors have demonstrated beneficial effects in DME treatment[166-169]. Current VEGF inhibitors include aflibercept (Eylea®), ranibizumab (Lucentis®), pegaptanib (Macugen®), and bevacizumab (Avastin®). Ranibizumab and aflibercept are approved by FDA for DME. Other anti-VEGF agents are also being considered due to cost effectiveness[170, 171].

Ranizubimab (RBZ) is a monoclonal antibody, approved for DME [172]. Ranibizumab has strong affinity binding to VEGF-A and blocks all isoforms of VEGF-A. Nguyen et al. demonstrated long term effects of ranizumab in diabetic patients with DME[173]. In this study, subjects were treated with RBZ, focal or grid laser or combination. The mean best-corrected visual acuity indicated that RBZ had significant effect to control edema in DME subjects. Moreover, a combination treatment with RBZ and focal /grid laser treatment can reduce edema also. Similarly, a clinical study, RIDE/RISE (NCT00473382 /NCT00473330) of RBZ demonstrated significantly improve of macula edema, and slowed down the progress of vision loss in DME subjects[174-176].

Bevacizumab is full-length humanized monoclonal antibody that is approximately 3 times bigger in size than ranibizumab. Bevacizumab was also approved by FDA for the treatment of glioblastoma and colorectal cancer. However, it is being used as an “off-label” drug for DME treatment due to low cost. Several studies have reported bevacizumab to significantly improve macula edema and vision in DME subjects[177-183]. Intravitreal injections of bevacizumab alone or in combinations with triamcinolone or

photocoagulation were investigated. Interestingly, combination of intravitreal bevacizumab and triamcinolone acetonide demonstrated marginal advantage over bevacizumab alone in DME [184].

Aflibercept: (Eylea®), VEGF Trap for eye, is a soluble protein composed of binding domain for human VEGF receptor 1 (VEGFR1), 2 and Fc domain of human immunoglobulin G1[185]. Aflibercept has 100 times higher binding affinity to VEGF isoforms relative to bevacizumab or ranibizumab [186]. Moreover, aflibercept binds to special P1GF and VEGF-B and inhibits the activation of VEGFR1[186]. Jean et al. conducted VISTA^{DME} and VIVID^{DME} phase 3 studies to compare the efficacy and safety of intravitreal aflibercept at 4 weeks, 8 weeks after initial monthly doses and laser treatment[185]. Aflibercept demonstrated significant effects over laser treatment. These results suggest that aflibercept is safe and well-tolerated. Best-corrected visual acuity (BCVA) can be achieved with aflibercept [187]. Many other studies such as VIBRANT, COPERNICUS, and GALILEO have reported significant benefits for aflibercept with better visual acuity[188-191]. Aflibercept had no significant difference at mild level of initial visual acuity relative to bevacizumab and ranibizumab. In fact, aflibercept can improve vision more effectively at worse level of initial visual acuity (NCT01627249)[170].

Pegaptanib (Macugen®) is a ribonucleic acid aptamer which was the first anti-VEGF approved be FDA for age-related macular degeneration (AMD). Pegaptanib is another "off-label" drug for DME and has selective target to VEGF 165[192]. Several studies demonstrated pegaptanib to be safe, well-tolerated and superior in efficacy in DME treatment[193-196].

Small molecule:

Rapamycin (or sirolimus) is an immunosuppressive drug with anti-inflammation, antiangiogenic, antifibrotic, and antifungal properties. Sirolimus blocks interleukin-2-mediated signaling pathway and reduces VEGF production by inhibiting S6K1 phosphorylation[197-200]. Recently subconjunctival and intravitreal injections of sirolimus were applied for the treatment of DME, AMD and non-infectious uveitis patients which appear well tolerated. (NCT01271270, NCT01033721)[201-203]. Efficacy studies with sirolimus in DME subjects have also been conducted. (NCT00711490, NCT00656643). Moreover, aqueous nanomicellar topical drop of sirolimus has been developed. These nanomicellar constructs have been demonstrated to deliver sirolimus in high concentrations to back-of-the-eye tissues (retina/choroid) with topical drop [197].

Steroids and other treatments in DME: Inflammation plays a crucial role in DME pathogenesis. Though the exact mechanism of glucocorticoid action is unclear. Anti-inflammatory agents are readily prescribed. Glucocorticoids lower VEGF activity with beneficial effects in DME[103, 204-208]. Steroids may inhibit inflammatory cytokine production, leukostasis, and phosphorylation of cell-junction proteins [209].

Triamcinolone acetonide (TA), is a synthetic steroid, recommended for DME treatment. TA possess anti-inflammatory and anti-angiogenic properties [17], improves tight-junctional levels between endothelial cells and reduces the vascular leakage [210]. The widespread biological effects and large therapeutic window of intravitreal TA (IVTA) in the treatment of various ocular disorder is well known. It is prescribed as an “off-label” drug for DME and DR[211-214]. Several studies have been conducted to compare the safety and efficacy between IVTA and other treatments[163, 184, 215-218]. In a meta-analysis of randomized controlled trials study, IVTA demonstrated better vision acuity relative to

standard care for ocular inflammation [217]. Moreover, IVTA administrations demonstrated better short-term efficacy to treat retinal vein occlusion [219]. However, after intravitreal administration of IVTA, it can also increase IOP, accelerate cataract formation and produce other associated side effects such as endophthalmitis and pseudo endophthalmitis [220-224]. To overcome such side effects, aqueous nanomicellar topical drop of dexamethasone were reported by our laboratory [225, 226] to delivers therapeutic levels to both anterior and posterior ocular tissues. Other studies for DME with glucocorticoids include biodegradable dexamethasone implant (Ozurdex), surgically implantable reservoir of fluocinolone (Retisert), the dexamethasone intravitreal implant (Posidurex), and non-bioerodible injectable fluocinolone polymer (Iluvien) [227-233].

3.3 Emerging Formulations for Treatment of Diabetic Macular Edema

Ophthalmic complications associated with diabetes are the leading cause of blindness in adults. In recent years, several formulations emerged that have been applied for treating DME and other back-of-the-eye diseases. FDA approved drugs such as ranibizumab and bevacizumab have shown promising results for the treatment of DME in various trials[173, 234, 235].

Inhibition of vascular endothelial growth factor (VEGF) has been used for treatment of age related macular degeneration in recent years. Recent studies have shown that inhibition of VEGF can also be used in treatment and management of DME. Furthermore, when intravitreal injection of anti-VEGF therapeutic was compared with laser monotherapy for treatment of DME, anti VEGF therapeutic was pharmacologically superior to laser monotherapy. Nguyen et al conducted a phase III randomized trial on 377 adult patients with vision loss due to DME. This study was conducted to evaluate efficacy

and safety of ranibizumab administered at different dosages. Results indicated that after 24 months of treatment 18.1% of sham patients gained more than 15 letters compared to 44.8% of patients treated with 0.3mg of ranibizumab [175]. In addition, ranibizumab showed fast and sustainable improved vision, lower risk for further vision loss and improved macular edema for DME patients[175].

Combination formulations are also emerging in treatment of some diseases associated with posterior segment of the eye. Combined regimens are utilized where the disease is not responding to one kind of therapy/treatment [236]. Liegl et al conducted a study to evaluate a combined treatment of laser photocoagulation and ranibizumab in the treatment of DME for a one-year period. One group received combination therapy which involved three monthly ranibizumab injections followed by laser photocoagulation. The second group was treated with ranibizumab injections and best corrected visual acquit (BCVA) was measured in both groups after treatment. An improvement in BCVA letter sore from 6.31 to 8.41 on both groups is observed. However, patients in monotherapy group require repeated ranibizumab injections (84%) relative to subjects in combined therapy (35%) [149]. These findings suggest that with combination therapy, the number of injections required was significantly reduced relative to monotherapy. This may be beneficial to subjects since frequent intravitreal injections may result local ocular complications including but not limited to: endophthalmitis, retinal hemorrhage retinal detachment and patient noncompliance[237, 238].

In addition to antibody therapeutics for treatment of DME, there are some promising non-antibody drug products that have been used in the treatment and management of DME. Fluocinolone Acetonide (ILUVIEN®) was approved in 2014 by the

FDA for treatment of DME. A long term follow-up study was conducted on DME subjects after receiving fluocinolone acetonide intravitreal implant [239]. In this study subjects not responding to laser photocoagulation or anti-VEGF were treated with fluocinolone acetonide implant (FAc) in one eye and were compared with contralateral eye that was treated with anti-VEGF therapy. Intravitreal FAc implant eye has demonstrated reduction of central macular thickness from 642 μm to 364 μm in the first month. In contrast, eye treated with anti-VEGF therapy was unresponsive [239]. Similarly, another study was conducted with FAc to treat patients with chronic DME[240]. Results indicated an improvement of more than 15 letters on 34.0% patients treated with FAc compared to 13.4% of control patients[240]. Such results provide option for physicians to treat subjects who do not respond to laser or anti-VEGF therapy. Moreover, FAc implant provided a long term sustained drug release of 0.2 μg/day for up to 3 years [239, 240] which may overcomesdrawbacks associated with intravitreal drug administration.

Misra et al have developed an insulin therapy that can be delivered to the retina. This is a sub-conjuctivally implantable hydrogel with thermosensitive and biodegradable properties for sustained release of insulin to the retina. Hydrogels are synthesized with UV photo-polymerization of N-isopropylacrylamide monomer and dextran containing biodegradable oligolactate-(2-hydroxyetheyl methacrylate) units. Insulin loading efficiency was very high (98%) [241]. *In vitro* studies demonstrated that hydrogels were nontoxic when subjected to R28 retinal cells and can release active insulin for seven days [241]. Such hydrogel implant may be utilized to load other macromolecular drugs intended to treat back-of-the-eye diseases.

Adelman et al conducted a non-randomized, multicenter study, with 2603 patients with macular edema and DME, to compare efficacy of anti-VEGF, triamcinolone monotherapy and laser treatments [242]. Despite the fact that all treatments revealed some improvement in visual acquit, anti-VEGF treatment showed the most improvement. However, surgery with pars plana vitrectomy and inner limiting membrane (ILM) peeling can improve vision acuity more than observed with anti-VEGF alone [242]. Consequently, this result indicates that treatment with ILM peeling and vitrectomy may be a better option to treat DME compared to other therapies.

Similarly, some other studies have also been conducted to evaluate the efficacy of combined treatments on DME. Vitrectomy combined with triamcinolone acetonide injection (IVTA) and macular laser photocoagulation was studied by Kim et al for treatment of nontractional DME. This study was performed on 28 patients, who were sequentially subjected to vitrectomy, IVTA and macular laser photocoagulation. Best corrected visual acuity (BCVA) and central subfield thickness (CST) were observed before vitrectomy, 1, 3, and 6 months after the treatment. Results indicated substantial improvement in BCVA from 0.44 to 0.34 and from 433.3 to 310.1 for CST [236]. These results suggest that vitrectomy, IVTA and laser photocoagulation may be combined for treatment of DME.

Enzymatic vitrectomy for DME patients has recently been explored [243]. Diaz-Llopis et al. investigated the role of enzymatic vitrectomy through intravitreal injection of autologous plasmin enzyme in management of DME and diabetic retinopathy. In a clinical study 63 eyes were treated with intravitreal injection of autologous plasmin enzyme and reexamined after one month for central macular thickness, BCVA and hyaloid. A second

injection of this enzyme was given to patients who did not develop posterior vitreous detachment (PVD)[244]. Results showed a massive improvement in central macular thickness by 100% and BCVA by 89%. However, PDV was observed to be 38% after first injection, which then increased to 51% after second injection [244]. Enzymatic vitrectomy is still new in the world of ophthalmology and further studies are required to understand the mechanism of action, efficacy and safety of the formulation. Enzymatic vitrectomy may be considered as an alternative therapy for treatment of DME.

In a study with nine patients who had persistent DME Zucchiati et al evaluated the effect of single injection of dexamethasone implant (0.7 mg) over 6 months period. Results indicated a significant improvement in BCVA and central retina thickness which was sustained for 4 months [245]. A similar study was performed in DME patients with vitrectomized eyes for 26 weeks by Boyer et al to evaluate safety and efficacy of dexamethasone. A significant improvement in BCVA and central retina thickness was maintained throughout treatment period [231]. In comparison, dexamethasone implant appeared to achieve superior outcomes in terms of BCVA, CMT and fewer injections compared to bevacizumab bevacizumab by (Gillies et al). Both treatments exhibited good progress on vision impairment score. However, 11% of patients treated with dexamethasone implant lost ten letters or more which was due to cataracts [246]. FDA approved dexamethasone implant (Ozurdex®) for the treatment of DME in 2014. Dexamethasone implant was previously approved for treatment of non-infectious uveitis affecting posterior segment of the eye. Table 1 summarizes major clinical trials that have been performed to study macromolecules and implants in treatment of DME

Nanotechnology formulations

As described earlier, DME is a back-of-the-eye disease. For local drug delivery, sub-conjunctival or intravitreal route of administration may be recommended. Frequent administrations are required in order to maintain therapeutic levels, and this may incur complications such as retinal detachment, endophthalmitis, pseudoendophthalmitis and retina hemorrhage. Nanoparticle-mediated sustained release formulations may lower injection frequency, and improve efficacy leading to reduced side effects and better patient compliance. Recently, several groups have developed topical nanomicelle formulations for delivery to the retina. Cholkar et al reported a topical administration of mixed nanomicelle formulation (MNF) loaded with dexamethasone, rapamycin (sirolimus) and cyclosporine for back-of-the-eye delivery [16]. The MNF was found to be safe when tested on human retinal pigment epithelial cells (D407) and rabbit primary corneal epithelial cells (rPCEC) *in vitro*. The MNF comprised high drug loading and entrapment efficiency with average size of 10.84 ± 0.11 nm. Furthermore, *in vivo* studies exhibited higher rapamycin concentration of 362.35 ± 56.17 ng/g in retina-choroid area but no drug was found in the vitreous humor [16]. Topical administration may provide patient compliance since no injections are involved.

In addition, Fujisawa et al have explored a liposomal diclofenac eye drop formulation along with improving formulation stability with the aid of surface modification of liposomes for delivery to retina. Liposomal formulation was prepared by using calcium acetate gradient method which increased entrapment efficiency from 51.3% (obtained by using hydration method) to 97% [247]. They utilized liposome surface modification with poly vinyl alcohol (PVA) or its derivatives PVA-R) and found that particle size of liposome with PVA modification to be 134.8 nm and with PVA-R was 176.7 nm. *In vivo* studies

performed on Japanese albino rabbits indicated an enhancement in accumulation of diclofenac in the retina-choroid by 1.8 fold with surface modified liposome compared unmodified liposomes [247]. Higher entrapment efficiency may result in a longer period of drug release. This delivery system may be suitable to deliver drug treatment of DME or any other diseases associated with posterior segment of the eye.

RNA has been also indicated as a therapeutic agent for treatment of wide variety of diseases. This involves modification, engineering, and/or assembly of organized materials on the nanometer scale. The 117-nucleotide (nt) RNA, called the packaging RNA (pRNA) of bacteriophage and small interfering RNA (siRNA) have been widely applied in the treatment of cancer, viral infection, genetic diseases, and other human ailments. Recently, Feng et al have reported ocular delivery of pRNA (pRNA-3WJ and pRNA-X) nanoparticles and investigated distribution and clearance after subconjunctival injection. pRNA-3WJ and pRNA-X-nanoparticles labelled with Alexa647 and dsRNA were prepared and administered to mice by subconjunctival injection [248]. It was observed that all nanoparticles (pRNA-3WJ, pRNA-X and dsRNA) were found in corneal, sclera, and conjunctiva cells, but pRNA-X was the only one found in retina cells. This study suggests that RNA therapy for ocular diseases including back of the eye delivery is possible.

Similarly, gene therapy for treatment of inherited and acquired ocular diseases has rapidly been evolving. The main challenge for gene therapy is to overcome barriers associated with ocular gene delivery. This can be achieved by developing a suitable nanotechnology that can cross ocular barriers and deliver genes at target site. A polymer (natural or synthetic) or peptides have been employed to encapsulate DNA to make a polymer or peptide compacted DNA gene delivery nanoparticles [249]. Safety of compacted DNA nanoparticles

for ocular delivery has also been investigated by Ding et al. Polyethylene glycol substituted lysine peptide (CK30PEG) compacted DNA nanoparticles encapsulating EGFP vector were subretinally injected in mice at different dosages [250]. Retin were observed at 1, 2, 4, 7 days post injection for any inflammatory signs or mediators. No inflammatory responses were observed in the retina [250]. In addition, chitosan DNA nanoparticles for retina gene delivery have been reported by Mitra et al[251]. Results indicates that compacted DNA nanoparticles may be exploited as gene therapies for treatment of posterior diseases and diseases associated with RPE.

Carbon nanotubes are nanometer-scale tube-like cylindrical 33 nanostructures. These cylindrical carbon molecules have unusual properties, which are valuable for nanotechnology, particularly in drug delivery. Nanotubes have also been explored for therapeutic delivery at back of the eye. Panda et al studied self-assembly dipeptide phenylalanine-α, β-hydrophenylalanine nanotubes for sustained intravitreal delivery of targeted tyrosine kinase inhibitor (pazopanib). The nanotube has a diameter range of 15-30 nm and 1500 nm in length and can be injected using 33G needle. Nanotubes were found to be nontoxic during *in vitro* studies with a 25% w/w pazopanib loading [252]. *In vivo* investigation indicated the presence of nanotube for 15 days and pazopanib drug was observed in vitreous humor, retina and choroid RPE at 4.5, 5 and 2.5 folds higher respectively compared to pazopanib alone [252]. These results suggest that nanotubes can be applied as a delivery system which may sustain higher concentration of drug in tissues.

Biodegradable polymers have been extensively utilized for preparation of nanoparticles in-drug delivery. Also, nanoparticle in gel formulation of steroids has been reported for treatment of macular edema by Boddu et al. In this formulation poly (lactic-

co-glycolic acid) PLGA (50:50 and 65:35) nanoparticles loaded with dexamethasone, hydrocortisone acetate, and prednisolone acetate were prepared by water in oil emulsion and then suspended in thermosensitive gel. Results indicated that entrapment efficiency for dexamethasone, hydrocortisone acetate and prednisolone acetate was 77.3%, 91.3% and 92.3 % respectively. Drug release studies indicated no burst release and followed zero order kinetics[253]. This nanoparticle suspended in thermosensitive gel may provide sustained release of drug at retina-choroid and may be exploited for DME and other eye diseases.

A quench technology where nanoparticles in porous microparticles (NPinPMP) were prepared by superficial infusion and pressure for sustained delivery of bevacizumab. Bevacizumab coated Poly(lactic acid) (PLA) nanoparticles were prepared and then mixed with PLGA microparticles and allowed to pass through supercritical carbon dioxide gas [254]. This allows expansion of PLGA matrix but not PLA matrix. Hence it created porous PLGA microparticles in which encapsulated bevacizumab PLA nanoparticles are incorporated to make NP in PMP. *In vitro* study indicated sustained release of bevacizumab for 4 months along with no change in conformation and activity [254]. Therefore, this formulation may be utilized with other protein therapeutics for treatment of back of the eye diseases and reduce frequent injections to maintain therapeutic levels. However, the size of microparticles may cause some problem for intravitreal injections.

In addition, tailor made pentablock copolymer-based formulation for sustained ocular delivery of protein therapeutics was extensively investigated by Patel et al. Biodegradable pentablock copolymers (FDA approved) were synthesized by ring opening polymerization method using different monomers [238, 255]. *In vitro* studies confirmed that polymers and monomers are safe and biocompatible when tested in ocular cell lines

(APRE-19, SIRC, HCEC and RAW-264.7). Furthermore, pentablock nanoparticles loaded with FITC-BSA, IgG and bevacizumab were tested for particle size distribution which ranges from 320 to 355 nm in diameter. The entrapment efficiency, however, widely varied from 35% to 70%. *In vitro* studies indicate 40 days release of FITC-BSA and 60 days for IgG when nanoparticles are suspended in gel [255]. This IgG has similar molecular weight as bevacizumab, which can be delivered at the back of the eye for treatment of posterior diseases. Therefore, this formulation may be adopted to prepare other anti-VEGF therapies and be delivered to the posterior segment of eye for DME and other diseases.

Since DME is a disease associated with the posterior segment of the eye, it remains a challenge to deliver drugs. Most of the drugs do not reach the back of the eye due to associated barriers such as blood retina barrier, blood aqueous barrier, and vitreous barrier, consequently only a small amount of drug reaches the back of eye. In order to maintain therapeutic drug levels, frequent injections are generally required, thereby lowering patient compliance. Therefore, it is very important when designing a formulation or a delivery system to insure higher therapeutic levels at the target site, particularly when it is ocular delivery. In addition, delivery systems that can sustain drug release for a prolonged period of time should be adopted so that frequent injections can be minimized. Also, stable therapeutics with safety is mandatory to deliver drugs at back of the eye.

Table 3-1: Current Therapeutic Drugs for DME

TRADE NAME	GENERIC NAME	STUDY	MAIN CONCLUSION	REF
Lucentis®	Ranibizumab	RISE/RIDE	Ranibizumab improved vision and macular edema in DME patients	[256]
Eylea®	Aflibercept	VISTA/VIVID	Intravitreal injection of aflibercept was shown to be superior compared to laser therapy in treatment of DME	[185]
Ozurdex®	Dexamethasone implant	MEAD	Dexamethasone implant were well tolerated and improved BCVA in DME patients	[257]
Iluvien®	Fluocinolone Acetonide	FAME	Both low and high dose of Fluocinolone Acetonide exhibited improved BCVA in treatment of DME	[258]

CHAPTER 4

4 MICELLE APPLICATION FOR DRUG DELIVERY

Micelles are colloidal constructs (5 to 100 nm) formed from amphiphilic monomers (surface active agents) that self-aggregate above certain concentration in solvent system. Such a concentration at which self-assembly of monomers is initiated and known as "critical micellar concentration (CMC)". In general, such monomer molecules have two distinct segments namely, hydrophobic head and hydrophilic tail. Depending on concentration (low to high) monomers exists in three different phases in the aqueous solvent; a) monomers b) an arranged monolayer of amphiphilic at the air-solvent interphase and c) micelles. Constructs formed from amphiphilic monomers offer unique advantages such as improved solubility of fairly insoluble compounds, stability, reproducibility and ease of manufacturing at pilot and bulk scale with ease of sterilization. Lipophilic molecules are embraced inside the hydrophobic core of micelles formed by van der Waals forces [259]. On the other hand, the outer hydrophilic corona helps to (a) provide stearic stability by forming hydrogen bonding with the surrounding aqueous solution [259, 260]; (b) protect the construct from being recognized and engulfed by reticuloendothelial system (RES) causing prolonged systemic circulation; (c) conjugate ligand for active targeting; (d) makes the encapsulated molecule non-detectable by analytical methods such as nuclear magnetic resonance and UV-visible spectroscopy and (e) develops clear solutions [15, 197, 261]. Also, micellar constructs may be comprised of pH and temperature sensitive polymers that release the cargo under surrounding conditions. However, micellar constructs suffer with limitations such as premature release of cargo, lack of controlled/sustained drug release and inability to encapsulate hydrophilic molecules. Micellar shape is largely

dependent on the size of head or tail of amphiphilic monomer. In case, if the monomer head i.e, hydrophobic part is sufficiently larger than hydrophilic portion then micelles may have structures such as rods and lamellae whereas, vice versa results in spherical construct [262].

4.1 Nanomicelle Preparations

Nanomicelles may be prepared from surface active agents such as surfactants and synthetic block copolymers. Amphiphilic monomers exists as ionic, nonionic and zwitterionic forms. Ionic surfactants may carry a charge (anion or cation). Examples of anionic and cationic surfactants include sodium dodecyl sulfate and dodecyltrimethyl ammonium bromide, respectively [263]. Nonionic surfactants such as n-dodecyl tetra (ethylene oxide) do not carry any charge. On the other hand, zwitterionic surfactant such as dioctanoyl phosphatydyl choline carry both positive and negative charges. Amphiphilic block copolymers are synthesized with U.S. FDA approved biocompatible and biodegradable polyester or polyamino acid derivatives. Polymer blocks may be arranged as linear diblock, triblock and pentablock (A-B; A-B-A or A-A-B-A-A type) and branched type copolymer. In the block copolymers A and B may represent any of the polymers such as, but not limited to poly(lactic acid)-poly(ethylene glycol)-poly(L-lysine) [PLA, PEG,PLL], poly ethyelen oxide, poly(D,L-lactic acid), polypropylene oxide, poly glycolic acid, poly (aspartic acid), poly (glutamic acid), poly (L-lysine) and poly-(histidine). In most of the copolymer blocks polyethylene glycol (PEG) is commonly used as hydrophilic segment because of its advantages such as high water-solubility, low toxicity, escape reticuloendothelial recognition, biocompatibility and stearic stability[264].

Nanomicelles may be prepared following different protocols depending upon the physicochemical properties of the copolymer. The method of preparation may be broadly divided into two processes, (a) direct dissolution and (b) solvent casting. Direct dissolution as known as simple equilibrium method has been employed with moderately hydrophobic block co-polymers. Examples include poloxamers and poly (butyl acrylate) block copolymers with hydrophilic end made from one anionic, one cationic, and four nonionic hydrophilic blocks [265]. In this method, drug and co-polymer are simultaneously dissolved in aqueous solution. Nanomicelle formation is initiated by heating the aqueous solution. Application of heat allows dehydration of micellar core and ultimately develops micelles. An appropriate combination of drug-to-copolymer ratio and application of heat induces micelle formation in the aqueous solution.

Solvent casting procedures may be further divided into four methods namely, (a) dialysis, (b) oil in water emulsion, (c) solution casting and (d) freeze drying. Dialysis method involves application of high boiling point, water soluble organic solvents such as dimethyl sulfoxide (DMSO), N,N-dimethylformamide (DMF), tetrahydrofuran (THF), dimethylacetamide and ethanol. Dialysis method is suitable to block copolymers that are not readily soluble in aqueous medium. In this method, copolymer and drug are separately dissolved in water soluble organic solvents. The organic solvent with copolymer and drug solution are loaded into a dialysis membrane bag and dialyzed against water for more than 12 hours with subsequent replacement of water at predetermined time points. This process involves slow removal of water soluble organic solvent that triggers micelle formation and encapsulation of drug. However, such method is associated with limitation such as low encapsulation efficiency and loss of drug in the dialysis process. The second method, o/w

emulsion method involves physical entrapping of molecules. In this process, lipophilic organic solvents such as dichloromethane, ethyl acetate and acetone are used. Encapsulation process involves dissolving the copolymer and drug in organic solvent with small amount of water. Organic solvent is removed by continuous stirring the mixture. In this method, evaporation of organic solvent triggers micelle formation with simultaneous physical entrapment of hydrophobic drug in the core of micelle [266]. The third method, solvent casting method involves use of organic solvent and aqueous solvent. In this method, both drug and polymer/s are dissolved in organic solvent such as ethanol to obtain clear solution. The organic solution is removed under high vacuum that results in a thin film. Evaporation of organic solvent favors polymer-drug interactions. Rehydration of this thin film with aqueous solvent spontaneously develops drug loaded micelles[15, 225, 261]. The final method of micelle preparation i.e., freeze drying is one step procedure. A mixture of water and tert-butanol are used to dissolved copolymer and drug. This mixture (drug and copolymer in water/tert-butanol) is subjected to freeze drying (lyophilization). During lyophilization, tert/butanol induces the formation of fine ice crystals that rapidly sublime leaving behind the freeze-thawed cake. Rehydration of this cake spontaneously develops drug loaded micelles.

4.2 Application of Nanomicelles in Drug Delivery

As discussed above, nanomicelles have several advantages in drug delivery carriers, including (a) small size (less than 100 nm), (b) structural stability, (c) low RES uptake, (d) enhance EPR effect, (e) less toxic, (f) entrap large amount of hydrophobic drugs and solubilize in water and (g) simple modification with target ligand. Several successful drug loaded micelle carriers have been studied in clinical trial which are summarized in

Table 1. This section will be divided into 3 main categories of nanomicelle applications in drug delivery.

4.2.1 Solubilize Poor Water-Soluble Drugs

Many current drugs possess poor water solubility. These compounds are classified as class II and IV according to the Biopharmaceutics Classification System (BCS) [267]. It is a big challenge for scientists to deliver hydrophobic drugs/diagnostic agents at therapeutic levels. Nanomicelles may assist in that respect. It can act a promising carrier to solubilize hydrophobic drugs[268, 269]. Since nanomicelles are made of amphiphilic polymers where the hydrophobic core can incorporate the hydrophobic drugs inside and the hydrophilic corona helps the construct with the aqueous phase. This approach has been studied over many decades and has demonstrated that nanomicelles have significantly increased the solubility lipophilic drugs many fold (10 to 8400 folds)[15, 197, 225, 270, 271]. For example, efavirenz, an antiretroviral, is poorly water soluble (about 4 μg/mL). Polymeric micelles of efavirenz increased its solubility up to 34 mg/mL (8400 fold) and its pharmacokinetic (PK) profile was evaluated in Wistar rats [271]. The PK parameters such as Cmax all rise up to 3 times for all doses range between 20 and 80mg/kg. Kishore Cholkar et al. has developed clear, aqueous nanomicellar topical eye drop containing 0.1 % (1.0 mg/mL) cyclosporine (CsA) while cyclosporine has a solubility of only 12 ng/mL [15]. CsA nanomicelles delivered drug to back-of-the-eye tissues such as retina/choroid with high level (53.7 ng/g tissue) following topical eye drop administration.

4.2.2 Targeted Nanomicelles

In order to maximize the drug delivery and minimize the side effects, the target moieties have been utilized to develop active targeting nanomicelles. Those nanomicelles

will target cells based on different approaches: (a) interaction with specific biological targets such as cell surface receptors, transporters and (b) use of locally applied signal protein (phage fusion proteins) [272]. Wang et al. have developed the paclitaxel-loaded phosphatidyl ethanolamine (PEG- PE) micelles which was modified with MCF-7-specific phage fusion proteins targeting tumor[273]. The targeted phage micelles demonstrated higher tumor selectivity in cancer cells than normal cells. Therefore, such targeting enhanced the anticancer effect of paclitaxel in xenograft mice model. Several target ligands have been exploited including monoclonal antibody[274, 275], peptides[276-280], and aptamer[281, 282]. Ahn J et al have prepared the antibody fragment conjugated nanomicelles loaded platinum to target the pancreatic cancer and tested on tumor xenografts [275]. Compared to the non-targeted micelles, Fab'- nanomicelles showed 15-fold higher *in vitro* cellular uptake and significant anti-tumor effect for more than 40 days in pancreatic tumor xenografts.

4.2.3 Stimuli Responsive Nanomicelles

pH sensitive: The pH of tumor environment is acidic (6.5–7.2) compare to normal tissues (7.4). These differences in pH have been exploited to stimulate, cleavage the pH-sensitive response ligands to release drugs from the micelle carriers. In brief, under physiological condition (pH 7.4) the drugs stay inside micelles while drugs are released selectively under acidic conditions such as tumor, endosomes or lysosomes. Several conjugates of pH-sensitive nanomicelles have been developed and shown effective with low toxicity and higher selectivity[283-287]. There are some anionic groups (polyacrylic acid, polymethacrylic acid, polyglutamic acid) and cationic groups (dimethylamino ethyl methacrylate, poly histidine) are very common in pH-sensitive components. For example, Bae et al have prepared the pH-sensitive poly (ethylene glycol)-poly (aspartate hydrazone

adriamycin) loaded nanomicelle which released selectively in the low pH environment through acid-sensitive hydrazine linker[288].

Temperature sensitive micelles: Similarly, the temperature difference of the environment may have effect on the CMC which allows micelle forming. The most common temperature-sensitive polymers are poly (N-isopropylacrylamide) (PNIPAAm) which shifts to hydrophobic insoluble polymer around 32°C from hydrophilic polymer. Soga et al have developed different thermosensitive polymeric micelles[289-292].

Light sensitive: Few studies indicate that the hydrophobicity and hydrophilicity of micelles is shifted under light where micelles got disrupted or reversible by light. This aspect is another potential development of drug release and delivery[293, 294]. Andrew et al. have reported that micellar system was very sensitive to infrared light to release fluorescence probe as Nile red [295].

Ultrasound-responsive: Ultrasound which has a frequency around 20 kHz or above has been utilized to increase drug uptake by tumor. Ultrasound has enhanced the drugs delivery by inducing (a) deeper tissue penetration, (b) perturbation of normal and tumor cell membrane, and (c) trigger drug release from micelle[296-300]. Marin et al. have studied the release and intracellular uptake of doxorubicin (Dox) from pluronic micelles, the most common ultrasound micelles. Higher Dox release from pluronic micelles was observed under high-frequency ultrasound[301].

Others: There are many other stimuli responsive micelles have been investigated including enzyme- responsive, redox-active. Enzymes present everywhere in body and over expresses in tumor. The oxidative and reductive enzymes are different between

intracellular and extracellular environment. Those differences are utilized in developing micelle carrier to deliver drugs to the target activation.

4.2.4 *Multifunctional Nanomicelle Carrier*: Multifunctional nanomicelle is the combination with at least two of the ligands which were discussed above. Multifunctional micelle could enhance the hydrophobic drug delivery to specific target as well as imaging agents which enable the micelle tracking or trigger released by pH sensitive or ultrasound. The combination provides many benefits over the conventional delivery. However, it is also very challenging for pharmaceutical field. Li et al. have developed the acid sensitive nanomicelle for both targeted drug delivery and magnetic resonance imaging in liver cancer cells[302]. Doxorubicin and superparamagnetic iron oxide nanoparticles (SPIONs – imaging agents) were encapsulated inside poly (ethylene glycol)-b-poly[N-(N',N'-diisopropylaminoethyl) glutamine (PEG-P(GA-DIP)) and surface modified with folate acid for targeting moiety. This multifunctional nanomicelles facilitated specific tumor targeted and enhance therapeutic effect as well as MRI diagnosis.

4.3 Conclusion

Over the decades micelles have become a hot topic in nanomedicine. Several nanomicelle formulations have now been developed and some are in clinical trials. Nanomicellar possess many advantages such as size, drug loading of both hydrophobic and hydrophilic agents, circulation time, safe, easily to conjugate target moiety for tumor uptake, imaging and triggered release. Those properties promise huge opportunity and challenges for pharmaceutical scientists explore to develop appropriate formulations which maximize the therapeutic efficacy and minimize the side effects. Fig. 4-1 shows different types of nanomicelle configurations.

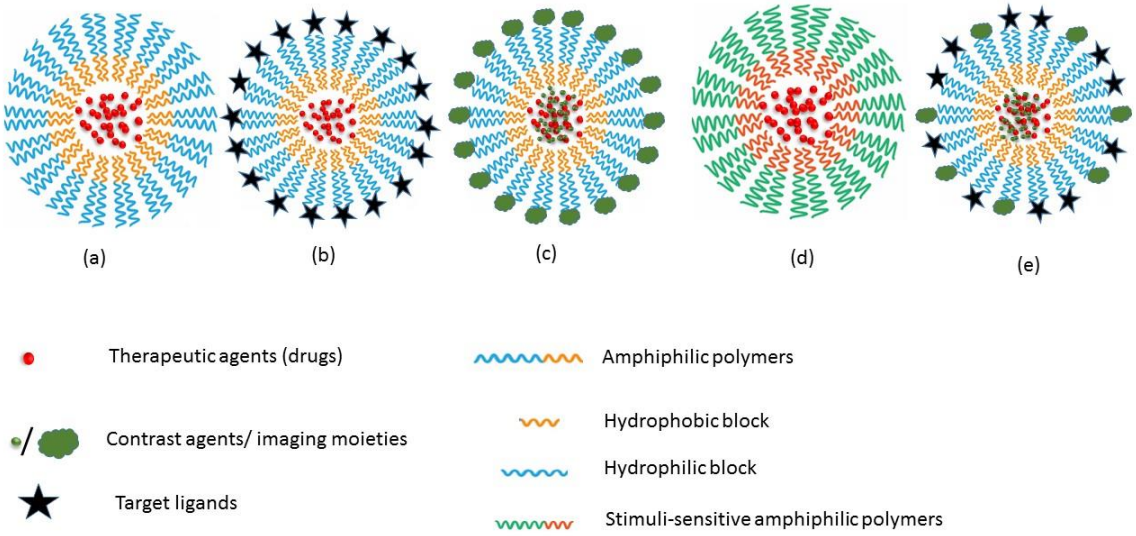

Figure 4-1: Schematic drawing image of (a). Polymeric micelle (b). Micelle conjugated with a targeting ligands (c). Micelle incorporating with contrast agents or imaging moieties (d). Stimuli-sensitive polymeric micelles (thermo/pH/ light/ultrasound-sensitive) (e). Multifunctional micelles with targeting ligands, contrast agents or imaging moieties, therapeutic drugs, etc. *Reproduce with permission.

CHAPTER 5

5 PREPARATION AND OPTIMIZATION OF TRIAMCINOLONE ACETONIDE-LOADED NANOMICELLES

5.1 Rationale

Diabetic macular edema (DME) is a back-of-the-eye chronic disease caused by the accumulation of fluid in the center of macula which may lead to vision loss [303]. DME originates from venous occlusions resulting in retina microvascular damage leading to leakage, capillary dropout, upregulation of angiogenic growth factors and neovascularization[304]. Diabetes causes degeneration of the inner lining of the blood vessels rendering them porous and leaky. Blood leakage through retinal vasculature causes the center of the retina to swell developing a condition known as DME. Such swelling leads to macular detachment and is responsible for the vision loss. Current treatment of DME includes laser photocoagulation, surgery, intravitreal anti-vascular endothelial growth factor (anti-VEGF) and steroid implant [303]. Delivery of drugs at therapeutic concentrations to back of the eye tissues (retina/choroid) is a very challenging task. Corticosteroids are prescribed routinely for the treatment of DME. However, steroids have many limitations such as the low aqueous solubility, sub-optimal physic-chemical properties, and poor ocular membrane permeability. Steroids are available under implant or intravitreal injection and associate with side effects like inducing intraocular pressure (IOP) leading to glaucoma and cataract [305].

Triamcinolone acetonide (TA) is a synthetic steroid, possessing anti-inflammatory and anti-angiogenic properties [17]. It is highly lipophilic with poor oral bioavailability and systemic side effects. Alternative invasive route of drug administration i.e. intravitreal

injection (IVT) of TA produced promising results for the treatment of DME [18] [19] [20]. However, IVT is an invasive procedure which is associated with adverse side effects such as retinal detachment, endophthalmitis, pseudoendophthalmitis, intraocular pressure (IOP) elevation and cataract formation [17, 18, 306].The current delivery strategies for steroids including TA are local administration such as implant and IVT, which are highly invasive and may cause low patient compliance. After IVT administration, TA particles may distribute homogenously in vitreous humor and interfere with vision. Such treatment can also accelerate cataract formation and elevate IOP[220, 307]. Therefore, there is an urgent need to develop a clear, aqueous topical eye drop formulation to deliver TA in therapeutic levels to back of the eye tissues (macula region). In such a scenario, aqueous nanomicellar formulation with amphiphilic polymers appear to be a promising approach. Hydrophobic-TA will be encapsulated in the core of nanomicelles. Hydrophilic corona aids in the development of clear, aqueous solution. This novel nanomicellar strategy may (i) improve drug solubility, (ii) improve drug uptake and cell permeability, (iii) allow for non-invasive delivery of hydrophobic drugs to posterior ocular tissues and (iv) improve patient acceptability and compliance due to its noninvasive, nonirritating clear and aqueous system. Nanomicelle structure has been sketched as Fig.5-1. Nanomicelles may primarily follow non-corneal pathway such as conjunctival-scleral rather than uveo-sclera pathway after topical administration to reach the retina [197].

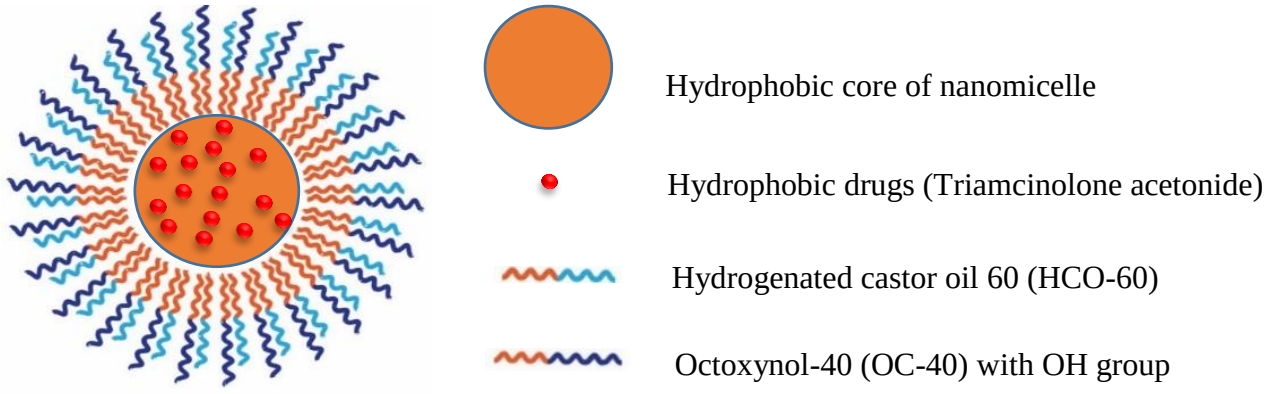

Figure 5-1: Schematic drawing image of TA-loaded NMF. Reproduce with Permission.

In the present study, two amphiphilic polymers namely; hydrogenated castor oil 40, 60, 80 and 100 (HCO-40, HCO-60, HCO-80 and HCO-100) and octoxynol-40 (Oc-40) are selected. Both HCOs and Oc-40 are safe and approved by FDA for human use. Amphiphilic nature of HCOs and Oc-40 consist of hydrophobic core and hydrophilic corona allowing spontaneous formation of spherical nanomicelles in aqueous solution. Hydrophobic TA may partition into hydrophobic core of nanomicellar structure whereas the corona is comprised of hydrophilic groups which extend towards surrounding aqueous environment in a manner to stabilize the inner hydrophobic core. Based on the experiment results, HCO-60 gave the highest entrapment efficiency and chosen as the The objective of current study is to develop and optimize nanomicellar aqueous TA-loaded formulation utilizing full-factorial statistical design of experiment (DOE). The ratio of the combination HCO-60 and Oc-40 was optimized with JMP 13.0 software and characterized for their size, polydispersity (PDI), shape, surface morphology, entrapment efficiency (EE), loading efficient (LE) and critical micellar concentration (CMC). Standard least square fit analysis was carried out to identify the optimal NMF which generates the highest desirability.

Moreover, this formulation was evaluated for *in vitro* cytotoxicity on human corneal epithelial cells (HCEC) and human retinal pigment epithelial cells (D407 cells).

5.2 Materials

TA was obtained from MP Biomedicals, LLC USA. Hydrogenated castor oil 40, 60, 80 and 100 (HCO-40, HCO-60, HCO-80, HCO-100) was procured from Barnet Products Corp., NJ, USA. Octoxynol-40 (Oc-40) (Igepal CA-897) was purchased from Rhodio Inc., NJ, USA. HPLC grade methanol, ethanol and dichloromethane were purchased from Fisher Scientific, USA. Povidone K 90 (PVP-K-90, Kollidon® 90 F, Ph.Eur, USP) was purchased from Mutchler, Inc. Pharmaceutical Ingredients, NJ, USA. CellTiter 96® AQueous nonradioactive cell proliferation assay (MTS) kit and lactate dehydrogenase (LDH) assay kit were obtained from Promega Corp and Takara Bio Inc., respectively. D407 cells were procured from the American Type Culture Collection (ATCC). HCEC are SV-40 virus transfected human immortalized corneal cells; this cell line was a generous gift from Dr. Araki-Sasaki (Kinki Central Hospital, Japan)

5.3 Methods

5.3.1 Film-Hydration Method for Nanomicelle Preparation

Triamcinolone acetonide-loaded nanomicelles, here on referred to as TA NMF were prepared following a previously described procedure reported from our laboratory [197, 225, 308]. Briefly, HCO-60, Oc-40 and TA were accurately weighed and separately dissolved in ethanol. All three solutions were mixed together to obtain a homogenous solution. Organic solvent was removed under rotary evaporation followed by high vacuum (GeneVac) to generate a thin film. Subsequently, this film was hydrated and resuspended in phosphate buffer. This solution was filtered sterilized through 0.2 µm nylon filter to

separate unentrapped TA and other foreign particles. Similarly, the blank formulation was prepared without TA

5.3.2 Drug Concentration Determination Using High Performance Liquid Chromatography (HPLC)

Reverse phase HPLC method described earlier was used with necessary modifications [309]. Reversed phase HPLC (RP-HPLC) method was applied to analyze samples with Shimadzu LC pump (Waters Corporation, Milford, MA), Alcott autosampler (model 718 AL), Shimadzu UV/Vis detector (SPD-20AV), and Phenomenex C8 column (spherisorb 250 x 4.60 mm, 5µm). The mobile phase was composed of methanol and water (52.5:47.5 %v/v) with the flow rate set at 0.5 mL/min and UV detector at 254 nm. Calibration curve (1 to 25 µg/mL) for TA was constructed by injecting 50 µL into the column.

5.3.3 Exploratory Model (Design of Experiments (DOE))

In order to understand the factors and the effect of polymers on the formulation variables such as entrapment efficiency (EE), loading efficiency (LE), and critical micellar concentration (CMC), the design of experiments (DOE) was employed. A preliminary study was conducted to screen the effect of polymers on the formulation variables such as EE, LE and CMC. To develop the experimental design and analyze the data, student version of JMP® 13.0 software (SAS institute, USA) was selected and "Screening design" was adopted. In this study, X1 (HCO-60) and X2 (Oc-40) serve as independent variables. On the other hands EE (Y1), LE (Y2) and CMC (Y3), respectively were selected as dependent variables.

Statistical Analysis:

The experimental design and data analysis were performed by JMP 13.0 software student version. The effect of two factors - polymer (HCO-60 and Oc-40) amounts on dependent variables (EE, LE and CMC) was studied with statistical models. These models will denote interactive and polynomial influences on the dependent outcome in order to predict fit model (Eq.5-1)

$$Y = b0 + b1\ X1 + b2X2 + b3\ X1X2 \quad \text{(Eq. 5-1)}$$

Where Y is response outcome, b0 denotes intercept, b1, b2, b3 represent the regression coefficients for factors X1, X2 and interaction X1 and X2, respectively. X1 denotes amount of HCO-60 and X2 represents amount of Oc-40. The t-test at $\alpha = 0.05$ level was used to determine the significant relationship between independent and dependent variables. R2 and adjusted R2 were also calculated for the regression model. The model was validated by checking model assumptions and lack of fit test. Results from this design were analyzed with one-way analysis of variance (ANOVA). F-test was carried out at $\alpha = 0.05$ to determine significance of regression relationship between independent and dependent variables. The design runs (coded and uncoded) and corresponding variables are summarized in Table 5-1.

In vitro experiments were performed at least in quadruplicate ($n = 4$) and the results were expressed as mean ± standard deviation (SD). Student t-test was applied to compare mean values. And a p value of ≤ 0.05 is considered as statistically significant.

Table 5-1: Details Design of Experimental (DOE) Coded and Uncoded Runs

Formulation Code	Coded Design		Uncoded Design	
	X1	X2	HCO-60 (wt%)	OC-40 (wt%)
F1	+	+	5	3
F2	+	-	5	1
F3	0	0	3.5	2
F4	-	+	2	3
F5	-	-	2	1
F6	+	+	5	3
F7	+	-	5	1
F8	0	0	3.5	2
F9	-	+	2	3
F10	-	_	2	1

5.3.4 Entrapment Efficiency (EE) and Loading Efficiency (LE)

Following a published protocol [197], reversed micellization was achieved in organic solvent (dichloromethane) and TA was extracted from the core of nanomicelles. The amount of TA encapsulated within NMF was measured with HPLC. The percentage EE and LE of TA in NMF were calculated with equation 5-2 and 5-3.

$$\text{EE (\%)} = \frac{amount\ of\ TA\ quantified\ in\ NMF}{amount\ of\ TA\ added\ in\ the\ NMF} * 100 \quad \text{(Eq. 5-2)}$$

$$\text{LE (\%)} = \frac{amount\ of\ TA\ quantified\ in\ NMF}{(amount\ of\ TA\ added + amount\ of\ polymers\ used)} * 100 \quad \text{(Eq. 5-3)}$$

5.3.5 Determination of Critical Micellar Concentration (CMC)

CMC of single polymer HCO-60, Oc-40 and a binary mixture of HCO-60 and Oc-40 were determined with iodine as hydrophobic probe following a published method from our laboratory. The absorbance of hydrophobic iodine partitioned into nanomicellar core was measured with UV-Vis spectrometer DDX 880, Beckman Coulter. The absorption intensity was plotted against logarithm of polymer concentration to calculate CMC.

5.3.6 Micelle Size, Polydispersity and Surface Potential Charge

The nanomicellar size, PDI, and surface potential were determined by dynamic light scattering analyzer (DLS) (Brookhaven Zeta Plus instrument, Holsville, NY, USA). A sample volume of 500 µL without dilution was subjected to size measurement at a laser wavelength of 659 nm at room temperature. All measurements were performed in triplicate.

5.3.7 Morphology Transmission Electron Microscopy (TEM)

To determine shapes of TA-loaded NMF, a drop of nanomicelles formulation was placed on TEM grid with carbon film, excess of liquid was removed with filter paper and grid was air dried. Specimens were negatively stained with 1% uranyl acetate and TA nanomicelles were witnessed with CM12 electron microscope (FEI, Hillsboro, OR) at 80 kV accelerating voltage. Image acquisition was performed with Orius CCD camera (GATAN, Pleasanton, CA)

5.3.8 Light Transmittance

The percentage transmittance of light through samples (N=4) was measured at different wavelength range from 400nm to 600 nm with a UV-Vis spectrometer (Model: Biomate-3, Thermo Spectronic, Waltham, MA). Percent light transmitted was recorded. Distilled deionized water served as blank. All measurements were performed in triplicate.

5.3.9 Dilution Effect

The dilution effect of NMF were studied by diluting the sample from 0 to 200 times with phosphate buffer. Diluted TA nanomicelles were measured for size characterization following an earlier described protocol. Briefly, the TA loaded NMF were diluted with appropriate volume of phosphate buffer according to dilution factor and NMF size and PDI were recorded from DLS analyzer.

5.3.10 Powder X-Ray Diffraction (XRD)

XRD analysis was performed for TA, freeze-dried blank NMF, and freeze-dried TA -NMF formulation. A Rigaku MiniFlex powder automated X-ray diffractometer (Rigaku, The Woodland, Texas, USA) was utilized for the analysis at RT. Cu Kα radiation (λ=1.5418Å) at 30 kv and 15mA was utilized. The diffraction angle covered from 2Θ 4.0° to 45.0°, and a step of 0.05° with 3 sec/step were applied. The diffraction patterns were processed using Jade 8 (Materials Data, Inc., Livermore, CA).

5.3.11 ^{1}H-NMR Spectroscopy of Nanomicelles

Proton nuclear magnetic resonance (^{1}H NMR) was applied to identify any unentrapped (or) free TA in the NMF solution. ^{1}H NMR studies were conducted for TA, blank NMF and TA-loaded NMF. ^{1}H NMR spectra were recorded on Varian 400 MHz

spectrometer (Varian, USA) in deuterated water (D_2O) or deuterated chloroform ($CDCl_3$). NMR data was processed using VNMRJ or ACD labs software.

5.3.12 Osmolality and pH

Osmolality is an important attribute for the topical eye drop formulation. It was measured using the Wescor Vapor Pressure Osmometer Vapro 5520 follow the manufacture manual. Briefly, 10 µl of NMF was loaded in the center of the sample disc and immediately the instrument measure and show osmolality value. The pH of the NMF was adjusted similar to the tear pH ~ 6.8 with phosphate buffer.

5.3.13 Viscosity

The viscosity of all the formulations was measured with Ostwald-Cannon-Fenske viscometer following conventional method as previously described. Briefly, the travel time or efflux time of NMF and distilled deionized water freely go through ranged distance was measured and calculated with equation 5-4 (Eq. 5-4). All measurements were performed in triplicate.

$$\text{Viscosity}_{(liq)} = \frac{Density\ (liq)\ X\ time\ (liq)\ X\ Viscosity(water)}{Density\ (water)\ X\ time\ (water)} \quad \text{(Eq. 5-4)}$$

Where $\text{viscosity}_{(water)} = 0.89$ centipoise (Cp), 25 ˚C and $\text{density}_{(water)} = 1$ g/mL

5.3.14 Cell Culture

Human corneal epithelial cells (HCEC cells) were cultured following a previously published protocol[310]. Briefly, DMEM/F-12 medium comprising of 15% (v/v) heat inactivated fetal bovine serum (FBS), 22mM $NaHCO_3$, 15mM HEPES and 5 mg/L insulin, 10 µg/L human epidermal growth factor, 100 mg/L penicillin and 100 mg/L streptomycin was prepared. Cells with passage numbers between 15 and 25 were utilized for all studies. Human retinal pigment epithelial cells (D407 cells) were grown as described earlier in

DMEM medium supplemented with 10% (v/v) heat inactivated FBS, 15 mM HEPES, 29 mM $NaHCO_3$, 100 mg/L penicillin, 100 mg/L streptomycin, and 1% nonessential amino acid. Both cell lines were incubated at 37 ˚C, 5% CO_2 and 90% humidity. Both media were changed every alternate day.

5.3.15 In vitro Cytotoxicity

In vitro cytotoxicity studies of NMF were carried out with Premix WST-1 cell proliferation assay kit (Takara Bio Inc.) and Lactate dehydrogenase (LDH) assays (Takara Bio Inc.) on HCEC and D407 cells respectively. Briefly, HCEC and D407 cells were cultured in flasks and harvested at 80–90% confluency with TrypLE™ Express (Invitrogen, Carlsbad, CA, USA). Cells were transferred to 96-well plates at a density of 10,000 cells/well and cytotoxicity studies were initiated following manufacturing protocol. NMF solution (blank and TA loaded) were prepared and re-suspended in serum free media and filtered with 0.2 µm nylon membrane to obtain sterile formulations.

Premix WST-1 cell proliferation assay: Experiments were performed following a published method [197]. To each well 100µL of NMF was added and incubated for 1h at physiological conditions. Serum free media and Triton X-100 (10%) served as negative and positive controls, respectively. Following incubation, 10 µL of premixed WST-1 was added to each well, incubated for 30 mins and absorbance was measured for the formazan product at 440 nm. An increase in absorbance of formazan denotes the % viable cells.

LDH assay: To evaluate cell membrane damage caused by NMF in each well, 100µL of serum free media and 100µL NMFs were added and incubated for 1 h at 37 ˚C. Serum free media and Triton X-100 10% served as negative and positive samples. After incubation period, 96 wells plate was centrifuged at 250X G for 10 mins and 100 µL of

supernatant was collected into 96-well flat bottom plate. LDH released from damaged cells was measured with LDH assay kit and absorbance of samples was measured at 490 nm. The % membrane damage was calculated with equation 5-5 (Eq. 5-5).

$$\% \text{ Cytotoxicity} = \frac{exp.value - cell\ culture\ medium\ value}{Triton\ X\_100 - cell\ culture\ medium\ value} * 100 \quad \text{(Eq. 5-5)}$$

5.3.16 In Vitro Drug Release Study

TA release kinetics from NMF was studied following previously described protocol[225]. Briefly, TA NMF and TA ethanoic solution (control) were transferred to dialysis bag with a molecular weight cut-off of 1,000 Da. The bags were immediately transferred to 15ml centrifuge tubes, previously thermostated at 37 ˚C, containing 5 mL Dulbecco's Phosphate-Buffered Saline (DPBS) (pH = 7.4) buffer solution, tween-80 (0.5% w/v). All samples were placed in shaking water bath at 37 ˚C and 60 rpm. At predetermined time points, drug release medium (5 mL) was collected and replaced with equal volume of fresh buffer to maintain sink conditions. Collected DPBS was immediately stored at – 80 ˚C until further analysis. Before analysis, samples were thawed, vortexed and extracted for TA (reverse micellization). Extracted samples were injected into RP-HPLC to determine TA concentrations. Release study was performed in triplicates. The results were plotted as mean ± SD. The release data was fitted for zero order, first order, Higuchi and Korsmeyer-Peppas model to determine the kinetics of TA release.

5.4 Results & Discussion:

5.4.1 Exploratory Model (design of experiments (DOE))

In this study, a full-factorial DOE with one center point and one replicate was selected to screen the independent factors for dependent variables. All formulations were characterized for EE, LE, CMC, size, PDI, surface potential, light transmittance and

cytotoxicity. The design runs (coded and uncoded) and corresponding variables are summarized in Table 5-1.

The nanomicellar size, PDI, surface potential and light transmittance did not show significant difference among formulations. The size and distribution of all NMFs were determined by the DLS method and presented in Table 5-2 ranged from 20- 26 nm. The PDI for all run were below 0.45 indication narrow size distribution. All light transmittance were above 90% indicating that the formulations allow the light pass through as close as water. The percent of cell viability of all NMFs were compared with medium and Triton X-100 10% which served as positive and negative controls, respectively (Fig 5-2). Because DOE used one replicate, the cytotoxicity only performed from F1 to F5 for both blank NMF and TA loaded NMF. More than ~ 80% cell viability was observed as compared to the control, where Triton X-100 generated less than 20% viability. However, a significant difference in EE, LE, and CMC were observed. Therefore, dependent variables such as EE, LE, and CMC were selected to identify the most essential influencing factor for each dependent variable. The standard least square fit analysis in JMP® 13.0 software was conducted and data analyzed to identify the most important variables. The parameters and pareto plot of estimates showed the significant effect with probability for each dependent factor on each outcome. Pareto plots were applied to identify the factors with significant effect on the outcome. The estimated coefficient with $p < 0.05$ were considered to be significant. Results shown in Fig. 5-3a indicate that different weight percent of HCO-60 and Oc-40 polymers had significant effect ($p < 0.05$) on EE. The pareto chart shows the significant of HCO-60 ($p < 0.0001$), OC-40 ($p = 0.0003$) and interaction HCO-60*OC-40 ($p = 0.0011$) cumulative percentage effect of the polymer weight percentage (Fig 5-3b).

The parameter estimates indicate that HCO-60 percentage offer significant contribution on entrapment efficiency relative to Oc-40. The fit model represents the relationship between independent and dependent variables, which are shown in the following equations (Eq. 5-6):

$$Y1= 33.7 + 14.625\ X1 + 4.625\ X2 + 3.625\ X1X2\ R^2 =0.99,\ p < 0.0001, \text{(Eq. 5-6)}$$

X1 (HCO-60) and X2 (Oc-40).

The correlation coefficient (R^2) for the regression model was 0.99 and *p* value less than 0.05 suggest that the model was significant and could predict EE. The model was also validated by plotting the response surface of predictive model for EE as a function of HCO-60 and OC-40 (Fig 5-3c).

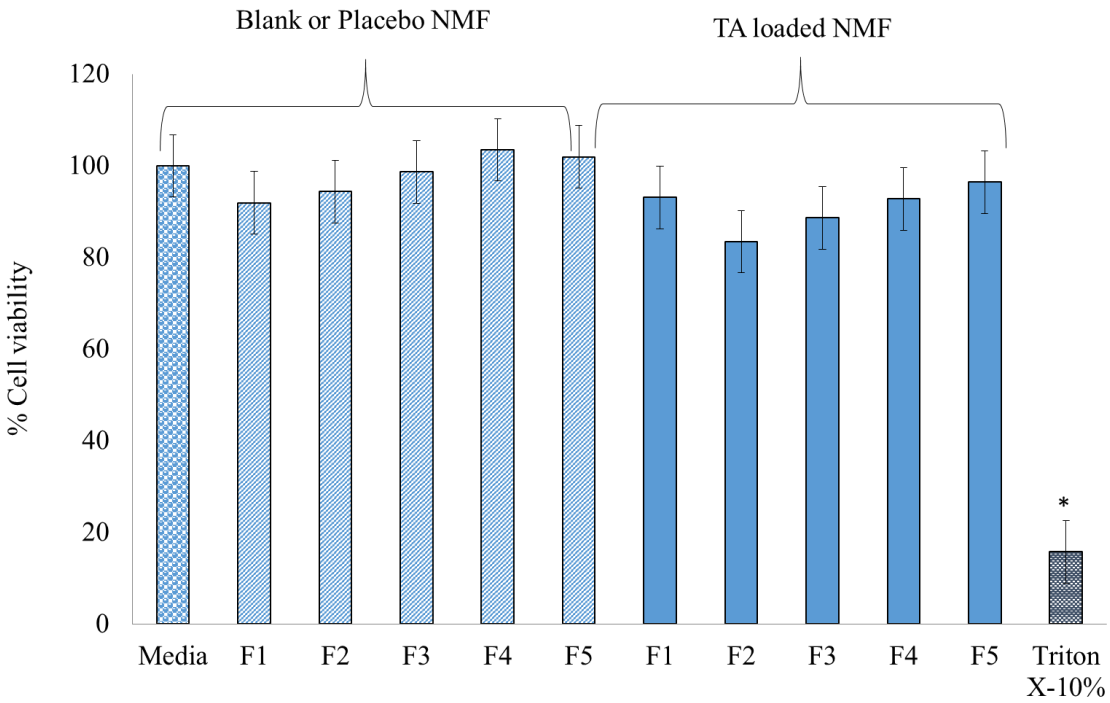

Figure 5-2: Cytotoxicity Studies Conducted on HCEC Cells. Cells Treated with Blank and Loaded TA NMFs Solutions for 1h

a **Parameter Estimates**

Term	Estimate	Std Error	t Ratio	Prob>|t|
Intercept	33.7	0.558644	60.32	<.0001*
HCO-60(2,5)	14.625	0.624583	23.42	<.0001*
OC-40(1,3)	4.625	0.624583	7.40	0.0003*
HCO-60*OC-40	3.625	0.624583	5.80	0.0011*

b **Sorted Parameter Estimates**

Term	Estimate	Std Error	t Ratio	Prob>|t|
HCO-60(2,5)	14.625	0.624583	23.42	<.0001*
OC-40(1,3)	4.625	0.624583	7.40	0.0003*
HCO-60*OC-40	3.625	0.624583	5.80	0.0011*

c

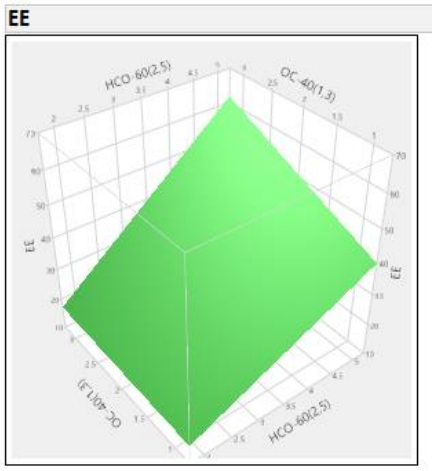

Figure 5-3: Summary of Variable Effects on Entrapment Efficiency (EE)

a

Parameter Estimates

Term	Estimate	Std Error	t Ratio	Prob>|t|
Intercept	0.5922	0.01318	44.93	<.0001*
HCO-60(2,5)	0.09625	0.014735	6.53	0.0006*
OC-40(1,3)	-0.03875	0.014735	-2.63	0.0391*
HCO-60*OC-40	0.05925	0.014735	4.02	0.0070*

b.

Sorted Parameter Estimates

Term	Estimate	Std Error	t Ratio	Prob>|t|
HCO-60(2,5)	0.09625	0.014735	6.53	0.0006*
HCO-60*OC-40	0.05925	0.014735	4.02	0.0070*
OC-40(1,3)	-0.03875	0.014735	-2.63	0.0391*

c.

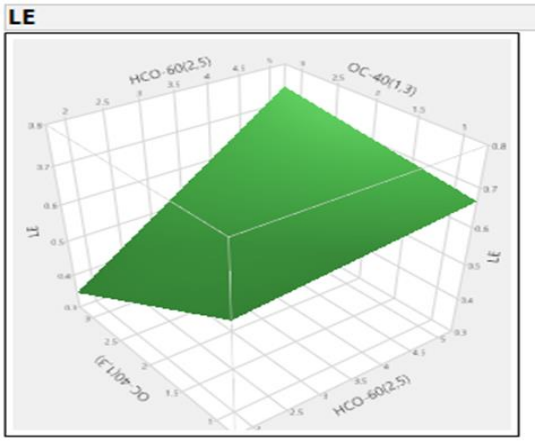

Figure 5-4: Summary of Variable Effects on Loading Efficiency (LE)

a.

Parameter Estimates

Term	Estimate	Std Error	t Ratio	Prob>|t|
Intercept	0.02426	0.002907	8.35	0.0002*
HCO-60(2,5)	0.00125	0.00325	0.38	0.7138
OC-40(1,3)	0.0091	0.00325	2.80	0.0312*
HCO-60*OC-40	0.00695	0.00325	2.14	0.0763

b

Sorted Parameter Estimates

Term	Estimate	Std Error	t Ratio	Prob>|t|
OC-40(1,3)	0.0091	0.00325	2.80	0.0312*
HCO-60*OC-40	0.00695	0.00325	2.14	0.0763
HCO-60(2,5)	0.00125	0.00325	0.38	0.7138

c

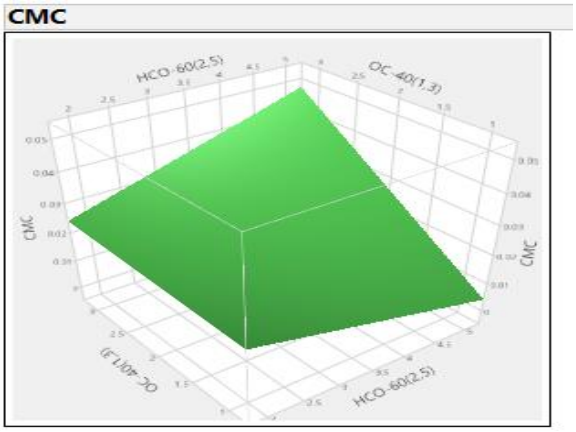

Figure 5-5: Summary of Variable Effects on Critical Micellar Concentration (CMC)

Similarly, Fig.5-4a shows that both HCO-60 and Oc-40 generated significant effect on loading efficiency with probability of 0.0006 and 0.0391, respectively. The regression equation is represented by Eq. 5-7.

$Y2 = 0.5922 + 0.09625\ X1 - 0.03875\ X2 + 0.05925\ X1X2$ (Eq. 5-7) $R^2 = 0.92$, $p = 0.0012$

The correlation coefficient (R^2) for the regression model was 0.92 and *p* value less than 0.05 suggest that the model was significant and could predict LE. The model was also validated by plotting the response surface of predictive model for LE as a function of HCO-60 and OC-40 (Fig 5-4b).

On the other hand, there is no significant effect of HCO-60 polymer was observed on CMC (Fig. 5-5) while OC-40 had lightly effect on CMC with *p* value 0.0312. The regression equation is presented by Eq.5-8.

$Y3 = 0.02426 + 0.00125\ X1 + 0.0091\ X2 + 0.00695\ X1X2$ (Eq. 5-8) $R^2 = 0.68$, $p = 0.0642$

The correlation coefficient (R^2) for the regression model was 0.68 and *p* value greater than 0.05 suggests and that the model was not significant.

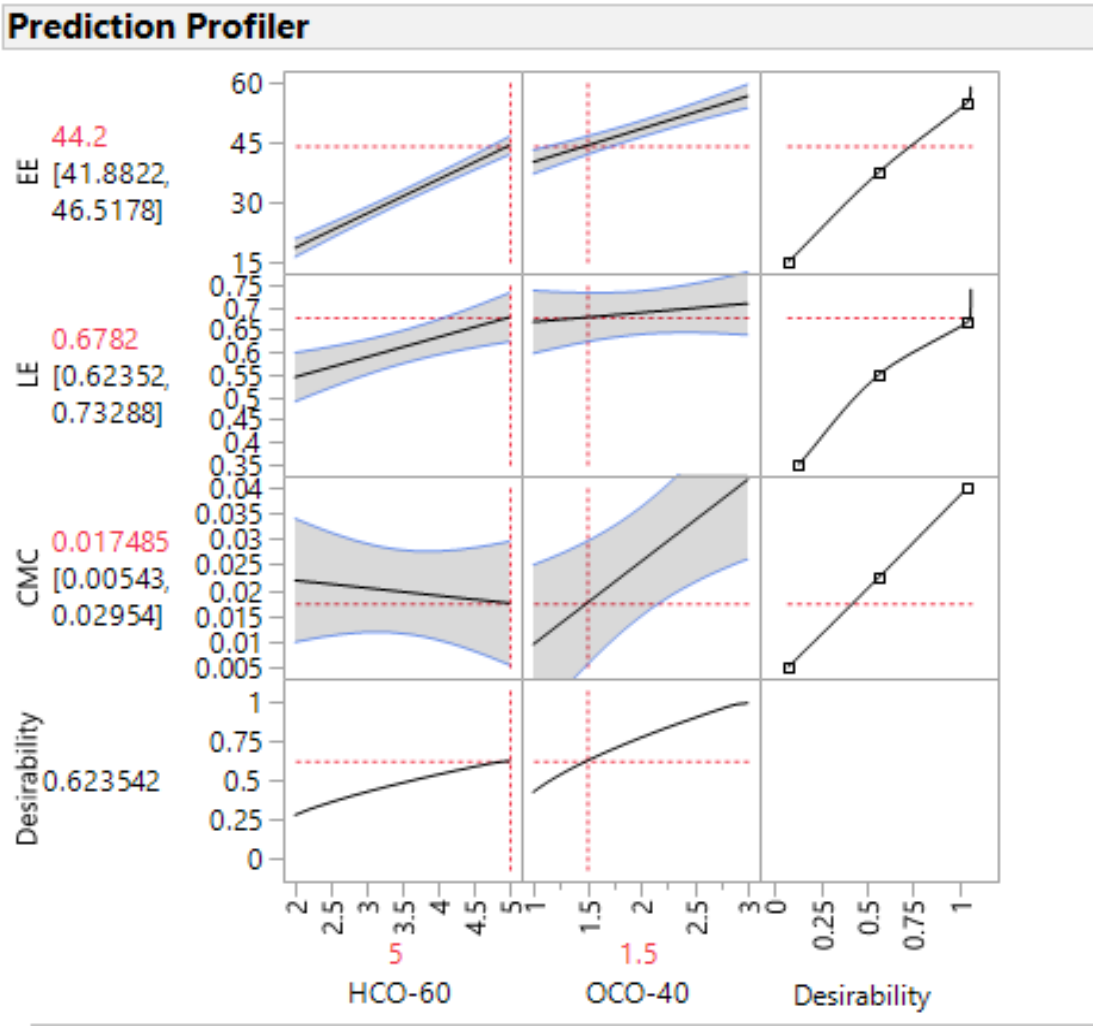

Figure 5-6: Prediction Profiler for Optimized TA NMF

The prediction profiler was generated to determine the optimal point with highest desirability. It also predicts the combination effects of variables at different levels. Prediction profiler helps to predict the levels of independent variables which may be adjusted to achieve high EE, LE and low CMC. TA loaded NMF with such characteristics was assumed to be the better formulation. Prediction profiler indicated that the optimized formula (HCO-60 at 5.0 wt% and OC-40 at 1.5 wt%) may provide optimal EE, LE and low CMC of 44.0%, 0.676% and 0.0216, respectively (Fig. 5-6). This optimized formulation produces the most reasonable desirability between independent and dependent variables.

TA loaded NMF was prepared with HCO-60 and Oc-40 with weight percent predicted by the profiler. EE, LE and CMC were determined following described earlier procedure and results were summarized in Table 5-3. EE, LE and CMC for the new NMF were 46%, 0.70% and 0.0210, respectively. Experimental results appear to be in agreement with the prediction profiler. The DOE was successfully applied to understand the interaction between the polymers and/or drugs and thus achieve the optimal formulation with high desirability. Further, the optimized NMF was subjected to characterization such as size, PDI, surface potential, light transmittance, viscosity, morphology, ^{1}H NMR, dilution effects, cytotoxicity, and *in vitro* release.

5.4.2 Entrapment Efficiency and Loading Efficiency

TA entrapment and loading into NMFs was determined with RP-HPLC method as described previously. NMFs EE, LE are summarized in Table 5-2 and 5-3. TA is a highly lipophilic drug with poor aqueous solubility 25.4 µg/mL (US patent US 2006/0141049), and octanol/water partition coefficient is 2.53. Because of the hydrophobic interaction, hydrophobic drug get encapsulated inside hydrophobic core of nanomicelle. Results indicate that entrapment of TA in the core of nanomicelles improved TA solubility by 20 times. Nanomicelle has improved the solubility of TA with increased EE.

Table 5-2: Summary of Uncoded Design and Corresponding EE, LE, CMC, Size, PDI, Zeta Potential and % Light Transmittance

Formulation code	HCO-60 (wt%)	OCO-40 (wt%)	EE (%)	LE (%)	CMC	Size (nm)	PDI	Zeta potential (mV)	T (%)
F1	5	3	55	0.682	0.0380	24.05	0.394	-0.78	98.51
F2	5	1	39	0.645	0.0059	25.04	0.378	-0.469	94.76
F3	3.5	2	35	0.632	0.0385	22.02	0.393	-0.254	93.76
F4	2	3	19	0.379	0.0216	23.08	0.392	+0.418	95.77
F5	2	1	17	0.563	0.0173	25.37	0.404	-0.084	93.05
F6	5	3	57	0.707	0.0380	23.94	0.397	-0.81	98.56
F7	5	1	40	0.662	0.0059	25.13	0.379	-0.458	95
F8	3.5	2	37	0.668	0.0385	22.04	0.393	-0.261	93.76
F9	2	3	20	0.398	0.0216	23.21	0.4	+0.418	95.89
F10	2	1	18	0.596	0.0173	25.07	0.43	-0.089	93.25

HCO-60 = Hydrogenated castor oil-60; Oc-40=octoxynol-40; EE=Entrapment Efficiency; LE=Loading Efficiency;

CMC=Critical Micellar Concentration; nm=nanometer; PDI=Polydispersity Index; mV=milli Volts;

NMF=Nanomicellar Formulation; T=Transmittance

Table 5-3: Characterization of Optimized TA NMF

Formulation code	HCO-60 (wt%)	OC-40 (wt%)	Size (nm)	PDI	Zeta potential (mV)	T (%)	EE (%)	LE (%)	CMC	Viscosity (cP)	Osmolality (mmol/kg)	pH
Blank optimized NMF	5	1.5	17.01±0.03	0.198	-0.745	96.69	-	-	0.0210	1.89 ± 0.01	300 ± 6	6.81
0.1% TA optimized NMF	5	1.5	16.64± 0.02	0.200	-0.447	95.58	46 ± 1	0.70± 0.05	-	1.95 ± 0.01	317 ± 5	6.85

5.4.3 Micellar Size, Polydispersity Index (PDI), Zeta Potential

Nanomicellar size, polydispersity index (PDI), Zeta potential were determined by dynamic light scattering (DLS). The results are summarized in Tables 5-2 and 5-3. Both blank and TA-loaded NMF were in the size range between 20-30 nm with narrow distribution. Fig. 5-7a and 5-7b illustrated the distribution of blank and TA- loaded NMF. The significantly small size of NMF may sufficiently allow NMF to travel across ocular tissues such as scleral channels/pores, are in the size range between 20 and 80 nm[311]. The PDI of all runs bellow 0.4 zeta potential is negligible. Such property of nanomicelles may help to deliver TA to back of the eyes by the conjunctival/ sclera pathway.

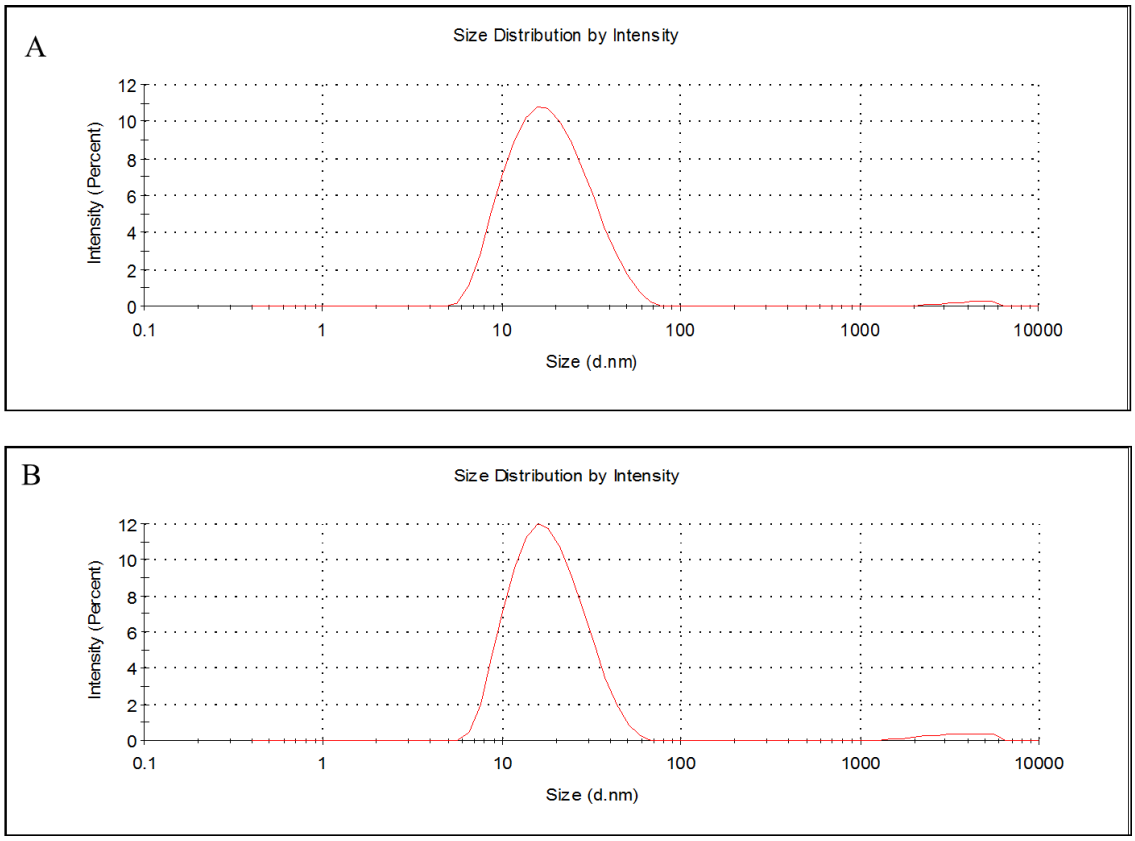

Figure 5-7: Size Distribution of NMF Formulations (A) Blank NMF (B) Optimized TA Loaded NMF

5.4.4 Morphology TEM

The morphology of optimal nanomicelle was studied by TEM. Results show that NMFs are spherical in shape with smooth surface architecture without any signs of aggregation (Fig. 5-8A). Nanomicelles are clearly defined and distinguished as bright, discrete spherical globules on the TEM grid. TA loaded NMF displays a size of about 20 nm which is in agreement with the size measurement with DLS.

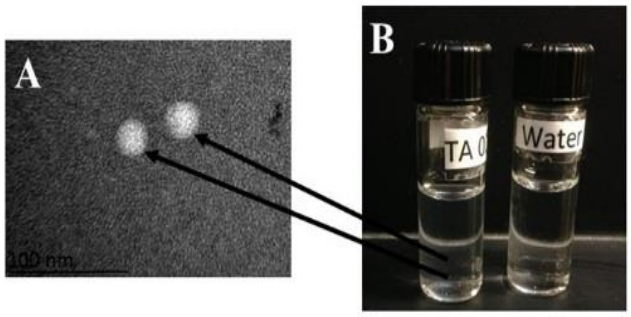

Figure 5-8: (A) Real-Time Scanning Transmission Electron Microscope (STEM) Image of Triamcinolone Acetonide-Loaded Nanomicelles (X147,000). Scale Bar 100 nm. (B) Image Showing Visual Appearance of 0.1% Triamcinolone Acetonide Loaded Nanomicelles on the Left Side in Comparison to Water on the Right Side

5.4.5 Optical Clarity/Appearance

Optical appearance / clarity is defined as the ability of light to be transmitted 90% or more through a 1.0-cm path length at 400nm wavelength. The major reason for light

scattering is due to interference produced by particles. However, particles of extremely small size i.e. nanometers will not produce enough hindrance or light scattering results in a clear and transparent solution. TA NMF is clear as water (Fig. 5-8B) or transparent and more than 90% of light has been transmitted (Table 5-2 and 5-3) compared with TA suspension. All NMFs can be compared with distilled deionized water measured by transmittance. Percentage light transmittance of optimized formulations (blank and TA loaded NMF) at different wavelength range from 400nm to 600 nm ranged from 91 % to 96 % (Fig. 5-9). It was observed that there is no particle interfering with light scattering. The nanomicelles help to develop a clear solution with no solid particles.

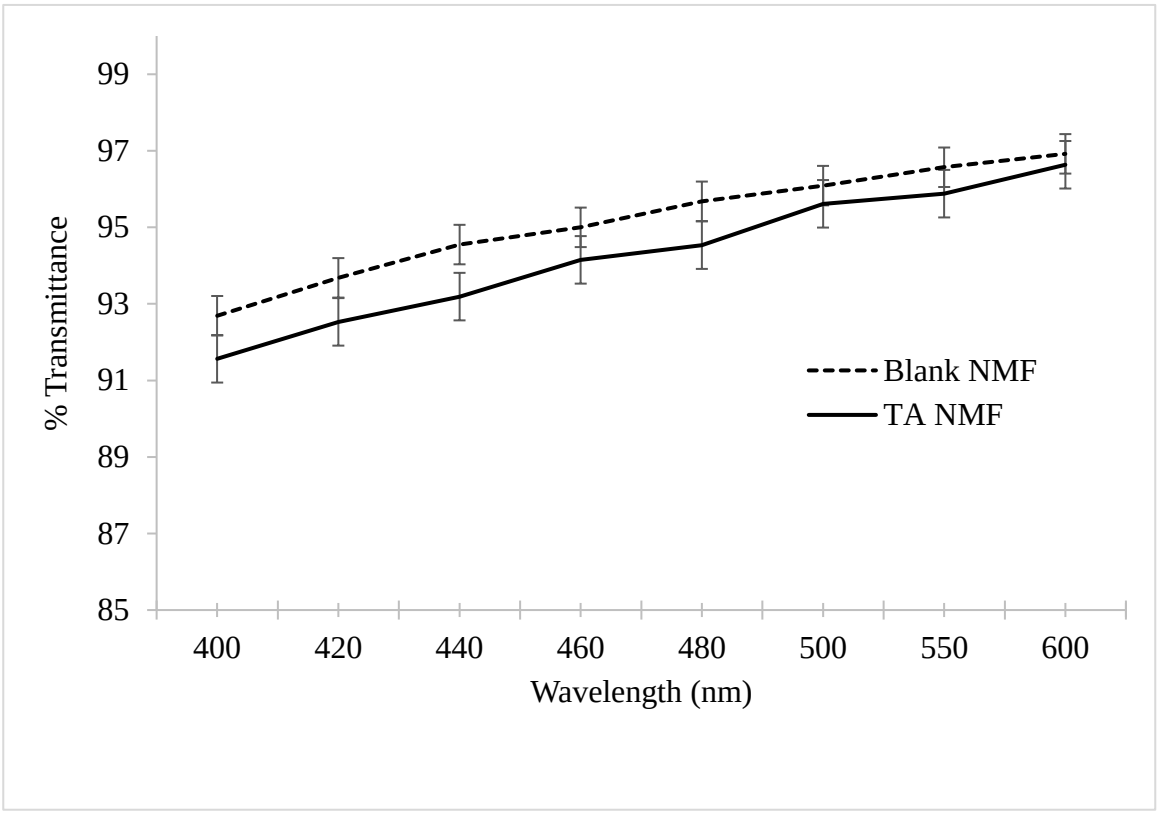

Figure 5-99: Light Transmittance of Formulations (Blank, TA NMF)

5.4.6 Critical Micellar Concentration (CMC)

Ocular static and dynamic barriers are the most challenging barriers for delivery of drugs to back-of-the-eye at therapeutic levels [312]. CMC is the most critical factor which regulates drug release in tear film. Only 20% of applied topical drop may be available for absorption [312]. Continuous tear production may dilute the NMF which may cause micelle disruption and premature TA release. In order to prevent such disruption, low CMC for nanomicelles are prepared since it imparts high stability to NMF after topical administration. In this study, CMC for blend of HCO-60 and OC-40 was determined and results are summarized in Tables 5-2 and 5-3. The optimized formulations display low CMC and are not in agreement with the prediction profiler. Since the correlation coefficient (R^2) for the regression model was 0.68 and *p* value greater than 0.05 suggest that the model was not significant and not good model in predicting CMC.

5.4.7 Viscosity

High viscosity of formulation can have effect on its residence time in the cul-de-sac enhancing therapeutic effect. The results summarized in Table 5-3 show that NMF produce viscosity less than 2.0 centipoise (cP), well below critical point of 4.4 cP, such that the drainage rate is not affected [313]. Formulation viscosity may offer advantages due to longer residence in the cul-de-sac which may increase ocular absorption.

5.4.8 Dilution Effect

Human eyes have many different mechanism and barriers to protect and prevent any harm from external particles from body. Major ocular barriers are static (corneal epithelium, corneal stroma, and blood–aqueous barrier) and dynamic barriers (blood-retinal barrier, conjunctival blood flow, lymph flow, and tear drainage). Tear drainage is

one of those barriers that clear out much of topical application. Therefore, the stability of the NMF was studied upon the effect of dilution. The results shown in Table 5-4 demonstrated that there is no significant effect on nanomicelle size and PDI with dilution up to 200 times.

Table 5- 4: Effect of Dilution on Nanomicellar Size and PDI of Optimized TA Loaded NMF.

Dilution factor	Average size (nm)	PDI
0	16.64	0.200
10	17.02	0.193
20	18.1	0.228
40	17.09	0.233
50	16.86	0.222
100	16.01	0.323
200	18.04	0.360

5.4.9 Osmolality and pH

Osmolality is an important attribute for the topical eye drop formulation. The hyper-osmolality is a main pathogenic factor in dry eye [314]. The osmolality and pH of the NMF was adjusted similar to the tear pH ~ 6.8 with phosphate buffer as depicted in Table 5-3. Osmolality of TA NMF was 317 mmol/kg or mOsm/kg and pH was around 6.8.

5.4.10 ^{1}H NMR Characterization

The free drug molecules in solution was identified by ^{1}H NMR analysis at parts per million (ppm) levels. In order to confirm TA entrapment into the mixed nanomicelles core qualitative ^{1}H NMR spectral analysis was performed in $CDCl_3$ and D_2O. Blank and TA-loaded NMFs were prepared in different solvent such as $CDCl_3$ and D_2O.

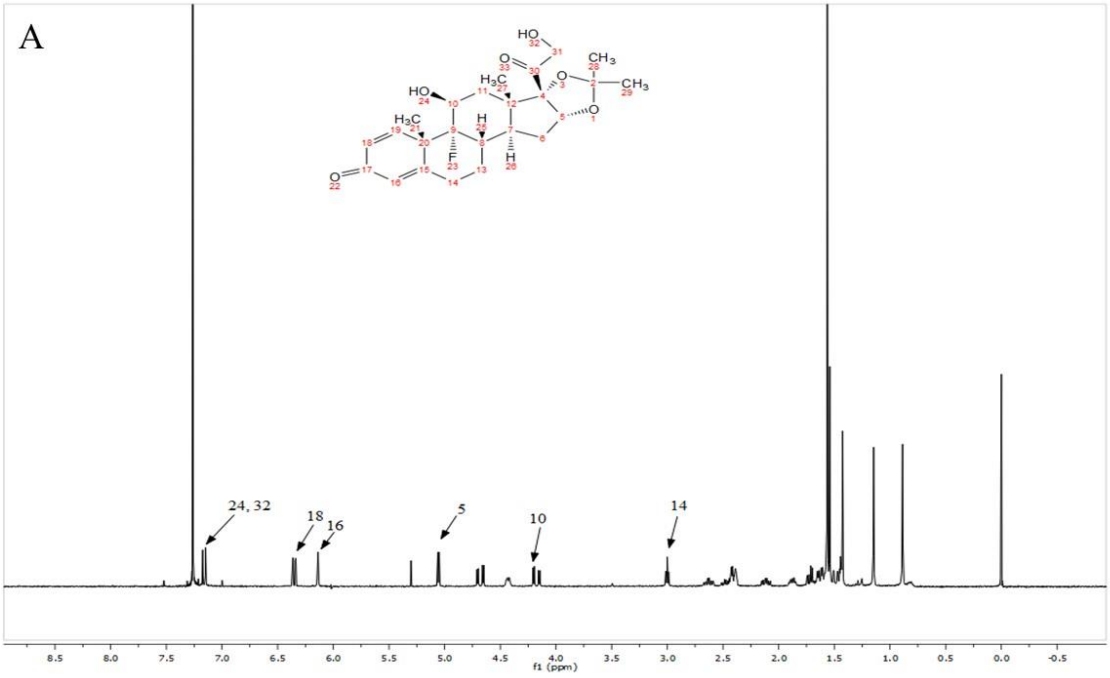

Figure 5-10: Qualitative ^{1}H NMR Studies (A) ^{1}H NMR Spectrum for TA Pure Drug in $CDCl_3$; (B) ^{1}H NMR Spectrum For Placebo Polymer Micelles in $CDCl_3$; (C) ^{1}H NMR Spectrum for TA Nanomicelles in D_2O; (D) ^{1}H NMR Spectrum For TA Micelles in $CDCl_3$.

B.

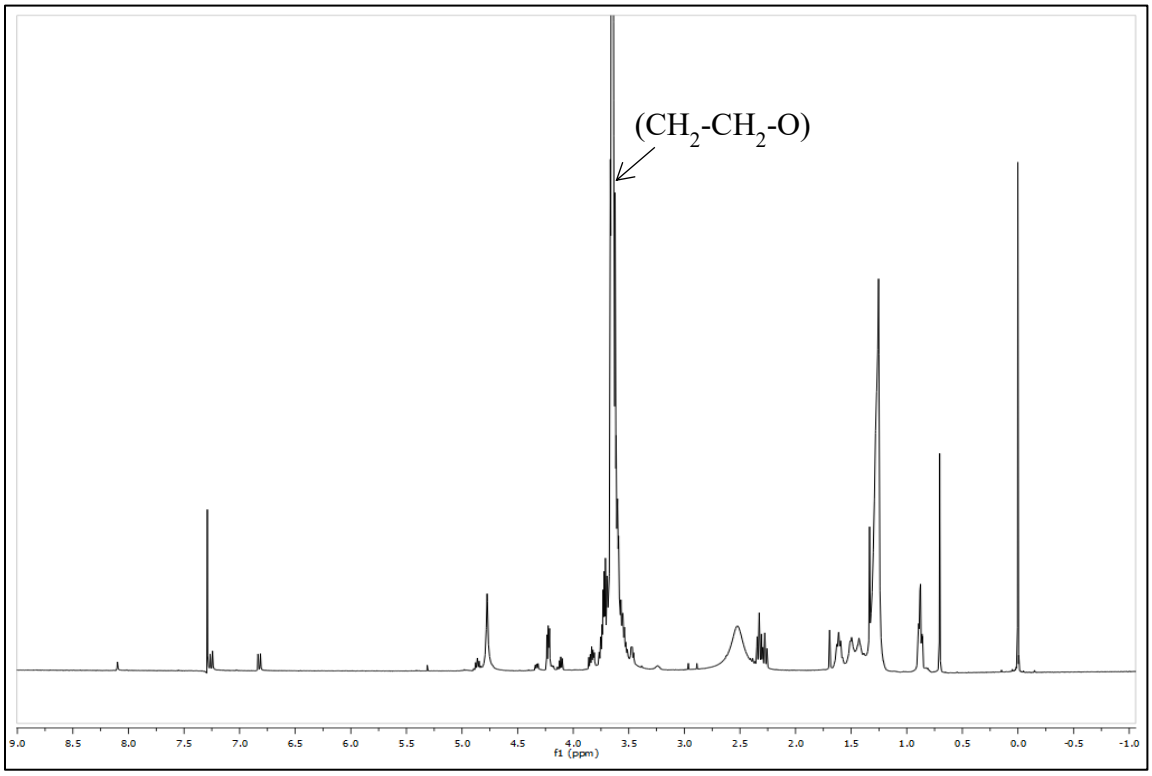
(CH2-CH2-O)
9.0 8.5 8.0 7.5 7.0 6.5 6.0 5.5 5.0 4.5 4.0 3.5 3.0 2.5 2.0 1.5 1.0 0.5 0.0 -0.5 -1.0
f1 (ppm)

C.

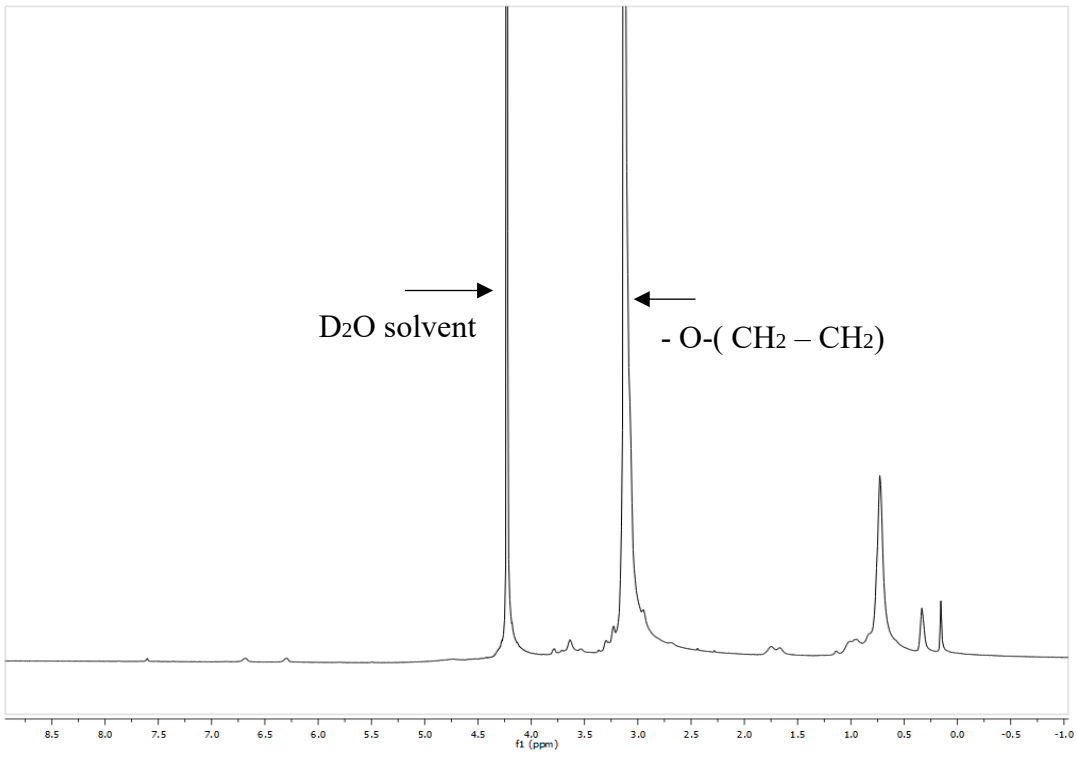
D2O solvent
- O-(CH2 – CH2)
8.5 8.0 7.5 7.0 6.5 6.0 5.5 5.0 4.5 4.0 3.5 3.0 2.5 2.0 1.5 1.0 0.5 0.0 -0.5 -1.0
f1 (ppm)

D

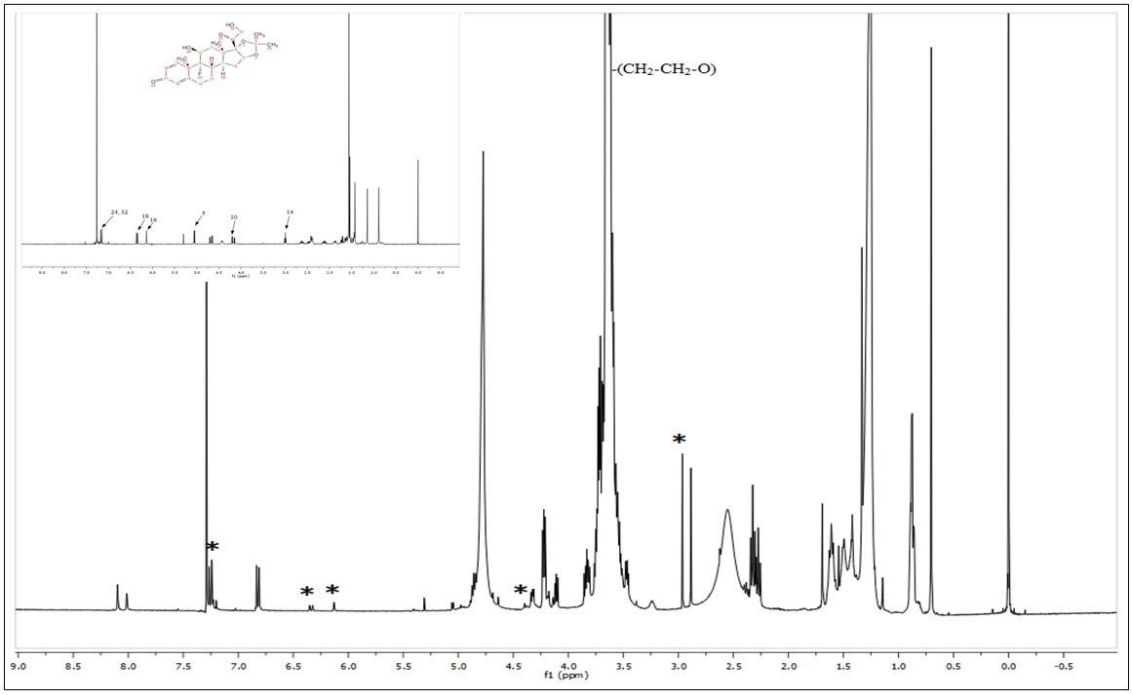

In Fig. 5-10A the resonance peaks were identified with pure triamcinolone acetonide standard in $CDCl_3$. For the blank formulation (Fig. 5-10B) in chloroform $CDCl_3$, there was no observable peak corresponding to triamcinolone acetonide except polymer peak. However, with the TA loaded formulation in $CDCl_3$ (Fig. 5-10D) the resonance peaks similar to pure TA are evident. The spectra indicated that drug is present in organic solvent $CDCl_3$ where reverse micelles are formed, and the drug is in the solvent. However, resonance signals for TA were absent when suspended in D_2O (Fig. 5-10C). The results indicate that TA is inside nanomicellar vesicles in aqueous solution. All triamcinolone acetonide in solution was entrapped inside nanomicelles and there was no free/unentrapped TA in the D_2O. Since amphiphilic polymers have encapsulated TA inside the core which muted the NMR signal during micelle formulation. This explains the absence of TA signal in D_2O.

5.4.11 Powder XRD Analysis of Blank NMF and TA NMF

TA, polymer HCO-60, OC-40, blank NMF and TA NMF were studied by XRD to find the further information about physical state of polymer and when inside micelles. Fig. 5-11 presented the results. XRD pattern showed the characteristic peaks of the HCO-60 widely at two-theta 20 degree and 32 degree while OC-40 showed at same 19 and 23 degree but higher intensity with smaller peak width. Peak width due to crystallite size, the peak gets broader as the crystallite size gets smaller. TA raw powder had characteristic peak at near 10, 14, and 18 degree. The characteristic peaks of HCO-60 and TA were disappeared for freeze-dried blank NMF and TA NMF. Because the polymers have interacted with each other and self-assemble in water to form nanomicelle, there were no more characteristic peaks for individual. Both blank nanomicelle and TA nanomicelle gave the same peaks at 19, 23, and 27 degree indicating the drug TA was molecularly dispersed in naomicelle. As the X-rays interact with crystalline lattice, a diffraction pattern is formed which reveals spacing between planes of atoms. The nanomicelles thermo-dynamically arrange atoms close together and forming very stable bond. The spacing between planes of atoms are smaller where there were no peaks observed with high intensity or broadening width. Such rigid structure may resist sheer stress while transport across the scleral pores which allows transport through the membrane.

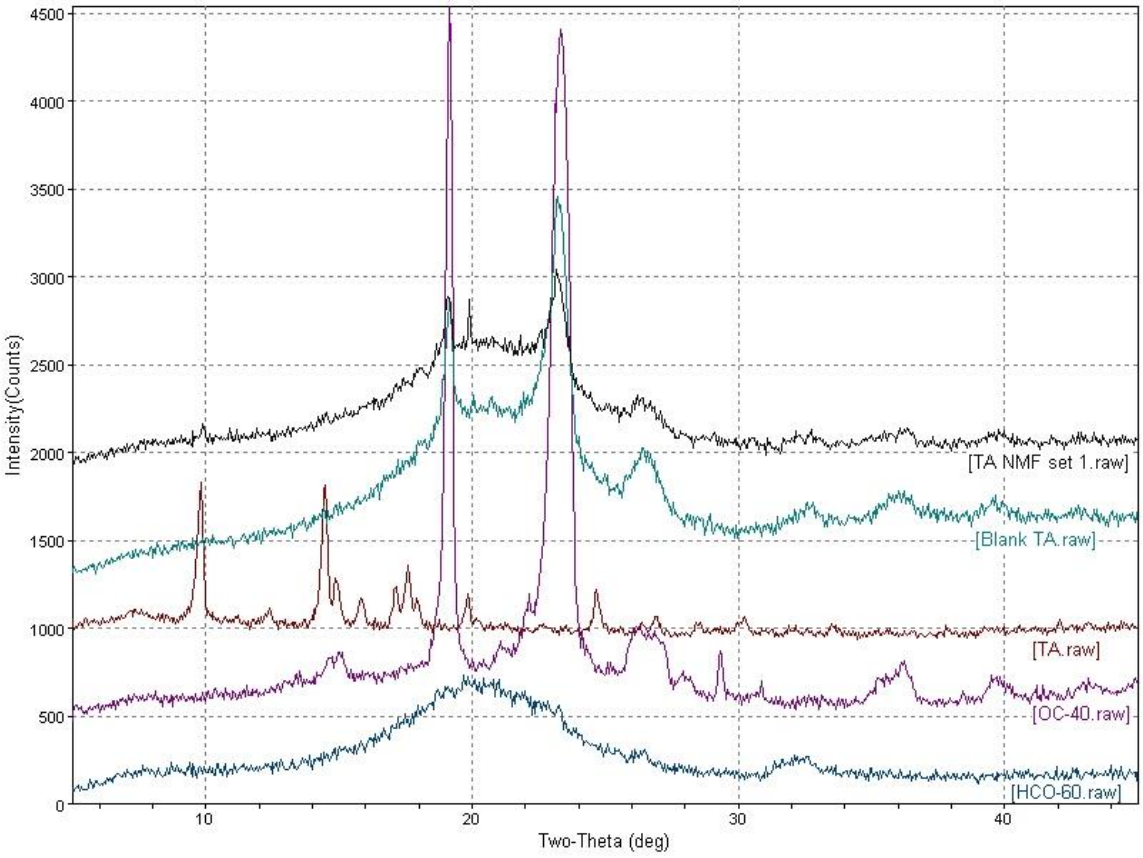

Figure 5-11: XRD Pattern of TA Raw, TA NMF and Polymers HCO-60, OC-40

5.4.12 In Vitro Cytotoxicity

The formulations/solutions are rapidly washed (within 5 to 10 min) after topical ophthalmic drop instillation into pre-corneal pocket [312]. Previous results from our laboratory showed drug molecules in nanomicelles reaching back of the eye tissues (retina/choroid) [315]. Therefore, cytotoxicity studies were conducted on human corneal epithelial cells (HCEC cells) and human retinal pigment epithelial cells (D407 cells) for 1 h incubation period. In order to evaluate the cytotoxicity of NMF, WST assay was performed on HCEC. The % cell viability of all NMFs were compared with medium and

Triton X-100 10% which served as positive and negative controls, respectively (Fig 2). Because DOE used one replicate, the cytotoxicity only performed from F1 to F5 for both blank NMF and TA loaded NMF. More than ~ 80% cell viability was observed as compared to the control, where Triton X-100 generated less than 20% viability.

In another study, only optimized formulation was evaluated for cytotoxicity with both WST and LDH (Fig. 5-12, 5-13). The amount of LDH released in the culture medium directly correlates with membrane damage and cytotoxicity. Triton-X 100 caused significant toxicity/ membrane damage and serves as positive control. LDH study NMF was found to be safe without any cytotoxic effects the results are compared with the blank culture medium. Results from these assays clearly suggest that NMF do not cause cell death or damage to plasma membrane, are safe and well-tolerated for further *in-vivo* studies with topical drop application to eye. Therefore, these formulations are safe, maybe potentially aqueous base formulation suitable to topical ocular application without much irritation.

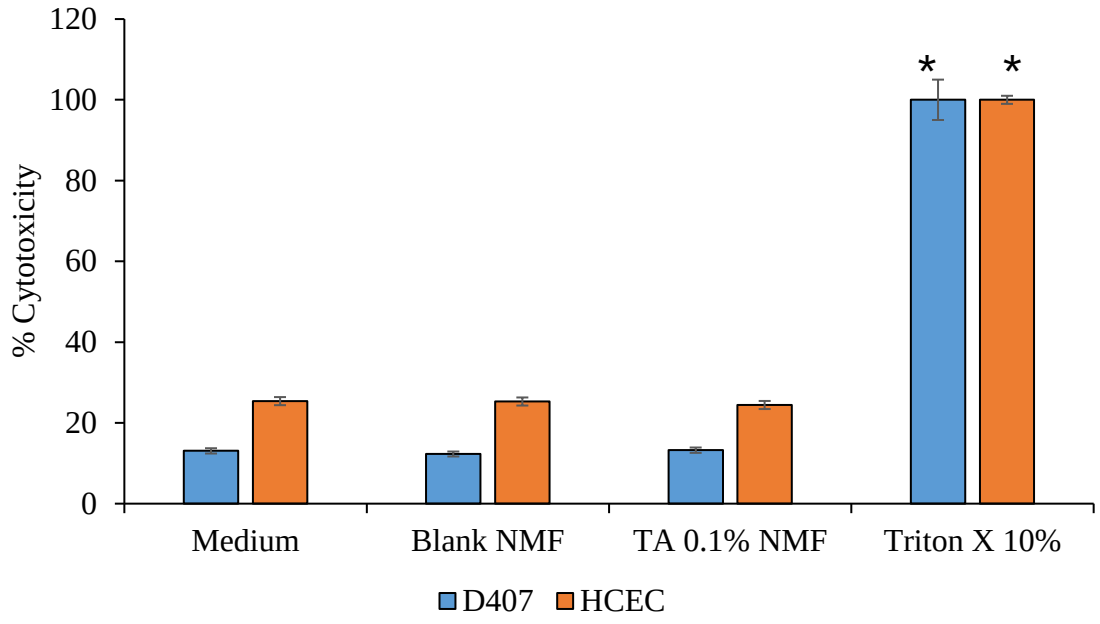

Figure 5-12: Cytotoxicity Studies (LDH Assay) Conducted on D407 and HCEC Cells. Cells Treated with NMF for 1h

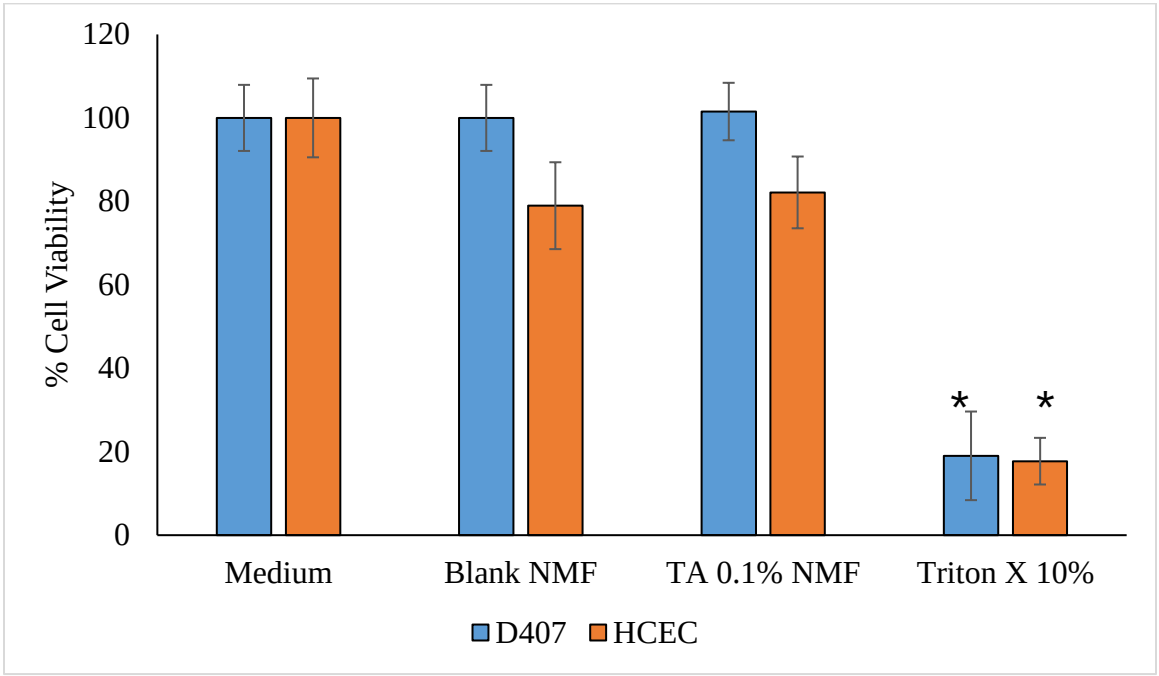

Figure 5-13: Cytotoxicity Studies (WST Assay) Conducted on D407 and HCEC Cells. Cells Treated with NMF for 1h

5.4.13 In Vitro Drug Release Study

To determine the release kinetic of TA from HCO-60 and OC-40 in optimized NMF (F6) was investigated under sink condition at a physiological pH of 7.4 at 37°C. The control represented an equal quantity of TA (1 mg) in 1 ml of absolute ethanol. TA release from NMF was slower than TA release from ethanolic solution. The release kinetic profiles of ethanolic and encapsulated TA from the nanomicelles are illustrated in Fig. 5-14. Almost 100 % of TA was cumulative released in approximately 24 h from ethanolic TA solution. However, TA release from NMF was very slow (nearly one month) without any burst effect. Results suggest that, topical administration of TA NMF helps to sustain release of TA under physiological conditions. Consequently, this nanomicelle formulation may aid in reducing dosing frequency but still achieving therapeutic TA concentrations in ocular tissues.

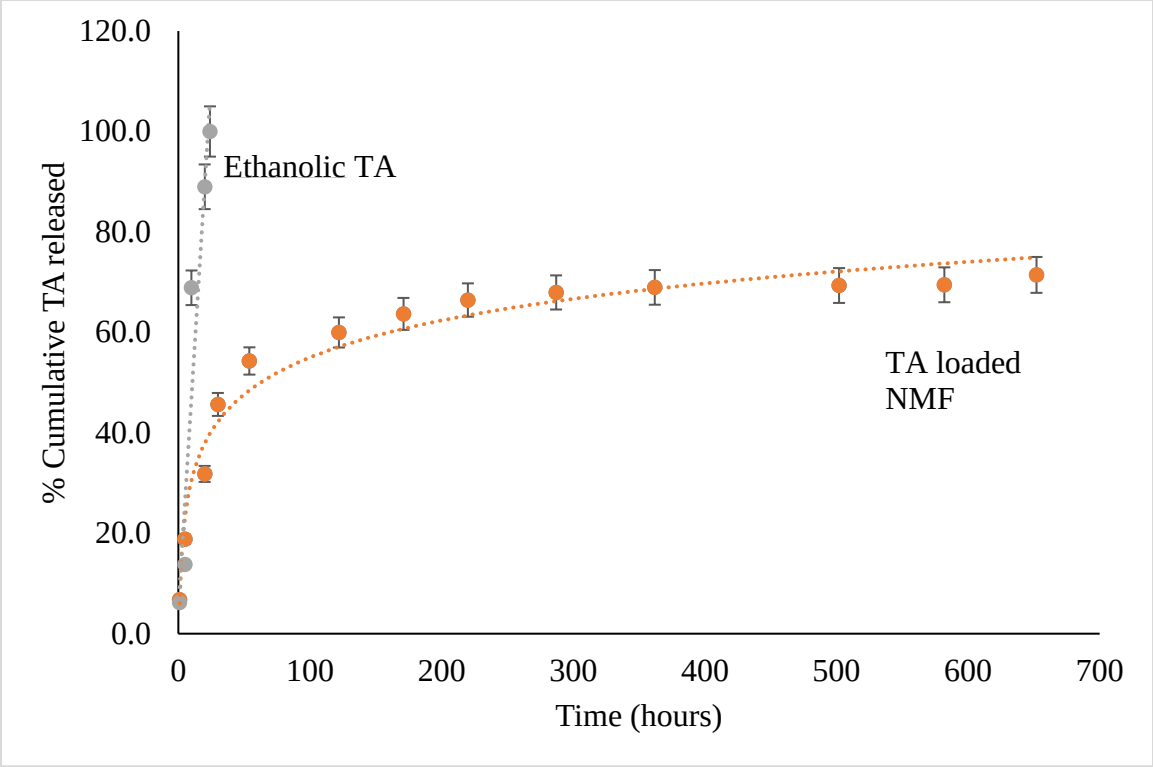

Figure 5-14: In Vitro Releases Profile of TA from Nanomicelles and Ethanolic TA Solution under Sink Conditions At 37 ˚C

5.5 Conclusion

In summary, a clear, stable, aqueous TA-loaded NMF have successfully been optimized and prepared with full-factorial statistical DOE. Results suggest that TA EE was dependent on the combination of polymer HCO-60 and OC-40. Predictive model was produced to determine the amount of independent factors to achieve the highest outcome. The specific blend of HCO-60 at 5.0 wt% and OC-40 at 1.5 wt% generated excellent EE, LE and low CMC. Optimal TA NMF was clear as water with no light scattering. Nanomicelles are spherical in shape and encapsulated TA in the core NMF display small size, narrow PDI, and are well-tolerated in human cell lines. The release profile showed controlled release under physiological conditions. The results indicate that TA NMF may

be suitable for human application as ocular drops for anterior and posterior ocular inflammations.

CHAPTER 6

6 PREPARATION AND OPTIMIZATION DEVELOPMENT OF FLUOCINOLONE ACETONIDE-LOADED NANOMICELLES

6.1 Rationale:

Diabetic macular edema (DME) is a retinal disease, the sight threatening condition caused by buildup of fluid in the center of macula [303, 316]. It is a painstaking back-of-the-eye chronic disease that causes changes in vision and leads to vision loss. DME patients are estimated to be around 21 million [317]. In type II diabetic patients, more than thirty percent suffer from diabetic retinopathy after five years, and up to 80% after 15 years [318, 319]. For type I diabetic patient, it was 17% after five years and 98% after 15 years [320, 321]. DME formation is known as significant cause for visual impairment for type II patient while diabetic retinopathy is observed in type I diabetes [322]. Due to the upregulation of angiogenic growth factors, neovascularization occurs as the result the microvascular becomes fragile and easily cause damage leading to leakage and breakdown of blood retinal barrier. [304, 323]. Sustained hyper-glycemia can lead to the destruction of the interior blood vessels walls, resulting in porosities and micro-vascular leakage. The resultant retinal vascular hemorrhage accumulates in the medial aspect of the retina resulting in swelling, which is pathognomonic for DME (11). Several treatment options of DME are available such as surgery, laser photocoagulation, intravitreal injection of anti-vascular endothelial growth factor (anti-VEGF), intravitreal injection of VEGF inhibitors (ranibizumab - Lucentis®, aflibercept – Eylea®, bevacizumab - Avastin®) and steroid implant (dexamethasone – Ozurdex®) [141, 303, 323, 324]. Corticosteroids have generally been indicated not only to reduce the effect of VEGF overexpression but also attenuate the inflammation by suspending VEGF-A, ICAM-1, IL-6 pathway, decreasing AQP4, reducing paracellular

permeability, and raising up the tight junction integrity[325]. Delivery of drugs at therapeutic levels to posterior eye tissues (retina/choroid) is a very difficult clinical task. Because of the static and dynamic barriers, topically delivered medicaments that travel to posterior segments of the eye are measured to be less than 5% of the original administered dose [5]. Since steroids possess many physicochemical chemical properties including low aqueous solubility, and poor ocular membrane permeability, intravitreal injection or implant are the treatment options. Complications associated with invasive administrations include increased intraocular pressure (IOP) resulting in glaucoma and cataracts [305, 326, 327].

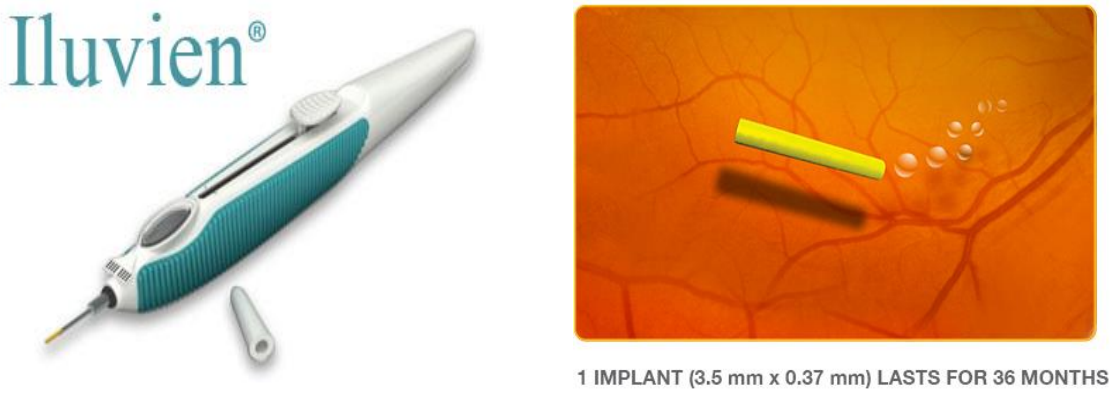

Figure 6- 1: Illuvien® Intravitreal Implant

Fluocinolone acetonide (FA) is a synthetic glucocorticoid, similar to triamcinolone acetonide and dexamethasone. FA have both anti-angiogenic and anti-inflammatory properties [17]. It is a hydrophobic compound with poor oral bioavailability. Currently most steroids including FA have been administered locally by intravitreal injections or implant. Those are highly invasive and costly procedures with low patient compliance. FA intravitreal implant (Iluvien® 0.19mg) is an injectable, non-bioerodible, corticosteroid

implant that is approved by FDA for DME (Fig. 6-1). It releases the drug at an initial rate 0.25 µg/day and last for 36 months. FA intravitreal implant has been improved significantly to deliver the best-corrected visual acuity (BCVA). In comparison with the control without the implant, FA intravitreal implants cause more cataract and IOP elevation [220, 307]. Common side effects include cataracts, acceleration of IOP, eye pain or irritation. Since topical administration is the most patient compliant route with fewer side effects, a topical eye drop of FA would be potentially a novel and self-delivery system. Consequently, aqueous nanomicellar formulation with amphiphilic polymers appear to be a promising approach. Therefore, hydrophobic-FA was encapsulated inside of nanomicelles. Hydrophilic groups on the surface of nanomicelles produced clear, aqueous solution. This novel nanomicellar delivery system may (i) enhance FA solubility (ii) expand cellular uptake and penetration, (iii) permit for non-invasive delivery of lipophilic drugs to back of the eye and (iv) improve patient compliance and economical since the formulation is non-invasive, self-dosing. After topical administration, NMF may travel around sclera and conjunctiva and spread to retina region. This route is known as conjunctival-scleral pathway [197].

In the current study, we selected amphiphilic polymers to optimize the formulation namely: hydrogenated castor oil (HCO) 40, 60, 80 and 100 and octoxynol-40 (OC-40). Amphiphilic nature of HCO and OC-40 contains both hydrophilic corona and hydrophobic core allowing spontaneous self-assembly and formation of circular nanomicelles in water solution. Due to hydrophobic effect, the hydrophobic part will come together and form hydrophobic core, which interacts hydrophobic drugs such as FA. Consequently, the hydrophobic FA can be encapsulated inside the hydrophobic core of nanomicelles and

hydrophilic part interacts with water surrounding environment and forms very stable nanomicellar structure. Based on the preliminary studies (Table 6-1), HCO-40 provided the most promising results. Therefore, further for formulation optimization was continued with HCO-40. FDA has approved both HCO-40 and OC-40 for human application. The aim of this work is to optimize and develop a clear aqueous NMF of FA utilizing central composite design (CCD) with mixture of two nonionic polymers OC-40 and HCO-40. JMP 13.0 software applied in this investigation supported the determination of the appropriate ratio of blending HCO-40 and OC-40. Two design of experiments (DOE) are selected to maximize the solubility of FA. DOE 1 no heat was involved. However, DOE 2 film was heated at 65 ºC before rehydration. The size, polydispersity index (PDI), osmolality, viscosity, light transparency and pH of the optimized formulations have been produced and characterized. Based on these experiments, the data was inserted into the software JMP. It generates standard least square fit analysis to identify the optimal NMF. Furthermore, *in vitro* cytotoxicity studies were performed on human corneal and retinal cell lines to confirm the safety of NMF.

Table 6-1: Preliminary Data for FA Nanomicellar Formulations

FA 0.05 % OC-40 0.5%	HCO-40 2%	HCO-60 2%	HCO-80 2%	HCO-100 2%
Clarity	++++	+++	++ (white particle)	+ (turbid)
Size (nm)	20.08	20.81	22.26	21.28
PDI	0.127	0.206	0.221	0.291
Zeta potential	0.508	1.76	2.16	1.48
Solubility (mg/ml)	0.603	0.417	0.076	0.027

6.2 Materials

FA was obtained from Sigma-Aldrich, USA. Hydrogenated castor oil 40 (HCO-40) was procured from Barnet Products Corp., NJ, USA. Octoxynol-40 (OC-40) (Igepal CA-897) was purchased from Rhodio Inc., NJ, USA. HPLC grade methanol, ethanol and dichloromethane were purchased from Fisher Scientific, USA. CellTiter 96® AQueous nonradioactive cell proliferation assay (MTT) kit and lactate dehydrogenase (LDH) assay kit were obtained from Promega Corp and Takara Bio Inc., respectively. D407 cells were procured from the American Type Culture Collection (ATCC). HCEC are SV-40 virus transfected human immortalized corneal cells; this cell line was a generous gift from Dr. Araki-Sasaki (Kinki Central Hospital, Japan)

6.3 Methods

6.3.1 High performance liquid chromatography (HPLC) analysis

Reversed phase HPLC (RP-HPLC) method was applied to analyze samples with Shimadzu LC pump (Waters Corporation, Milford, MA), Alcott autosampler (model 718 AL), Shimadzu UV/Vis detector (SPD-20AV), and Phenomenex C8 column (spherisorb 250 x 4.60 mm, 5 µm). The mobile phase was composed of methanol and water (65:35 %v/v) with the flow rate set at 0.5 ml/min and UV detector was set at 235nm for quantifying FA. Calibration curve (1 to 75 µg/mL) for FA was constructed.

6.3.2 Experimental Design

To understand the factors and interactions between two factors on the effect of FA solubilization in nanomicelles, a response surface design with central composite design (CCD) with two continuous factors two degree was employed. The two factors under investigation here are the amount or percentage of HCO-40 and OC-40 for their effects on

FA solubility (Y) in nanomicelles. In order to develop the experimental design and analyze the data, student version of JMP® 13.0 software (SAS institute, USA) was selected. In this study, X1 (HCO-40) and X2 (OC-40) serve as independent variables and solubility (Y) serves as dependent variables. The design had ten runs including 2 center points (Table 6-2). HCO-40 was continuous factor and ranged from 0.5-2 % while OC-40 continuously ranged from 0.1-0.5%. The response surface design has been utilized with the central composite design (CCD) which provide the value not only inside the box but outside of the box. The run a0, A0, 0a and 0A were the point outside of the range (< 0.5%, >2%, <0.1% and >0.5%).

Table 6-2: Design of Experimental (DOE) Coded, Uncoded Runs and Solubility of Fluocinolone Acetonide for DOE 1 (Micelle Preparation Method 1)

Run No.	Pattern	HCO-40 (%)	OC-40 (%)	DOE 1 Solubility (mg/ml)
1	--	0.50	0.10	0.17
2	-+	0.50	0.50	0.12
3	+-	2.0	0.10	0.62
4	++	2.0	0.50	0.60
5	a0	0.19	0.30	0.14
6	A0	2.31	0.30	0.58
7	0a	1.25	0.017	0.51
8	0A	1.25	0.58	0.66
9	00	1.25	0.30	0.49
10	00	1.25	0.30	0.51

Statistical Analysis: The experimental design and data analysis were performed by JMP 13.0 software student version. The effect of two factors - polymers (HCO-40 and OC-40) amounts on dependent variables (solubility (mg/mL) was studied with statistical models. These models will denote interactive and polynomial influences on the dependent outcome in order to predict fit model (Eq. 6-1) and was used to evaluate their influence on the response variable (Y)

$$Y = b_0 + b_1 X1 + b_2X2 + b_3 X1X2 + b_4 X1X1 + b_5 X2X2 \quad \text{(Eq. 6-1)}$$

Where Y is response outcome, b_0 denotes intercept, b_1, b_2, b_3, b_4, b_5 represent the regression coefficients for factors X1, X2, interaction X1 and X2, interaction X1 and X1, interaction X2 and X2, respectively. X1 denotes amount of HCO-40 and X2 represents amount of OC-40. X1X1 and X1X2, X2X2 are polynomial term of individual effects which represent the polymer 1- polymer 1, polymer 1 -polymer 2 and polymer 2 -polymer 2 interactions.

Results from design were analyzed with one-way analysis of variance (ANOVA). *F*-test was carried at $\alpha = 0.05$ level was used to determine the significant relationship between independent and dependent variables. Significant factors and interactions were identified by the *t*-test at 95% significance level. R^2 and adjusted R^2 were also calculated for regression model and validated by checking model assumptions and summary of fit. Statistical analysis was done by the JMP 13.0 software student version.

6.3.3 Nanomicelle Preparation

Method 1 (Experiment of design 1 (DOE1)): Nanomicellar formulations (NMF) were prepared following a previously described procedure reported from our laboratory[197, 225, 308]. Briefly, HCO-40, OC-40 and FA were accurately weighed and separately dissolved in ethanol. All three solutions were mixed together to obtain a homogenous solution. Organic solvent was removed under rotary evaporation followed by high vacuum (GeneVac) to generate a thin film. Subsequently, this film was hydrated and resuspended in phosphate buffer. This solution was filtered sterilized through 0.2 µm nylon filter to separate unentrapped FA and other foreign particles. Similarly, the blank formulation was prepared without FA.

Method 2 (Experiment of design 2 (DOE2)): Based on the result of method 1, a small modification was made in method 1 to have higher drug solubility. Briefly, the drug and polymer film in method 1 was heated at 65 °C for 10-15 mins until the film was melted. The melted film was rehydrated and resuspended in phosphate buffer and follow the method 1. FA NMF was obtained and characterized as needed. Similarly, the blank formulation was prepared without FA.

6.3.4 Solubility

Following a previously described procedure reported from our laboratory[197, 225, 308], reversed micellization was achieved in organic solvent (dichloromethane), and FA was extracted from the core of nanomicelles. The amount of FA encapsulated within NMF was measured with HPLC. The solubility of FA in NMF were calculated.

6.3.5 Mixed Nanomicellar Size, Polydispersity Index (PDI), and Surface Potential

Following a previously described procedure reported from our laboratory[197, 225, 308]. Briefly, the nanomicellar size, PDI, and surface potential were determined by dynamic light scattering analyzer (DLS) (Brookhaven Zeta Plus instrument, Holsville, NY, USA). A sample volume of 500 µL without dilution was subjected to size measurement at a laser wavelength of 659 nm at room temperature. All measurements were performed in triplicate.

6.3.6 Light Transmittance

Following a previously described procedure reported from our laboratory[197, 225, 308]. Briefly, the percentage transmittance of light through samples (N=4) was measured at

different wavelength range from 400nm to 600 nm with a UV-Vis spectrometer (Model: Biomate-3, Thermo Spectronic, Waltham, MA). Percent light transmitted was recorded. Distilled deionized water served as blank. All measurements were performed in triplicate.

6.3.7 Viscosity

Viscosity of all the formulations was measured with Ostwald-Cannon-Fenske viscometer following conventional method as previously described. Briefly, the travel time or efflux time of NMF and distilled deionized water freely go through ranged distance was measured and calculated with equation 1 (Eq. 6-2). All measurements were performed in triplicate.

$$\text{Viscosity}_{(\text{liq})} = \frac{Density\ (liq)\ X\ time\ (liq)\ X\ Viscosity(water)}{Density\ (water)\ X\ time\ (water)} \quad \text{(Eq. 6-2)}$$

Viscosity $_{(\text{water})}$ = 0.89 centipoise (Cp), 25 ˚C and density $_{(\text{water})}$ = 1 g/mL

6.3.8 Dilution Effect

Stability of NMF was examined by diluting the sample 0 to 400 times with phosphate buffer. Diluted FA nanomicelles were characterized for size and PDI following an earlier established protocol using DLS instrument [197, 225, 308]. Diluted FA nanomicelles were measured for size characterization following an earlier described protocol [15]. FA loaded NMF were diluted with appropriate volume of phosphate buffer according to dilution factor and NMF size and PDI were recorded from DLS analyzer.

6.3.9 ^{1}H NMR Characterization

Proton nuclear magnetic resonance (^{1}H NMR) was applied to identify any unentrapped (or) free FA in the NMF solution following a previously procedure reported from our laboratory[197, 225, 308]. ^{1}H NMR studies were conducted for FA, blank NMF and

FA-loaded NMF. ^{1}H NMR spectra were recorded on Varian 400 MHz spectrometer (Varian, USA) in deuterated water (D_2O) or deuterated chloroform ($CDCl_3$).

6.3.10 In vitro Drug Release Study

FA release kinetics from NMF was studied following previously described protocol [225]. Briefly, FA NMF and FA ethanoic solution (control) were transferred to dialysis bag with a molecular weight cut-off of 1,000 Da. The bags were immediately transferred to 15ml centrifuge tubes, previously thermostated at 37 ˚C, containing 5 mL Dulbecco's Phosphate-Buffered Saline (DPBS) (pH = 7.4) buffer solution. All samples were placed in shaking water bath at 37 ˚C and 60 rpm. At predetermined time points, drug release medium (5 mL) was collected and replaced with equal volume of fresh buffer to maintain sink conditions. Collected DPBS was immediately stored at – 80 ˚C until further analysis. Before analysis, samples were thawed, vortexed and extracted for FA (reverse micellelization). Extracted samples were injected into RP-HPLC to determine FA concentrations.

6.3.11 Osmolality and pH

Osmolality is an important attribute for the topical eye drop formulation. It was measured using the Wescor Vapor Pressure Osmometer (Vapro 5520). The experiment was done following the manual procedure previously reported from our laboratory[197, 225, 308]. Briefly, 10 µL of NMF was loaded in the center of the sample disc and immediately the instrument measure and show osmolality value. The pH of the NMF was adjusted similar to the tear pH ~ 6.8 with phosphate buffer.

6.3.12 Powder X-ray Diffraction (XRD)

Following a previously described procedure reported from our laboratory [197, 225, 308]. XRD analyses were performed for freeze-dried FA, polymer HCO-40, OC-40, blank FA NMF and FA NMF. The diffractograms were collected on Rigaku MiniFlex using Cu Kα radiation, 30kV-15mA, at 1 degree 2-theta/minute.

6.3.13 Cell Culture

Briefly, Human corneal epithelial cells (HCEC cells) were cultured following a previously published protocol [308], [328]. Briefly, DMEM/F-12 medium comprising of 15% (v/v) heat inactivated fetal bovine serum (FBS), 22 mM NaHCO-60_3, 15 mM HEPES and 5 mg/L insulin, 10 µg/L human epidermal growth factor, 100 mg/L penicillin and 100 mg/L streptomycin was prepared. Cells with passage numbers between 15 and 25 were utilized for all studies. Human retinal pigment epithelial cells (D407 cells) were grown as described earlier [197] in DMEM medium supplemented with 10% (v/v) heat inactivated FBS, 15mM HEPES, 29mM NaHCO-60_3, 100 mg/L penicillin, 100 mg/L streptomycin, and 1% nonessential amino acid. Both cell lines were incubated at 37 ˚C, 5% CO_2 and 90% humidity. Both media were changed every alternate day.

6.3.14 In vitro Cytotoxicity

Briefly, *in vitro* cytotoxicity studies of NMF were carried out with Premix WST-1 cell proliferation assay kit (Takara Bio Inc.) and Lactate dehydrogenase (LDH) assays (Takara Bio Inc.) on HCEC and D407 cells respectively. Briefly, HCEC and D407 cells were cultured in flasks and harvested at 80–90% confluency with TrypLE™ Express (Invitrogen, Carlsbad, CA, USA). Cells were transferred to 96-well plates at a density of 10,000 cells/well and cytotoxicity studies were initiated following manufacturing protocol.

NMF solution (blank and FA loaded) were prepared and re-suspended in serum free media and filtered with 0.2 µm nylon membrane to obtain sterile formulations.

Premix WST-1 cell proliferation assay: Experiments were performed following a published method [197]. To each well 100µL of NMF was added and incubated for 1h at physiological conditions. Serum free media and Triton X-100 (10%) served as negative and positive controls, respectively. Following incubation, 10 µL of premixed WST-1 was added to each well, incubated for 30 mins and absorbance was measured for the formazan product at 440 nm. An increase in absorbance of formazan denotes the % viable cells.

LDH assay: To evaluate cell membrane damage caused by NMF in each well, 100µL of serum free media and 100µL NMFs were added and incubated for 1 h at 37 ˚C. Serum free media and Triton X-100 10% served as negative and positive samples. After incubation period, 96 well plate was centrifuged at 250X g for 10 mins and 100 µL of supernatant was collected into 96-well flat bottom plate. LDH released from damaged cells was measured with LDH assay kit and absorbance of samples was measured at 490 nm. The % membrane damage was calculated with equation 6-3 (Eq. 6-3).

$$\% \text{ Cytotoxicity} = \frac{exp.value - cell\ culture\ medium\ value}{Triton\ X\_100 - cell\ culture\ medium\ value} * 100 \quad \text{(Eq. 6-3)}$$

6.3.15 Statistical Analysis

All experiments were performed at least in quadruplicate (n=4) and the results were expressed as mean ± standard deviation (SD). Student *t*-test was applied to compare mean values. And a *p* value of ≤0.05 is considered as statistically significant.

6.4 Results and Discussion

6.4.1 HPLC to Quantity the Amount of FA in Solution:

The amount of FA was determined using HPLC, the mobile phase was composed of methanol and water (65:35 %v/v) with the flow rate set at 0.5 ml/min and UV detector was set at 235nm. Calibration standard curve (1 to 75 µg/mL) for FA was constructed. As Fig. 6-2 showed the linear equation relationship between the amount of FA (ug/ml) and area under curve. (Eq. 6-4)

$y = 152216\ x - 58049,\ R^2 = 0.9999$ (Eq. 6-4)

The R^2 is a statistical measure of how close the data are able to the fitted regression line given. It shows a percentage of the response variable variation that is explained by a linear model. In this case the standard curve is linear with an excellent R^2 (>0.99).

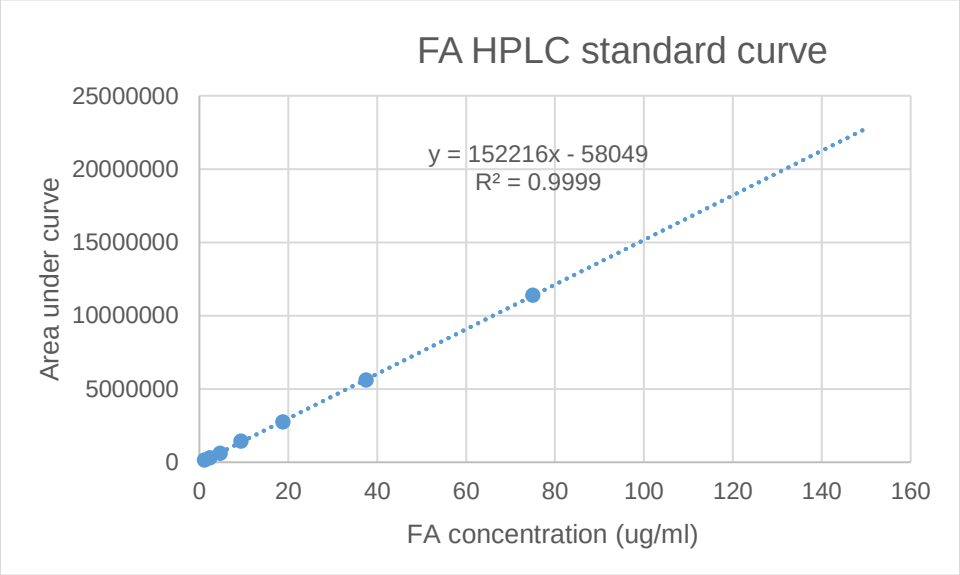

Figure 6- 2: FA HPLC Standard Curve

6.4.2 Experiment Design and FA Solubility

Design of experiment 1 (DOE1): nanomicelle preparation method 1

In this study, a central composite design with two level of two continuous factor, two center points along with axial value for rotatable 1.414 was selected to screen the independent factors for dependent variables. The FA solubility was determined using HPLC with the above method. All formulations were characterized for size, PDI, surface potential, light transmittance and cytotoxicity. The design runs (coded and uncoded) and corresponding variables are summarized in Table 6-2. The design had ten runs including 2 center points. HCO-40 was continuous factor and ranged from 0.5-2 % while OC-40 continuously ranged from 0.1-0.5%. The response surface design has been utilized with the central composite design (CCD) which provides the value not only inside the box but outside of the box. The run a0, A0, 0a and 0A were the point outside of the range (< 0.5%, >2%, <0.1% and >0.5%). FA solubility ranged from 0.12 to 0.66 mg/mL. Among all the run, the highest solubility of FA was 0.66 mg/mL, run no. 8 (coded 0A) where HCO-40 1.25% and OC-40 0.5828%. The FA solubility improved a lot where the HCO-40 were at medium or high level than low level. This appears that the amount of HCO-40 has more effect on FA solubility than OC-40. Statistical analysis was applied to analyze the data. And the software analyzed and gave the similar results. The fit model is given by Eq. 6-5.

$$Y= 0.5025 + 0.1937817\ X1 + 0.0175165\ X2 + 0.007\ X1X2 - 0.095125\ X1X1 + 0.017375\ X2X2 \quad \text{(Eq. 6-5)}$$

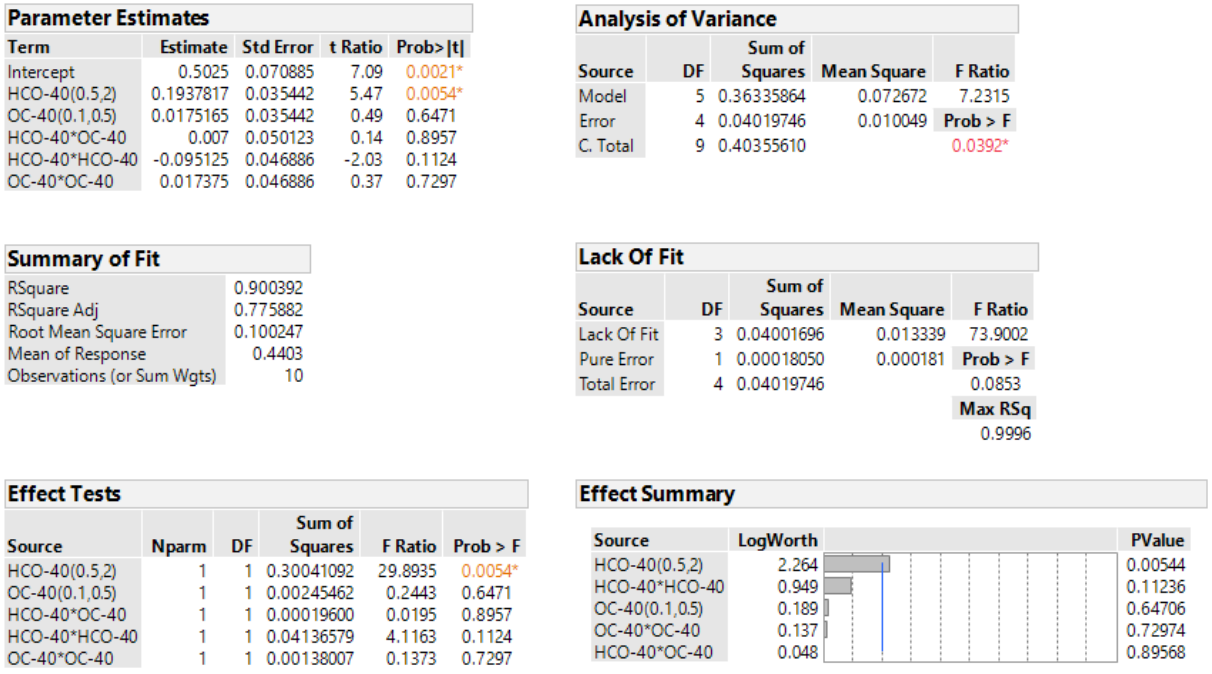

Parameter Estimates

Term	Estimate	Std Error	t Ratio	Prob>|t|
Intercept	0.5025	0.070885	7.09	0.0021*
HCO-40(0.5,2)	0.1937817	0.035442	5.47	0.0054*
OC-40(0.1,0.5)	0.0175165	0.035442	0.49	0.6471
HCO-40*OC-40	0.007	0.050123	0.14	0.8957
HCO-40*HCO-40	-0.095125	0.046886	-2.03	0.1124
OC-40*OC-40	0.017375	0.046886	0.37	0.7297

Analysis of Variance

Source	DF	Sum of Squares	Mean Square	F Ratio
Model	5	0.36335864	0.072672	7.2315
Error	4	0.04019746	0.010049	Prob > F
C. Total	9	0.40355610		0.0392*

Summary of Fit

RSquare	0.900392
RSquare Adj	0.775882
Root Mean Square Error	0.100247
Mean of Response	0.4403
Observations (or Sum Wgts)	10

Lack Of Fit

Source	DF	Sum of Squares	Mean Square	F Ratio
Lack Of Fit	3	0.04001696	0.013339	73.9002
Pure Error	1	0.00018050	0.000181	Prob > F
Total Error	4	0.04019746		0.0853
				Max RSq
				0.9996

Effect Tests

Source	Nparm	DF	Sum of Squares	F Ratio	Prob > F
HCO-40(0.5,2)	1	1	0.30041092	29.8935	0.0054*
OC-40(0.1,0.5)	1	1	0.00245462	0.2443	0.6471
HCO-40*OC-40	1	1	0.00019600	0.0195	0.8957
HCO-40*HCO-40	1	1	0.04136579	4.1163	0.1124
OC-40*OC-40	1	1	0.00138007	0.1373	0.7297

Effect Summary

Source	LogWorth	PValue
HCO-40(0.5,2)	2.264	0.00544
HCO-40*HCO-40	0.949	0.11236
OC-40(0.1,0.5)	0.189	0.64706
OC-40*OC-40	0.137	0.72974
HCO-40*OC-40	0.048	0.89568

Figure 6- 3: Statistical Summary of DOE1: Parameter Estimates, Summary of Fit, ANOVA, Effect Summary, Effect Tests

Statistical parameters for the fit model including Parameter Estimates, ANOVA for the fit model, summary of fit, lack of fit, effect tests and effect summary are summarized in Fig. 6-3. The fit model was found to be significant based on the *p*-value (p = 0.0392), R^2 = 0.90 and adjusted R^2= 0.77582. R^2 is the correlation coefficient for regression model. It shows 90% model can explain the variation in FA solubility. Also, the lack of fit suggested that the model was significant and could predict FA solubility. The model was validated based on the actual by predicted plot (Fig. 6-4). According to effect summary and parameter estimates, the only statistical significant factor was the amount of HCO-40 (X1, p= 0.0054). Another estimated coefficient for each factor and interaction between factors associated *p* value are presented in effect test and effect summary (Fig. 6-3). From the model, the amount of OC-40 (X2, p=0.64706), HCO-40 and OC-40 interaction (X1X2, p=0.89568), HCO-40 and HCO-40 (X1X1, p= 0.11236), OC-40 and OC-40 (X2X2,

p=0.72974) were presented. Only the estimated coefficients with p < 0.05 were considered to be significant. X2(OC-40), X1X2 (HCO-40 OC-40), X1X1 (HCO-40 HCO-40) and X2X2 (OC-40 OC-40) had negative effects on FA solubility while X1 (HCO-40) had a positive effect on FA solubility. As mentioned previously, solubility of FA improved with higher level of HCO-40.

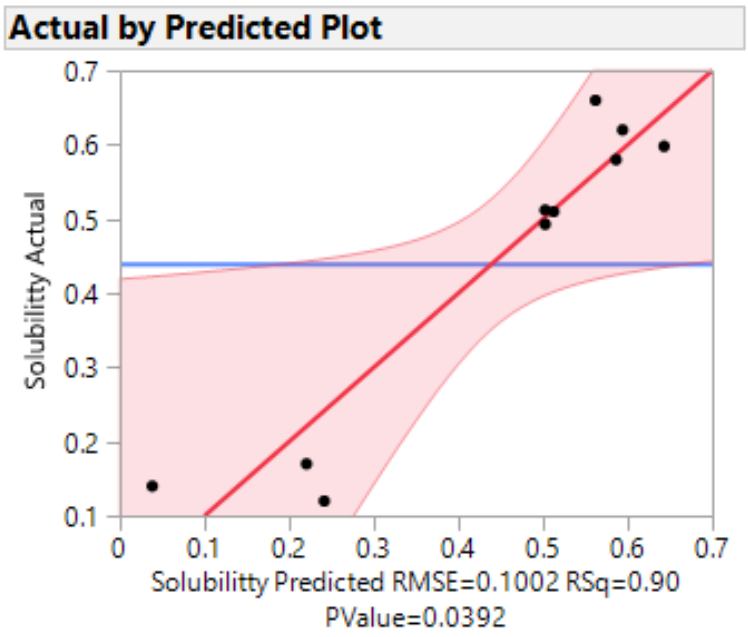

Figure 6- 4: Actual by Predicted Plot DOE1 FA NMF

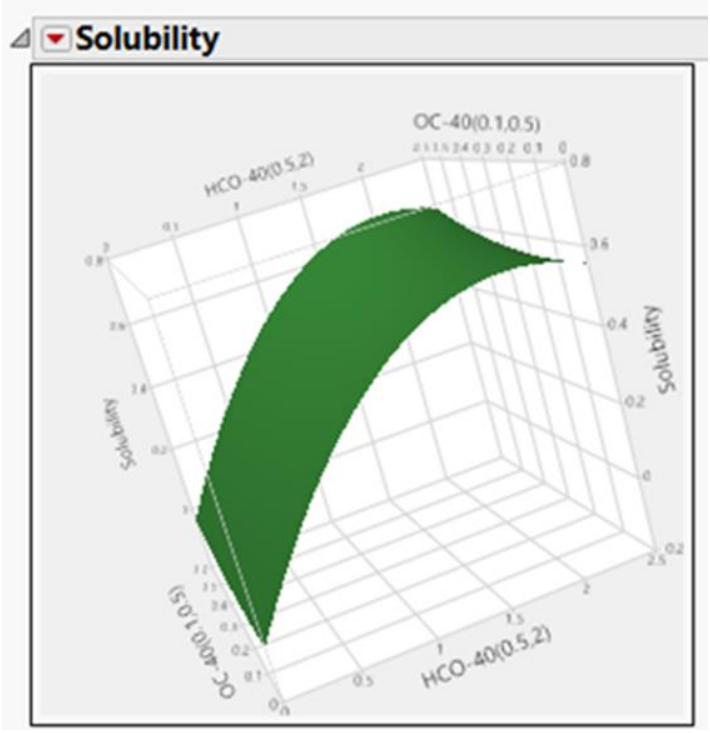

Figure 6- 5: DOE1 Response Surface Curve of FA Solubility

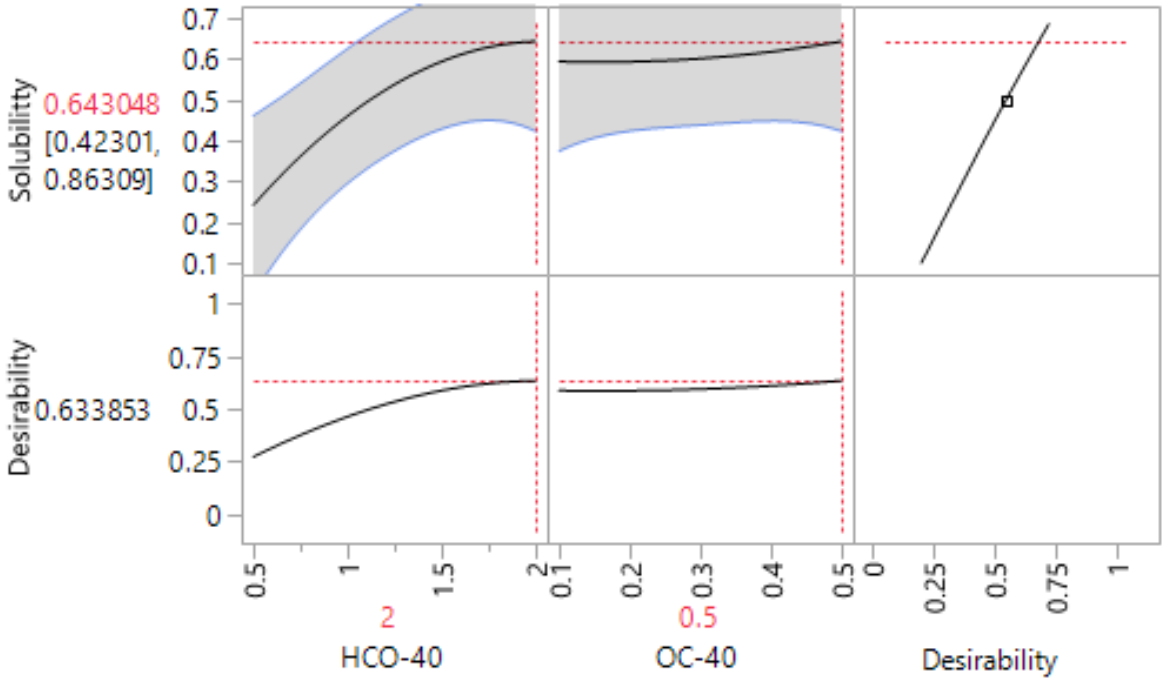

Figure 6- 6: DOE1 Prediction Profiler FA NMF

The response surface curve provides a diagrammatical representation of FA solubility as a function of the amount of HCO-40 and OC-40 in the prediction profiler (Fig. 6-5). The prediction profiler was generated to determine the optimal point with highest desirability (Fig. 6-6). It also predicts the combination effects of variables at different levels. As anticipated, increase the amount of HCO-40 the FA solubility will increase since the amount of HCO-40 had positive effect on the FA solubility. There was no change in solubility with various amount of OC-40. Based on the prediction profiler, HCO-40 2% and OC-40 0.5% gave the highest FA solubility with the highest desirability. The predicted solubility would be 0.643048 mg/mL. This value was very close to the actual value which was run no. 4, and it's lower than the run no. 8 (FA solubility 0.66 mg/mL). This discrepancy may be easy explained and understood since the prediction profiler just cooperate and predict inside the box, where HCO-40 had two level 0.5- 2% and OC-40 had two level 0.1 – 0.5%. And run no.8 (0A) was the augmented pointed with axial rotatable 1.414. This optimized nanomicelle formulation (HCO-40 2% and OC-40 0.5%) was used for the nanomicelle formulation characterizations and performed all the later studies.

Design of experiment 2 (DOE2): nanomicelle preparation method 2

Table 6-3: Design of Experimental (DOE) Coded, Uncoded Runs and Solubility of Fluocinolone Acetonide for DOE2 (Micelles Preparation Method 2)

Run No.	Pattern	HCO-40 (%)	OC-40 (%)	DOE 2 Solubility (mg/ml)
1	--	0.50	0.10	0.32
2	-+	0.50	0.50	0.46
3	+-	2.0	0.10	0.52
4	++	2.0	0.50	0.46
5	a0	0.19	0.30	0.22
6	A0	2.31	0.30	0.52
7	0a	1.25	0.017	0.44
8	0A	1.25	0.58	0.64
9	00	1.25	0.30	0.59
10	00	1.25	0.30	0.51

As mentioned above, DOE2 has been modified from DOE1 with the heating film at 65 ºC to allow the film melting before rehydration in order to improve the solubility. In this study, a central composite design with two level of two continuous factor, two center points along with axial value for rotatable 1.414 was selected to screen the independent factors for dependent variables. All formulations were characterized for solubility, size, PDI, surface potential, light transmittance and cytotoxicity. The design runs (coded and uncoded) and corresponding variables are summarized in Table 6-3.

The design also had ten runs including 2 center points. HCO-40 was a continuous factor and ranged from 0.5-2 % while OC-40 continuously ranged from 0.1-0.5%. The

response surface design has been utilized with the central composite design (CCD) which provided the value not only inside the box but outside of the box. The run a0, A0, 0a and 0A were the point outside of the range (< 0.5%, >2%, <0.1% and >0.5%). FA solubility ranged from 0.22 to 0.64 mg/mL. Among all runs, the highest solubility of FA was 0.64 mg/mL, run no. 8 (coded 0A) where 1.25% HCO-40 is added which is similar with DOE1. The FA solubility improved where the HCO-40 was added at medium or high level. Apparently, the amount of HCO-40 accelerated more effect on FA solubility than OC-40. Statistical analysis was applied to analyze the data. And the software analyzed and gave the similar results. The fit model is given by Eq. 6-6.

$$Y= 0.55 + 0.078033\ X1 + 0.0453553\ X2 – 0.05\ X1X2 - 0.09375\ X1X1 - 0.00875\ X2X2 \quad \text{(Eq.6-6)}$$

Statistical parameters for the fit model including Parameter Estimates, ANOVA for the fit model, summary of fit, lack of fit, effect tests and effect summary are summarized in Fig. 6-7. The fit model was found to be significant based on the *p*-value ($p = 0.0480$), $R^2 = 0.88905$ and adjusted $R^2= 0.750442$. R^2 is the correlation coefficient for regression model. It shows 88% model can explain the variation in FA solubility. Also, the lack of fit suggested that the model was significant and could predict FA solubility. The model was validated based on the actual by predicted plot (Fig. 6-8). According to effect summary and parameter estimates, the statistical significant factors were the amount of HCO-40 (X1, $p= 0.0229$) and interaction between HCO-40 and HCO-40 (X1X1, $p= 0.0309$). Another estimated coefficient for each factor and interaction between factors associated *p* value are presented in effect test and effect summary. From the model, the amount of OC-40 (X2, $p= 0.1049$), HCO-40 and OC-40 interaction (X1X2, $p= 0.1787$), and OC-40 and OC-40

(X2X2, *p*= 0.7758). Only the estimated coefficients with p < 0.05 were considered to be significant. X2(OC-40), X1X2 (HCO-40 OC-40), and X2X2 (OC-40 OC-40) had negative effect on FA solubility while X1 (HCO-40) and X1X1 (HCO-40 HCO-40) had positive effect on FA solubility. As mentioned above, solubility of FA increase at higher level of amount of HCO-40. Unlike DOE1, in DOE2 the heat was involved, and which may cause the interaction between polymers to change. The heat may have effect on the formation of the hydrogen bond between polymers and drugs. Also, the heating up and cooling down polymers could affect the recrystallization of polymer. However, this heating did not have any effect on FA solubility or the heating did not improve the FA solubility compare with DOE1.

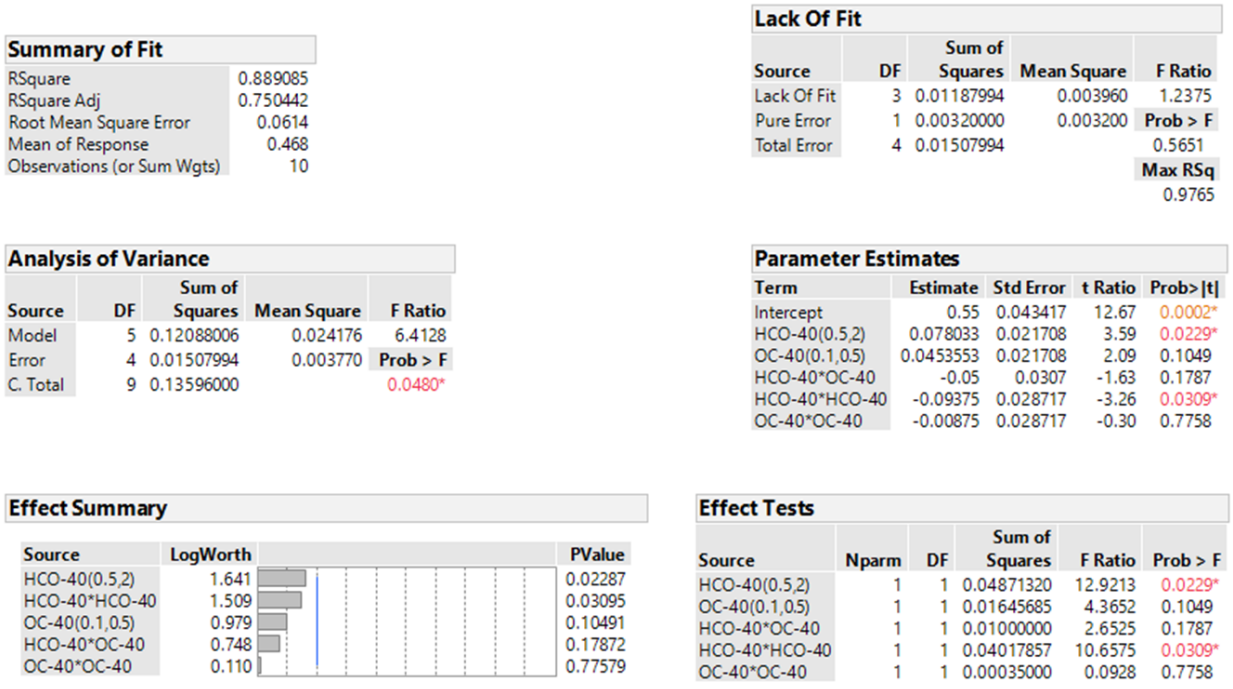

Summary of Fit

RSquare	0.889085
RSquare Adj	0.750442
Root Mean Square Error	0.0614
Mean of Response	0.468
Observations (or Sum Wgts)	10

Lack Of Fit

Source	DF	Sum of Squares	Mean Square	F Ratio
Lack Of Fit	3	0.01187994	0.003960	1.2375
Pure Error	1	0.00320000	0.003200	Prob > F
Total Error	4	0.01507994		0.5651
				Max RSq
				0.9765

Analysis of Variance

Source	DF	Sum of Squares	Mean Square	F Ratio
Model	5	0.12088006	0.024176	6.4128
Error	4	0.01507994	0.003770	Prob > F
C. Total	9	0.13596000		0.0480*

Parameter Estimates

Term	Estimate	Std Error	t Ratio	Prob>|t|
Intercept	0.55	0.043417	12.67	0.0002*
HCO-40(0.5,2)	0.078033	0.021708	3.59	0.0229*
OC-40(0.1,0.5)	0.0453553	0.021708	2.09	0.1049
HCO-40*OC-40	-0.05	0.0307	-1.63	0.1787
HCO-40*HCO-40	-0.09375	0.028717	-3.26	0.0309*
OC-40*OC-40	-0.00875	0.028717	-0.30	0.7758

Effect Summary

Source	LogWorth	PValue
HCO-40(0.5,2)	1.641	0.02287
HCO-40*HCO-40	1.509	0.03095
OC-40(0.1,0.5)	0.979	0.10491
HCO-40*OC-40	0.748	0.17872
OC-40*OC-40	0.110	0.77579

Effect Tests

Source	Nparm	DF	Sum of Squares	F Ratio	Prob > F
HCO-40(0.5,2)	1	1	0.04871320	12.9213	0.0229*
OC-40(0.1,0.5)	1	1	0.01645685	4.3652	0.1049
HCO-40*OC-40	1	1	0.01000000	2.6525	0.1787
HCO-40*HCO-40	1	1	0.04017857	10.6575	0.0309*
OC-40*OC-40	1	1	0.00035000	0.0928	0.7758

Figure 6- 7: Statistical Summary of DOE2 FA NMF

The response surface curve provides a diagrammatical representation of FA solubility as a function of the amount of HCO-40 and OC-40 in the prediction profiler (Fig. 6-9 and 6-10). The prediction profiler was generated to determine the optimal point with highest desirability. It also predicts the combination effects of variables at different levels. As anticipated, with increased amount of HCO-40 FA solubility will increase since the amount of HCO-40 had positive effect on the FA solubility, yet there is not much difference FA solubility when changing the amount of OC-40. Heating may have an effect on the formation of bonds which may explain the difference between DOE1 and DOE2. Based on the prediction profiler, HCO-40 1.5% and OC-40 0.5% gave the highest FA solubility with highest desirability. Unlike DOE1, the predicted solubility would be 0.585533 mg/mL which is lower than DOE1 and the curve was nonlinear. The OC-40 has negative effect on solubility. This optimized nanomicelle formulation (HCO-40 1.5% and OC-40 0.5%) was carried for the nanomicelle formulation characterization and all the later studies.

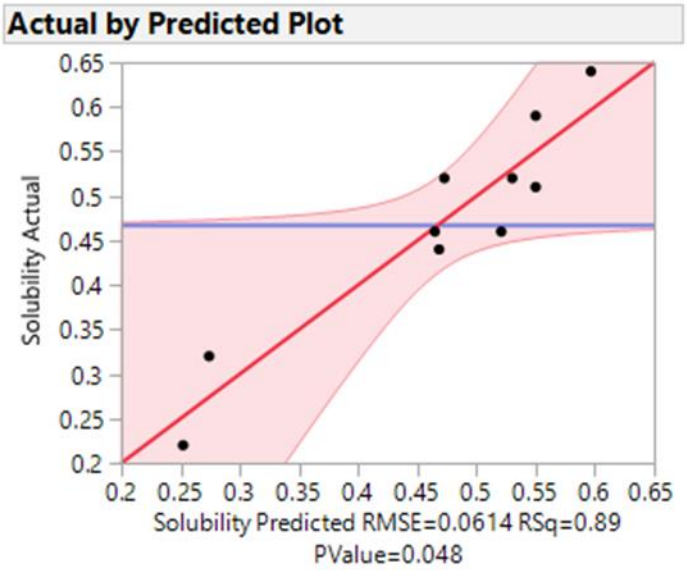

Figure 6- 8: DOE2 Actual By Predicted Plot

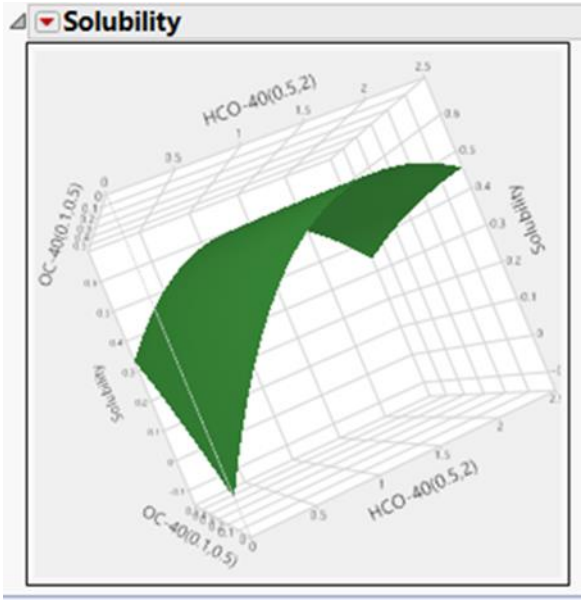

Figure 6- 9: DOE2 Response Surface of FA Solubility

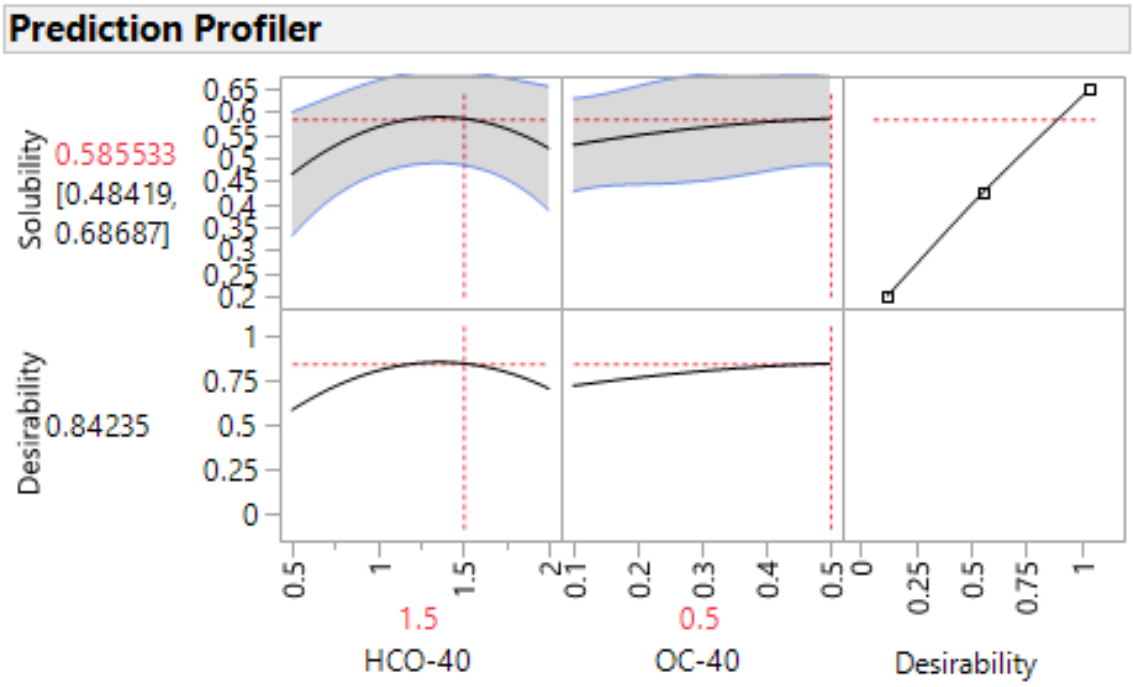

Figure 6- 10: DOE2 Prediction Profiler

6.4.3 Micellar Size, Polydispersity Index (PDI) and Surface Potential

Nanomicellar size, polydispersity index (PDI), Zeta potential and size distribution were determined by dynamic light scattering (DLS) method. The results are summarized in Tables 6-4 and 6-5. All FA-loaded NMFs were in the size range between 12-20 nm with unimodel distribution irrespective of the FA solubility and the DOE1 or DOE2. Heat does not have effect on the size of NMFs. The blank NMFs also were prepared with method 1 and measured the size, PDI and summarized in Table 6-. The blank NMFs are ranged from 19 -25 nm and PDIs were also small and negligible, ranged from 0.152 to 0.247. Since the blank NMFs do not contain the drugs, there were no change of drug and polymers interaction. It's increasing the distance between atoms thereby elevating the size of blank NMFs are bigger than FA-loaded NMFs. Fig. 6-11 illustrated the distribution of blank and FA- loaded NMF. The significantly small size of NMF may sufficiently allow NMF to travel across ocular tissues such as scleral channels/pores, are in the size range between 20 and 80 nm[311]. The PDI of all runs bellow 0.5 surface charge is negligible. Such property of nanomicelles may help to deliver FA to back of the eyes by the conjunctival/ sclera pathway. The surface potential of all blank and FA-loaded NMFs did not have any charge on it (Table 6-4 and 6-5) 0.141 for FA NMF DOE1 and -0.124 for FA NMF DOE2 was considered no charge or negligible. This charge may not cause any effect when nanomicelles across tissue membrane.

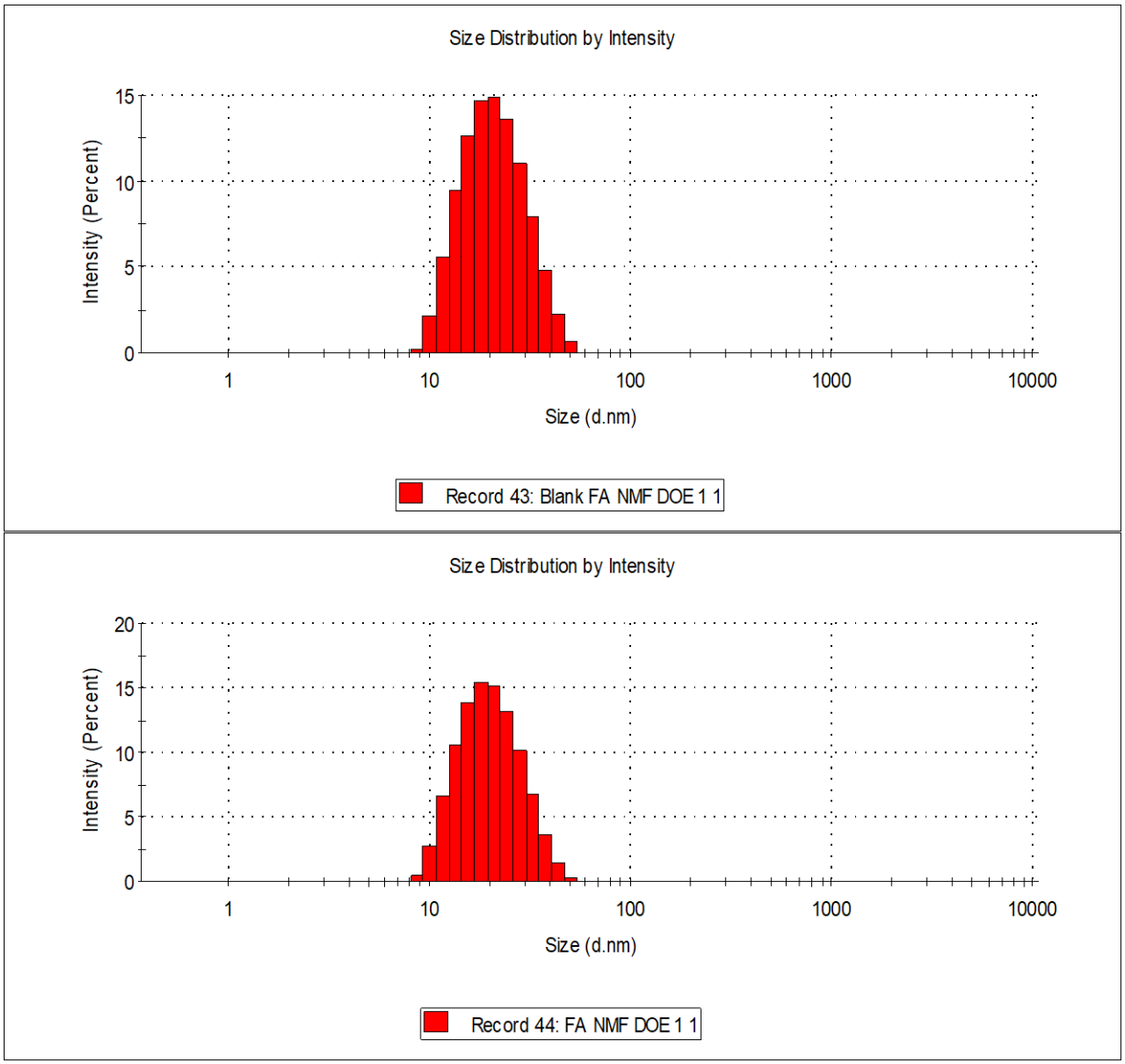

Figure 6- 11: Size of Blank NMF and FA NMF

Table 6-4: Summary of Size, PDI for DOE1 and DOE2 FA-Loaded Nanomicelle Formulations

Run No.	Pattern	HCO-40 (%)	OC-40 (%)	DOE1 Size (nm)	DOE1 PDI	DOE2 Size (nm)	DOE2 PDI
1	--	0.50	0.10	19.07	0.149	19.55	0.135
2	-+	0.50	0.50	17.75	0.166	18.12	0.156
3	+-	2.0	0.10	19.08	0.157	19.46	0.149
4	++	2.0	0.50	18.86	0.168	20.01	0.186
5	a0	0.19	0.30	18.98	0.153	19.62	0.162
6	A0	2.31	0.30	19.89	0.159	18.98	0.162
7	0a	1.25	0.02	16.89	0.142	18.15	0.156
8	0A	1.25	0.58	17.58	0.137	17.98	0.142
9	00	1.25	0.30	14.32	0.516	16.56	0.235
10	00	1.25	0.30	12.43	0.721	17.56	0.142

Table 6-5: Summary of Size, PDI for DOE1 Blank Nanomicellar Formulations

Formulations	HCO-40 (%)	OC-40 (%)	Size (nm)	PDI
Blank F1	2.0	0.50	21.95	0.174
Blank F2	2.0	0.10	19.70	0.152
Blank F3	1.25	0.30	21.44	0.188
Blank F4	1.25	0.30	21.25	0.205
Blank F5	0.50	0.50	25.19	0.247
Blank F6	0.50	0.10	24.55	0.222

6.4.4 Optical Clarity/Appearance

Optical appearance / clarity is defined as the ability of light to be transmitted 90% or more through a 1.0-cm path length at 400nm wavelength and compared with water. Due to the interference of particles, the light was scattered and give different angles. However, particles of extremely small size (i.e. nanometers) will not produce enough hindrance or light scattering resulting in a clear and transparent solution. FA NMF is clear as water (Fig. 6-12) or transparent and more than 97% of light has been transmitted (Table 6-6). All NMFs can be compared with distilled deionized water when measured by transmittance. Percentage light transmittance of optimized formulations (blank and FA loaded NMF DOE1 and DOE2) at wavelength 400nm ranged from 97 % to 99 %. It was observed that there was no particle interfering with light scattering, the FA-loaded NMF appeared as clear as water. The nanomicelles helped improve the FA solubility and formed clear, aqueous solution.

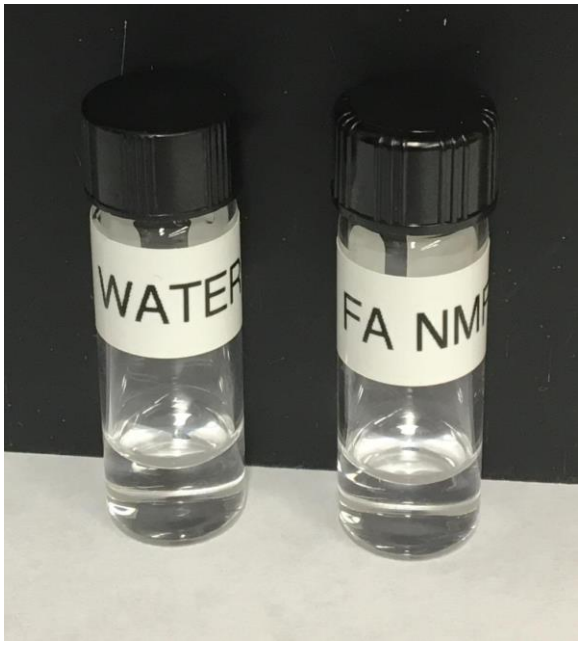

Figure 6-12: Visual Appearance of FA-Loaded NMF on the Right in Comparison to Water on the Left

Table 6-6: Characterizations of Optimal DOE1 and DOE2 FA NMFs

Formulation code	HCO-40 (wt%)	OCO-40 (wt%)	Size (nm)	PDI	Surface potential (mV)	T (%)	Osmolality (mmol/kg)	pH	Viscosity (Cp)	Solubility (mg/ml)
Blank FA NMF DOE 1	2.0	0.50	19.55	0.131	0.135	98	301	6.8	1.094	-
FA NMF DOE1	2.0	0.50	18.85	0.126	0.148	97.68	292	6.8	1.111	0.683
Blank FA NMF DOE 2	1.50	0.50	21.51	0.136	-0.082	98.5	299	6.8	1.052	-
FA NMF DOE 2	1.50	0.50	19.83	0.112	-0.124	97.69	289	6.8	1.069	0.596

6.4.5 Powder XRD Analysis of Blank Micelle and FA NMF

FA, polymer HCO-40, OC-40, blank NMF and FA NMF were studied by XRD to find the further information about physical state of polymer and when inside micelles. Fig. 6-13 presented the results. XRD pattern showed the characteristic peaks of the HCO-40 widely at two-theta 19 degree and 23 degree while OC-40 showed at same 19 and 23 degree but higher intensity with smaller peak width. Peak width due to crystallite size, the peak gets broader as the crystallite size gets smaller. FA raw powder had characteristic peak at near 10, 14, 17 and 24 degree. The characteristic peaks of HCO-40, OC-40 and FA were disappeared for freeze-dried blank NMF and FA NMF. Because the polymers have interacted with each other and self-assemble in water to form nanomicelle, there were no more characteristic peaks for individual components. Both blank nanomicelle and FA nanomicelle gave the same peaks at 22, 23, 32 and 33 degree indicating the drug FA was molecularly dispersed in naomicelles. As the X-rays interact with crystalline lattice, a diffraction pattern is formed which reveals spacing between planes of atoms. The nanomicelles have the intense to arrange the atoms close together and form very stable bond so spacing between planes of atoms are smaller where there were no peaks observed with high intensity or broaden width. And such rigid structure resists against sheer stress while travel across the scleral pores and will be beneficial for formulation during transport through the membrane.

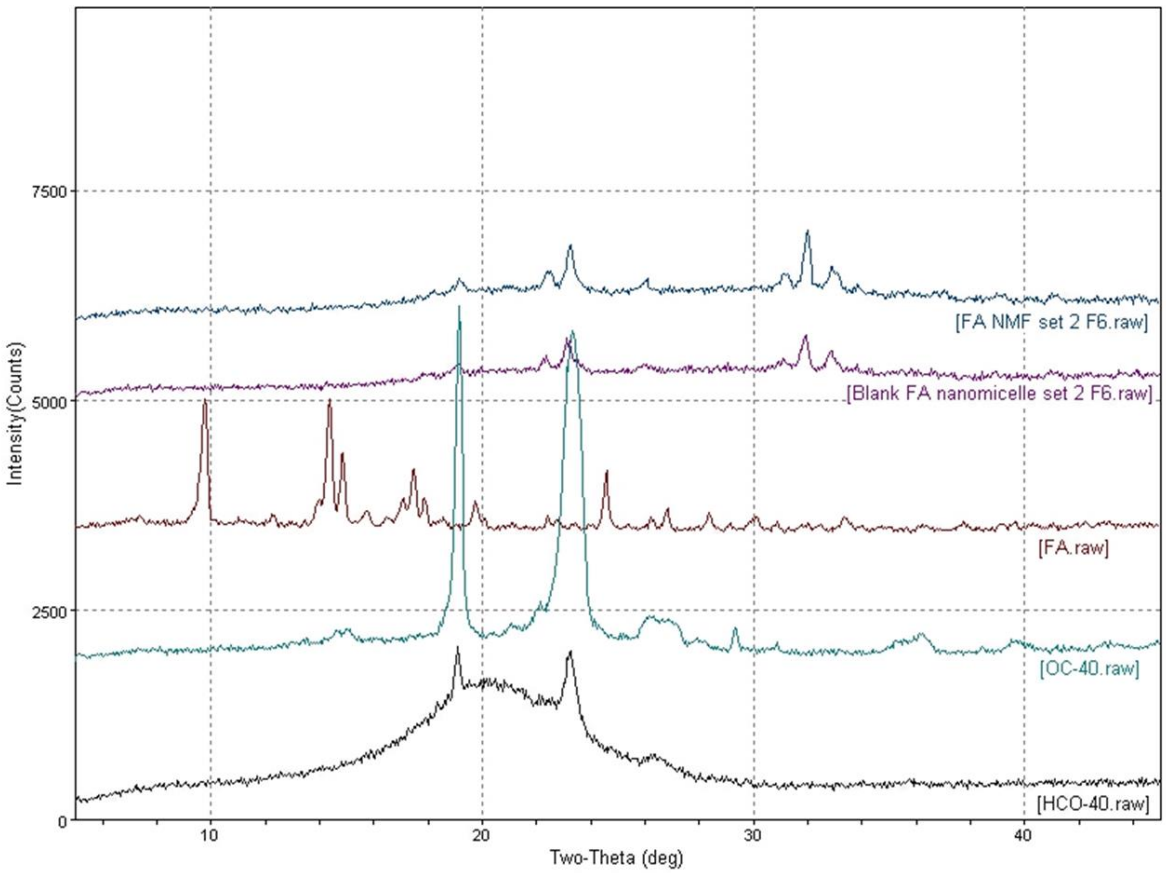

Figure 6-13: Power X-Ray Diffraction (XRD) Pattern for Freeze Dried FA NMF, Blank NMF, FA Raw, OC-40 Raw and HCO-40 Raw

6.4.6 Viscosity

The viscosity of all NMFs is summarized in Table 6-6. The viscosity of all formulations was ranged from 1.052 and 1.094 centipoise (Cp) for blank NMFs, 1.069 and 1.111 Cp for FA NMFs which are very close to water (0.89 Cp). This clear and aqueous formulation almost has water characteristic, which may help reducing the irritation for the eyes. NMFs produce viscosity well below critical point of 4.4 cP, such that the drainage rate is not affected [313]. However, the high viscosity of formulation may have effect on its residence time in the cul-de-sac enhancing therapeutic effect. The

viscosity of formulation may offer advantages due to longer residence in the cul-de-sac which may increase ocular absorption but again eye irritation should be considered carefully.

6.4.7 Dilution Effect

The dilution effect on NMF was investigated following the size and PDI and is summarized in Table 6-7. Since human eyes have many different mechanism and barriers to protect and prevent any harm from external particles. Major ocular barriers are static (corneal epithelium, corneal stroma, and blood–aqueous barrier) and dynamic barriers (blood-retinal barrier, conjunctival blood flow, lymph flow, and tear drainage). Tear drainage is one of those barriers that clear out much of topical application. Therefore, the effect of dilution on the stability of the NMF was studied. The results shown in Table 6-7 was found that there is no significant effect on nanomicelle size and PDI with dilution up to 400 times. The size of NMF was slightly increased from 18.23 nm to 26.23 nm upon 400 dilution times. However, the tear secreted in the eye following topical administration may form less than 10 times dilution. FA NMF was very stable at that dilution factor, almost approximately the same 18.35 nm. The formulation stability with continuous dilution may help the formulation reach the target.

Table 6-7: Effect of Dilution on Nanomicelles Size and PDI of Optimal FA NMF

Dilution factor (times)	Average size (nm)	PDI
0	18.23	0.126
10	18.35	0.107
20	18.55	0.140
50	19.03	0.195
100	19.62	0.220
200	23.79	0.347
400	26.23	0.332

6.4.8 Osmolality and pH

Osmolality is an important attribute for the topical eye drop formulation. The hyper-osmolality is a main pathogenic factor in dry eye [314]. The osmolality and pH of the NMF was adjusted similar to the tear pH ~ 6.8 with phosphate buffer as depicted in Table 6-6. Osmolality of FA NMF was ranged from 289 to 301 mmol/Kg or mOsm/kg and pH was around 6.8. The physiological tear has osmolarity of 289 mOsm/L[329] and osmolality of 290 mOsm/L which is equivalent to 0.9% saline.

6.4.9 ^{1}H NMR Characterization

We have already reported that ^{1}H NMR spectral analysis of nanomicelles. The free drug molecules in nanomicelle solution was identified by ^{1}H NMR analysis at parts

per million (ppm) levels. ^{1}H NMR studies were conducted for FA in $CDCl_3$ to identify the corresponded resonance peaks of FA to compare or serve as positive control. ^{1}H NMR studies of blank NMF in $CDCl_3$ and FA-loaded NMF were conducted in different solvent such as $CDCl_3$ and D_2O.

As similar with our previous chapter, the resonance signals for TA were absent, the resonance signals for FA were absent when suspended FA NMF in D_2O (Fig. 6-14). All FA in solution was entrapped inside nanomicelles and there was no free/unentrapped FA in the D_2O or water. Since amphiphilic polymers have encapsulated FA inside the core which muted the NMR signal during micelle formulation. This explains the absence of FA signal in D_2O.

There were obvious resonance peaks of FA for the pure FA in $CDCl_3$ and the similar corresponding peak of FA was observed for FA NMF in $CDCl_3$ (data not shown). The spectra indicated that FA was presented in organic solvent ($CDCl_3$) where the reverse micelles was formed. However, there was no observable peak corresponding to FA except polymer peak for blank NMF in $CDCl_3$ (data not shown). FA NMF was dissolved in both organic solvent and water, free FA was presented only in organic solvent ($CDCl_3$) not in water (D_2O). That means no free FA in FA NMF solution and this FA NMF will not cause any irritation for the eyes due to free FA particles.

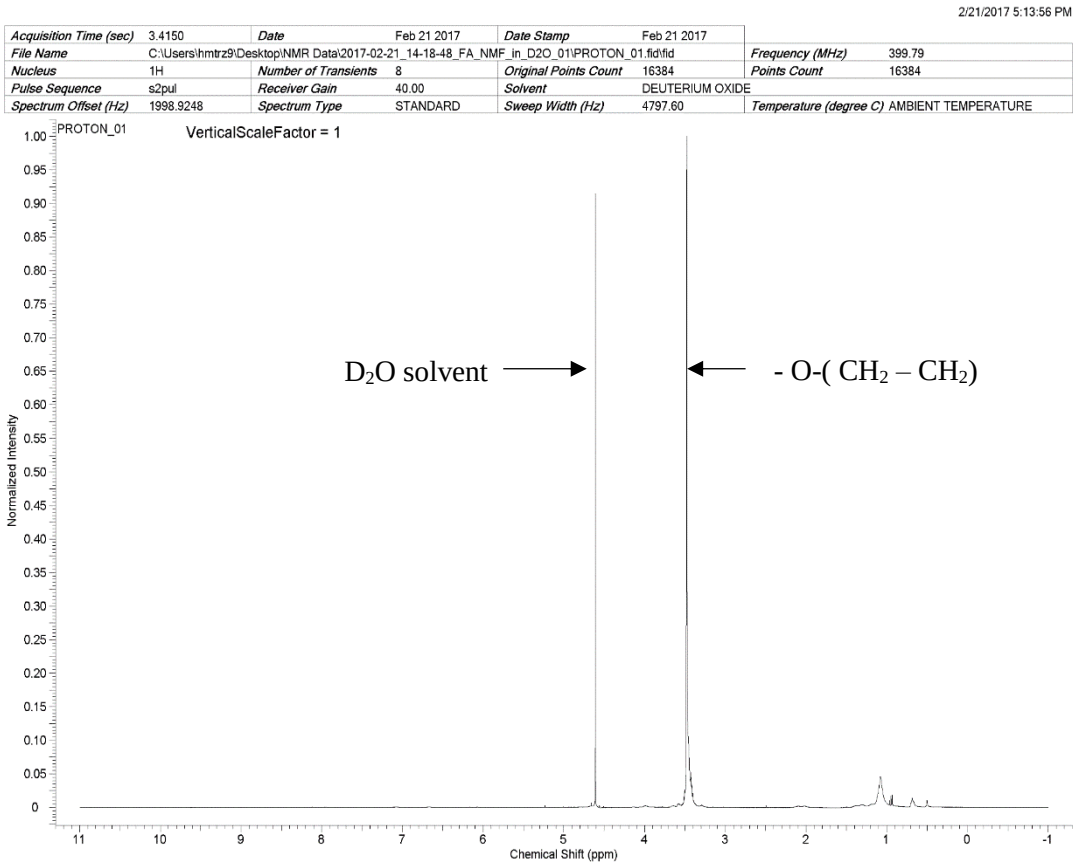

Figure 6- 14: Qualitative ^{1}H NMR Studies, ^{1}H NMR Spectrum for FA Nanomicelles in D_2O

6.4.10 In vitro Cytotoxicity

Following the topical administered, the formulations/solutions are rapidly washed (within 5 to 10 min) [312]. Previous results from our laboratory showed drug molecules in nanomicelles reaching back of the eye tissues (retina/choroid) [315] and we target back of the eyes disease. Therefore, cytotoxicity studies were conducted on human corneal epithelial cells (HCEC cells) and human retinal pigment epithelial cells (D407 cells) and ARPE-19 for 1 h incubation period. The experiments have been conducted with all DOE blank and FA loaded formulations, optimal FA NMFs.

In order to evaluate the cytotoxicity of NMF, MTT assay was performed on HCEC. The medium and Triton X-100 10% served as positive and negative controls, the % cell viability of all NMFs were compared with negative and positive control (Fig. 6-15 and 6-16). On all cell lines, HCEC, ARPE 19 and D407, all blank and FA-loaded NMFs had more than 80% cell viability as compared to medium, where Triton X-100 showed less than 10 % viability.

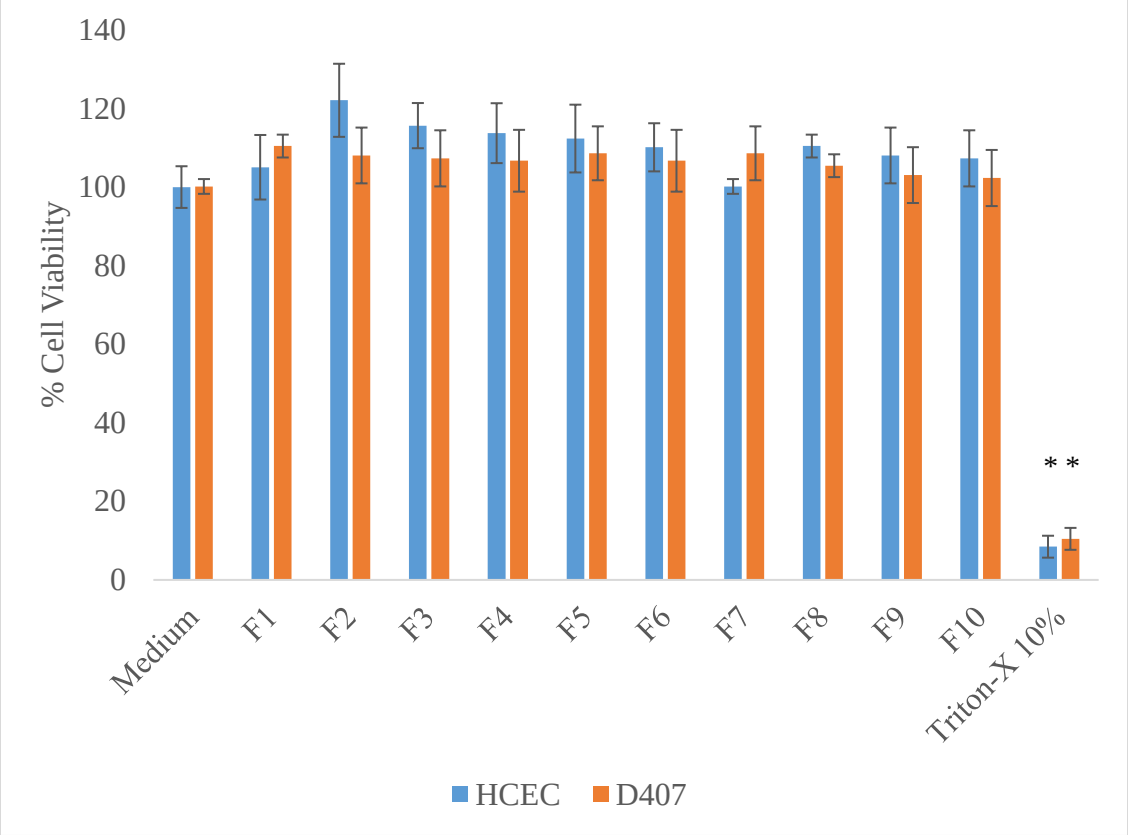

Figure 6- 15: MTT Cytotoxicity of FA-Loaded NMFs on HCEC and D407

In another study, all blank and FA-loaded NMF were evaluated for cytotoxicity by LDH leakage (Fig. 6-17). The amount of LDH released in the culture medium directly correlates with membrane damage and cytotoxicity. Triton-X 100 caused significant toxicity/ membrane damage and served as positive control. LDH study NMFs were found

to be safe without any cytotoxic effects the results are compared with the blank culture medium. Results from these assays clearly suggest that NMF do not cause cell death or damage to plasma membrane. NMFs are safe, and well-tolerated. These NMF may potentially be suitable for further *in-vivo* and human studies.

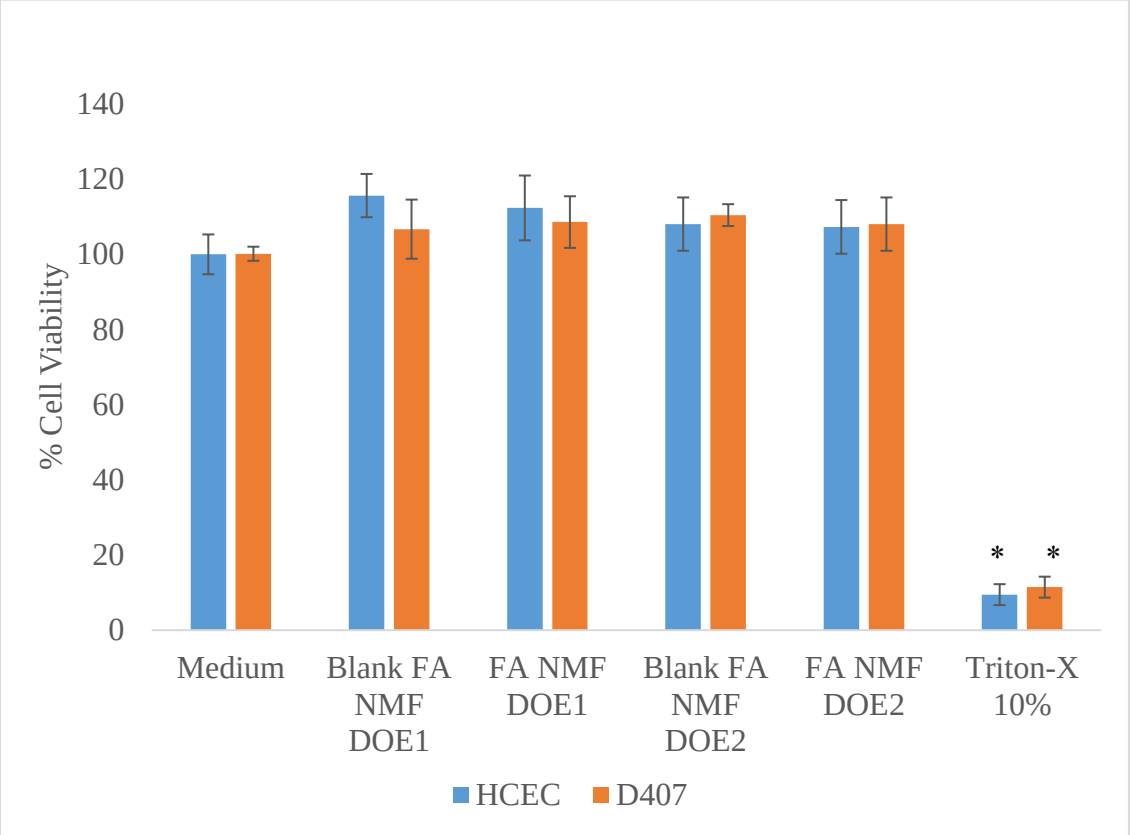

Figure 6- 16: MTT Cytotoxicity of Optimal NMFs on HCEC and D407

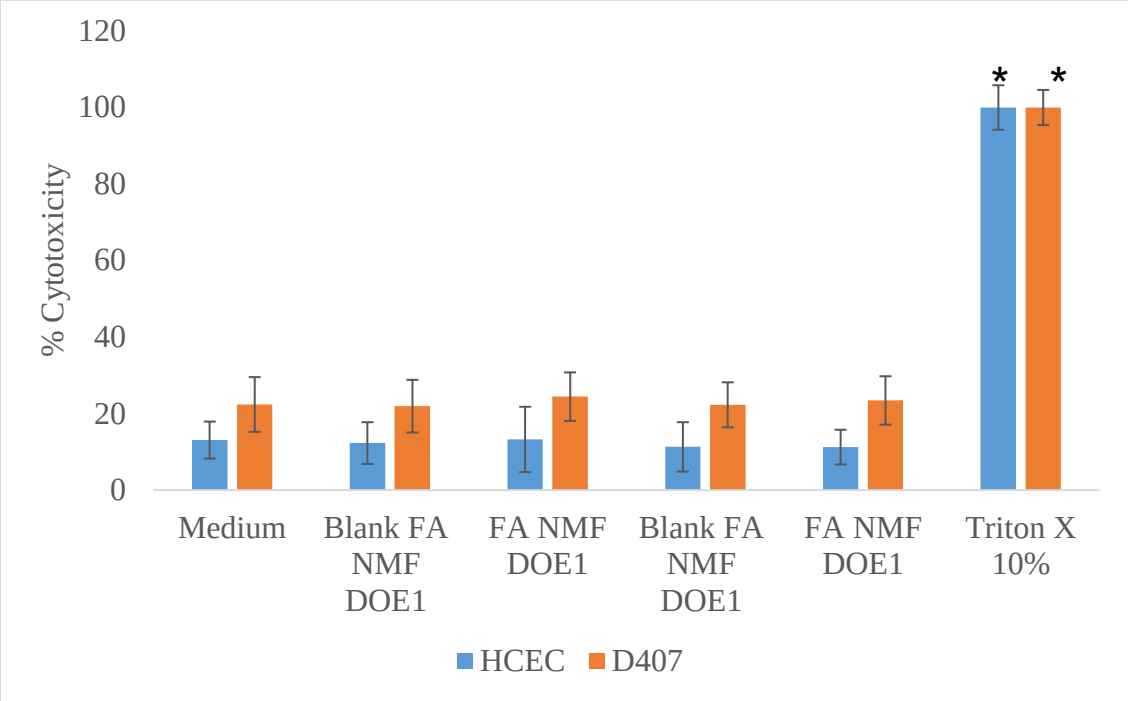

Figure 6- 17: LDH Cytotoxicity of Optimal NMFs on HCEC and D407

6.4.11 In Vitro Drug Release

To determine the release kinetics of FA from nanomicelles formulation, the optimal FA NMF (HCO-40 2% and OC-40 0.5%) was investigated under sink condition in physiological buffer pH of 7.4 at 37°C. The control represented an equal quantity of FA (1 mg) in 1 ml of absolute ethanol with a clear solution however FA in water cause a FA suspension. FA release from NMF was slower than FA release from ethanolic solution and higher than FA suspension. The release kinetic profiles of ethanolic and encapsulated FA from the nanomicelles and FA suspension are shown in Fig. 6-18. The release study has been performed for more than 72 hours. Within this time almost 100% of FA was released. At the beginning, the amount of FA was released very fast and enough to have effect. Different drugs have different logP, surface polar area, the

interaction between polymer and drug, the release mechanism from nanomicelle may change. Results suggest that, topical administration of FA NMF may release FA at a slow rate under physiological conditions. Consequently, this NMF dosing frequency can be reduced. However, achieving therapeutic FA concentrations in ocular tissues has not examined.

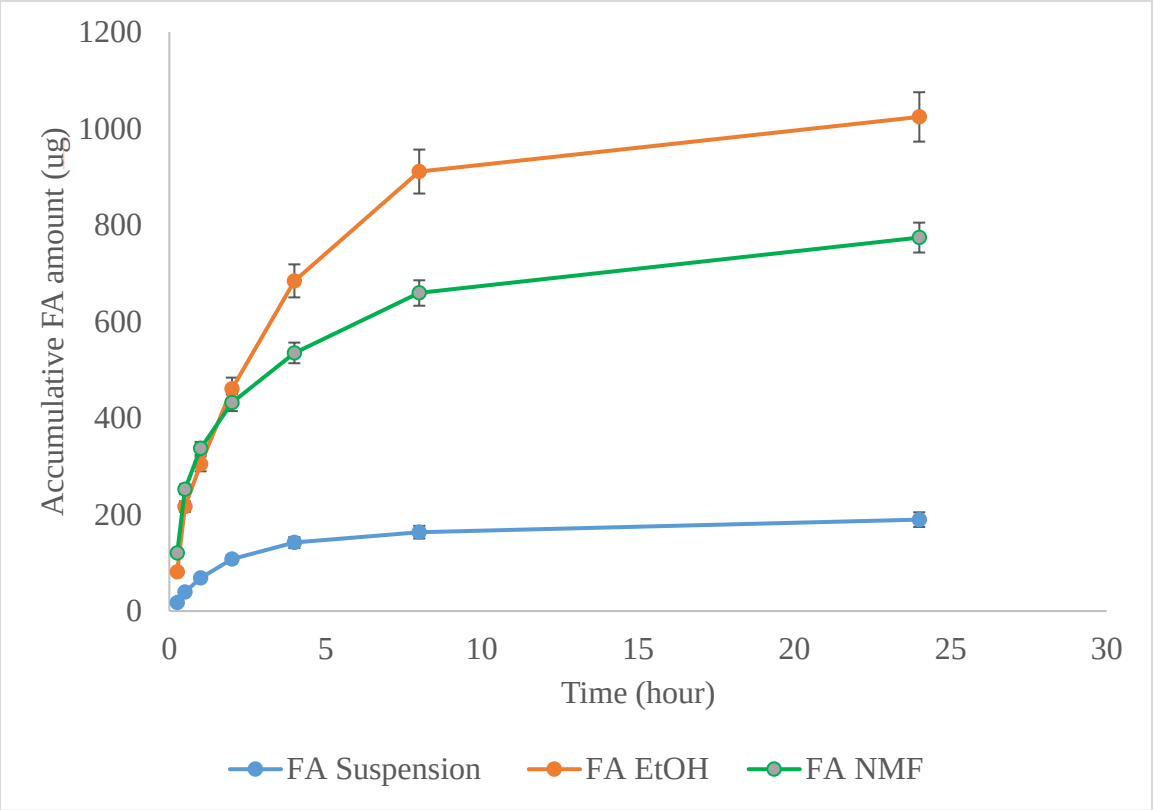

Figure 6- 18: Release Study of FA-Loaded NMF

6.5 Conclusion

In summary, a clear, stable, aqueous FA-loaded NMF have successfully been optimized, prepared and characterized with size, PDI, surface charge, osmolality, pH, % T transparent, release and cytotoxicity. The micelles preparation method was optimized

to achieve higher solubility utilizing the DOE and exploratory model. HCO-40 plays the most important role in improving FA solubility with significant *p*-value. HCO-40 and HCO-40 interaction also found to be significant in statistical model. The predictive profiler was generated to fit highest desirability and achieve the highest FA solubility. The optimal FA solubility has agreed with prediction profiler. Optimal FA NMF has small size with unimodal distribution, negligible charge, and the osmolality and pH of FA NMF were very good for crossing tissue membrane. Moreover, the FA NMF was very stable in dilution study. Qualitative ^{1}H NMR showed the absence of free FA in micelles solution. Also, the FA NMFs were safe and well-tolerated on cell viability on HCEC and ARPE-19. These results indicate that FA NMF was safe and used for further *in vivo* studies.

CHAPTER 7

7 APPLICATION OF MATHEMATICAL ENGINEERING STEEPEST ASCENT METHOD TO OPTIMIZE TOPICAL OCULAR NANOMICELLAR FORMULATION

7.1 Rationale

Triamcinolone (T1) ($C_{21}H_{27}FO_6$) is a synthetic glucocorticoid. T1 acts as a corticosteroid hormone receptor agonist with anti-inflammatory and immunomodulating properties. Upon cell entry, T1 binds to and activates the glucocorticoid receptor, and switch on multiple anti-inflammatory genes [330]. The activation of glucocorticoid receptors leads to translocation of the ligand-receptor complex to the nucleus. It induces expression of glucocorticoid-responsive genes such as annexin-1 (lipocortins), interleukin-6, (IL-6), IL-10 and secretory leukoprotease inhibitor (SLPI) [331-333]. Lipocortins inhibit phospholipase A2, therefore blocking the release of arachidonic acid from membrane phospholipids and inhibiting the synthesis of mediators of inflammation such as prostaglandins and leukotrienes. In addition, pro-inflammatory cytokine production, including interleukin (IL)-1and IL-6, and the activation of cytotoxic T-lymphocytes and nuclear factor (NF) kappa-B are also inhibited. T-cells are prevented from secreting IL-2 and proliferating. This agent also decreases the number of circulating lymphocytes, induces cell differentiation, and stimulates apoptosis through Ikappa-B expression and curtailing activation of nuclear factor (NF) kappa-B.

Diabetic macular edema (DME) is a back-of-the-eye chronic disease, a sight threatening condition caused by the accumulation of fluid in the center of the macula which may lead to vision loss[303, 316]. DME affects an estimated around 21 million

individuals with diabetes worldwide[317]. The common pathogenesis of DME is the breakdown of blood retinal barrier resulting in retina microvascular damage leading to leakage, capillary dropout, upregulation of angiogenic growth factors and neovascularization[304, 323]. Sustained hyper-glycemia causes degeneration of the inner lining of the blood vessels rendering them porous and leaky. Blood leakage through retinal vasculature accumulates in the center of the retina causing swelling and developing a condition known as DME [108]. Such swelling leads to macular detachment and is responsible for the vision loss. Current treatment of DME includes laser photocoagulation, surgery, intravitreal injection of anti-vascular endothelial growth factor (anti-VEGF), intravitreal injection of VEGF inhibitors (ranibizumab - Lucentis, aflibercept – Eylea®, bevacizumab - Avastin®) and steroid implant (dexamethasone – Ozurdex®) [141, 303, 323, 324]. Corticosteroids have been used not only to reduce the effect of VEGF overexpression but also attenuate the inflammation by suspending VEGF-A, ICAM-1, IL-6 pathway, decreasing AQP4, reducing paracellular permeability, raising up the tight junction integrity[325]. K Kriechbaum et al has compared the retinal morphology and function after intravitreal injection administering of bevacizumab (Avastin®) and triamcinolone (Volon A®) in early DME patients[334]. After one-year result, both triamcinolone and bevacizumab equally reduced central retinal subfield thickness and bevacizumab improved best corrected visual acuity more than triamcinolone. Delivery of drugs at therapeutic concentrations to back of the eye tissues (retina/choroid) is a very challenging task. Because of static and dynamic barriers, less than 5% of topical administered dose reaches the back of the eye segment [5]. Steroids have many limitations such as low aqueous solubility, sub-optimal physiochemical properties, and poor ocular

membrane permeability. Therefore, glucocorticoids must be administered by implant or intravitreal injection. Those invasive modalities are associated with side effects like higher intraocular pressure (IOP) leading to glaucoma, moreover continuous exposure to the lens may cause cataract[305, 326, 327].

Therefore, there is an urgent need to develop a clear, aqueous topical eye drop formulation to deliver T1 in therapeutic levels to back of the eye tissues (macula region). Topical administration is the most patient compliant route. In such a scenario, aqueous nanomicellar formulation with amphiphilic polymers appear to be a promising approach. Hydrophobic-T1 will be encapsulated in the core of nanomicelles. Hydrophilic corona covers the outside and aids in the development of clear, aqueous solutions. This novel nanomicellar strategy may (i) improve drug solubility (ii) improve drug uptake and cell permeability, (iii) allow for non-invasive delivery of hydrophobic drugs to posterior ocular tissues and (iv) improve patient acceptability and compliance due to its noninvasive, nonirritating clear and aqueous system. Nanomicelles may primarily follow the non-corneal pathway such as conjunctival-scleral rather than uveo-sclera pathway after topical administration to reach the retina [197].

Design of Experiment (DOE) is a systematic method to determine the relationship between factors affecting a process and the output of that process. DOE can accentuate the pattern of interaction between independent and dependent factors. This method can reduce the number of experiments required for optimization which can save time and cost.

Steepest ascent: is a simple and economical method to estimate the operating conditions, which are far from the actual optimum, but based on the initial optimum. It

is the procedure for increasing maximum response. Steepest ascent has been applied in engineering and pharmaceutical industry since numerous factors involve in manufacturing. For pharmaceutical companies saving time and money are crucial and they employ DOE and steepest ascent to quickly increase their profit by determining the main factor and optimize the ideal manufacturing conditions. Salih Dincer has demonstrated how to apply steepest ascent to determine the most suitable combinations for enteric film coating of tablets [335].

In the present study, the amphiphilic polymers approved by FDA namely Octoxynol-40 (OC-40) and hydrogenated castor oil 40, 60, 80 and 100 are selected to improve the solubility of T1. Both OC-40 and HCO-40 are amphiphilic nature containing both hydrophobic and hydrophilic branches. These characteristics allow natural form self-assembly of spherical nanomicelles in aqueous solution. Consequently, hydrophobic T1 stays into hydrophobic core and hydrophilic corona allows aqueous solubility. Based on the preliminary studies (data not shown, similarly to table 6-1, page 105), hydrogenated castor oil 40 (HCO-40) provide the best results in solubility. For the reason, HCO-40 was selected to continue further for formulation optimization. The objective of study is to improve T1 solubility utilizing nanomicellar technology with the help of design of experiment (DOE). The amounts of HCO-40 and OC-40 were considered as independent factors while T1 solubility was presented the response outcome. The best ratio of the combination HCO-40 and OC-40 is determined by JMP 13.0 software. The optimized formulation was checked for size, polydispersity index (PDI), % light transparency, viscosity, osmolality and pH. Moreover, we have examined *in vitro*

cytotoxicity on both human retinal pigment epithelial cells (D407 cells) and human corneal epithelial cells (HCEC).

7.2 Methods

7.2.1 Nanomicelle Preparation

T1 encapsulated nanomicelles were prepared using solvent evaporation film hydration methods, see section 5.3.1 for method.

7.2.2 Solubility Determination using HPLC

We analyzed and quantified the samples by reversed-phase HPLC (RP-HPLC). Also, we applied Shimadzu UV/Vis detector (SPD-20AV), Alcott autosampler (model 718 AL), Phenomenex C8 column (spherisorb 250x4.60 mm, 5µm), and Shimadzu LC pump (Waters Corporation, Milford, MA) for this HPLC analyses. We carried out detection and separation of samples utilizing a gradient method developed in HPLC with the mobile phase containing methanol (40%-60%) and water. The flow rate and UV detector remained at 0.5 ml/min and 252 nm, respectively. We calibrated samples using standard curve (1.5 to 200 µg/mL) of T1.

7.2.3 Design of Experiment (DOE)

Primarily we have investigated the two crucial factors: the amount or percentage of two polymers, HCO-40 and OC-40 and their effects on T1 solubility (Y) in nanomicelles. To understand the factors and interactions between these two factors that affect T1 solubilization in nanomicelles, we employed a response surface design with full factorial design combining two degrees with continuous factors. We selected the student version of JMP® 13.0 software (SAS Institute, USA) to develop the experimental design and analyze the data. The study consisted of X1 (HCO-40) and X2 (OC-40), which

served as independent variables and solubility (Y) served as a dependent variable. The design had eight runs including two times repeat (Table 7-1). HCO-40 assigned as a continuous factor ranging from 0.5-2 % while OC-40 continuously varied from 0.1-0.5%. We utilized the response surface design with full factorial, which provides the value only inside the box.

Statistical Analysis: JMP 13.0 software student version was selected to perform the experimental design and data analysis. We investigated the proportional effect of two polymers (HCO-40 and OC-40) on dependent variables (solubility (mg/mL) with statistical models. Then we predicted the interactive and polynomial influences depending on the outcome the fit model (Eq.6-1) and evaluated their influence on the response variable (Y)

$$Y = b_0 + b_1 X1 + b_2X2 + b_3 X1X2 + b_4 X1X1 + b_5 X2X2 \text{ (Eq. 6-1)}$$

Where Y is response outcome, b_0 denotes intercept, b_1, b_2, b_3, b_4, b_5 represent the regression coefficients for factors X1, X2, interaction X1 and X2, interaction X1 and X1, interaction X2 and X2, respectively. X1 denotes amount of HCO-40 and X2 represents amount of OC-40. X1X1 and X1X2, X2X2 are polynomial terms of individual effects which represent the polymer 1- polymer 1, polymer 1 -polymer 2 and polymer 2 -polymer 2 interactions.

We utilized one-way analysis of variance (ANOVA) to evaluate the results from DOE. We determined the important relationship between dependent and independent variables using *F*-test at $\alpha = 0.05$. The t-test identified significant factors and interactions at 95% significance level. We calculated a regression model with the help of R^2 and

adjusted R^2 values. We established validation by checking model assumptions and summary of fit. The JMP 13.0 software student version did statistical analysis.

7.2.4 Steepest Ascent

As mentioned previous, steepest ascent should be applied to rapidly move the initial estimate to optimum region which can maximize the response outcome. All calculations were done according to the book "Design and Analysis of Experiments" by Douglas C. Montgomery. The fit model followed first model with single response, as shown in previous section with following equation:

$$Y=\beta 0 + \beta 1X1 + \beta 2X2 + \cdots + \beta kXk + \epsilon \text{ (Eq. 7-1)}$$

Where Y: response variable, X1, X2,…..Xk: independent factors

β0, β1, β2, ….., βk: regression coefficients for first-order polynomial

The path of steepest ascent is defined and continuous increase with the constant step size (parallel) from the center point where we assume the X1= X2= …. =Xk =0. We called this point as the original or base point. For steepest ascent, the scientists have used coded unit and uncoded unit or physic unit (real value) for processing data. The central point is considered as 0.000 for coded unit. And the physic unit of central point is the central point true value. From this central point, the basic step size (Δ) has been added to move along the path of steepest ascent.

The following procedure shows all steps to calculate in steepest ascent and move from small region to optimum region in details:

Step 1: Select the step size of standard variable ΔXj, Calculate the step size of other variables ΔXi:

The step size of standard variable ΔXj was selected subjectively based on how fast we want to move from the center to optimum region, calculate the step size of other variables ΔXi following the equation 7-2 (Eq. 7-2):

$\Delta Xi = \beta i / (\beta j / \Delta Xj)$ (Eq. 7-2)

Where i, j =1,2 3, 4….,k; i≠j: independent factor and j is chosen as a standard variable or known factor.

Step 2: Calculate the $X^n c(i)$ coded variables based on coded standard variable $X^n c(j)$

$X^n c(j)$ coded variable of independent factor j at n step size. $X^n c(j) = origin + n * \Delta$

$X^n c(i)$ coded variable of independent factor i at n step size, n = 1, 2, 3,….,n

$X^n c(i)$ was calculated by equation 7-3 (Eq. 7-3):

$$X^n_{c(i)} = \frac{\beta i}{\beta j / X^n_{c(j)}} \quad \text{(Eq. 7-3)}$$

Where βi, βj: regression coefficients of independent factor i, j; i, j =1, 2 3, 4…., k; i≠j: independent factor and n: the step size level; n = 1, 2, 3,….,n

Step 3: Calculate the uncoded $X^n p(i)$ and uncoded $X^n p(j)$ or physical unit variables:

1. Convert coded $X^n c(j)$ to Uncoded $X^n p(j)$ follow equation 7-4 (Eq. 7-4)

$X^n p(j) = X^{(n-1)} p(j) + X^n c(j)$ (Eq. 7-4)

Where $X^n p(j)$: uncoded variable (physical unit) of independent factor j at n step size. n = 1, 2, 3,….,n

$X^n p(i)$: uncoded variable (physical unit) of independent factor i at n step size, n = 1, 2, 3,….,n

i, j =1,2 3, 4….,k; i≠j: independent factor and n: the step size level

2. Convert uncoded $X^n p(i)$ to Uncoded $X^n p(i)$ follow equation 7-5 (Eq. 7-5)

$$X_p^n(i) = X_p^{(n-1)}(i) + \frac{Xpi(+1) - Xpi(0)}{Xci(+1) - Xci(0)} * \Delta \text{ Xi} \quad \text{(Eq. 7-5)}$$

Where $X^n p(i)$: uncoded variable (physical unit) of independent factor i at n step size, n = 1, 2, 3,….,n

$X^{(n-1)} p(i)$: uncoded variable (physical unit) of independent factor i at (n-1) step size

Xpi(+1): physical value of independent factor i at high level

Xpi(0) physical value of independent factor i at central level

Xci(+1) coded value of independent factor i at high level; Xci(+1) = +1 = constant

Xci(0) coded value of independent factor i at central level; Xci(0) =0 = constant

$\Delta Xi = \beta i / (\beta j / \Delta Xj)$ (Eq. 7-2)

Step 4: Calculate the predicted response coded and uncoded

With new coded and uncoded variables, the coded and uncoded predicted response are calculated following the first order polynomial

$$Y=\beta 0 + \beta 1X1 + \beta 2X2 + \cdots + \beta kXk + \epsilon \text{ (Eq. 7-1)}$$

Where Y: response variable, X1, X2,…..Xk: independent factors

β0, β1, β2, ….., βk: regression coefficients for first-order polynomial

7.2.5 Micellar Size, Polydispersity Index and Surface Potential

See section 5.3.6 for method.

7.2.6 Viscosity

See section 5.3.13 for method.

7.2.7 Dilution Effect

See section 5.3.9 for method.

7.2.8 Optical Clarity/ Appearance

See section 6.3.6 for method.

7.2.9 Osmolality and pH

See section 5.3.12 for method.

7.2.10 ^{1}H-NMR Spectroscopy of Blank NMF and T1 NMF

See section 5.3.15 for method.

7.2.11 In Vitro Cytotoxicity

See section 5.3.11 for method.

7.3 Results & discussion

7.3.1 HPLC Analysis:

The amount of T1 was determined using HPLC. The detection and separation was carried on gradient HPLC with the mobile phase containing methanol (40%-60%) and water. The flow rate set at 0.5 ml/min and UV detector was set at 252 nm. A calibration

standard curve (1.5 to 200 µg/mL) for T1 was constructed. As Fig. 7-1 showed the linear equation relationship between the amount of T1 (ug/ml) and area under curve. (Eq. 7-6)

$$y = 235104\ x + 783548,\ R^2 = 0.9992 \quad \text{(Eq. 7-6)}$$

The R^2 is a statistical measure of how close the data are able to the fitted regression line given. It shows a percentage of the response variable variation that is explained by a linear model. In this case the standard curve is linear with an excellent R^2 (>0.99).

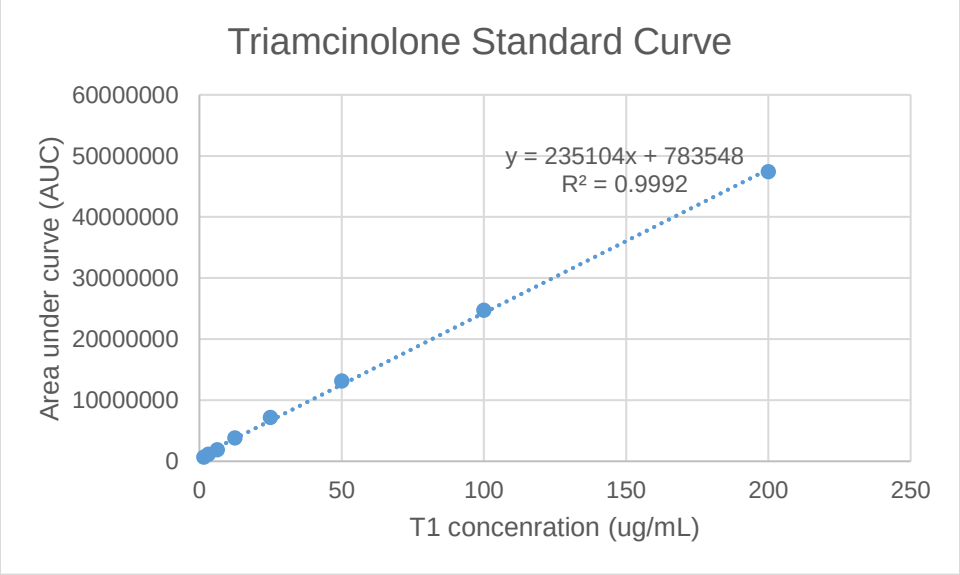

Figure 7- 1: HPLC Triamcinolone Standard Curve

7.3.2 Design of Experiment (DOE1) and T1 Solubility

In this study, a full factorial with two level of two continuous factor, (2^2 runs) was selected to screen the independent factors for dependent variables. The T1 solubility was determined using HPLC with the above method. The design runs (coded and uncoded) and corresponding variables are summarized in Table 7-1. The design had eight runs with repeated. HCO-40 was continuous factor and ranged from 0.5-2 % while OC-40 continuously ranged from 0.1-0.5%.

Table 7-1: Design of Experiment (DOE) 1 Runs Coded, Uncoded Designs

Run No.	Pattern	HCO-40 (%)	OC-40 (%)	DOE1 Solubility (mg/ml)
1	--	0.50	0.10	0.074
2	-+	0.50	0.50	0.089
3	+-	2.0	0.10	0.089
4	++	2.0	0.50	0.101
5	--	0.50	0.10	0.074
6	-+	0.50	0.50	0.092
7	+-	2.0	0.10	0.009
8	++	2.0	0.50	0.109

T1 solubility ranged from 0.0735 to 0.109 mg/mL. Among all runs, the highest solubility of T1 was 0.109 mg/mL, run no. 8 and 4 (coded ++) with 2% HCO-40 and 0.5% OC-40. T1 solubility was markedly higher at HCO-40 were at high level. Apparently, the amount of HCO-40 has more effect on T1 solubility than OC-40. Statistical analysis was applied to analyze the data. The software analyzed and gave the similar results. The fit model is given by Eq.7-7.

$$Y= 0.0896963 + 0.0075988\ X1 + 0.0082513\ X2 -0.000346\ X1X2 \quad \text{(Eq.7-7)}$$

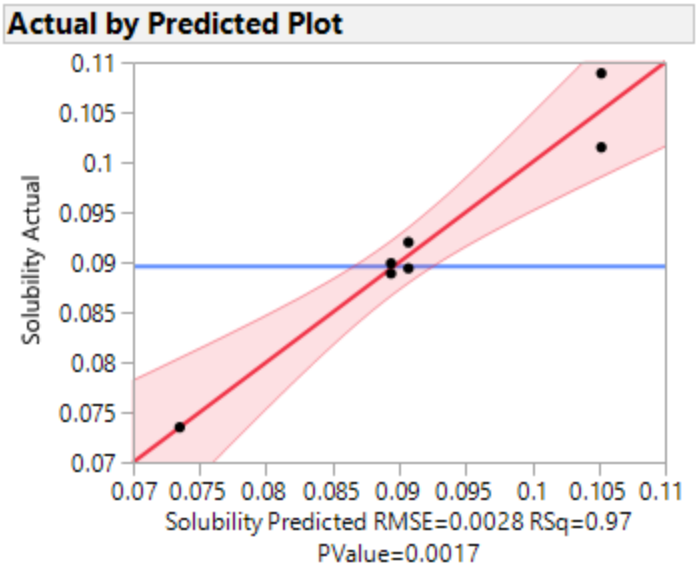

Figure 7- 2: Actual by Predicted Plot DOE1 of T1 NMF

The model was validated based on the actual by predicted plot Fig. 7-2. Statistical parameters for the fit model including Parameter Estimates, ANOVA for the fit model, summary of fit, lack of fit, effect tests and effect summary are summarized in Fig. 7-3. The fit model was found to be significant based on the *p*-value (p = 0.0017), R^2 = 0.969865 and adjusted R^2= 0.947263. R^2 is the correlation coefficient for the regression model. It shows 97% model can explain the variation in T1 solubility. Also, the lack of fit suggested that the model was significant and could predict T1 solubility. According to effect summary and parameter estimates, statistical significant factor was the amount of HCO-40 (X1, p= 0.0015) and OC-40 (X2, p= 0.0011). Another estimated coefficient for each factor and interaction between factors associated *p* value are presented in effect test and effect summary. From the model, HCO-40 and OC-40 interaction (X1X2, p=0.7439). Only the estimated coefficients with $p < 0.05$ were considered to be significant. X1X2 had a negative effect on T1 solubility while X1 (HCO-40) and X2

(OC-40) had positive effect on T1 solubility. As mentioned above, solubility of T1 increase at higher level of amount of HCO-40.

Effect Tests

Source	Nparm	DF	Sum of Squares	F Ratio	Prob > F
HCO-40(0.5,2)	1	1	0.00046193	59.0205	0.0015*
OC-40(0.1,0.5)	1	1	0.00054467	69.5919	0.0011*
HCO-40*OC-40	1	1	0.00000096	0.1225	0.7439

Effect Summary

Source	LogWorth	PValue
OC-40(0.1,0.5)	2.947	0.00113
HCO-40(0.5,2)	2.811	0.00154
HCO-40*OC-40	0.128	0.74395

Parameter Estimates

Term	Estimate	Std Error	t Ratio	Prob>|t|
Intercept	0.0896963	0.000989	90.68	<.0001*
HCO-40(0.5,2)	0.0075988	0.000989	7.68	0.0015*
OC-40(0.1,0.5)	0.0082513	0.000989	8.34	0.0011*
HCO-40*OC-40	-0.000346	0.000989	-0.35	0.7439

Analysis of Variance

Source	DF	Sum of Squares	Mean Square	F Ratio
Model	3	0.00100755	0.000336	42.9117
Error	4	0.00003131	7.827e-6	Prob > F
C. Total	7	0.00103886		0.0017*

Summary of Fit

RSquare	0.969865
RSquare Adj	0.947263
Root Mean Square Error	0.002798
Mean of Response	0.089696
Observations (or Sum Wgts)	8

Figure 7- 3: Statistical Summary of DOE1 of T1 NMF Optimization

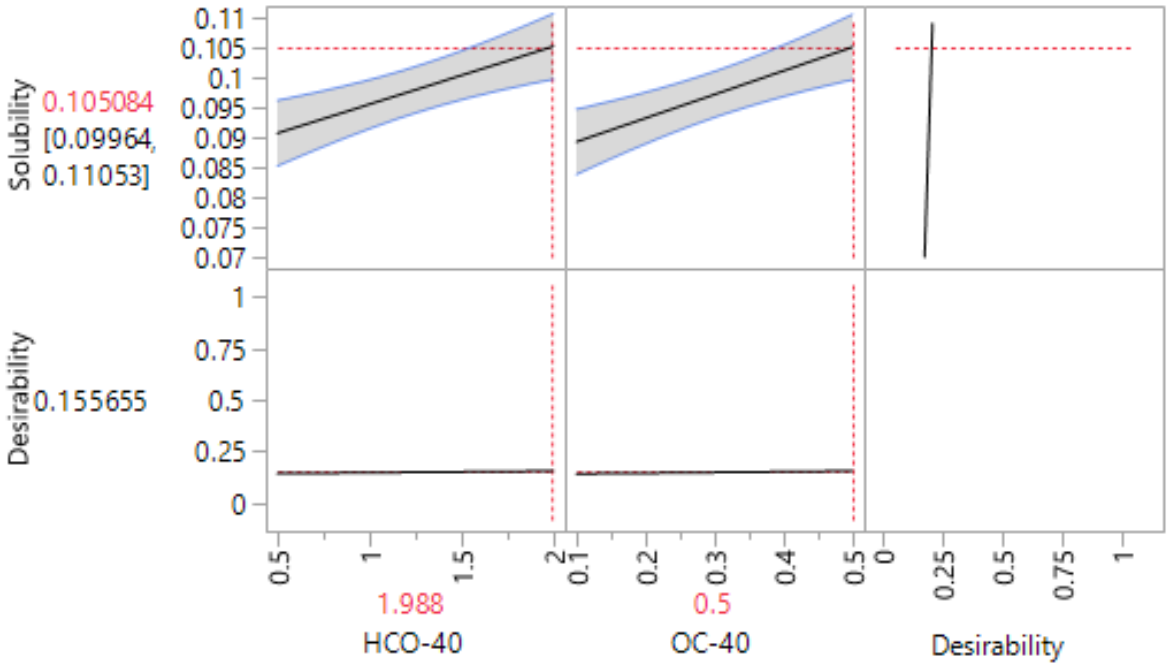

Figure 7- 4: Prediction Profiler of T1 DOE1

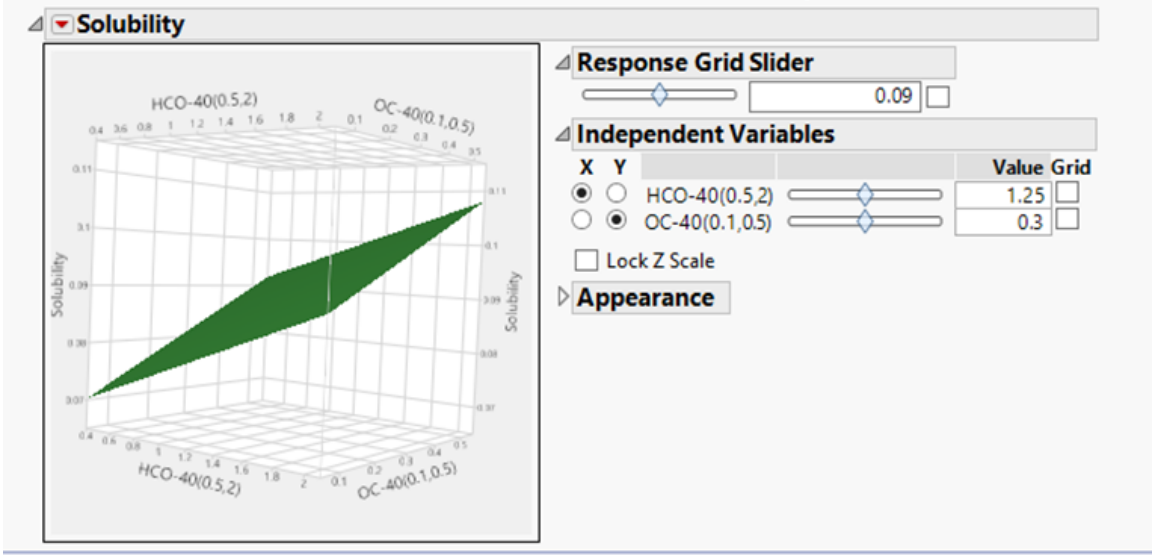

Figure 7- 5: Surface Response of T1 DOE1

The response surface curve provides a diagrammatical representation of T1 solubility as a function of the amount of HCO-40 and OC-40 in the prediction profiler (Fig. 7-4). The prediction profiler was generated to determine the optimal point with highest desirability. It also predicts the combination effects of variables at different levels. As anticipated, increase the amount of HCO-40 and OC-40 the T1 solubility will increase since the amount of HCO-40 and OC-40 had positive effect on the T1 solubility. Based on the prediction profiler, HCO-40 2% and OC-40 0.5% produced the highest T1 solubility with highest desirability. The predicted solubility is 0.1052 mg/mL. This value is very close to the actual value which was run no. 4 and 8. Based on the graph, the T1 solubility followed the first order response. The surface response can allow us to predict higher solubility with various amounts of polymers (Fig 7-5). This solubility may rise higher since the curve is very linear. This is the reason for the steepest ascent to be utilized. Steepest ascent is recommended for moving sequentially in the direction of

maximum escalation in the response or T1 solubility (Fig. 7-6). The DOE2 is another experimental design after applying steepest ascent.

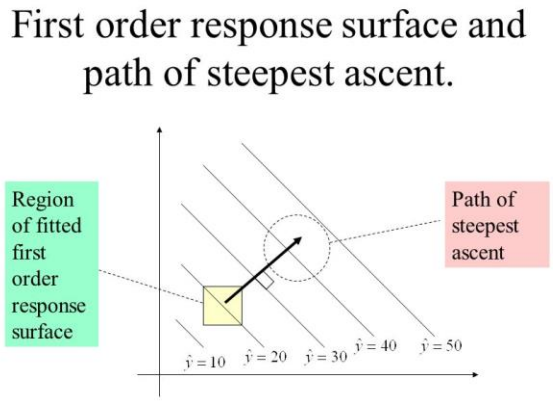

Figure 7- 6: Path of Steepest Ascent

7.3.3 Steepest Ascent Steps and T1 Solubility

As mentioned above, steepest ascent was used to maximize the T1 solubility in nanomicelles (Fig. 7-6). Based on DOE1, both HCO-40 and OC-40 have effect on T1 solubility and the fit model followed first model with single response, as shown in previous section with following equation:

$Y=\beta 0 + \beta 1X1 + \beta 2X2$ (Eq. 7-1 modified in this case, only 2 factors)

Where Y: response variable T1 solubility, X1, X2: independent factors

β0, β1, β2: regression coefficients for first-order polynomial

For steepest ascent, scientists have used coded unit and uncoded unit or physic unit (real value) for processing data. The central point was considered as 0.000 for coded unit. From this central point, the basic step size (Δ) has been added to move along the

path of steepest ascent. This step the coded variables and uncoded variables have been calculated based on the step size of increase (Δ).

Table 7- 2: Coded and Uncoded Levels of Factors X1 And X2

Level	Low	Central Point	High
Coded	-1	0	+1
X1 (HCO-40)	0.50%	1.25%	2.0%
X2 (OC-40)	0.10%	0.30%	0.50%

Table 7-2 showed levels of factors X1 and X2 or polymers HCO-40 and OC-40 at low high and central point.

The central point with coded unit of X1 and X2 is 0 or 0.000 while the uncoded central point of X1 is 1.25% and X2 is 0.3%. In this calculation, X1 was chosen as standard variable and other variable X2 calculated according to X1. Based on the linear equation (Eq. 7-7), if rising X1 and X2, Y will increase.

The following calculations showed how the data in Table 3 were calculated. Hence, we used the black bond region where 1 step increases, and 2 step increases as the example.

Step 1: Choose the step size of standard variable ΔX1, Calculate the step size of other variables ΔX2.

In this experiment, the first-order model of solubility was presented as uncoded:

$Y= 0.0896963 + 0.0075988\ X1 + 0.0082513\ X2$ (Eq. 7-7 modified)

The step size of X1: ΔX1 = 0.100 (objective chosen since we want to increase or maximize Y)

Apply Eq. 7-2, $\Delta X2 = \frac{\beta 2}{\beta 1/\Delta X1}$ where β1 =0.0075988, β2 =0.0082513

The step size of X2: $\Delta X2 = \frac{0.0082513}{0.0075988/0.1} = 0.1086$

Step 2: Calculate the $X^n c(2)$ coded variables based on coded standard variable $X^n c(1)$

For example, β1 =0.0075988, β2 =0.0082513

For 1 Δ step increase n=1, Coded $X^1c(1)$= origin + Δ= 0.000 + 0.100 = 0.1 for independent factor X1, apply Eq. 7-3 to calculate coded $X^1c(2) = \frac{0.0082513}{0.0075988/0.1}$ =0.1086 independent factor X2

For 2 Δ step increase n=2, Coded $X^2c(1)$= origin + 2Δ= 0.000 + 2x 0.100 = 0.2 for independent factor X1, apply Eq. 7-3 to calculate coded $X^2c(2) = \frac{0.0082513}{0.0075988/0.2}$ =0.2172 independent factor X2

Step 3: Calculate the uncoded $X^n p(1)$ and uncoded $X^n p(2)$ or physic unit variables:

1. Convert coded $X^n c(1)$ to uncoded $X^n p(1)$ follow Eq. 7-4

Apply Eq. 7-4 to calculate Xp1, physical unit or uncoded variables

For 1 Δ step increase, physical value or uncoded variables $X^1p(1) = X^0p(1) + X^1c(1)$ = 1.25% + 0.100 = 1.35 (%)

For 2 Δ step increase, that mean 1 Δ step increase from the previous (X^1p1) , physical value or uncoded variables $X^2p(1) = X^1p(1) + X^2c(1)$ = 1.35% + 0.200 = 1.55 (%)

2. Convert uncoded $X^np(1)$ to uncoded $X^np(2)$ follow Eq. 7-5

$$X_p^n(i) = X_p^{(n-1)}(i) + \frac{Xpi(+1)-Xpi(0)}{Xci(+1)-Xci(0)} * \Delta \text{ Xi} \quad \text{(Eq. 7-5)}$$

Where Xpi(+1) = 0.5%; Xpi(0) = 0.3%; Xci(+1) = +1; Xci(0) = 0

Therefore, Eq. 7-5 could be re-written as:

$$X_p^n(i) = X_p^{(n-1)}(i) + \frac{0.5-0.3}{+1-0} * \Delta \text{ Xi} \quad \text{(Eq. 7-5 modified)}$$

ΔXi= βi/ (βj/ΔXj) (Eq. 7-2)

For 1 Δ step increase, apply Eq. 7-5 modified where ΔXi = 0.1086, Physical value of $X^1p(2)$ = 0.3 + 0.2x 0.1086 = 0.32172 (%)

For 2 Δ step increase, apply Eq. 7-5 modifed ΔXi = 0.2172, physical value of $X^2p(2)$ = 0.32172 + 0.2x0.2172 = 0.3652 (%)

Step 4: Calculate the coded and uncoded predicted response

In this experiment, the first-order model of solubility was presented

Y= 0.0896963 + 0.0075988 X1 + 0.0082513 X2 (Eq. 7-7- modified)

For example

For 1 Δ step increase, $X^1c(1)$ = 0.1000, $X^1c(2)$ = 0.1086; predicted response coded: Y = 0.0896963 + 0.0075988 (0.1000) + 0.0082513 (0.1086) = 0.09152163

For 2 Δ step increase, $X^2c(1) = 0.2000$, $X^2c(2) = 0.2172$; predicted response coded: $Y = 0.0896963 + 0.0075988 (0.2000) + 0.0082513 (0.2172) = 0.093008026$

Similar with uncoded predicted response

For 2 Δ step increase, $X^2p(1) = 1.5500$, $X^2p(2) = 0.3652$; predicted response uncoded: $Y = 0.0896963 + 0.0075988 (1.5500) + 0.0082513 (0.3652) = 0.10448742$

Table 7- 3: Steepest Ascent Calculations for Coded, Uncoded Variables and Predicted Response Value

	Coded level variables ($X^n c$)		UnCoded Variables in units ($X^n p$)		Predicted response (Solubility) (Y)	
Steps	**X1 ($X^n c(1)$)**	**X2 ($X^n c(2)$)**	**X1 (%) ($X^n p(1)$)**	**X2 (%) ($X^n p(2)$)**	**Coded ($Y^n c$)**	**Uncoded ($Y^n p$)**
Origin	0.0000	0.0000	1.2500	0.3000	0.0896963	0.10167019
Δ	0.1000	0.1086	0.1000			
Origin +1Δ n =1	**$X^1 c(1)$= 0.1000**	**$X^1 c(2)$= 0.1086**	**$X^1 p(1)$ = 1.3500**	**$X^1 p(2)$ = 0.3217**	**0.091352163**	**0.102609267**
Origin +2Δ n =2	**$X^2 c(1)$ = 0.2000**	**$X^2 c(2)$ = 0.2172**	**$X^2 p(1)$ = 1.5500**	**$X^2 p(2)$ = 0.3652**	**0.093008026**	**0.10448742**
Origin +3Δ	0.3000	0.3258	1.8500	0.4303	0.094663889	0.10730465
Origin +4Δ	0.4000	0.4343	2.2500	0.5172	0.096319752	0.111060956
Origin +5Δ	0.5000	0.5429	2.7500	0.6258	0.097975615	0.115756339
Origin +6Δ	0.6000	0.6515	3.3500	0.7561	0.099631478	0.121390798
Origin +7Δ	0.7000	0.7601	4.0500	0.9081	0.101287341	0.127964334
Origin +8Δ	0.8000	0.8687	4.8500	1.0818	0.102943204	0.135476947
Origin +9Δ	0.9000	0.9773	5.7500	1.2773	0.104599066	0.143928636
Origin +10Δ	1.0000	1.0859	6.7500	1.4945	0.106254929	0.153319402
Origin +11Δ	1.1000	1.1945	7.8500	1.7333	0.107910792	0.163649245
Origin +12Δ	1.2000	1.3030	9.0500	1.9940	0.109566655	0.174918164
Origin +13Δ	1.3000	1.4116	10.3500	2.2763	0.111222518	0.18712616
Origin +14Δ	1.4000	1.5202	11.7500	2.5803	0.112878381	0.200273232
Origin +15Δ	1.5000	1.6288	13.2500	2.9061	0.114534244	0.214359381

Origin +16Δ	1.6000	1.7374	14.8500	3.2536	0.116190107	0.229384606
Origin +17Δ	1.7000	1.8460	16.5500	3.6228	0.11784597	0.245348908
Origin +18Δ	1.8000	1.9546	18.3500	4.0137	0.119501833	0.262252287
Origin +19Δ	1.9000	2.0632	20.2500	4.4263	0.121157696	0.280094742
Origin +20Δ	2.0000	2.1717	22.2500	4.8606	0.122813559	0.298876274
Origin +21Δ	2.1000	2.2803	24.3500	5.3167	0.124469422	0.318596882
Origin +22Δ	2.2000	2.3889	26.5500	5.7945	0.126125285	0.339256567
Origin +23Δ	2.3000	2.4975	28.8500	6.2940	0.127781148	0.360855328
Origin +24Δ	2.4000	2.6061	31.2500	6.8152	0.129437011	0.383393166
Origin +25Δ	2.5000	2.7147	33.7500	7.3581	0.131092874	0.406870081

From DOE1, the fit model equation first order is

Y= 0.0896963 + 0.0075988 X1 + 0.0082513 X2 (Eq. 7-7 modified)

The steepest ascent has been calculated in the Table 7-3 where the solubility has been increased when the amount of HCO-40 and OC-40 increase. However, the amount of polymer may be limited due to potential cytotoxicity, side effects as well as the economic consideration. The amount of HCO-40 and OC-40 in the range 3% to 6% gave better than expected results. Even further increasing polymer, the solubility increased but slowly. DOE2 has been designed with HCO-40 3% - 6% while OC-40 ranged from 0.7%-1.5%. In this study, a central composite design with two level of two continuous factor, two center points along with axial value for rotatable 1.414 was selected to screen the independent factors for dependent variables.

7.3.4 Design of Experiment (DOE2) and T1 Solubility

DOE2 was modified from DOE1 to maximize the solubility of T1 after applying steepest ascent. Fig. 7-7 showed HCO-40 ranged from 3% - 6% ad OC-40 ranged from 0.7% - 1.5%. Response surface design CCD has been utilized with 5 center point and Table 7-4 presented all the runs.

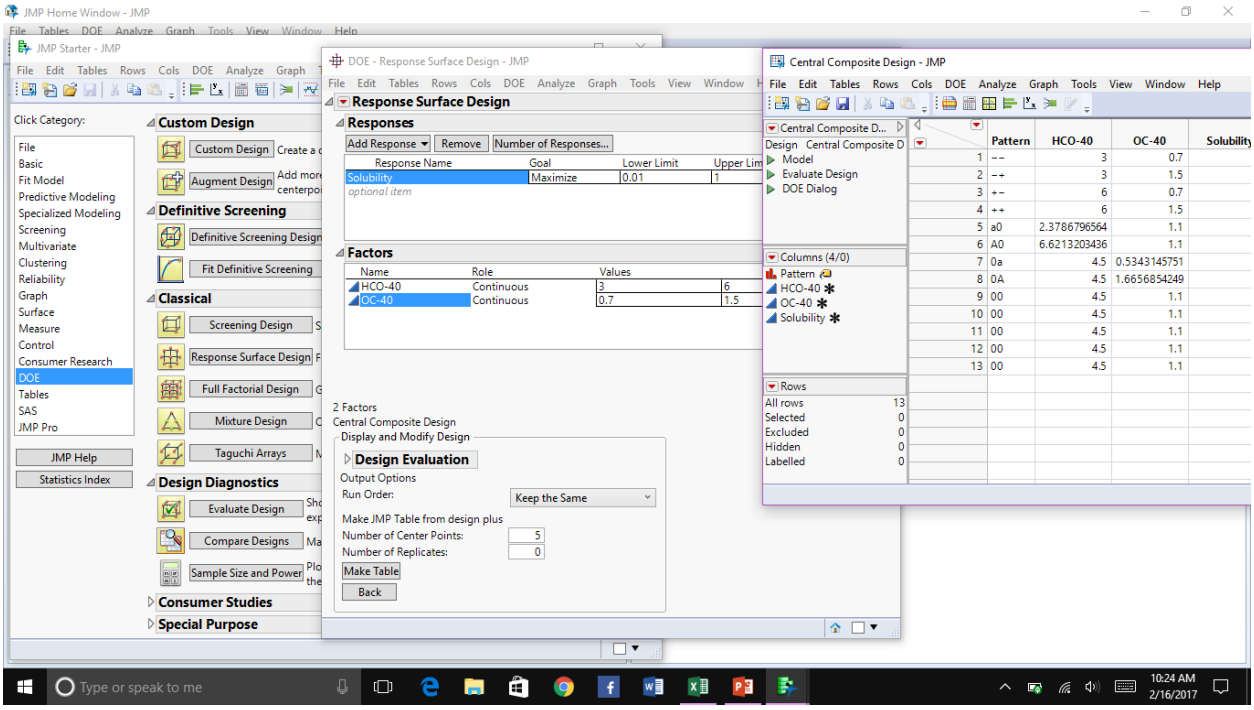

Figure 7- 7: DOE2 JMP

Table 7-4: DOE2 Runs and Solubility

Run No.	Pattern	HCO-40 (%)	OC-40 (%)	DOE2 Solubility (mg/ml)
1	−−	3.0	0.70	0.52
2	−+	3.0	1.50	0.42
3	+−	6.0	0.70	0.40
4	++	6.0	1.50	0.38
5	a0	2.37	1.10	0.39
6	A0	6.62	1.10	0.43
7	0a	4.50	0.53	0.39
8	0A	4.50	1.67	0.41
9	0	4.50	1.10	0.39
10	0	4.50	1.10	0.32
11	0	4.50	1.10	0.36
12	0	4.50	1.10	0.39
13	0	4.50	1.10	0.37

The design runs (coded and uncoded) and corresponding variables are summarized in Table 7-4. The design also had thirteen runs including 5 center points. HCO-40 was continuous factor and ranged from 3-6% while OC-40 continuously ranged from 0.7-1.5%. The response surface design has been utilized with the central composite design (CCD) which provide the value not only inside the box but outside of the box. The run a0, A0, 0a and 0A were the point outside of the range (< 3%, >6%, <0.7% and

>1.5%). T1 solubility ranged from 0.32 to 0.52 mg/mL. Among all the runs, the highest solubility of T1was 0.52 mg/mL, run no. 1 (coded --) where HCO-40 is at 3.0% and OC-40 0.70%. T1 solubility improved when the HCO-40 was at medium or low levels compared to high level. Apparently, the amount of HCO-40 has more effect on T1 solubility than OC-40. Statistical analysis was applied to data. And the software analyzed and gave the similar results. The fit model is given by Eq. 7-8.

Y= 0.366 – 0.011972 X1 - 0.010684 X2 + 0.023 X1X2 - 0.0290625 X1X1 + 0.0228125 X2X2 (Eq. 7-8)

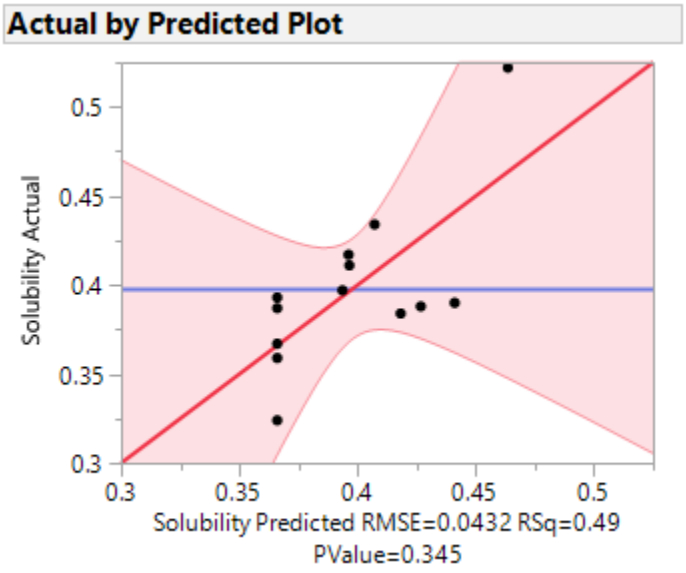

Figure 7- 8: Actual By Predicted Plot for DOE2 T1 NMF

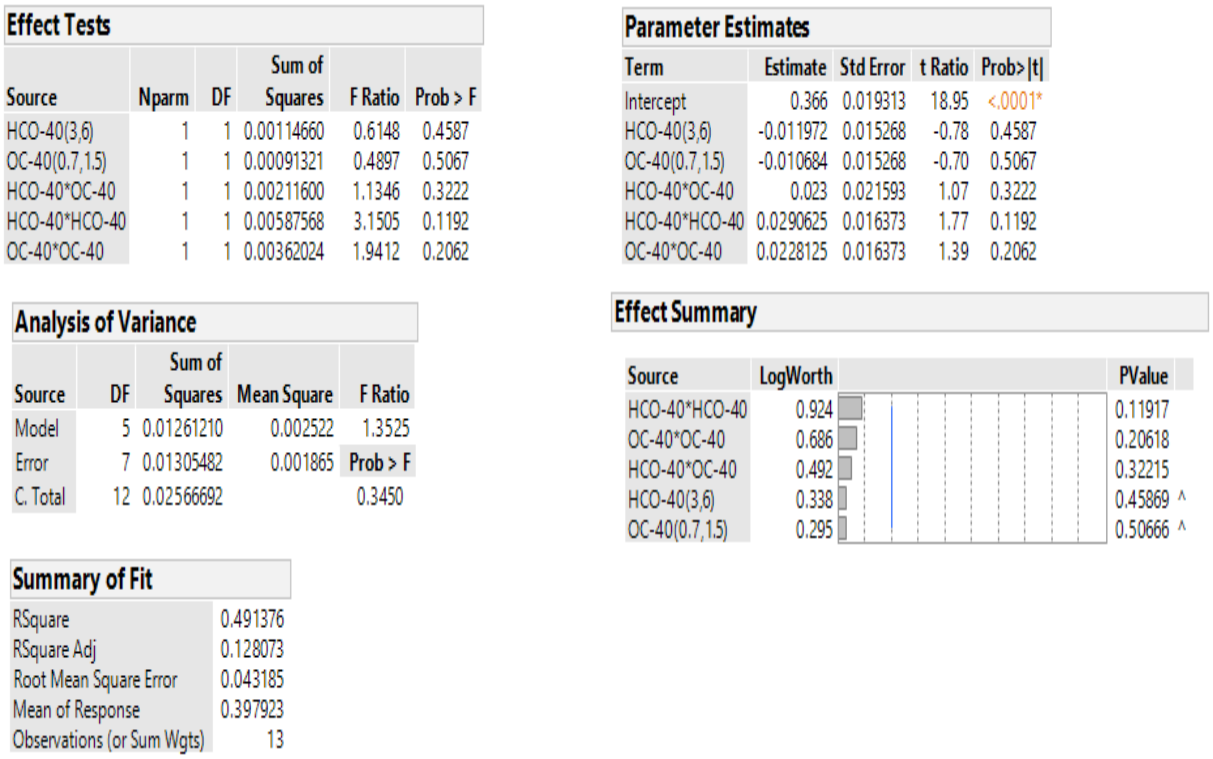

Effect Tests

Source	Nparm	DF	Sum of Squares	F Ratio	Prob > F
HCO-40(3,6)	1	1	0.00114660	0.6148	0.4587
OC-40(0.7,1.5)	1	1	0.00091321	0.4897	0.5067
HCO-40*OC-40	1	1	0.00211600	1.1346	0.3222
HCO-40*HCO-40	1	1	0.00587568	3.1505	0.1192
OC-40*OC-40	1	1	0.00362024	1.9412	0.2062

Parameter Estimates

Term	Estimate	Std Error	t Ratio	Prob>|t|
Intercept	0.366	0.019313	18.95	<.0001*
HCO-40(3,6)	-0.011972	0.015268	-0.78	0.4587
OC-40(0.7,1.5)	-0.010684	0.015268	-0.70	0.5067
HCO-40*OC-40	0.023	0.021593	1.07	0.3222
HCO-40*HCO-40	0.0290625	0.016373	1.77	0.1192
OC-40*OC-40	0.0228125	0.016373	1.39	0.2062

Analysis of Variance

Source	DF	Sum of Squares	Mean Square	F Ratio
Model	5	0.01261210	0.002522	1.3525
Error	7	0.01305482	0.001865	Prob > F
C. Total	12	0.02566692		0.3450

Effect Summary

Source	LogWorth	PValue
HCO-40*HCO-40	0.924	0.11917
OC-40*OC-40	0.686	0.20618
HCO-40*OC-40	0.492	0.32215
HCO-40(3,6)	0.338	0.45869 ^
OC-40(0.7,1.5)	0.295	0.50666 ^

Summary of Fit

RSquare	0.491376
RSquare Adj	0.128073
Root Mean Square Error	0.043185
Mean of Response	0.397923
Observations (or Sum Wgts)	13

Figure 7- 9: Statistical Parameter of DOE2 T1 NMF

The model was validated based on the actual by predicted plot (Fig. 7-8). Statistical parameters for the fit model including Parameter Estimates, ANOVA for the fit model, summary of fit, lack of fit, effect tests and effect summary are summarized in Fig. 7-9. The fit model was found not to be significant based on the *p*-value ($p = 0.3450$), $R^2 = 0.491376$ and adjusted $R^2 = 0.128073$. R^2 is the correlation coefficient for regression model. The model can explain 49% of the variation in T1 solubility. Also, the lack of fit suggested that the model was significant and could predict T1 solubility. According to effect summary and parameter Estimates, the statistical factors had negative effect on T1 solubility the amount of HCO-40 (X1, $p = 0.4587$) and interaction between HCO-40 HCO-40 (X1X1, $p = 0.1192$), the amount of OC-40 (X2, $p = 0.5067$), HCO-40 and OC-

40 interaction (X1X2, *p*= 0.3222), and OC-40 and OC-40 (X2X2, *p*= 0.2062). Only the estimated coefficients with p < 0.05 were considered to be significant. X2(OC-40).

The response surface curve provides a representation of T1 solubility as a function of the amount of HCO-40 and OC-40 in the prediction profiler (Fig. 7-10 and 7-11). The prediction profiler was generated to determine the optimal point with highest desirability. It also predicts the combination effects of variables at different levels. Even the model does not have very powerful to predict the solubility (*p*=0.345, R^2 =0.491376), the predicted solubility (0.462307 mg/mL) was very close to the actual one (0.522 mg/mL). This optimized nanomicelle formulation (HCO-40 3% and OC-40 0.7%) was carried for the nanomicelle formulation characterizations and for all the later studies.

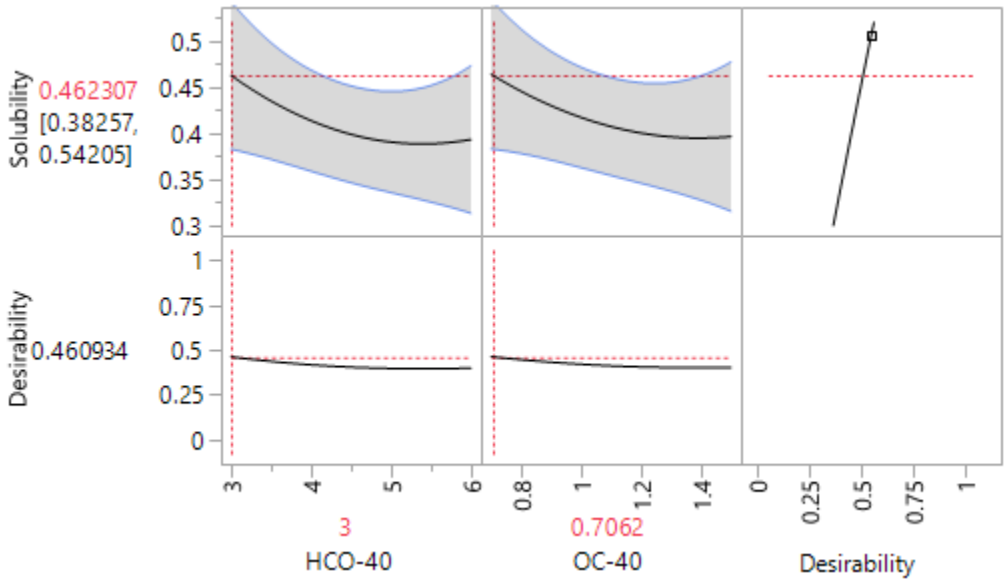

Figure 7-10: Prediction Profiler of DOE2 T1 NMF

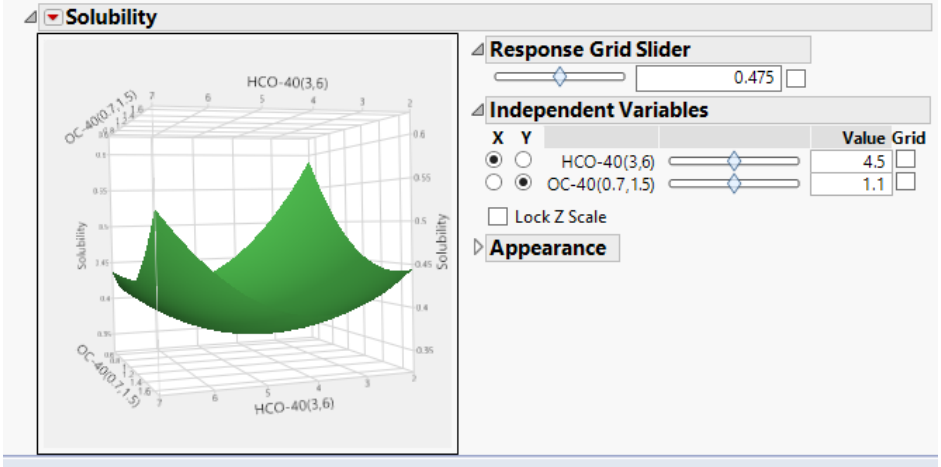

Figure 7- 11: Surface Response T1 DOE2

7.3.5 Micellar Size, Polydispersity Index (PDI) and Surface Potential

Nanomicellar size, polydispersity index (PDI), Zeta potential and size distribution were determined by dynamic light scattering (DLS) method. The results are summarized in Tables 7-5. All T1-loaded NMFs were in the size range around 18 nm with unimodel distribution irrespective of the T1 solubility and the DOE1 or DOE2. The blank NMFs also were prepared with method 1 and measured the size, PDI and summarized in Table 7-5. Fig. 7-12 and 7-13 illustrated the distribution of T1- loaded NMFs. The small size may sufficiently allow NMF to travel across ocular tissues such as scleral channels/pores, are in the size range between 20 and 80 nm[311]. The PDI of all runs bellow 0.5 surface charge was negligible. Such properties of nanomicelles may help to deliver T1 to back of the eyes by the conjunctival/ sclera pathway. The surface potential of all blank and T1-loaded NMFs did not have any charge on it (Table 7-5) 0.212 for blank NMF DOE2 and 0.126 for T1 NMF DOE2 was considered no charge or negligible. This charge will not cause any effect when nanomicelles across tissue membrane.

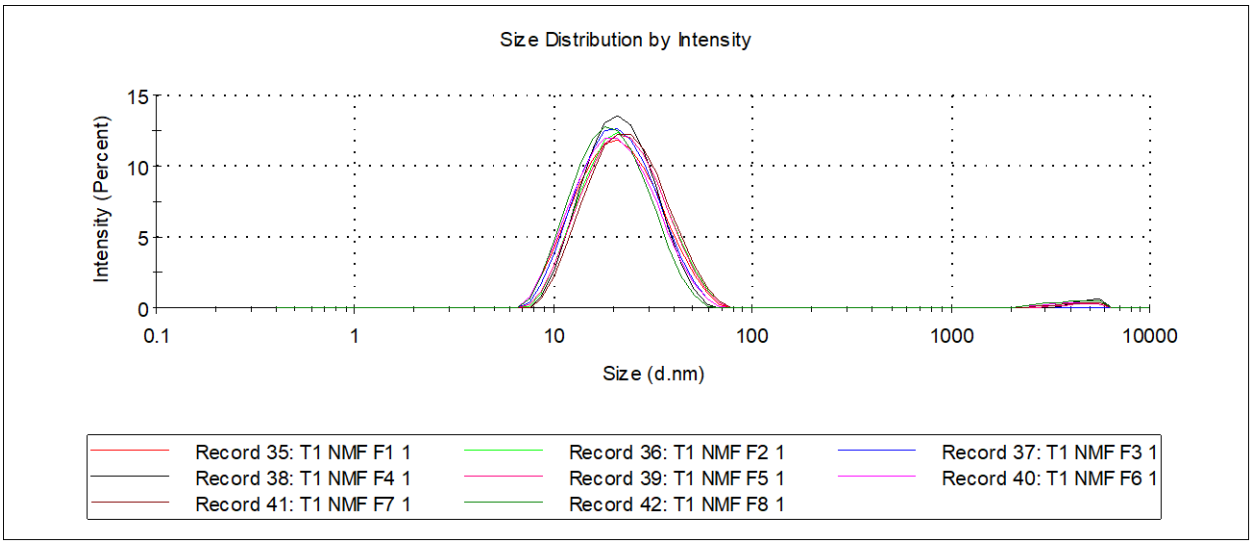

Figure 7-12: Size distribution of T1 NMF1 to T1 NMF8

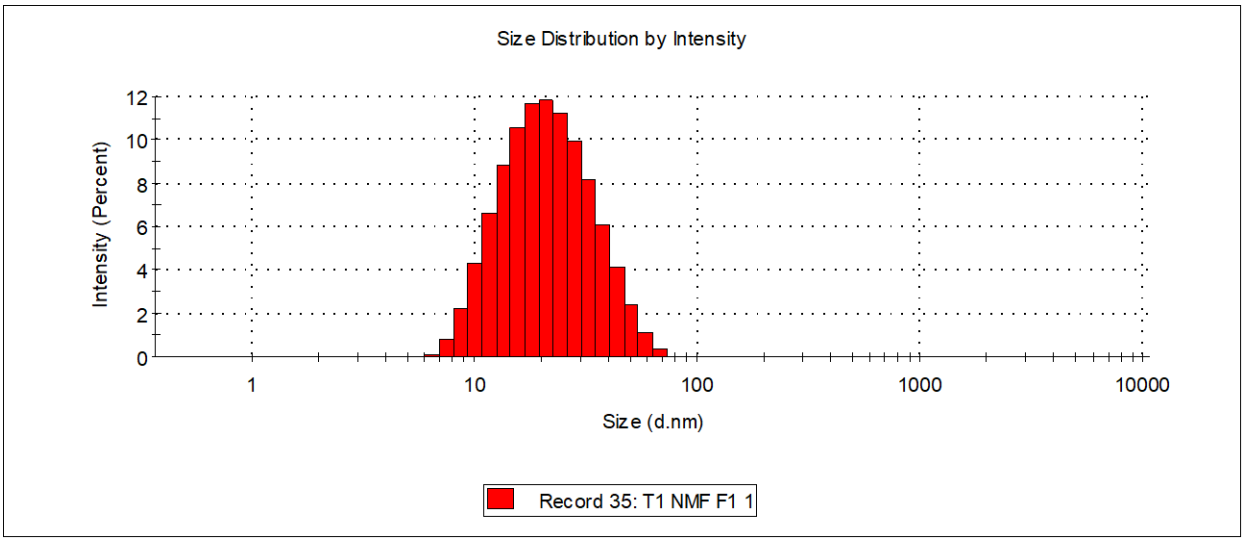

Figure 7-13: Size Distribution of Optimized T1 NMF

Table 7-5: Characterizations of Optimized T1 NMF

Formulation code	HCO-40 (wt%)	OCO-40 (wt%)	Size (nm)	PDI	Surface potential (mV)	T (%)
Blank T1 NMF DOE 2	3.0	0.70	18.72	0.109	0.212	98.5
T1 NMF DOE 2	3.0	0.70	18.35	0.126	0.139	98.0

7.3.6 Optical Clarity/Appearance

Optical appearance / clarity is defined as the ability of light to be transmitted 90% or more through a 1.0-cm path length at 400nm wavelength and compared with water. Due to the interference of particles, the light was scattered and give different angles. However, particles of extremely small size i.e. nanometers will not produce enough hindrance or light scattering results in a clear and transparent solution. T1 NMF is clear as water (Fig. 7-14) or transparent and more than 97% of light has been transmitted (Table 7-5). All NMFs can be compared with distilled deionized water measured by transmittance. Percentage light transmittance of optimized formulations (blank and T1 loaded NMF DOE1 and DOE2) at wavelength 400nm ranged from 97 % to 99 %. It was observed that there was no particle interfering with light scattering, the T1 NMF looks as clear as water. The nanomicelles helped improve the T1 solubility and formed clear, aqueous solution

Figure 7-14: Clarity of T1 NMF Compared with Water

7.3.7 Viscosity

The viscosity of optimized NMFs has been summarized in Table 7-6. The viscosity of formulations was 1.13 centipoise (Cp) for blank NMFs, and 1.25 Cp for T1 NMFs which are very close to water (0.89 Cp). This clear, aqueous formulation completely water like, which may help reduce the ocular irritation. NMFs produce viscosity well below critical point of 4.4 cP, such that the drainage rate is not affected [313]. However, high viscosity of formulation can have effect on its residence time in the cul-de-sac enhancing therapeutic effect. The viscosity of formulation may offer advantages due to longer residence in the cul-de-sac which may increase ocular absorption but again eye irritation should be considered carefully.

Table 7-6: Viscosity of Blank NMF Vs T1 NMF

Formulation code	HCO-40 (wt%)	OCO-40 (wt%)	Viscosity (cP)
Blank T1 NMF DOE 2	3.0	0.70	1.13
T1 NMF DOE 2	3.0	0.70	1.25

7.3.8 Dilution Effect

The dilution effect on NMF was investigated following the size and PDI and was summarized in Table 7-7. Since human eyes have many different mechanism and barriers to protect and prevent any harm from external particles from body. Major ocular barriers are static (corneal epithelium, corneal stroma, and blood–aqueous barrier) and dynamic barriers (blood-retinal barrier, conjunctival blood flow, lymph flow, and tear drainage). Tear drainage is one of those barriers that clear out much of topical application. Therefore, the stability of the NMF was studied upon the effect of dilution. The results shown in Table 7-7 was found that there is no significant effect on nanomicelle size and PDI with dilution up to 400 times. The size of NMF was slightly increased from 18.35 nm to 35.53 nm upon 400 dilution times. However, the tear secreted in the eye following topical administered should be less than 10 times dilution and FA NMF was very stable at that dilution factor, very close 19.62 nm. The formulation stability with dilution will help the formulation across the membrane as it is.

Table 7-7: Dilution Effect of Optimized T1 NMF

Dilution factor	Average size (nm)	PDI
0	18.35	0.119
10	19.62	0.154
20	26.51	0.218
50	31.21	0.223
100	31.33	0.254
200	32.03	0.207
400	35.53	0.322

7.3.9 Osmolality and pH

Osmolality is an important attribute for the topical eye drop formulation. The hyper-osmolality is a main pathogenic factor in dry eye [314]. The osmolality and pH of the NMF was adjusted similar to the tear pH ~ 6.8 with phosphate buffer as depicted in Table 7-8. Osmolality of T1 NMF was 385 mmol/L or mOsm/kg and pH was around 6.8. The physiological tear osmolality of 289 mOsm/L and osmolality of 290 mOsm is equivalent to 0.9% saline.

Table 7-8: Osmolality ond pH of Blank and T1 Optimized NMF

Formulation code	HCO-40 (wt%)	OCO-40 (wt%)	Osmolality (mmol/Kg)	pH
Blank T1 NMF DOE2	3.0	0.70	335	6.8
T1 NMF DOE2	3.0	0.70	385	6.8

7.3.10 ^{1}H NMR Characterization

As we have presented in many of our paper about the ^{1}H NMR spectral analysis of nanomicelle. The free drug molecules in nanomicelle solution was identified by ^{1}H NMR analysis at parts per million (ppm) levels. ^{1}H NMR studies were conducted for T1 in $CDCl_3$ to identify the corresponded resonance peaks of T1 to compare or serve as positive control. ^{1}H NMR studies of blank NMF in $CDCl_3$ and T1-loaded NMF in different solvent such as $CDCl_3$ and D_2O.

Similar with our previous papers, the resonance signals for T1 were absent when suspended T1 NMF in D_2O (Fig. 7-15). All T1 in solution was entrapped inside nanomicelles and there was no free/unentrapped T1 in the D_2O or water. Since amphiphilic polymers have encapsulated T1 inside the core which muted the NMR signal during micelle formulation. This explains the absence of T1 signal in D_2O.

There were obvious resonance peaks of T1 for the pure T1 in $CDCl_3$ and the similar corresponding peak of T1 was observed for T1 NMF in $CDCl_3$ (data not shown). The spectra indicated that T1 was presented in organic solvent ($CDCl_3$) where the reverse micelles was formed. However, there was no observable peak corresponding to T1 except

polymer peak for blank NMF in $CDCl_3$ (data not shown). T1 NMF was dissolved in both organic solvent and water, free T1 was presented only in organic solvent ($CDCl_3$) not in water (D_2O). That means no free T1 in T1 NMF solution and this T1 NMF will not cause any irritation for the eyes due to free T1 particles.

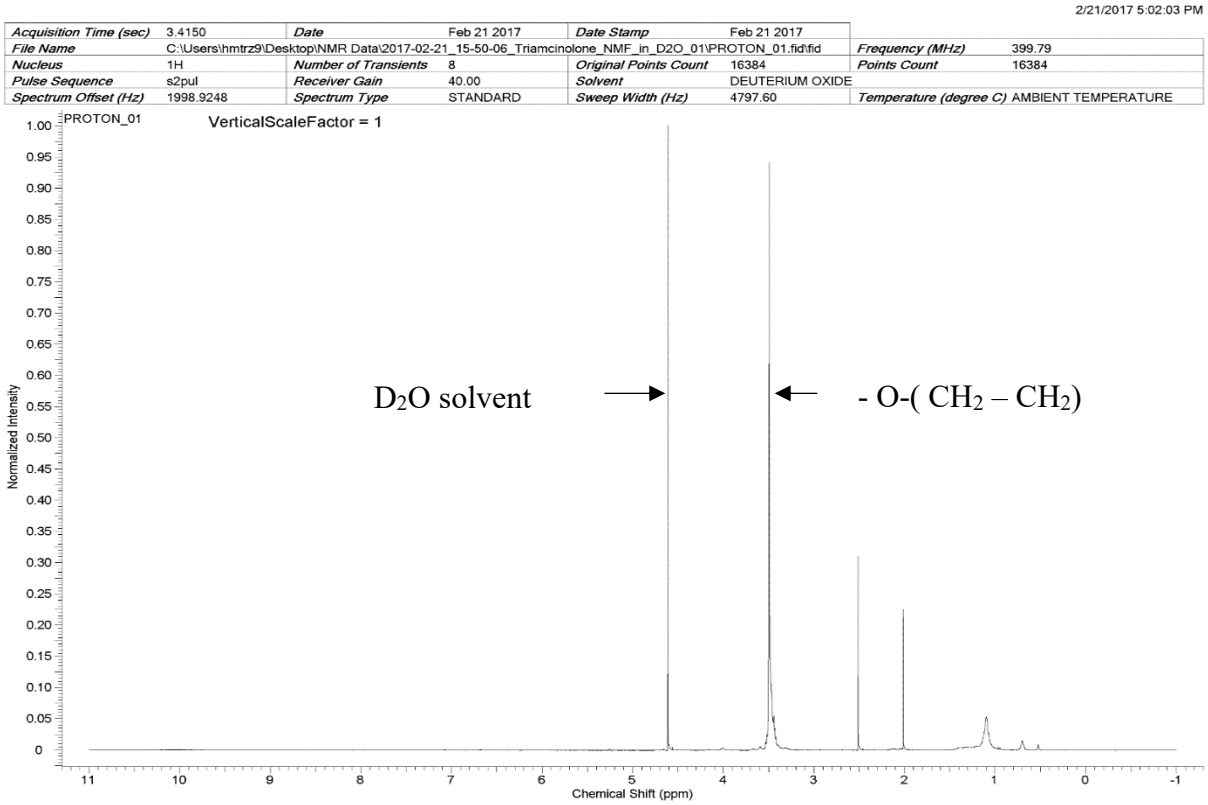

Figure 7-15: Proton NMR of T1 Optimized NMF in D_2O

7.3.11 In vitro Cytotoxicity

Following the topical administered, the formulations/solutions are rapidly washed (within 5 to 10 min) [312]. Previous results from our laboratory showed drug molecules in nanomicelles reaching back of the eye tissues (retina/choroid) [315] and we target back of the eyes disease. Therefore, cytotoxicity on human retinal pigment epithelial cells (ARPE-19) was performed for 1 h incubation period. The cytotoxicity of optimized

DOE1 blank and T1 loaded formulations were compared with medium and Triton-X 10%.

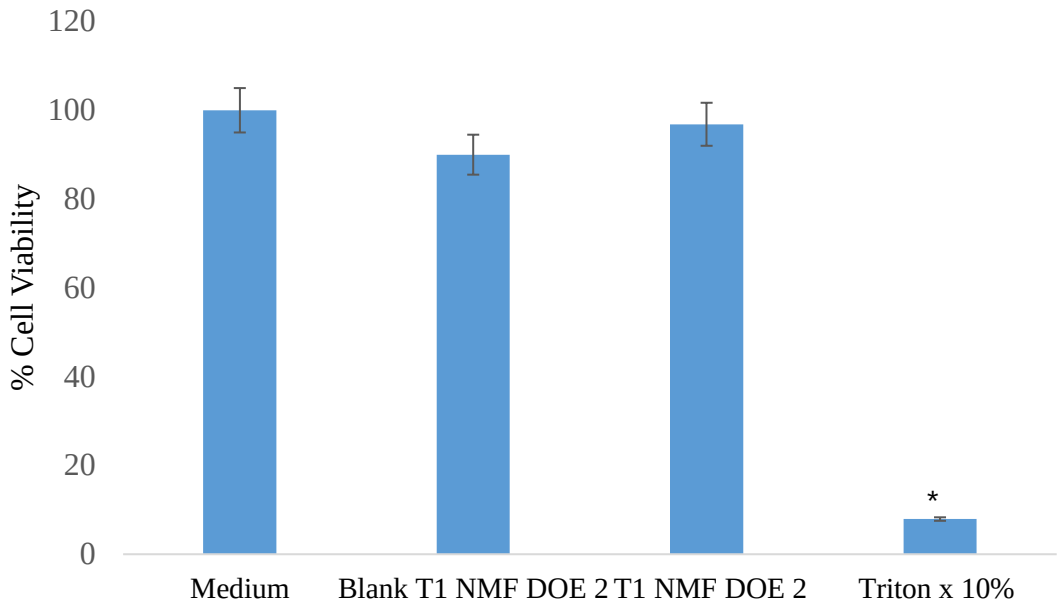

Figure 7- 16: MTT Cytotoxicity of Blank and T1 Optimized NMF on ARPE-19

MTT assay was conducted on ARPE-19 to check the cytotoxicity of NMFs. The medium was positive control while Triton X-100 10% was negative controls, the percentage of cell viability of all NMFs were recorded and plotted in Fig. 7-16. On ARPE 19 cell line, less than 10 % cell viability was observed with Triton X-100 while more than 90% cell viability was shown for both blank and T1-loaded NMFs relative to medium (100%).

In alternative study, both T1-loaded and blank NMFs were estimated for LDH cytotoxicity (Fig. 7-17). The amount of LDH released in the culture medium is directly proportional to the membrane damage and toxicity. Again, Triton-X 100 was served as positive control and medium as negative control. In this study NMFs were found to be

safe and doesn't showed any signs of cytotoxicity as compared to blank. These results clearly suggest that NMF do not cause cell death or harm to plasma membrane, the formulations are safe enough and well-tolerated for further *in-vivo* studies. On basis of above results and observations, these formulations are not toxic and safe for topical ocular application.

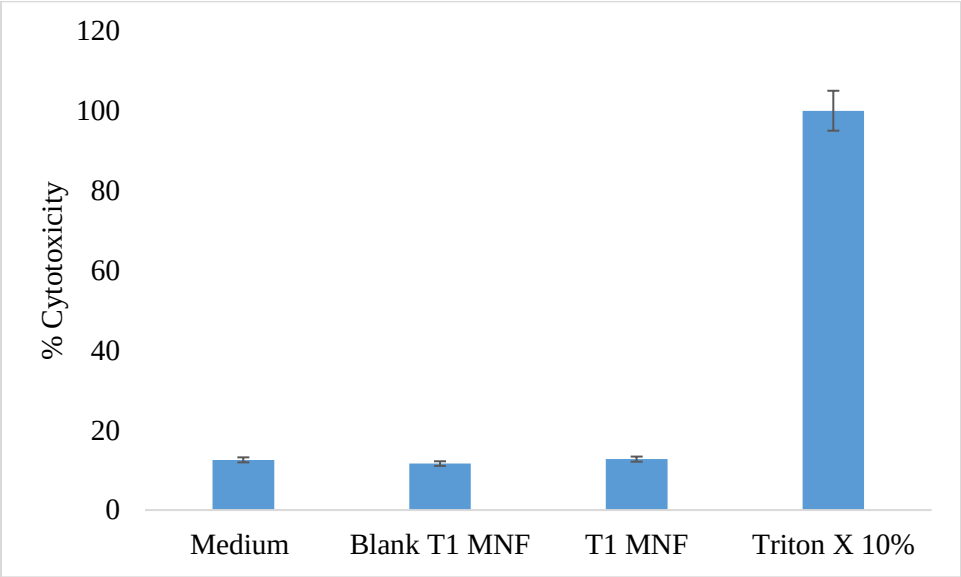

Figure 7- 17: LDH Cytotoxicity of Blank and T1 NMF on ARPE-19

7.4 Conclusion

In summary, we successfully incorporated T1 solubility and improved with nanomicellar technology. We prepared a clear, stable, aqueous T1-loaded NMF with the best combination ratio of HCO-40 and OC-40 using design of experiment software JMP. Both HCO-40 and OC-40 have significant effect on T1 solubility and steepest ascent has improved a noticeable solubility of T1. We optimized the highest solubility with T1-loaded NMF where the combination ratio of HCO-40 and OC-40 is 3% and 0.7% respectively. We further characterized this T1-loaded NMF for size, PDI, zeta potential, viscosity, osmolality, pH, clarity, % light transparent and cytotoxicity. The optimized T1

loaded NMF is clear like water. It has small nanoparticle size (18nm) with uniform distribution, negligible charge, which is very good for crossing tissue membrane. The osmolality, pH, and viscosity of T1 loaded NMF appear appropriate for topical purpose. Moreover, the T1 loaded NMF is very stable in dilution test and there is no free T1 drug in micelles solution presented in ^{1}H NMR. Moreover, the *in vitro* cytotoxicity of T1 NMFs showed more than 80% of cell viability, which indicates that T1 NMF is safe enough for further *in vivo* studies.

.

CHAPTER 8

8 SUMMARY AND RECOMMENDATIONS

8.1 Summary

Topical formulation administration is non-invasive and the most patient compliance route. However, delivery of therapeutic level of drugs following topical administration is very challenging due to structure of the eye, ocular static and dynamic barriers. Less than 5% of topical administered dose is absorbed, and 95% is washed out through the eye tissues.

Nanomicelles is one of the carriers which have been studied to enhance the solubility of drugs and target drug delivery due to their advantages over conventional formulations. Nanomicelles has been developed for posterior as well as anterior ocular delivery. It is an excellent vehicle for hydrophobic drugs and has significantly overcome the ocular barriers to deliver the drugs to the back-of- the eye. Nanomicelles has small size which helps to pass through the slera pore as well as follow trans-sclera pathway. Our laboratory has shown that nanomicelle formulation is an effective carrier system for hydrophobic drugs such as Cys-A, dexamethasone to intraocular tissues. These formulations followed trans-scleral pathway more than trans-corneal pathway due to their small size.

Glucocorticoids including fluocinolone acetonide, triamcinolone acetonide have been used widely to treat ocular disease including DME. Because glucocorticoids are hydrophobic and have poor water solubility, they are administered locally by intravitreal injection or implants. There are many side effects associated with those routes. Therefore, there is an urgent need to develop a clear formulation for topical administration.

Nanomicelle is an ideal system to improve aqueous solubility of FA, TA and T1 by dissolving it in the hydrophobic micelle core. This is a very simple method and can be scaled up at industrial level.

In order to achieve this goal, we utilized the statistical design of experiment to optimize the formulation. An exploratory model was employed to identify factors or interactions influencing drug solubilization in nanomicelles.

In chapter 5, the objective of this chapter was to develop a clear aqueous mixed nanomicellar formulation (NMF) of triamcinolone acetonide (TA) with a combination of nonionic surfactant hydrogenated castor oil 60 (HCO-60) and octoxynol-40 (Oc-40). In order to delineate the effects of drug-polymer interactions on entrapment efficiency (EE), loading efficiency (LE) and critical micellar concentration (CMC), a design of experiment (DOE) was performed to optimize the formulation. In this study, full factorial design has been used with HCO-60 and OC-40 as independent variables. All formulations were prepared following solvent evaporation and film rehydration method, characterized with size, polydispersity, shape, morphology, EE, LE and CMC. A specific blend of HCO-60 and Oc-40 at a particular wt% ratio (5:1.5) produced highest drug EE, LE, and smallest CMC (0.0216 wt %). Solubility of TA in NMF improved twenty times relative to normal aqueous solubility. Qualitative ^{1}H NMR studies confirmed the absence of free drug in the outer aqueous NMF medium. Moreover, TA loaded NMF appeared to be highly stable and well tolerated on human corneal epithelial cells (HCEC) and human retinal pigment epithelial cells (D407 cells). Overall, this study suggests that TA in NMF is safe and potentially could be used for human topical ocular drop application.

In chapter 6, the objective of this chapter was to develop a clear aqueous nanomicellar formulation (NMF) of fluocinolone acetonide (FA) with a combination of nonionic surfactant hydrogenated castor oil 40 (HCO-40) and octoxynol-40 (OC-40). To delineate the effects of polymer-polymer interactions on solubility (mg/ml) a design of experiment (DOE) was performed to optimize the formulation. In this study, central composite design was employed with two continuous factors, the amount of polymers HCO-40 and OC-40 as independent variables and resultant solubility is response outcome. All formulations were prepared following solvent evaporation and film rehydration method and characterized for size, polydispersity (PDI), zeta potential, percentage light transmittance (%T), osmolality, pH and cytotoxicity. DOE1 devoid of heating but DOE2 the film was heated at 65 ºC for 10-15 mins to allow the film melt before rehydration. Different ratios of HCO-40 and Oc-40 by two DOEs produced highest solubility. Solubility of FA in NMF improved fifteen and fourteen times, respectively for DOE1 and DOE2 relative to normal aqueous solubility. Qualitative ^{1}H NMR studies confirmed the absence of free drug in the outer aqueous NMF medium. Moreover, FA loaded NMF appeared very stable with dilution factors up to 400 times and well tolerated on human corneal epithelial cells (HCEC) and human retinal pigment epithelial cells (D407 cells). Overall this study suggests that FA in NMF is safe and potentially could be used for human topical ocular drop application.

In chapter 7, the objective of this chapter is to enhance Triamcinolone (T1) solubility by applying nanomicellar technology and design of experiment (DOE). We have prepared T1-nanomicellar formulation (NMF) with a mixture of nonionic surfactant hydrogenated castor oil 40 (HCO-40) and Octoxynol-40 (OC-40). We have established

the experimental strategies utilizing full factorial design and central composite base on interaction between polymers HCO-40 and OC-40 on drug solubility (mg/ml). In this paper, two continuous factors HCO-40 and OC-40 serve as independent variables while the dependent response is solubility. We have developed this nanomicellar formulation (NMFs) by solvent evaporation and film rehydration method. So we exploited DOE1 full factorial design to establish positive effect of both HCO-40 and OC-40 improving T1solubility, R square 0.97, (p-value 0.0015 for HCO-40 and 0.0011 for OC-40) and followed first order response. In addition, we applied steepest ascent to optimize outside the feasible region and to maximize the solubility with first order response. Steepest ascent is a numerical method for approaching local maxima of differentiable functions. It is a simple but convergent method for system of nonlinear equations. Steepest ascent allows moving the optimal region to the higher solubility. Applying steepest ascent, we designed the DOE2 to optimize different ratios of HCO-40 and OC-40 resulting in higher solubility. T1-solubility in NMF improved almost four times from DOE1 to DOE2. The optimal T1-NMF has small size, negligible polydispersity (PDI) and zeta potential. It allows more than 95% light transmitted. The osmolality, pH of T1-NMF are suitable for eye drop formulation with no cytotoxicity on human retinal ARPE-19 cells. Qualitative 1H NMR studies show no free drug T1 in nanomicellar solution. T1-NMF appears well established with dilution factors up to 400 times. These results establish the T1 loaded NMF a nontoxic and potentially could be used for human topical ocular drop application.

All the hydrophobic drugs are successfully encapsulated inside the nanomicelle and the solubility of drugs has been enhanced. All the NMFs are clear, no free drug articles present in the solution. Also, all NMFs are safe and well tolerated on human

corneal and retinal cell lines. Moreover, the small size of NMFs will help them penetrate through the tissue and release the drug.

8.2 Recommendations

The above studies were aimed at improving solubility and developing aqueous formulation of drug molecules and safely delivery to ocular tissues without any side effects. A few recommendations can be made to move further with this work based on the results obtained from the above studies.

First, as we can see that different drugs including triamcinolone acetonide, triamcinolone, fluocinolone acetonide, the ratio of polymers was different. Those drugs have different chemical structure and will have different interactions with polymers. Therefore, the ratio of polymers in different formulations are different. Different chain length of polyethylene may cause different pocket to encapsulate the hydrophobic drugs inside. Those different formulations may need further studies to investigate to know the hydrogen bond formation.

Second, investigations for FA, TA and T1 NMF *in vivo* ocular tolerability and pharmacokinetic studies with single and multiple drop administration of NMF should be undertaken. Such studies allow identification of the best possible dose to treat ocular diseases such as dry eye syndrome, uveitis and ocular neovascularization.

Third, these drug molecules may be conjugated with targeting moieties and loaded into NMF. Such carriers may deliver the cargo non-invasively to back-of- the-eye tissues. Moreover, targeted drugs (constructs) may help to improve drug permeability and overcome efflux transporters. Peptide transporter and folate receptor are expressed on the choroidal side of RPE. Conjugation of peptide and/or folate molecule to drug and

simultaneous loading into NMF should be undertaken in order to come up with the best possible formulation.

APPENDIX

ELSEVIER ORDER DETAILS

Mar 08, 2018

This Agreement between Hoang My Trinh ("You") and Elsevier ("Elsevier") consists of your order details and the terms and conditions provided by Elsevier and Copyright Clearance Center.

Order Number	501364437
Order date	Feb 12, 2018
Licensed Content Publisher	Elsevier
Licensed Content Publication	Elsevier Books
Licensed Content Title	Emerging Nanotechnologies for Diagnostics, Drug Delivery and Medical Devices
Licensed Content Author	Hoang M. Trinh,Mary Joseph,Kishore Cholkar,Ranjana Mitra,Ashim K. Mitra
Licensed Content Date	2017
Licensed Content Volume	n/a
Licensed Content Issue	n/a
Licensed Content Pages	14
Start Page	45
End Page	58
Type of Use	reuse in a thesis/dissertation
I am an academic or government institution with a full-text subscription to this journal and the audience of the material consists of students and/or employees of this institute?	No
Portion	full chapter
Format	both print and electronic
Are you the author of this Elsevier chapter?	Yes
Will you be translating?	No
Title of your thesis/dissertation	CLEAR, AQUEOUS TOPICAL NANOMICELLE FOR DIABETIC MACULA EDEMA
Expected completion date	Mar 2018
Estimated size (number of pages)	200
Requestor Location	Hoang My Trinh 4100 N Harrison ave Kansas City, MO 64116 United States Attn:
Publisher Tax ID	98-0397604
Billing Type	Invoice

SPRINGER NATURE LICENSE
TERMS AND CONDITIONS

Feb 13, 2018

This Agreement between Hoang My Trinh ("You") and Springer Nature ("Springer Nature") consists of your license details and the terms and conditions provided by Springer Nature and Copyright Clearance Center.

License Number	4287210153038
License date	Feb 13, 2018
Licensed Content Publisher	Springer Nature
Licensed Content Publication	Springer eBook
Licensed Content Title	Compositions, Formulation, Pharmacology, Pharmacokinetics, and Toxicity of Topical, Periocular, and Intravitreal Ophthalmic Drugs
Licensed Content Author	Kishore Cholkar, Aswani Dutt Vadlapudi, Hoang M. Trinh et al
Licensed Content Date	Jan 1, 2013
Type of Use	Thesis/Dissertation
Requestor type	academic/university or research institute
Format	print and electronic
Portion	full article/chapter
Will you be translating?	no
Circulation/distribution	<501
Author of this Springer Nature content	yes
Title	CLEAR, AQUEOUS TOPICAL NANOMICELLE FOR DIABETIC MACULA EDEMA
Instructor name	n/a
Institution name	n/a
Expected presentation date	Mar 2018
Requestor Location	Hoang My Trinh 4100 N Harrison ave Kansas City, MO 64116 United States Attn:
Billing Type	Invoice
Billing Address	Hoang My Trinh 4100 N Harrison ave Kansas City, MO 64116 United States Attn: Hoang My Trinh
Total	0.00 USD
Terms and Conditions	

SPRINGER NATURE LICENSE
TERMS AND CONDITIONS

Feb 13, 2018

This Agreement between Hoang My Trinh ("You") and Springer Nature ("Springer Nature") consists of your license details and the terms and conditions provided by Springer Nature and Copyright Clearance Center.

License Number	4287210445935
License date	Feb 13, 2018
Licensed Content Publisher	Springer Nature
Licensed Content Publication	AAPS PharmSciTech
Licensed Content Title	Clear, Aqueous Topical Drop of Triamcinolone Acetonide
Licensed Content Author	Hoang M. Trinh, Kishore Cholkar, Mary Joseph et al
Licensed Content Date	Jan 1, 2017
Licensed Content Volume	18
Licensed Content Issue	7
Type of Use	Thesis/Dissertation
Requestor type	academic/university or research institute
Format	print and electronic
Portion	full article/chapter
Will you be translating?	no
Circulation/distribution	<501
Author of this Springer Nature content	yes
Title	CLEAR, AQUEOUS TOPICAL NANOMICELLE FOR DIABETIC MACULA EDEMA
Instructor name	n/a
Institution name	n/a
Expected presentation date	Mar 2018
Requestor Location	Hoang My Trinh 4100 N Harrison ave Kansas City, MO 64116 United States Attn:
Billing Type	Invoice
Billing Address	Hoang My Trinh 4100 N Harrison ave Kansas City, MO 64116 United States Attn: Hoang My Trinh
Total	0.00 USD

ELSEVIER LICENSE
TERMS AND CONDITIONS

May 25, 2018

This Agreement between Hoang My Trinh ("You") and Elsevier ("Elsevier") consists of your license details and the terms and conditions provided by Elsevier and Copyright Clearance Center.

License Number	4355910684109
License date	May 25, 2018
Licensed Content Publisher	Elsevier
Licensed Content Publication	Progress in Retinal and Eye Research
Licensed Content Title	The multifunctional choroid
Licensed Content Author	Debora L. Nickla,Josh Wallman
Licensed Content Date	Mar 1, 2010
Licensed Content Volume	29
Licensed Content Issue	2
Licensed Content Pages	25
Start Page	144
End Page	168
Type of Use	reuse in a thesis/dissertation
Portion	figures/tables/illustrations
Number of figures/tables/illustrations	2
Format	both print and electronic
Are you the author of this Elsevier article?	No
Will you be translating?	No
Original figure numbers	Figure 2
Title of your thesis/dissertation	CLEAR, AQUEOUS TOPICAL NANOMICELLE FOR DIABETIC MACULA EDEMA
Expected completion date	Mar 2018
Estimated size (number of pages)	200
Requestor Location	Hoang My Trinh 4100 N Harrison ave Kansas City, MO 64116 United States Attn:
Publisher Tax ID	98-0397604
Total	0.00 USD
Terms and Conditions	

x.x.song <x.x.song@wjgnet.com>

Wed 11/23/2016 12:50 AM

To:Trinh, Hoang M. (UMKC-Student) <hmtrz9@mail.umkc.edu>;

Dear Dr. Trinh,

Ok, you can use.

Best Regards,

Xiu-Xia Song, Vice Director, Editorial Office
Baishideng Publishing Group Inc
Telephone: +86-10-8538-1891
Fax: +86-10-8538-1893
E-mail: x.x.song@wjgnet.com
Help desk: http://www.wjgnet.com/esps/helpdesk.aspx
http://www.wjgnet.com

2016-11-23

收件人： publicationfee@wjgnet.com
抄送：
主题： Re: Manuscript acceptance-ESPS-Ms NO: 22810

Dear editor,

I have recently published this paper in your journal. I would like to include it in the introduction of my thesis. I would like to ask the copyright for it.

Please let me know what should I do.

I really appreciate that.

Thanks,
Holly Hoang Trinh
Doctoral Candidate
Graduate Teaching & Research Assistant
University of Missouri-Kansas City
School of Pharmacy
Division of Pharmaceutical Sciences
Email : hmtrz9@mail.umkc.edu

REFERENCES

1. Kim, S. H.; Lutz, R. J.; Wang, N. S.; Robinson, M. R., Transport barriers in transscleral drug delivery for retinal diseases. *Ophthalmic Res* **2007,** *39* (5), 244-54.
2. Saraiya, N. V.; Goldstein, D. A., Dexamethasone for ocular inflammation. *Expert Opin Pharmacother* **2011,** *12* (7), 1127-31.
3. Moshfeghi, D. M.; Kaiser, P. K.; Scott, I. U.; Sears, J. E.; Benz, M.; Sinesterra, J. P.; Kaiser, R. S.; Bakri, S. J.; Maturi, R. K.; Belmont, J.; Beer, P. M.; Murray, T. G.; Quiroz-Mercado, H.; Mieler, W. F., Acute endophthalmitis following intravitreal triamcinolone acetonide injection. *American journal of ophthalmology* **2003,** *136* (5), 791-6.
4. Fong, A. H.; Chan, C. K., Presumed Sterile Endophthalmitis After Intravitreal Triamcinolone (Kenalog)-More Common and Less Benign Than We Thought? *Asia Pac J Ophthalmol (Phila)* **2016**.
5. Gaudana, R.; Ananthula, H. K.; Parenky, A.; Mitra, A. K., Ocular drug delivery. *AAPS J* **2010,** *12* (3), 348-60.
6. HariKrishna Ananthula; Ravi Vaishya; Megha Barot; Mitra, A., Bioavailability. Tasman W; EA, J., Eds. Philadelphia: Lippincott Williams & Wilkins: 2009.
7. Lowder, C.; Belfort, R., Jr.; Lightman, S.; Foster, C. S.; Robinson, M. R.; Schiffman, R. M.; Li, X. Y.; Cui, H.; Whitcup, S. M., Dexamethasone intravitreal implant for noninfectious intermediate or posterior uveitis. *Arch Ophthalmol* **2011,** *129* (5), 545-53.
8. Robert H Janigian Jr; Jr, R. H. J. Uveitis Evaluation and Treatment http://emedicine.medscape.com/article/1209123-overview (accessed 06/25/2013).
9. Tang, D. L.; Song, F.; Chen, C.; Wang, X. L.; Wang, Y. Z., A pH-responsive chitosan-b-poly(p-dioxanone) nanocarrier: formation and efficient antitumor drug delivery. *Nanotechnology* **2013,** *24* (14), 145101.
10. Gu, Q.; Xing, J. Z.; Huang, M.; He, C.; Chen, J., SN-38 loaded polymeric micelles to enhance cancer therapy. *Nanotechnology* **2012,** *23* (20), 205101.
11. Zhang, Z.; Mei, L.; Feng, S. S., Paclitaxel drug delivery systems. *Expert opinion on drug delivery* **2013,** *10* (3), 325-40.
12. Sun, M.; Su, X.; Ding, B.; He, X.; Liu, X.; Yu, A.; Lou, H.; Zhai, G., Advances in nanotechnology-based delivery systems for curcumin. *Nanomedicine* **2012,** *7* (7), 1085-100.
13. Amrite, A. C.; Kompella, U. B., Size-dependent disposition of nanoparticles and microparticles following subconjunctival administration. *J Pharm Pharmacol* **2005,** *57* (12), 1555-63.
14. Inokuchi, Y.; Hironaka, K.; Fujisawa, T.; Tozuka, Y.; Tsuruma, K.; Shimazawa, M.; Takeuchi, H.; Hara, H., Physicochemical properties affecting retinal drug/coumarin-6 delivery from nanocarrier systems via eyedrop administration. *Investigative ophthalmology & visual science* **2010,** *51* (6), 3162-70.
15. Cholkar, K.; Gilger, B. C.; Mitra, A. K., Topical, Aqueous, Clear Cyclosporine Formulation Design for Anterior and Posterior Ocular Delivery. *Transl Vis Sci Technol* **2015,** *4* (3), 1.

16. Cholkar, K.; Gunda, S.; Earla, R.; Pal, D.; Mitra, A. K., Nanomicellar Topical Aqueous Drop Formulation of Rapamycin for Back-of-the-Eye Delivery. *AAPS PharmSciTech* **2015,** *16* (3), 610-22.
17. Veritti, D.; Di Giulio, A.; Sarao, V.; Lanzetta, P., Drug safety evaluation of intravitreal triamcinolone acetonide. *Expert opinion on drug safety* **2012,** *11* (2), 331-40.
18. Smithen, L. M.; Ober, M. D.; Maranan, L.; Spaide, R. F., Intravitreal triamcinolone acetonide and intraocular pressure. *American journal of ophthalmology* **2004,** *138* (5), 740-3.
19. Grover, D.; Li, T. J.; Chong, C. C., Intravitreal steroids for macular edema in diabetes. *The Cochrane database of systematic reviews* **2008,** (1), CD005656.
20. Romero-Aroca, P., Current status in diabetic macular edema treatments. *World journal of diabetes* **2013,** *4* (5), 165-9.
21. Edelman, J. L., Differentiating intraocular glucocorticoids. *Ophthalmologica* **2010,** *224 Suppl 1*, 25-30.
22. Turvey, T. A.; Golden, B. A., Orbital anatomy for the surgeon. *Oral Maxillofac Surg Clin North Am* **2012,** *24* (4), 525-36.
23. Martins, C.; Costa E Silva, I. E.; Campero, A.; Yasuda, A.; Aguiar, L. R.; Tatagiba, M.; Rhoton, A., Microsurgical anatomy of the orbit: the rule of seven. *Anat Res Int* **2011,** *2011*, 468727.
24. Demer, J. L., Compartmentalization of extraocular muscle function. *Eye (Lond)* **2015,** *29* (2), 157-62.
25. McCaa, C. S., The eye and visual nervous system: anatomy, physiology and toxicology. *Environ Health Perspect* **1982,** *44*, 1-8.
26. Dua, H. S.; Faraj, L. A.; Said, D. G.; Gray, T.; Lowe, J., Human corneal anatomy redefined: a novel pre-Descemet's layer (Dua's layer). *Ophthalmology* **2013,** *120* (9), 1778-85.
27. DelMonte, D. W.; Kim, T., Anatomy and physiology of the cornea. *J Cataract Refract Surg* **2011,** *37* (3), 588-98.
28. Schermer, A.; Galvin, S.; Sun, T. T., Differentiation-related expression of a major 64K corneal keratin in vivo and in culture suggests limbal location of corneal epithelial stem cells. *J Cell Biol* **1986,** *103* (1), 49-62.
29. Wiley, L.; SundarRaj, N.; Sun, T. T.; Thoft, R. A., Regional heterogeneity in human corneal and limbal epithelia: an immunohistochemical evaluation. *Invest Ophthalmol Vis Sci* **1991,** *32* (3), 594-602.
30. Stiemke, M. M.; Edelhauser, H. F.; Geroski, D. H., The developing corneal endothelium: correlation of morphology, hydration and Na/K ATPase pump site density. *Curr Eye Res* **1991,** *10* (2), 145-56.
31. Geroski, D. H.; Matsuda, M.; Yee, R. W.; Edelhauser, H. F., Pump function of the human corneal endothelium. Effects of age and cornea guttata. *Ophthalmology* **1985,** *92* (6), 759-63.
32. Lacouture, A., [Anatomy-physiology of the eye]. *Rev Infirm* **2006,** (120), 16-7.
33. Delamere, N. A., Ciliary Body and Ciliary Epithelium. *Adv Organ Biol* **2005,** *10*, 127-148.
34. Goel, M.; Picciani, R. G.; Lee, R. K.; Bhattacharya, S. K., Aqueous humor dynamics: a review. *Open Ophthalmol J* **2010,** *4*, 52-9.

35. Civan, M. M.; Macknight, A. D., The ins and outs of aqueous humour secretion. *Exp Eye Res* **2004,** *78* (3), 625-31.
36. Bill, A.; Phillips, C. I., Uveoscleral drainage of aqueous humour in human eyes. *Exp Eye Res* **1971,** *12* (3), 275-81.
37. Pederson, J. E.; Toris, C. B., Uveoscleral outflow: diffusion or flow? *Invest Ophthalmol Vis Sci* **1987,** *28* (6), 1022-4.
38. Johnstone, M. A., The aqueous outflow system as a mechanical pump: evidence from examination of tissue and aqueous movement in human and non-human primates. *J Glaucoma* **2004,** *13* (5), 421-38.
39. Petrash, J. M., Aging and age-related diseases of the ocular lens and vitreous body. *Invest Ophthalmol Vis Sci* **2013,** *54* (14), ORSF54-9.
40. Lee, C. J.; Vroom, J. A.; Fishman, H. A.; Bent, S. F., Determination of human lens capsule permeability and its feasibility as a replacement for Bruch's membrane. *Biomaterials* **2006,** *27* (8), 1670-8.
41. Delamere, N. A.; Mandal, A.; Shahidullah, M., The Significance of TRPV4 Channels and Hemichannels in the Lens and Ciliary Epithelium. *J Ocul Pharmacol Ther* **2016,** *32* (8), 504-508.
42. Candia, O. A., Electrolyte and fluid transport across corneal, conjunctival and lens epithelia. *Exp Eye Res* **2004,** *78* (3), 527-35.
43. Bassnett, S.; Shi, Y.; Vrensen, G. F., Biological glass: structural determinants of eye lens transparency. *Philos Trans R Soc Lond B Biol Sci* **2011,** *366* (1568), 1250-64.
44. Wride, M. A., Lens fibre cell differentiation and organelle loss: many paths lead to clarity. *Philos Trans R Soc Lond B Biol Sci* **2011,** *366* (1568), 1219-33.
45. Danysh, B. P.; Czymmek, K. J.; Olurin, P. T.; Sivak, J. G.; Duncan, M. K., Contributions of mouse genetic background and age on anterior lens capsule thickness. *Anat Rec (Hoboken)* **2008,** *291* (12), 1619-27.
46. Norman, R. E.; Flanagan, J. G.; Rausch, S. M.; Sigal, I. A.; Tertinegg, I.; Eilaghi, A.; Portnoy, S.; Sled, J. G.; Ethier, C. R., Dimensions of the human sclera: Thickness measurement and regional changes with axial length. *Exp Eye Res* **2010,** *90* (2), 277-84.
47. Edelhauser, H.; Ubels, J., Cornea and sclera. In *Physiology of the eye*, Kaufman, P.; Aam, A., Eds. Moses, RA

Mosby, CV: St. Louis, 2003; pp 47-116.
48. Ambati, J.; Canakis, C. S.; Miller, J. W.; Gragoudas, E. S.; Edwards, A.; Weissgold, D. J.; Kim, I.; Delori, F. C.; Adamis, A. P., Diffusion of high molecular weight compounds through sclera. *Investigative ophthalmology & visual science* **2000,** *41* (5), 1181-5.
49. Nickla, D. L.; Wallman, J., The multifunctional choroid. *Prog Retin Eye Res* **2010,** *29* (2), 144-68.
50. May, C. A., Non-vascular smooth muscle cells in the human choroid: distribution, development and further characterization. *J Anat* **2005,** *207* (4), 381-90.
51. Sharma, R.; Ehinger, B., Development and structure of retina. In *Physiology of the eye*, Kaufman, P.; Aam, A., Eds. Moses, RA

Mosby, CV: St. Louis, 2003; pp 47-116.

52. Cour, M., The retinal pigmented epithelium. In *Physiology of the eye*, Kaufman, P.; Aam, A., Eds. Moses, RA

Mosby, CV: St. Louis, 2003; pp 47-116.
53. Boulton, M.; Dayhaw-Barker, P., The role of the retinal pigment epithelium: topographical variation and ageing changes. *Eye (Lond)* **2001,** *15* (Pt 3), 384-9.
54. Curcio, C. A.; Sloan, K. R.; Kalina, R. E.; Hendrickson, A. E., Human photoreceptor topography. *J Comp Neurol* **1990,** *292* (4), 497-523.
55. Gollisch, T.; Meister, M., Eye smarter than scientists believed: neural computations in circuits of the retina. *Neuron* **2010,** *65* (2), 150-64.
56. Ma, J.; Ke, Y.; Wu, D.; Gu, X.; Gao, R., Experimental study on relationship between retinal vein occlusion and loss of vitreous gel mass. *Mol Vis* **2005,** *11*, 744-8.
57. Andersen, H.; Sander, B., The vitreous. In *Physiology of the eye*, Kaufman, P.; Aam, A., Eds. Moses, RA

Mosby, CV: St. Louis, 2003; pp 47-116.
58. Mitra, A. K., *Ocular Transporters and Receptors*. Elsevier: 2013; Vol. 1.
59. Fischbarg, J., The Corneal Endothelium. Advances in Organ Biology. *Elsevier* **2005**.
60. I, A., *The noncorneal route in ocular drug delivery*. Marcel Dekker: New York, 2003.
61. Kim, Y. C.; Chiang, B.; Wu, X.; Prausnitz, M. R., Ocular delivery of macromolecules. *J Control Release* **2014,** *190*, 172-81.
62. Dey, S.; Gunda, S.; Mitra, A. K., Pharmacokinetics of erythromycin in rabbit corneas after single-dose infusion: role of P-glycoprotein as a barrier to in vivo ocular drug absorption. *The Journal of pharmacology and experimental therapeutics* **2004,** *311* (1), 246-55.
63. Yang, J. J.; Kim, K. J.; Lee, V. H., Role of P-glycoprotein in restricting propranolol transport in cultured rabbit conjunctival epithelial cell layers. *Pharm Res* **2000,** *17* (5), 533-8.
64. Chen, P.; Chen, H.; Zang, X.; Chen, M.; Jiang, H.; Han, S.; Wu, X., Expression of efflux transporters in human ocular tissues. *Drug Metab Dispos* **2013,** *41* (11), 1934-48.
65. Constable, P. A.; Lawrenson, J. G.; Dolman, D. E.; Arden, G. B.; Abbott, N. J., P-Glycoprotein expression in human retinal pigment epithelium cell lines. *Exp Eye Res* **2006,** *83* (1), 24-30.
66. Schoenwald, R. D., Ocular drug delivery. Pharmacokinetic considerations. *Clin Pharmacokinet* **1990,** *18* (4), 255-69.
67. Booij, J. C.; Baas, D. C.; Beisekeeva, J.; Gorgels, T. G.; Bergen, A. A., The dynamic nature of Bruch's membrane. *Prog Retin Eye Res* **2010,** *29* (1), 1-18.
68. Lee, S. J.; Kim, E. S.; Geroski, D. H.; McCarey, B. E.; Edelhauser, H. F., Pharmacokinetics of intraocular drug delivery of Oregon green 488-labeled triamcinolone by subtenon injection using ocular fluorophotometry in rabbit eyes. *Investigative ophthalmology & visual science* **2008,** *49* (10), 4506-14.
69. Ghate, D.; Brooks, W.; McCarey, B. E.; Edelhauser, H. F., Pharmacokinetics of intraocular drug delivery by periocular injections using ocular fluorophotometry. *Investigative ophthalmology & visual science* **2007,** *48* (5), 2230-7.

70. Janoria, K. G.; Gunda, S.; Boddu, S. H.; Mitra, A. K., Novel approaches to retinal drug delivery. *Expert opinion on drug delivery* **2007,** *4* (4), 371-88.
71. Reddy, I. K., *Ocular Therapeutics and Drug Delivery: A Multi-disciplinary Aapproach*. CRC Press: 1995.
72. Edman, P., *Biopharmaceutics of Ocular Drug Delivery*. Informa Health Care: 1993.
73. Kumar, S.; Karki, R.; Meena, M.; Prakash, T.; Rajeswari, T.; Goli, D., Reduction in drop size of ophthalmic topical drop preparations and the impact of treatment. *J Adv Pharm Technol Res* **2011,** *2* (3), 192-4.
74. Lederer, C. M.; Harold, R. E., Drop size of commercial glaucoma medications. *Am J Ophthalmol* **1986,** *101* (6), 691-4.
75. Van Santvliet, L.; Ludwig, A., Determinants of eye drop size. *Surv Ophthalmol* **2004,** *49* (2), 197-213.
76. Barar, J.; Javadzadeh, A. R.; Omidi, Y., Ocular novel drug delivery: impacts of membranes and barriers. *Expert opinion on drug delivery* **2008,** *5* (5), 567-81.
77. Hamalainen, K. M.; Kananen, K.; Auriola, S.; Kontturi, K.; Urtti, A., Characterization of paracellular and aqueous penetration routes in cornea, conjunctiva, and sclera. *Investigative ophthalmology & visual science* **1997,** *38* (3), 627-34.
78. Raghava, S.; Hammond, M.; Kompella, U. B., Periocular routes for retinal drug delivery. *Expert opinion on drug delivery* **2004,** *1* (1), 99-114.
79. Van Santvliet, L.; Ludwig, A., Determinants of eye drop size. *Survey of Ophthalmology* **2004,** *49* (2), 197-213.
80. Urtti, A.; Salminen, L., Minimizing systemic absorption of topically administered ophthalmic drugs. *Survey of Ophthalmology* **1993,** *37* (6), 435-456.
81. Shell, J. W., Pharmacokinetics of topically applied ophthalmic drugs. *Survey of Ophthalmology* **1982,** *26* (4), 207-218.
82. Letocha, C. E., Methods for self-administration of eyedrops. *Ann Ophthalmol* **1985,** *17* (12), 768-9.
83. Mishima, S.; Gasset, A.; Klyce, S. D., Jr.; Baum, J. L., Determination of tear volume and tear flow. *Invest Ophthalmol* **1966,** *5* (3), 264-76.
84. Fraunfelder, F. T.; Meyer, S. M., Systemic side effects from ophthalmic timolol and their prevention. *J Ocul Pharmacol* **1987,** *3* (2), 177-84.
85. Gray, R. H., The influence of drop size on pupil dilatation. *Eye* **1991,** *5 (Pt 5)*, 615-9.
86. Falavarjani, K. G.; Nguyen, Q. D., Adverse events and complications associated with intravitreal injection of anti-VEGF agents: a review of literature. *Eye (Lond)* **2013,** *27* (7), 787-94.
87. Nomoto, H.; Shiraga, F.; Kuno, N.; Kimura, E.; Fujii, S.; Shinomiya, K.; Nugent, A. K.; Hirooka, K.; Baba, T., Pharmacokinetics of bevacizumab after topical, subconjunctival, and intravitreal administration in rabbits. *Invest Ophthalmol Vis Sci* **2009,** *50* (10), 4807-13.
88. Heiduschka, P.; Fietz, H.; Hofmeister, S.; Schultheiss, S.; Mack, A. F.; Peters, S.; Ziemssen, F.; Niggemann, B.; Julien, S.; Bartz-Schmidt, K. U.; Schraermeyer, U.; Group, T. B. S., Penetration of bevacizumab through the retina after intravitreal injection in the monkey. *Invest Ophthalmol Vis Sci* **2007,** *48* (6), 2814-23.

89. Duvall, B.; Kershner, R. M., Ophthalmic Medications and Pharmacology. 2nd ed.; Slack Incorporated: 2006.
90. Dastjerdi, M. H.; Sadrai, Z.; Saban, D. R.; Zhang, Q.; Dana, R., Corneal penetration of topical and subconjunctival bevacizumab. *Invest Ophthalmol Vis Sci* **2011,** *52* (12), 8718-23.
91. Peeters, L.; Lentacker, I.; Vandenbroucke, R. E.; Lucas, B.; Demeester, J.; Sanders, N. N.; De Smedt, S. C., Can ultrasound solve the transport barrier of the neural retina? *Pharm Res* **2008,** *25* (11), 2657-65.
92. Eljarrat-Binstock, E.; Orucov, F.; Aldouby, Y.; Frucht-Pery, J.; Domb, A. J., Charged nanoparticles delivery to the eye using hydrogel iontophoresis. *J Control Release* **2008,** *126* (2), 156-61.
93. Kumar, C. M.; Eid, H.; Dodds, C., Sub-Tenon's anaesthesia: complications and their prevention. *Eye (Lond)* **2011,** *25* (6), 694-703.
94. Falavarjani, K. G.; Khadamy, J.; Karimi Moghaddam, A.; Karimi, N.; Modarres, M., Posterior sub-tenon's bevacizumab injection in diabetic macular edema; a pilot study. *Saudi J Ophthalmol* **2015,** *29* (4), 270-3.
95. Canavan, K. S.; Dark, A.; Garrioch, M. A., Sub-Tenon's administration of local anaesthetic: a review of the technique. *Br J Anaesth* **2003,** *90* (6), 787-93.
96. TRIVEDI, H.; TODKAR, H.; ARBHAVE, V.; BHATIA, P., OCULAR ANAESTHESIA FOR CATARACT SURGERY. *Lancet* **2003,** *3*, 1312-1313,1319.
97. Ebner, R.; Devoto, M. H.; Weil, D.; Bordaberry, M.; Mir, C.; Martinez, H.; Bonelli, L.; Niepomniszcze, H., Treatment of thyroid associated ophthalmopathy with periocular injections of triamcinolone. *Br J Ophthalmol* **2004,** *88* (11), 1380-6.
98. van den Berg, A. A., An audit of peribulbar blockade using 15 mm, 25 mm and 37.5 mm needles, and sub-Tenon's injection. *Anaesthesia* **2004,** *59* (8), 775-80.
99. McGrath, L. A.; Bradshaw, C. P., Transconjunctival approach to peribulbar block. *Clin Ophthalmol* **2013,** *7*, 1073-6.
100. Bandello, F.; Battaglia Parodi, M.; Tremolada, G.; Lattanzio, R.; De Benedetto, U.; Iacono, P., Steroids as part of combination treatment: the future for the management of macular edema? *Ophthalmologica* **2010,** *224 Suppl 1*, 41-5.
101. Varma, R.; Bressler, N. M.; Doan, Q. V.; Gleeson, M.; Danese, M.; Bower, J. K.; Selvin, E.; Dolan, C.; Fine, J.; Colman, S.; Turpcu, A., Prevalence of and risk factors for diabetic macular edema in the United States. *JAMA ophthalmology* **2014,** *132* (11), 1334-40.
102. https://nei.nih.gov/health/diabetic/retinopathy.
103. Romero-Aroca, P., Managing diabetic macular edema: The leading cause of diabetes blindness. *World J Diabetes* **2011,** *2* (6), 98-104.
104. Frank, R. N., Diabetic retinopathy and systemic factors. *Middle East Afr J Ophthalmol* **2015,** *22* (2), 151-6.
105. Cunha-Vaz, J.; Bernardes, R.; Lobo, C., Blood-retinal barrier. *Eur J Ophthalmol* **2011,** *21 Suppl 6*, S3-9.
106. Wenick, A. S.; Bressler, N. M., Diabetic macular edema: current and emerging therapies. *Middle East Afr J Ophthalmol* **2012,** *19* (1), 4-12.
107. Klaassen, I.; Van Noorden, C. J.; Schlingemann, R. O., Molecular basis of the inner blood-retinal barrier and its breakdown in diabetic macular edema and other pathological conditions. *Prog Retin Eye Res* **2013,** *34*, 19-48.

108. Bhagat, N.; Grigorian, R. A.; Tutela, A.; Zarbin, M. A., Diabetic macular edema: pathogenesis and treatment. *Surv Ophthalmol* **2009,** *54* (1), 1-32.
109. Kim, B. Y.; Smith, S. D.; Kaiser, P. K., Optical coherence tomographic patterns of diabetic macular edema. *American journal of ophthalmology* **2006,** *142* (3), 405-12.
110. Ehrlich, R.; Harris, A.; Ciulla, T. A.; Kheradiya, N.; Winston, D. M.; Wirostko, B., Diabetic macular oedema: physical, physiological and molecular factors contribute to this pathological process. *Acta Ophthalmol* **2010,** *88* (3), 279-91.
111. Pham, I.; Uchida, T.; Planes, C.; Ware, L. B.; Kaner, R.; Matthay, M. A.; Clerici, C., Hypoxia upregulates VEGF expression in alveolar epithelial cells in vitro and in vivo. *American journal of physiology. Lung cellular and molecular physiology* **2002,** *283* (5), L1133-42.
112. Sotoodehnejadnematalahi, F.; Burke, B., Human activated macrophages and hypoxia: a comprehensive review of the literature. *Iranian journal of basic medical sciences* **2014,** *17* (11), 820-30.
113. Lange, C. A.; Stavrakas, P.; Luhmann, U. F.; de Silva, D. J.; Ali, R. R.; Gregor, Z. J.; Bainbridge, J. W., Intraocular oxygen distribution in advanced proliferative diabetic retinopathy. *American journal of ophthalmology* **2011,** *152* (3), 406-412 e3.
114. Tangvarasittichai, S., Oxidative stress, insulin resistance, dyslipidemia and type 2 diabetes mellitus. *World journal of diabetes* **2015,** *6* (3), 456-80.
115. Stefánsson, E., Ocular oxygenation and the treatment of diabetic retinopathy. *Surv Ophthalmol* **2006,** *51* (4), 364-80.
116. Kohner, E. M.; Patel, V.; Rassam, S. M., Role of blood flow and impaired autoregulation in the pathogenesis of diabetic retinopathy. *Diabetes* **1995,** *44* (6), 603-7.
117. Altabas, V., Diabetes, Endothelial Dysfunction, and Vascular Repair: What Should a Diabetologist Keep His Eye on? *International journal of endocrinology* **2015,** *2015*, 848272.
118. Hadi, H. A.; Suwaidi, J. A., Endothelial dysfunction in diabetes mellitus. *Vascular health and risk management* **2007,** *3* (6), 853-76.
119. Georgescu, A., Vascular dysfunction in diabetes: The endothelial progenitor cells as new therapeutic strategy. *World journal of diabetes* **2011,** *2* (6), 92-7.
120. Chen, Y. H.; Lin, S. J.; Lin, F. Y.; Wu, T. C.; Tsao, C. R.; Huang, P. H.; Liu, P. L.; Chen, Y. L.; Chen, J. W., High glucose impairs early and late endothelial progenitor cells by modifying nitric oxide-related but not oxidative stress-mediated mechanisms. *Diabetes* **2007,** *56* (6), 1559-68.
121. Huang, P. H.; Chen, J. S.; Tsai, H. Y.; Chen, Y. H.; Lin, F. Y.; Leu, H. B.; Wu, T. C.; Lin, S. J.; Chen, J. W., Globular adiponectin improves high glucose-suppressed endothelial progenitor cell function through endothelial nitric oxide synthase dependent mechanisms. *Journal of molecular and cellular cardiology* **2011,** *51* (1), 109-19.
122. Soliman, W.; Sander, B.; Jørgensen, T. M., Enhanced optical coherence patterns of diabetic macular oedema and their correlation with the pathophysiology. *Acta Ophthalmol Scand* **2007,** *85* (6), 613-7.

123. Sikorski, B. L.; Malukiewicz, G.; Stafiej, J.; Lesiewska-Junk, H.; Raczynska, D., The diagnostic function of OCT in diabetic maculopathy. *Mediators of inflammation* **2013,** *2013*, 434560.
124. Dabhi, B.; Mistry, K. N.; Patel, H.; Lal, S., Vascular endothelial growth factor insertion/deletion gene polymorphism in West Indian patients of type 2 diabetes and diabetic nephropathy. *Indian journal of biochemistry & biophysics* **2015,** *52* (2), 209-12.
125. Shams, N.; Ianchulev, T., Role of vascular endothelial growth factor in ocular angiogenesis. *Ophthalmology clinics of North America* **2006,** *19* (3), 335-44.
126. Andreoli, C. M.; Miller, J. W., Anti-vascular endothelial growth factor therapy for ocular neovascular disease. *Current opinion in ophthalmology* **2007,** *18* (6), 502-8.
127. Patel, N., Targeting leukostasis for the treatment of early diabetic retinopathy. *Cardiovascular & hematological disorders drug targets* **2009,** *9* (3), 222-9.
128. Miyamoto, K.; Ogura, Y., [Diabetic retinopathy and leukocytes--feasibility of anti-leukostasis therapy for diabetic retinopathy]. *Nihon rinsho. Japanese journal of clinical medicine* **2002,** *60 Suppl 10*, 183-8.
129. Frey, T.; Antonetti, D. A., Alterations to the blood-retinal barrier in diabetes: cytokines and reactive oxygen species. *Antioxidants & redox signaling* **2011,** *15* (5), 1271-84.
130. Morgan, L.; Shah, B.; Rivers, L. E.; Barden, L.; Groom, A. J.; Chung, R.; Higazi, D.; Desmond, H.; Smith, T.; Staddon, J. M., Inflammation and dephosphorylation of the tight junction protein occludin in an experimental model of multiple sclerosis. *Neuroscience* **2007,** *147* (3), 664-73.
131. Raleigh, D. R.; Boe, D. M.; Yu, D.; Weber, C. R.; Marchiando, A. M.; Bradford, E. M.; Wang, Y.; Wu, L.; Schneeberger, E. E.; Shen, L.; Turner, J. R., Occludin S408 phosphorylation regulates tight junction protein interactions and barrier function. *The Journal of cell biology* **2011,** *193* (3), 565-82.
132. Bennett, J.; Basivireddy, J.; Kollar, A.; Biron, K. E.; Reickmann, P.; Jefferies, W. A.; McQuaid, S., Blood-brain barrier disruption and enhanced vascular permeability in the multiple sclerosis model EAE. *Journal of neuroimmunology* **2010,** *229* (1-2), 180-91.
133. Pacher, P.; Beckman, J. S.; Liaudet, L., Nitric oxide and peroxynitrite in health and disease. *Physiological reviews* **2007,** *87* (1), 315-424.
134. El-Remessy, A. B.; Behzadian, M. A.; Abou-Mohamed, G.; Franklin, T.; Caldwell, R. W.; Caldwell, R. B., Experimental diabetes causes breakdown of the blood-retina barrier by a mechanism involving tyrosine nitration and increases in expression of vascular endothelial growth factor and urokinase plasminogen activator receptor. *The American journal of pathology* **2003,** *162* (6), 1995-2004.
135. Awata, T.; Neda, T.; Iizuka, H.; Kurihara, S.; Ohkubo, T.; Takata, N.; Osaki, M.; Watanabe, M.; Nakashima, Y.; Sawa, T.; Inukai, K.; Inoue, I.; Shibuya, M.; Mori, K.; Yoneya, S.; Katayama, S., Endothelial nitric oxide synthase gene is associated with diabetic macular edema in type 2 diabetes. *Diabetes care* **2004,** *27* (9), 2184-90.
136. Navaratna, D.; McGuire, P. G.; Menicucci, G.; Das, A., Proteolytic degradation of VE-cadherin alters the blood-retinal barrier in diabetes. *Diabetes* **2007,** *56* (9), 2380-7.

137. Galvez, M. I., Protein kinase C inhibitors in the treatment of diabetic retinopathy. Review. *Current pharmaceutical biotechnology* **2011,** *12* (3), 386-91.
138. Gao, B. B.; Clermont, A.; Rook, S.; Fonda, S. J.; Srinivasan, V. J.; Wojtkowski, M.; Fujimoto, J. G.; Avery, R. L.; Arrigg, P. G.; Bursell, S. E.; Aiello, L. P.; Feener, E. P., Extracellular carbonic anhydrase mediates hemorrhagic retinal and cerebral vascular permeability through prekallikrein activation. *Nature medicine* **2007,** *13* (2), 181-8.
139. Sjølie, A. K.; Klein, R.; Porta, M.; Orchard, T.; Fuller, J.; Parving, H. H.; Bilous, R.; Chaturvedi, N.; Group, D. P. S., Effect of candesartan on progression and regression of retinopathy in type 2 diabetes (DIRECT-Protect 2): a randomised placebo-controlled trial. *Lancet* **2008,** *372* (9647), 1385-93.
140. Singh, A.; Stewart, J. M., Pathophysiology of diabetic macular edema. *International ophthalmology clinics* **2009,** *49* (2), 1-11.
141. Jain, A.; Varshney, N.; Smith, C., The evolving treatment options for diabetic macular edema. *Int J Inflam* **2013,** *2013*, 689276.
142. Park, Y. G.; Kim, E. Y.; Roh, Y. J., Laser-based strategies to treat diabetic macular edema: history and new promising therapies. *J Ophthalmol* **2014,** *2014*, 769213.
143. Perente, I.; Alkin, Z.; Ozkaya, A.; Dardabounis, D.; Ogreden, T. A.; Konstantinidis, A.; Kyratzoglou, K.; Yazici, A. T., Focal laser photocoagulation in non-center involved diabetic macular edema. *Med Hypothesis Discov Innov Ophthalmol* **2014,** *3* (1), 9-16.
144. Kozak, I.; Luttrull, J. K., Modern retinal laser therapy. *Saudi J Ophthalmol* **2015,** *29* (2), 137-46.
145. Chalam, K. V.; Murthy, R. K.; Brar, V.; Radhakrishnan, R.; Khetpal, V.; Grover, S., Evaluation of a Novel, Non Contact, Automated Focal Laser with Integrated (NAVILAS) Fluorescein Angiography for Diabetic Macular Edema. *Middle East African journal of ophthalmology* **2012,** *19* (1), 158-62.
146. Romero-Aroca, P.; Reyes-Torres, J.; Baget-Bernaldiz, M.; Blasco-Sune, C., Laser treatment for diabetic macular edema in the 21st century. *Current diabetes reviews* **2014,** *10* (2), 100-12.
147. Romero-Aroca, P., Is laser photocoagulation treatment currently useful in diabetic macular edema? *Med Hypothesis Discov Innov Ophthalmol* **2015,** *4* (1), 5-8.
148. Dalos, B.; Doklen, A.; Horvath, M., Depression of mitosis by gamma-globulin from splenic x-irradiated animals. *Int J Radiat Biol Relat Stud Phys Chem Med* **1969,** *16* (5), 501-2.
149. Liegl, R.; Langer, J.; Seidensticker, F.; Reznicek, L.; Haritoglou, C.; Ulbig, M. W.; Neubauer, A. S.; Kampik, A.; Kernt, M., Comparative evaluation of combined navigated laser photocoagulation and intravitreal ranibizumab in the treatment of diabetic macular edema. *PLoS One* **2014,** *9* (12), e113981.
150. Grigorian, R.; Bhagat, N.; Lanzetta, P.; Tutela, A.; Zarbin, M., Pars plana vitrectomy for refractory diabetic macular edema. *Seminars in ophthalmology* **2003,** *18* (3), 116-20.
151. Hartley, K. L.; Smiddy, W. E.; Flynn, H. W.; Murray, T. G., Pars plana vitrectomy with internal limiting membrane peeling for diabetic macular edema. *Retina* **2008,** *28* (3), 410-9.

152. Yanyali, A.; Horozoglu, F.; Celik, E.; Nohutcu, A. F., Long-term outcomes of pars plana vitrectomy with internal limiting membrane removal in diabetic macular edema. *Retina* **2007,** *27* (5), 557-66.
153. Iwase, T.; Oveson, B. C., Long-term outcome after vitrectomy for macular edema with retinal vein occlusion dividing into the occlusion site. *Journal of ophthalmology* **2014,** *2014*, 198782.
154. Rosenblatt, B. J.; Shah, G. K.; Sharma, S.; Bakal, J., Pars plana vitrectomy with internal limiting membranectomy for refractory diabetic macular edema without a taut posterior hyaloid. *Graefe's archive for clinical and experimental ophthalmology = Albrecht von Graefes Archiv fur klinische und experimentelle Ophthalmologie* **2005,** *243* (1), 20-5.
155. Haller, J. A.; Qin, H.; Apte, R. S.; Beck, R. R.; Bressler, N. M.; Browning, D. J.; Danis, R. P.; Glassman, A. R.; Googe, J. M.; Kollman, C.; Lauer, A. K.; Peters, M. A.; Stockman, M. E.; Committee, D. R. C. R. N. W., Vitrectomy outcomes in eyes with diabetic macular edema and vitreomacular traction. *Ophthalmology* **2010,** *117* (6), 1087-1093.e3.
156. Stefansson, E., Physiology of vitreous surgery. *Graefe's archive for clinical and experimental ophthalmology = Albrecht von Graefes Archiv fur klinische und experimentelle Ophthalmologie* **2009,** *247* (2), 147-63.
157. Stolba, U.; Binder, S.; Gruber, D.; Krebs, I.; Aggermann, T.; Neumaier, B., Vitrectomy for persistent diffuse diabetic macular edema. *American journal of ophthalmology* **2005,** *140* (2), 295-301.
158. Thomas, D.; Bunce, C.; Moorman, C.; Laidlaw, D. A., A randomised controlled feasibility trial of vitrectomy versus laser for diabetic macular oedema. *The British journal of ophthalmology* **2005,** *89* (1), 81-6.
159. Patel, J. I.; Hykin, P. G.; Schadt, M.; Luong, V.; Bunce, C.; Fitzke, F.; Gregor, Z. J., Diabetic macular oedema: pilot randomised trial of pars plana vitrectomy vs macular argon photocoagulation. *Eye* **2006,** *20* (8), 873-81.
160. Yanyali, A.; Horozoglu, F.; Celik, E.; Ercalik, Y.; Nohutcu, A. F., Pars plana vitrectomy and removal of the internal limiting membrane in diabetic macular edema unresponsive to grid laser photocoagulation. *European journal of ophthalmology* **2006,** *16* (4), 573-81.
161. Hoerauf, H.; Bruggemann, A.; Muecke, M.; Luke, J.; Muller, M.; Stefansson, E.; Hammes, H. P.; Weiss, C., Pars plana vitrectomy for diabetic macular edema. Internal limiting membrane delamination vs posterior hyaloid removal. A prospective randomized trial. *Graefe's archive for clinical and experimental ophthalmology = Albrecht von Graefes Archiv fur klinische und experimentelle Ophthalmologie* **2011,** *249* (7), 997-1008.
162. Simunovic, M. P.; Hunyor, A. P.; Ho, I. V., Vitrectomy for diabetic macular edema: a systematic review and meta-analysis. *Canadian journal of ophthalmology. Journal canadien d'ophtalmologie* **2014,** *49* (2), 188-95.
163. Aksoy, S.; Yilmaz, G.; Akkoyun, I.; Yazici, A. C., Comparison of intravitreal bevacizumab and triamcinolone acetonide theraphies for diffuse diabetic macular edema. *Int J Ophthalmol* **2015,** *8* (3), 550-5.
164. Keating, G. M., Aflibercept: A Review of Its Use in Diabetic Macular Oedema. *Drugs* **2015,** *75* (10), 1153-60.

165. Lim, L. T.; Chia, S. N.; Ah-Kee, E. Y.; Chew, N.; Gupta, M., Advances in the management of diabetic macular oedema based on evidence from the Diabetic Retinopathy Clinical Research Network. *Singapore medical journal* **2015,** *56* (5), 237-47.
166. Stefanini, F. R.; Badaro, E.; Falabella, P.; Koss, M.; Farah, M. E.; Maia, M., Anti-VEGF for the management of diabetic macular edema. *Journal of immunology research* **2014,** *2014*, 632307.
167. Ford, J. A.; Lois, N.; Royle, P.; Clar, C.; Shyangdan, D.; Waugh, N., Current treatments in diabetic macular oedema: systematic review and meta-analysis. *BMJ open* **2013,** *3* (3).
168. Stewart, M. W., Critical appraisal of ranibizumab in the treatment of diabetic macular edema. *Clinical ophthalmology* **2013,** *7*, 1257-67.
169. Boyer, D. S.; Hopkins, J. J.; Sorof, J.; Ehrlich, J. S., Anti-vascular endothelial growth factor therapy for diabetic macular edema. *Therapeutic advances in endocrinology and metabolism* **2013,** *4* (6), 151-69.
170. Wells, J. A.; Glassman, A. R.; Ayala, A. R.; Jampol, L. M.; Aiello, L. P.; Antoszyk, A. N.; Arnold-Bush, B.; Baker, C. W.; Bressler, N. M.; Browning, D. J.; Elman, M. J.; Ferris, F. L.; Friedman, S. M.; Melia, M.; Pieramici, D. J.; Sun, J. K.; Beck, R. W.; Network, D. R. C. R., Aflibercept, bevacizumab, or ranibizumab for diabetic macular edema. *N Engl J Med* **2015,** *372* (13), 1193-203.
171. Regnier, S. A.; Malcolm, W.; Haig, J.; Xue, W., Cost-effectiveness of ranibizumab versus aflibercept in the treatment of visual impairment due to diabetic macular edema: a UK healthcare perspective. *ClinicoEconomics and outcomes research : CEOR* **2015,** *7*, 235-47.
172. Krispel, C.; Rodrigues, M.; Xin, X.; Sodhi, A., Ranibizumab in diabetic macular edema. *World journal of diabetes* **2013,** *4* (6), 310-8.
173. Nguyen, Q. D.; Shah, S. M.; Khwaja, A. A.; Channa, R.; Hatef, E.; Do, D. V.; Boyer, D.; Heier, J. S.; Abraham, P.; Thach, A. B.; Lit, E. S.; Foster, B. S.; Kruger, E.; Dugel, P.; Chang, T.; Das, A.; Ciulla, T. A.; Pollack, J. S.; Lim, J. I.; Eliott, D.; Eliot, D.; Campochiaro, P. A.; Group, R.-S., Two-year outcomes of the ranibizumab for edema of the mAcula in diabetes (READ-2) study. *Ophthalmology* **2010,** *117* (11), 2146-51.
174. Brown, D. M.; Nguyen, Q. D.; Marcus, D. M.; Boyer, D. S.; Patel, S.; Feiner, L.; Schlottmann, P. G.; Rundle, A. C.; Zhang, J.; Rubio, R. G.; Adamis, A. P.; Ehrlich, J. S.; Hopkins, J. J.; Group, R. a. R. R., Long-term outcomes of ranibizumab therapy for diabetic macular edema: the 36-month results from two phase III trials: RISE and RIDE. *Ophthalmology* **2013,** *120* (10), 2013-22.
175. Nguyen, Q. D.; Brown, D. M.; Marcus, D. M.; Boyer, D. S.; Patel, S.; Feiner, L.; Gibson, A.; Sy, J.; Rundle, A. C.; Hopkins, J. J.; Rubio, R. G.; Ehrlich, J. S.; Group, R. a. R. R., Ranibizumab for diabetic macular edema: results from 2 phase III randomized trials: RISE and RIDE. *Ophthalmology* **2012,** *119* (4), 789-801.
176. Domalpally, A.; Ip, M. S.; Ehrlich, J. S., Effects of intravitreal ranibizumab on retinal hard exudate in diabetic macular edema: findings from the RIDE and RISE phase III clinical trials. *Ophthalmology* **2015,** *122* (4), 779-86.
177. Liu, X. D.; Zhou, X. D.; Wang, Z.; Shen, H. J., Comparison of intravitreal bevacizumab with macular photocoagulation for treatment of diabetic macular edema: a

systemic review and Meta-analysis. *International journal of ophthalmology* **2014,** *7* (6), 1048-55.
178. Rajendram, R.; Fraser-Bell, S.; Kaines, A.; Michaelides, M.; Hamilton, R. D.; Esposti, S. D.; Peto, T.; Egan, C.; Bunce, C.; Leslie, R. D.; Hykin, P. G., A 2-year prospective randomized controlled trial of intravitreal bevacizumab or laser therapy (BOLT) in the management of diabetic macular edema: 24-month data: report 3. *Archives of ophthalmology* **2012,** *130* (8), 972-9.
179. Soheilian, M.; Ramezani, A.; Obudi, A.; Bijanzadeh, B.; Salehipour, M.; Yaseri, M.; Ahmadieh, H.; Dehghan, M. H.; Azarmina, M.; Moradian, S.; Peyman, G. A., Randomized trial of intravitreal bevacizumab alone or combined with triamcinolone versus macular photocoagulation in diabetic macular edema. *Ophthalmology* **2009,** *116* (6), 1142-50.
180. Soheilian, M.; Garfami, K. H.; Ramezani, A.; Yaseri, M.; Peyman, G. A., Two-year results of a randomized trial of intravitreal bevacizumab alone or combined with triamcinolone versus laser in diabetic macular edema. *Retina* **2012,** *32* (2), 314-21.
181. Soheilian, M.; Ramezani, A.; Bijanzadeh, B.; Yaseri, M.; Ahmadieh, H.; Dehghan, M. H.; Azarmina, M.; Moradian, S.; Tabatabaei, H.; Peyman, G. A., Intravitreal bevacizumab (avastin) injection alone or combined with triamcinolone versus macular photocoagulation as primary treatment of diabetic macular edema. *Retina* **2007,** *27* (9), 1187-95.
182. Poku, E.; Rathbone, J.; Wong, R.; Everson-Hock, E.; Essat, M.; Pandor, A.; Wailoo, A., The safety of intravitreal bevacizumab monotherapy in adult ophthalmic conditions: systematic review. *BMJ open* **2014,** *4* (7), e005244.
183. Jin, Z. Y.; Zhu, D.; Tao, Y.; Wong, I. Y.; Jonas, J. B., Meta-analysis of the effect of intravitreal bevacizumab versus intravitreal triamcinolone acetonide in central retinal vein occlusion. *Journal of ocular pharmacology and therapeutics : the official journal of the Association for Ocular Pharmacology and Therapeutics* **2013,** *29* (9), 826-31.
184. Liu, X.; Zhou, X.; Wang, Z.; Li, T.; Jiang, B., Intravitreal bevacizumab with or without triamcinolone acetonide for diabetic macular edema: a meta-analysis of randomized controlled trials. *Chin Med J (Engl)* **2014,** *127* (19), 3471-6.
185. Korobelnik, J. F.; Do, D. V.; Schmidt-Erfurth, U.; Boyer, D. S.; Holz, F. G.; Heier, J. S.; Midena, E.; Kaiser, P. K.; Terasaki, H.; Marcus, D. M.; Nguyen, Q. D.; Jaffe, G. J.; Slakter, J. S.; Simader, C.; Soo, Y.; Schmelter, T.; Yancopoulos, G. D.; Stahl, N.; Vitti, R.; Berliner, A. J.; Zeitz, O.; Metzig, C.; Brown, D. M., Intravitreal aflibercept for diabetic macular edema. *Ophthalmology* **2014,** *121* (11), 2247-54.
186. Papadopoulos, N.; Martin, J.; Ruan, Q.; Rafique, A.; Rosconi, M. P.; Shi, E.; Pyles, E. A.; Yancopoulos, G. D.; Stahl, N.; Wiegand, S. J., Binding and neutralization of vascular endothelial growth factor (VEGF) and related ligands by VEGF Trap, ranibizumab and bevacizumab. *Angiogenesis* **2012,** *15* (2), 171-85.
187. Do, D. V.; Nguyen, Q. D.; Boyer, D.; Schmidt-Erfurth, U.; Brown, D. M.; Vitti, R.; Berliner, A. J.; Gao, B.; Zeitz, O.; Ruckert, R.; Schmelter, T.; Sandbrink, R.; Heier, J. S.; Group, d. V. S., One-year outcomes of the da Vinci Study of VEGF Trap-Eye in eyes with diabetic macular edema. *Ophthalmology* **2012,** *119* (8), 1658-65.
188. Campochiaro, P. A.; Clark, W. L.; Boyer, D. S.; Heier, J. S.; Brown, D. M.; Vitti, R.; Kazmi, H.; Berliner, A. J.; Erickson, K.; Chu, K. W.; Soo, Y.; Cheng, Y.;

Haller, J. A., Intravitreal aflibercept for macular edema following branch retinal vein occlusion: the 24-week results of the VIBRANT study. *Ophthalmology* **2015,** *122* (3), 538-44.
189. Brown, D. M.; Heier, J. S.; Clark, W. L.; Boyer, D. S.; Vitti, R.; Berliner, A. J.; Zeitz, O.; Sandbrink, R.; Zhu, X.; Haller, J. A., Intravitreal aflibercept injection for macular edema secondary to central retinal vein occlusion: 1-year results from the phase 3 COPERNICUS study. *American journal of ophthalmology* **2013,** *155* (3), 429-437 e7.
190. Evoy, K. E.; Abel, S. R., Aflibercept: newly approved for the treatment of macular edema following central retinal vein occlusion. *The Annals of pharmacotherapy* **2013,** *47* (6), 819-27.
191. Korobelnik, J. F.; Holz, F. G.; Roider, J.; Ogura, Y.; Simader, C.; Schmidt-Erfurth, U.; Lorenz, K.; Honda, M.; Vitti, R.; Berliner, A. J.; Hiemeyer, F.; Stemper, B.; Zeitz, O.; Sandbrink, R.; Group, G. S., Intravitreal Aflibercept Injection for Macular Edema Resulting from Central Retinal Vein Occlusion: One-Year Results of the Phase 3 GALILEO Study. *Ophthalmology* **2014,** *121* (1), 202-8.
192. Kourlas, H.; Schiller, D. S., Pegaptanib sodium for the treatment of neovascular age-related macular degeneration: a review. *Clinical therapeutics* **2006,** *28* (1), 36-44.
193. Querques, G.; Bux, A. V.; Martinelli, D.; Iaculli, C.; Noci, N. D., Intravitreal pegaptanib sodium (Macugen) for diabetic macular oedema. *Acta ophthalmologica* **2009,** *87* (6), 623-30.
194. Sivaprasad, S.; Browning, R. C.; Starita, C., An open-label, one-year, noncomparative study to evaluate the safety and tolerability of intravitreal pegaptanib sodium in patients with diabetic macular edema. *Clinical ophthalmology* **2014,** *8*, 1565-71.
195. Ishibashi, T.; Yuzawa, M.; Yoshimura, N.; Ohji, M.; Ishida, S.; Isogawa, N.; Esaka, E., [Japan phase 3 study of pegaptanib sodium in patients with diabetic macular edema]. *Nippon Ganka Gakkai Zasshi* **2014,** *118* (9), 773-82.
196. Sultan, M. B.; Zhou, D.; Loftus, J.; Dombi, T.; Ice, K. S.; Group, M. S., A phase 2/3, multicenter, randomized, double-masked, 2-year trial of pegaptanib sodium for the treatment of diabetic macular edema. *Ophthalmology* **2011,** *118* (6), 1107-18.
197. Cholkar, K.; Gunda, S.; Earla, R.; Pal, D.; Mitra, A. K., Nanomicellar Topical Aqueous Drop Formulation of Rapamycin for Back-of-the-Eye Delivery. *AAPS PharmSciTech* **2014**.
198. Xue, Q.; Nagy, J. A.; Manseau, E. J.; Phung, T. L.; Dvorak, H. F.; Benjamin, L. E., Rapamycin inhibition of the Akt/mTOR pathway blocks select stages of VEGF-A164-driven angiogenesis, in part by blocking S6Kinase. *Arteriosclerosis, thrombosis, and vascular biology* **2009,** *29* (8), 1172-8.
199. Stahl, A.; Paschek, L.; Martin, G.; Gross, N. J.; Feltgen, N.; Hansen, L. L.; Agostini, H. T., Rapamycin reduces VEGF expression in retinal pigment epithelium (RPE) and inhibits RPE-induced sprouting angiogenesis in vitro. *FEBS letters* **2008,** *582* (20), 3097-102.
200. Frost, P.; Berlanger, E.; Mysore, V.; Hoang, B.; Shi, Y.; Gera, J.; Lichtenstein, A., Mammalian target of rapamycin inhibitors induce tumor cell apoptosis in vivo primarily by inhibiting VEGF expression and angiogenesis. *Journal of oncology* **2013,** *2013*, 897025.

201. Krishnadev, N.; Forooghian, F.; Cukras, C.; Wong, W.; Saligan, L.; Chew, E. Y.; Nussenblatt, R.; Ferris, F.; Meyerle, C., Subconjunctival sirolimus in the treatment of diabetic macular edema. *Graefes Arch Clin Exp Ophthalmol* **2011,** *249* (11), 1627-33.
202. Nguyen, Q. D.; Ibrahim, M. A.; Watters, A.; Bittencourt, M.; Yohannan, J.; Sepah, Y. J.; Dunn, J. P.; Naor, J.; Shams, N.; Shaikh, O.; Leder, H. A.; Do, D. V., Ocular tolerability and efficacy of intravitreal and subconjunctival injections of sirolimus in patients with non-infectious uveitis: primary 6-month results of the SAVE Study. *Journal of ophthalmic inflammation and infection* **2013,** *3* (1), 32.
203. Dugel, P. U.; Blumenkranz, M. S.; Haller, J. A.; Williams, G. A.; Solley, W. A.; Kleinman, D. M.; Naor, J., A randomized, dose-escalation study of subconjunctival and intravitreal injections of sirolimus in patients with diabetic macular edema. *Ophthalmology* **2012,** *119* (1), 124-31.
204. Nauck, M.; Roth, M.; Tamm, M.; Eickelberg, O.; Wieland, H.; Stulz, P.; Perruchoud, A. P., Induction of vascular endothelial growth factor by platelet-activating factor and platelet-derived growth factor is downregulated by corticosteroids. *American journal of respiratory cell and molecular biology* **1997,** *16* (4), 398-406.
205. Edelman, J. L.; Lutz, D.; Castro, M. R., Corticosteroids inhibit VEGF-induced vascular leakage in a rabbit model of blood-retinal and blood-aqueous barrier breakdown. *Experimental eye research* **2005,** *80* (2), 249-58.
206. Stewart, M. W., Corticosteroid use for diabetic macular edema: old fad or new trend? *Current diabetes reports* **2012,** *12* (4), 364-75.
207. Wolfensberger, T. J.; Gregor, Z. J., Macular edema--rationale for therapy. *Developments in ophthalmology* **2010,** *47*, 49-58.
208. Bandello, F.; Casalino, G.; Loewenstein, A.; Goldstein, M.; Pelayes, D.; Battaglia Parodi, M., Pharmacological approach to diabetic macular edema. *Ophthalmic research* **2014,** *51* (2), 88-95.
209. Das, A.; McGuire, P. G.; Rangasamy, S., Diabetic Macular Edema: Pathophysiology and Novel Therapeutic Targets. *Ophthalmology* **2015,** *122* (7), 1375-94.
210. Sears, J. E.; Hoppe, G., Triamcinolone acetonide destabilizes VEGF mRNA in Muller cells under continuous cobalt stimulation. *Investigative ophthalmology & visual science* **2005,** *46* (11), 4336-41.
211. Tao, Y.; Jonas, J. B., Intravitreal triamcinolone. *Ophthalmologica. Journal international d'ophtalmologie. International journal of ophthalmology. Zeitschrift fur Augenheilkunde* **2011,** *225* (1), 1-20.
212. Jonas, J. B., Intravitreal triamcinolone acetonide: a change in a paradigm. *Ophthalmic research* **2006,** *38* (4), 218-45.
213. Jonas, J. B., Intravitreal triamcinolone acetonide for diabetic retinopathy. *Developments in ophthalmology* **2007,** *39*, 96-110.
214. Jonas, J. B.; Kreissig, I.; Kamppeter, B.; Degenring, R. F., [Intravitreal triamcinolone acetonide for the treatment of intraocular edematous and neovascular diseases]. *Der Ophthalmologe : Zeitschrift der Deutschen Ophthalmologischen Gesellschaft* **2004,** *101* (2), 113-20.

215. Network, D. R. C. R., A randomized trial comparing intravitreal triamcinolone acetonide and focal/grid photocoagulation for diabetic macular edema. *Ophthalmology* **2008,** *115* (9), 1447-9, 1449.e1-10.
216. Yumusak, E.; Buyuktortop, N.; Ornek, K., Early results of dexamethasone implant, ranibizumab, and triamcinolone in macular edema due to branch retinal vein occlusion. *Eur J Ophthalmol* **2016,** *26* (1), 54-9.
217. Bucolo, C.; Grosso, G.; Drago, V.; Gagliano, C., Intravitreal triamcinolone acetonide in the treatment of ophthalmic inflammatory diseases with macular edema: a meta-analysis study. *J Ocul Pharmacol Ther* **2015,** *31* (4), 228-40.
218. Beck, R. W.; Edwards, A. R.; Aiello, L. P.; Bressler, N. M.; Ferris, F.; Glassman, A. R.; Hartnett, E.; Ip, M. S.; Kim, J. E.; Kollman, C.; (DRCR.net), D. R. C. R. N., Three-year follow-up of a randomized trial comparing focal/grid photocoagulation and intravitreal triamcinolone for diabetic macular edema. *Arch Ophthalmol* **2009,** *127* (3), 245-51.
219. Yoo, S. G.; Kim, J. H.; Lee, T. G.; Kim, C. G.; Kim, J. W., Short-term efficacy of intravitreal triamcinolone acetonide for macular edema secondary to retinal vein occlusion that is refractory to intravitreal bevacizumab. *Indian journal of ophthalmology* **2015,** *63* (1), 25-9.
220. Gillies, M. C.; Kuzniarz, M.; Craig, J.; Ball, M.; Luo, W.; Simpson, J. M., Intravitreal triamcinolone-induced elevated intraocular pressure is associated with the development of posterior subcapsular cataract. *Ophthalmology* **2005,** *112* (1), 139-43.
221. Dodwell, D. G.; Krimmel, D. A.; de Fiebre, C. M., Sterile endophthalmitis rates and particle size analyses of different formulations of triamcinolone acetonide. *Clinical ophthalmology* **2015,** *9*, 1033-40.
222. Thompson, J. T., Cataract formation and other complications of intravitreal triamcinolone for macular edema. *American journal of ophthalmology* **2006,** *141* (4), 629-37.
223. Moshfeghi, D. M.; Kaiser, P. K.; Bakri, S. J.; Kaiser, R. S.; Maturi, R. K.; Sears, J. E.; Scott, I. U.; Belmont, J.; Beer, P. M.; Quiroz-Mercado, H.; Mieler, W. F., Presumed sterile endophthalmitis following intravitreal triamcinolone acetonide injection. *Ophthalmic Surg Lasers Imaging* **2005,** *36* (1), 24-9.
224. Bhavsar, A. R.; Ip, M. S.; Glassman, A. R.; Groups, D. a. t. S. S., The risk of endophthalmitis following intravitreal triamcinolone injection in the DRCRnet and SCORE clinical trials. *Am J Ophthalmol* **2007,** *144* (3), 454-6.
225. Cholkar, K.; Hariharan, S.; Gunda, S.; Mitra, A. K., Optimization of dexamethasone mixed nanomicellar formulation. *AAPS PharmSciTech* **2014,** *15* (6), 1454-67.
226. Earla, R.; Boddu, S. H.; Cholkar, K.; Hariharan, S.; Jwala, J.; Mitra, A. K., Development and validation of a fast and sensitive bioanalytical method for the quantitative determination of glucocorticoids--quantitative measurement of dexamethasone in rabbit ocular matrices by liquid chromatography tandem mass spectrometry. *J Pharm Biomed Anal* **2010,** *52* (4), 525-33.
227. Campochiaro, P. A.; Brown, D. M.; Pearson, A.; Chen, S.; Boyer, D.; Ruiz-Moreno, J.; Garretson, B.; Gupta, A.; Hariprasad, S. M.; Bailey, C.; Reichel, E.; Soubrane, G.; Kapik, B.; Billman, K.; Kane, F. E.; Green, K.; Group, F. S., Sustained

delivery fluocinolone acetonide vitreous inserts provide benefit for at least 3 years in patients with diabetic macular edema. *Ophthalmology* **2012,** *119* (10), 2125-32.
228. Pearson, P. A.; Comstock, T. L.; Ip, M.; Callanan, D.; Morse, L. S.; Ashton, P.; Levy, B.; Mann, E. S.; Eliott, D., Fluocinolone acetonide intravitreal implant for diabetic macular edema: a 3-year multicenter, randomized, controlled clinical trial. *Ophthalmology* **2011,** *118* (8), 1580-7.
229. Haller, J. A.; Kuppermann, B. D.; Blumenkranz, M. S.; Williams, G. A.; Weinberg, D. V.; Chou, C.; Whitcup, S. M.; Group, D. D. P. I. S., Randomized controlled trial of an intravitreous dexamethasone drug delivery system in patients with diabetic macular edema. *Arch Ophthalmol* **2010,** *128* (3), 289-96.
230. Campochiaro, P. A.; Hafiz, G.; Shah, S. M.; Bloom, S.; Brown, D. M.; Busquets, M.; Ciulla, T.; Feiner, L.; Sabates, N.; Billman, K.; Kapik, B.; Green, K.; Kane, F.; Group, F. S., Sustained ocular delivery of fluocinolone acetonide by an intravitreal insert. *Ophthalmology* **2010,** *117* (7), 1393-9.e3.
231. Boyer, D. S.; Faber, D.; Gupta, S.; Patel, S. S.; Tabandeh, H.; Li, X. Y.; Liu, C. C.; Lou, J.; Whitcup, S. M.; Group, O. C. S., Dexamethasone intravitreal implant for treatment of diabetic macular edema in vitrectomized patients. *Retina* **2011,** *31* (5), 915-23.
232. Gillies, M. C.; Sutter, F. K.; Simpson, J. M.; Larsson, J.; Ali, H.; Zhu, M., Intravitreal triamcinolone for refractory diabetic macular edema: two-year results of a double-masked, placebo-controlled, randomized clinical trial. *Ophthalmology* **2006,** *113* (9), 1533-8.
233. Chang-Lin, J. E.; Attar, M.; Acheampong, A. A.; Robinson, M. R.; Whitcup, S. M.; Kuppermann, B. D.; Welty, D., Pharmacokinetics and pharmacodynamics of a sustained-release dexamethasone intravitreal implant. *Investigative ophthalmology & visual science* **2011,** *52* (1), 80-6.
234. Nguyen, Q. D.; Shah, S. M.; Heier, J. S.; Do, D. V.; Lim, J.; Boyer, D.; Abraham, P.; Campochiaro, P. A.; Group, R.-S., Primary End Point (Six Months) Results of the Ranibizumab for Edema of the mAcula in diabetes (READ-2) study. *Ophthalmology* **2009,** *116* (11), 2175-81.e1.
235. Michaelides, M.; Kaines, A.; Hamilton, R. D.; Fraser-Bell, S.; Rajendram, R.; Quhill, F.; Boos, C. J.; Xing, W.; Egan, C.; Peto, T.; Bunce, C.; Leslie, R. D.; Hykin, P. G., A prospective randomized trial of intravitreal bevacizumab or laser therapy in the management of diabetic macular edema (BOLT study) 12-month data: report 2. *Ophthalmology* **2010,** *117* (6), 1078-1086 e2.
236. Kim, J. H.; Kang, S. W.; Ha, H. S.; Kim, J. R., Vitrectomy combined with intravitreal triamcinolone acetonide injection and macular laser photocoagulation for nontractional diabetic macular edema. *Korean J Ophthalmol* **2013,** *27* (3), 186-93.
237. Sampat, K. M.; Garg, S. J., Complications of intravitreal injections. *Curr Opin Ophthalmol* **2010,** *21* (3), 178-83.
238. Patel, S. P.; Vaishya, R.; Yang, X.; Pal, D.; Mitra, A. K., Novel thermosensitive pentablock copolymers for sustained delivery of proteins in the treatment of posterior segment diseases. *Protein Pept Lett* **2014,** *21* (11), 1185-200.
239. Bertelmann, T.; Schulze, S., Long-Term Follow-Up of Patient with Diabetic Macular Edema Receiving Fluocinolone Acetonide Intravitreal Implant. *Ophthalmol Ther* **2015,** *4* (1), 51-8.

240. Cunha-Vaz, J.; Ashton, P.; Iezzi, R.; Campochiaro, P.; Dugel, P. U.; Holz, F. G.; Weber, M.; Danis, R. P.; Kuppermann, B. D.; Bailey, C.; Billman, K.; Kapik, B.; Kane, F.; Green, K.; Group, F. S., Sustained delivery fluocinolone acetonide vitreous implants: long-term benefit in patients with chronic diabetic macular edema. *Ophthalmology* **2014,** *121* (10), 1892-903.
241. Misra, G. P.; Singh, R. S.; Aleman, T. S.; Jacobson, S. G.; Gardner, T. W.; Lowe, T. L., Subconjunctivally implantable hydrogels with degradable and thermoresponsive properties for sustained release of insulin to the retina. *Biomaterials* **2009,** *30* (33), 6541-7.
242. Adelman, R.; Parnes, A.; Michalewska, Z.; Parolini, B.; Boscher, C.; Ducournau, D., Strategy for the management of diabetic macular edema: the European vitreo-retinal society macular edema study. *BioMed research international* **2015,** *2015*, 352487.
243. Arevalo, J. F., Diabetic macular edema: Current management 2013. *World journal of diabetes* **2013,** *4* (6), 231-3.
244. Diaz-Llopis, M.; Udaondo, P.; Millán, J. M.; Arevalo, J. F., Enzymatic vitrectomy for diabetic retinopathy and diabetic macular edema. *World J Diabetes* **2013,** *4* (6), 319-23.
245. Zucchiatti, I.; Lattanzio, R.; Querques, G.; Querques, L.; Del Turco, C.; Cascavilla, M. L.; Bandello, F., Intravitreal dexamethasone implant in patients with persistent diabetic macular edema. *Ophthalmologica. Journal international d'ophtalmologie. International journal of ophthalmology. Zeitschrift fur Augenheilkunde* **2012,** *228* (2), 117-22.
246. Gillies, M. C.; Lim, L. L.; Campain, A.; Quin, G. J.; Salem, W.; Li, J.; Goodwin, S.; Aroney, C.; McAllister, I. L.; Fraser-Bell, S., A randomized clinical trial of intravitreal bevacizumab versus intravitreal dexamethasone for diabetic macular edema: the BEVORDEX study. *Ophthalmology* **2014,** *121* (12), 2473-81.
247. Fujisawa, T.; Miyai, H.; Hironaka, K.; Tsukamoto, T.; Tahara, K.; Tozuka, Y.; Ito, M.; Takeuchi, H., Liposomal diclofenac eye drop formulations targeting the retina: formulation stability improvement using surface modification of liposomes. *Int J Pharm* **2012,** *436* (1-2), 564-7.
248. Feng, L.; Li, S. K.; Liu, H.; Liu, C. Y.; LaSance, K.; Haque, F.; Shu, D.; Guo, P., Ocular delivery of pRNA nanoparticles: distribution and clearance after subconjunctival injection. *Pharmaceutical research* **2014,** *31* (4), 1046-58.
249. Conley, S. M.; Naash, M. I., Nanoparticles for retinal gene therapy. *Progress in retinal and eye research* **2010,** *29* (5), 376-97.
250. Ding, X. Q.; Quiambao, A. B.; Fitzgerald, J. B.; Cooper, M. J.; Conley, S. M.; Naash, M. I., Ocular delivery of compacted DNA-nanoparticles does not elicit toxicity in the mouse retina. *PLoS One* **2009,** *4* (10), e7410.
251. Mitra, R. N.; Han, Z.; Merwin, M.; Al Taai, M.; Conley, S. M.; Naash, M. I., Synthesis and characterization of glycol chitosan DNA nanoparticles for retinal gene delivery. *ChemMedChem* **2014,** *9* (1), 189-96.
252. Panda, J. J.; Yandrapu, S.; Kadam, R. S.; Chauhan, V. S.; Kompella, U. B., Self-assembled phenylalanine-α,β-dehydrophenylalanine nanotubes for sustained intravitreal delivery of a multi-targeted tyrosine kinase inhibitor. *J Control Release* **2013,** *172* (3), 1151-60.

253. Boddu, S. H.; Jwala, J.; Vaishya, R.; Earla, R.; Karla, P. K.; Pal, D.; Mitra, A. K., Novel nanoparticulate gel formulations of steroids for the treatment of macular edema. *Journal of ocular pharmacology and therapeutics : the official journal of the Association for Ocular Pharmacology and Therapeutics* **2010,** *26* (1), 37-48.
254. Yandrapu, S. K.; Upadhyay, A. K.; Petrash, J. M.; Kompella, U. B., Nanoparticles in porous microparticles prepared by supercritical infusion and pressure quench technology for sustained delivery of bevacizumab. *Mol Pharm* **2013,** *10* (12), 4676-86.
255. Patel, S. P.; Vaishya, R.; Mishra, G. P.; Tamboli, V.; Pal, D.; Mitra, A. K., Tailor-made pentablock copolymer based formulation for sustained ocular delivery of protein therapeutics. *J Drug Deliv* **2014,** *2014*, 401747.
256. Nguyen, Q. D.; Brown, D. M.; Marcus, D. M.; Boyer, D. S.; Patel, S.; Feiner, L.; Gibson, A.; Sy, J.; Rundle, A. C.; Hopkins, J. J.; Rubio, R. G.; Ehrlich, J. S.; Rise; Group, R. R., Ranibizumab for diabetic macular edema: results from 2 phase III randomized trials: RISE and RIDE. *Ophthalmology* **2012,** *119* (4), 789-801.
257. Boyer, D. S.; Yoon, Y. H.; Belfort, R., Jr.; Bandello, F.; Maturi, R. K.; Augustin, A. J.; Li, X. Y.; Cui, H.; Hashad, Y.; Whitcup, S. M.; Ozurdex, M. S. G., Three-year, randomized, sham-controlled trial of dexamethasone intravitreal implant in patients with diabetic macular edema. *Ophthalmology* **2014,** *121* (10), 1904-14.
258. Campochiaro, P. A.; Brown, D. M.; Pearson, A.; Ciulla, T.; Boyer, D.; Holz, F. G.; Tolentino, M.; Gupta, A.; Duarte, L.; Madreperla, S.; Gonder, J.; Kapik, B.; Billman, K.; Kane, F. E.; Group, F. S., Long-term benefit of sustained-delivery fluocinolone acetonide vitreous inserts for diabetic macular edema. *Ophthalmology* **2011,** *118* (4), 626-635 e2.
259. Torchilin, V. P., Micellar nanocarriers: pharmaceutical perspectives. *Pharm Res* **2007,** *24* (1), 1-16.
260. Jones, M.; Leroux, J., Polymeric micelles - a new generation of colloidal drug carriers. *Eur J Pharm Biopharm* **1999,** *48* (2), 101-11.
261. Cholkar, K.; Gilger, B. C.; Mitra, A. K., Topical delivery of aqueous micellar resolvin E1 analog (RX-10045). *Int J Pharm* **2016,** *498* (1-2), 326-34.
262. Cai, S.; Vijayan, K.; Cheng, D.; Lima, E. M.; Discher, D. E., Micelles of different morphologies--advantages of worm-like filomicelles of PEO-PCL in paclitaxel delivery. *Pharmaceutical research* **2007,** *24* (11), 2099-109.
263. Sammalkorpi, M.; Karttunen, M.; Haataja, M., Ionic surfactant aggregates in saline solutions: sodium dodecyl sulfate (SDS) in the presence of excess sodium chloride (NaCl) or calcium chloride (CaCl(2)). *J Phys Chem B* **2009,** *113* (17), 5863-70.
264. Koo, O. M.; Rubinstein, I.; Onyuksel, H., Camptothecin in sterically stabilized phospholipid micelles: a novel nanomedicine. *Nanomedicine : nanotechnology, biology, and medicine* **2005,** *1* (1), 77-84.
265. Garnier, S.; Laschewsky, A., New amphiphilic diblock copolymers: surfactant properties and solubilization in their micelles. *Langmuir : the ACS journal of surfaces and colloids* **2006,** *22* (9), 4044-53.
266. La, S. B.; Okano, T.; Kataoka, K., Preparation and characterization of the micelle-forming polymeric drug indomethacin-incorporated poly(ethylene oxide)-

poly(beta-benzyl L-aspartate) block copolymer micelles. *Journal of pharmaceutical sciences* **1996,** *85* (1), 85-90.
267. Wu, C. Y.; Benet, L. Z., Predicting drug disposition via application of BCS: transport/absorption/ elimination interplay and development of a biopharmaceutics drug disposition classification system. *Pharmaceutical research* **2005,** *22* (1), 11-23.
268. Xu, W.; Ling, P.; Zhang, T., Polymeric micelles, a promising drug delivery system to enhance bioavailability of poorly water-soluble drugs. *Journal of drug delivery* **2013,** *2013*, 340315.
269. Dian, L.; Yu, E.; Chen, X.; Wen, X.; Zhang, Z.; Qin, L.; Wang, Q.; Li, G.; Wu, C., Enhancing oral bioavailability of quercetin using novel soluplus polymeric micelles. *Nanoscale Res Lett* **2014,** *9* (1), 2406.
270. Savic, R.; Eisenberg, A.; Maysinger, D., Block copolymer micelles as delivery vehicles of hydrophobic drugs: micelle-cell interactions. *Journal of drug targeting* **2006,** *14* (6), 343-55.
271. Chiappetta, D. A.; Hocht, C.; Taira, C.; Sosnik, A., Oral pharmacokinetics of the anti-HIV efavirenz encapsulated within polymeric micelles. *Biomaterials* **2011,** *32* (9), 2379-87.
272. Sutton, D.; Nasongkla, N.; Blanco, E.; Gao, J., Functionalized micellar systems for cancer targeted drug delivery. *Pharmaceutical research* **2007,** *24* (6), 1029-46.
273. Wang, T.; Yang, S.; Mei, L. A.; Parmar, C. K.; Gillespie, J. W.; Praveen, K. P.; Petrenko, V. A.; Torchilin, V. P., Paclitaxel-loaded PEG-PE-based micellar nanopreparations targeted with tumor-specific landscape phage fusion protein enhance apoptosis and efficiently reduce tumors. *Molecular cancer therapeutics* **2014,** *13* (12), 2864-75.
274. Torchilin, V. P.; Lukyanov, A. N.; Gao, Z.; Papahadjopoulos-Sternberg, B., Immunomicelles: targeted pharmaceutical carriers for poorly soluble drugs. *Proc Natl Acad Sci U S A* **2003,** *100* (10), 6039-44.
275. Ahn, J.; Miura, Y.; Yamada, N.; Chida, T.; Liu, X.; Kim, A.; Sato, R.; Tsumura, R.; Koga, Y.; Yasunaga, M.; Nishiyama, N.; Matsumura, Y.; Cabral, H.; Kataoka, K., Antibody fragment-conjugated polymeric micelles incorporating platinum drugs for targeted therapy of pancreatic cancer. *Biomaterials* **2015,** *39*, 23-30.
276. Xiao, K.; Li, Y.; Lee, J. S.; Gonik, A. M.; Dong, T.; Fung, G.; Sanchez, E.; Xing, L.; Cheng, H. R.; Luo, J.; Lam, K. S., "OA02" peptide facilitates the precise targeting of paclitaxel-loaded micellar nanoparticles to ovarian cancer in vivo. *Cancer research* **2012,** *72* (8), 2100-10.
277. Zhan, C.; Gu, B.; Xie, C.; Li, J.; Liu, Y.; Lu, W., Cyclic RGD conjugated poly(ethylene glycol)-co-poly(lactic acid) micelle enhances paclitaxel anti-glioblastoma effect. *Journal of controlled release : official journal of the Controlled Release Society* **2010,** *143* (1), 136-42.
278. Danhier, F.; Le Breton, A.; Preat, V., RGD-based strategies to target alpha(v) beta(3) integrin in cancer therapy and diagnosis. *Molecular pharmaceutics* **2012,** *9* (11), 2961-73.
279. Sawant, R. R.; Jhaveri, A. M.; Koshkaryev, A.; Zhu, L.; Qureshi, F.; Torchilin, V. P., Targeted transferrin-modified polymeric micelles: enhanced efficacy

in vitro and in vivo in ovarian carcinoma. *Molecular pharmaceutics* **2014,** *11* (2), 375-81.
280. Sarisozen, C.; Abouzeid, A. H.; Torchilin, V. P., The effect of co-delivery of paclitaxel and curcumin by transferrin-targeted PEG-PE-based mixed micelles on resistant ovarian cancer in 3-D spheroids and in vivo tumors. *European journal of pharmaceutics and biopharmaceutics : official journal of Arbeitsgemeinschaft fur Pharmazeutische Verfahrenstechnik e.V* **2014,** *88* (2), 539-50.
281. Mu, C.; Dave, N.; Hu, J.; Desai, P.; Pauletti, G.; Bai, S.; Hao, J., Solubilization of flurbiprofen into aptamer-modified PEG-PLA micelles for targeted delivery to brain-derived endothelial cells in vitro. *J Microencapsul* **2013,** *30* (7), 701-8.
282. Li, X.; Yu, Y.; Ji, Q.; Qiu, L., Targeted delivery of anticancer drugs by aptamer AS1411 mediated Pluronic F127/cyclodextrin-linked polymer composite micelles. *Nanomedicine : nanotechnology, biology, and medicine* **2015,** *11* (1), 175-84.
283. Wang, X. Q.; Zhang, Q., pH-sensitive polymeric nanoparticles to improve oral bioavailability of peptide/protein drugs and poorly water-soluble drugs. *European journal of pharmaceutics and biopharmaceutics : official journal of Arbeitsgemeinschaft fur Pharmazeutische Verfahrenstechnik e.V* **2012,** *82* (2), 219-29.
284. Bae, Y.; Nishiyama, N.; Kataoka, K., In vivo antitumor activity of the folate-conjugated pH-sensitive polymeric micelle selectively releasing adriamycin in the intracellular acidic compartments. *Bioconjugate chemistry* **2007,** *18* (4), 1131-9.
285. Lee, E. S.; Na, K.; Bae, Y. H., Doxorubicin loaded pH-sensitive polymeric micelles for reversal of resistant MCF-7 tumor. *Journal of controlled release : official journal of the Controlled Release Society* **2005,** *103* (2), 405-18.
286. Wu, X. L.; Kim, J. H.; Koo, H.; Bae, S. M.; Shin, H.; Kim, M. S.; Lee, B. H.; Park, R. W.; Kim, I. S.; Choi, K.; Kwon, I. C.; Kim, K.; Lee, D. S., Tumor-targeting peptide conjugated pH-responsive micelles as a potential drug carrier for cancer therapy. *Bioconjugate chemistry* **2010,** *21* (2), 208-13.
287. Kim, D.; Lee, E. S.; Park, K.; Kwon, I. C.; Bae, Y. H., Doxorubicin loaded pH-sensitive micelle: antitumoral efficacy against ovarian A2780/DOXR tumor. *Pharmaceutical research* **2008,** *25* (9), 2074-82.
288. Bae, Y.; Nishiyama, N.; Fukushima, S.; Koyama, H.; Yasuhiro, M.; Kataoka, K., Preparation and biological characterization of polymeric micelle drug carriers with intracellular pH-triggered drug release property: tumor permeability, controlled subcellular drug distribution, and enhanced in vivo antitumor efficacy. *Bioconjugate chemistry* **2005,** *16* (1), 122-30.
289. Soga, O.; van Nostrum, C. F.; Hennink, W. E., Poly(N-(2-hydroxypropyl) methacrylamide mono/di lactate): a new class of biodegradable polymers with tuneable thermosensitivity. *Biomacromolecules* **2004,** *5* (3), 818-21.
290. Soga, O.; van Nostrum, C. F.; Ramzi, A.; Visser, T.; Soulimani, F.; Frederik, P. M.; Bomans, P. H.; Hennink, W. E., Physicochemical characterization of degradable thermosensitive polymeric micelles. *Langmuir : the ACS journal of surfaces and colloids* **2004,** *20* (21), 9388-95.
291. Soga, O.; van Nostrum, C. F.; Fens, M.; Rijcken, C. J.; Schiffelers, R. M.; Storm, G.; Hennink, W. E., Thermosensitive and biodegradable polymeric micelles for

paclitaxel delivery. *Journal of controlled release : official journal of the Controlled Release Society* **2005,** *103* (2), 341-53.
292. Soga, O.; van Nostrum, C. F.; Hennink, W. E., Thermosensitive and biodegradable polymeric micelles with transient stability. *Journal of controlled release : official journal of the Controlled Release Society* **2005,** *101* (1-3), 383-5.
293. Lin, H. M.; Wang, W. K.; Hsiung, P. A.; Shyu, S. G., Light-sensitive intelligent drug delivery systems of coumarin-modified mesoporous bioactive glass. *Acta Biomater* **2010,** *6* (8), 3256-63.
294. Alvarez-Lorenzo, C.; Bromberg, L.; Concheiro, A., Light-sensitive intelligent drug delivery systems. *Photochem Photobiol* **2009,** *85* (4), 848-60.
295. Goodwin, A. P.; Mynar, J. L.; Ma, Y.; Fleming, G. R.; Frechet, J. M., Synthetic micelle sensitive to IR light via a two-photon process. *Journal of the American Chemical Society* **2005,** *127* (28), 9952-3.
296. Marin, A.; Muniruzzaman, M.; Rapoport, N., Mechanism of the ultrasonic activation of micellar drug delivery. *Journal of controlled release : official journal of the Controlled Release Society* **2001,** *75* (1-2), 69-81.
297. Husseini, G. A.; Pitt, W. G.; Martins, A. M., Ultrasonically triggered drug delivery: breaking the barrier. *Colloids Surf B Biointerfaces* **2014,** *123*, 364-86.
298. Ahmed, S. E.; Martins, A. M.; Husseini, G. A., The use of ultrasound to release chemotherapeutic drugs from micelles and liposomes. *Journal of drug targeting* **2015,** *23* (1), 16-42.
299. Xia, H.; Zhao, Y.; Tong, R., Ultrasound-Mediated Polymeric Micelle Drug Delivery. *Adv Exp Med Biol* **2016,** *880*, 365-84.
300. Husseini, G. A.; Pitt, W. G., Ultrasonic-activated micellar drug delivery for cancer treatment. *J Pharm Sci* **2009,** *98* (3), 795-811.
301. Marin, A.; Sun, H.; Husseini, G. A.; Pitt, W. G.; Christensen, D. A.; Rapoport, N. Y., Drug delivery in pluronic micelles: effect of high-frequency ultrasound on drug release from micelles and intracellular uptake. *Journal of controlled release : official journal of the Controlled Release Society* **2002,** *84* (1-2), 39-47.
302. Li, X.; Li, H.; Yi, W.; Chen, J.; Liang, B., Acid-triggered core cross-linked nanomicelles for targeted drug delivery and magnetic resonance imaging in liver cancer cells. *International journal of nanomedicine* **2013,** *8*, 3019-31.
303. Hoang M Trinh, M. J., Kishore Cholkar, Dhananjay Pal, Ashim K Mitra Novel strategies for the treatment of diabetic macular Edema. *World Journal of Pharmacology* **2016**, 1-14.
304. Emerson, M. V.; Lauer, A. K., Emerging therapies for the treatment of neovascular age-related macular degeneration and diabetic macular edema. *BioDrugs : clinical immunotherapeutics, biopharmaceuticals and gene therapy* **2007,** *21* (4), 245-57.
305. Sihota, R.; Konkal, V. L.; Dada, T.; Agarwal, H. C.; Singh, R., Prospective, long-term evaluation of steroid-induced glaucoma. *Eye* **2008,** *22* (1), 26-30.
306. Chu, Y. K.; Chung, E. J.; Kwon, O. W.; Lee, J. H.; Koh, H. J., Objective evaluation of cataract progression associated with a high dose intravitreal triamcinolone injection. *Eye* **2008,** *22* (7), 895-9.

307. Jonas, J. B.; Degenring, R.; Vossmerbauemer, U.; Kamppeter, B., Frequency of cataract surgery after intravitreal injection of high-dosage triamcinolone acetonide. *European journal of ophthalmology* **2005,** *15* (4), 462-4.
308. Vadlapudi, A. D.; Cholkar, K.; Vadlapatla, R. K.; Mitra, A. K., Aqueous nanomicellar formulation for topical delivery of biotinylated lipid prodrug of acyclovir: formulation development and ocular biocompatibility. *Journal of ocular pharmacology and therapeutics : the official journal of the Association for Ocular Pharmacology and Therapeutics* **2014,** *30* (1), 49-58.
309. Korodi, T.; Lachmann, B.; Kopelent-Frank, H., Evaluation of different preparation methods for a preservative free triamcinolone acetonide preparation for intravitreal administration: a validated stability indicating HPLC-method. *Pharmazie* **2010,** *65* (12), 860-6.
310. Vadlapudi, A. D.; Vadlapatla, R. K.; Pal, D.; Mitra, A. K., Functional and molecular aspects of biotin uptake via SMVT in human corneal epithelial (HCEC) and retinal pigment epithelial (D407) cells. *AAPS J* **2012,** *14* (4), 832-42.
311. Chopra, P.; Hao, J.; Li, S. K., Iontophoretic transport of charged macromolecules across human sclera. *International journal of pharmaceutics* **2010,** *388* (1-2), 107-13.
312. Cholkar, K., Eye: anatomy, physiology and barriers to drug delivery. In *Ocular transporters and receptors their role in drug delivery*, Mitra, A. K., Ed. Woodhead publishing: 2013; pp 1-28.
313. Zhu, H.; Chauhan, A., Effect of viscosity on tear drainage and ocular residence time. *Optom Vis Sci* **2008,** *85* (8), 715-25.
314. Aragona, P.; Di Stefano, G.; Ferreri, F.; Spinella, R.; Stilo, A., Sodium hyaluronate eye drops of different osmolality for the treatment of dry eye in Sjogren's syndrome patients. *The British journal of ophthalmology* **2002,** *86* (8), 879-84.
315. Meencke, H. J., Pathology of childhood epilepsies. *Cleve Clin J Med* **1989,** *56 Suppl Pt 1*, S111-20; discussion S121-3.
316. Al Rashaed, S.; Arevalo, J. F., Combined therapy for diabetic macular edema. *Middle East African journal of ophthalmology* **2013,** *20* (4), 315-20.
317. Yau, J. W.; Rogers, S. L.; Kawasaki, R.; Lamoureux, E. L.; Kowalski, J. W.; Bek, T.; Chen, S. J.; Dekker, J. M.; Fletcher, A.; Grauslund, J.; Haffner, S.; Hamman, R. F.; Ikram, M. K.; Kayama, T.; Klein, B. E.; Klein, R.; Krishnaiah, S.; Mayurasakorn, K.; O'Hare, J. P.; Orchard, T. J.; Porta, M.; Rema, M.; Roy, M. S.; Sharma, T.; Shaw, J.; Taylor, H.; Tielsch, J. M.; Varma, R.; Wang, J. J.; Wang, N.; West, S.; Xu, L.; Yasuda, M.; Zhang, X.; Mitchell, P.; Wong, T. Y.; Meta-Analysis for Eye Disease Study, G., Global prevalence and major risk factors of diabetic retinopathy. *Diabetes care* **2012,** *35* (3), 556-64.
318. Singh, S. K.; Behre, A.; Singh, M. K., Diabetic retinopathy and microalbuminuria in lean type 2 diabetes mellitus. *J Assoc Physicians India* **2001,** *49*, 439-41.
319. Harris, M. I., Diabetes in America: epidemiology and scope of the problem. *Diabetes care* **1998,** *21 Suppl 3*, C11-4.
320. Wong, T. Y.; Cheung, N.; Tay, W. T.; Wang, J. J.; Aung, T.; Saw, S. M.; Lim, S. C.; Tai, E. S.; Mitchell, P., Prevalence and risk factors for diabetic retinopathy: the Singapore Malay Eye Study. *Ophthalmology* **2008,** *115* (11), 1869-75.

321. Romero, P.; Salvat, M.; Fernandez, J.; Baget, M.; Martinez, I., Renal and retinal microangiopathy after 15 years of follow-up study in a sample of Type 1 diabetes mellitus patients. *J Diabetes Complications* **2007,** *21* (2), 93-100.
322. Hammes, H. P.; Kerner, W.; Hofer, S.; Kordonouri, O.; Raile, K.; Holl, R. W.; Group, D. P.-W. S., Diabetic retinopathy in type 1 diabetes-a contemporary analysis of 8,784 patients. *Diabetologia* **2011,** *54* (8), 1977-84.
323. Kulkarni, A. D.; Ip, M. S., Diabetic macular edema: therapeutic options. *Diabetes Ther* **2012,** *3* (1), 1-14.
324. Shamsi, H. N.; Masaud, J. S.; Ghazi, N. G., Diabetic macular edema: New promising therapies. *World journal of diabetes* **2013,** *4* (6), 324-38.
325. Joussen, A. M.; Poulaki, V.; Le, M. L.; Koizumi, K.; Esser, C.; Janicki, H.; Schraermeyer, U.; Kociok, N.; Fauser, S.; Kirchhof, B.; Kern, T. S.; Adamis, A. P., A central role for inflammation in the pathogenesis of diabetic retinopathy. *FASEB J* **2004,** *18* (12), 1450-2.
326. Goni, F. J.; Stalmans, I.; Denis, P.; Nordmann, J. P.; Taylor, S.; Diestelhorst, M.; Figueiredo, A. R.; Garway-Heath, D. F., Elevated Intraocular Pressure After Intravitreal Steroid Injection in Diabetic Macular Edema: Monitoring and Management. *Ophthalmology and therapy* **2016,** *5* (1), 47-61.
327. Friedman, D. S.; Holbrook, J. T.; Ansari, H.; Alexander, J.; Burke, A.; Reed, S. B.; Katz, J.; Thorne, J. E.; Lightman, S. L.; Kempen, J. H.; Group, M. R., Risk of elevated intraocular pressure and glaucoma in patients with uveitis: results of the multicenter uveitis steroid treatment trial. *Ophthalmology* **2013,** *120* (8), 1571-9.
328. Cholkar, K.; Trinh, H. M.; Vadlapudi, A. D.; Wang, Z.; Pal, D.; Mitra, A. K., Interaction Studies of Resolvin E1 Analog (RX-10045) with Efflux Transporters. *Journal of ocular pharmacology and therapeutics : the official journal of the Association for Ocular Pharmacology and Therapeutics* **2015,** *31* (4), 248-55.
329. Dutescu, R. M.; Panfil, C.; Schrage, N., Osmolality of prevalent eye drops, side effects, and therapeutic approaches. *Cornea* **2015,** *34* (5), 560-6.
330. Barnes, P. J., How corticosteroids control inflammation: Quintiles Prize Lecture 2005. *British journal of pharmacology* **2006,** *148* (3), 245-54.
331. Miner, J. N.; Hong, M. H.; Negro-Vilar, A., New and improved glucocorticoid receptor ligands. *Expert Opin Investig Drugs* **2005,** *14* (12), 1527-45.
332. Muller-Ladner, U.; Gay, R. E.; Gay, S., Role of nuclear factor kappaB in synovial inflammation. *Curr Rheumatol Rep* **2002,** *4* (3), 201-7.
333. Mittelstadt, P. R.; Ashwell, J. D., Inhibition of AP-1 by the glucocorticoid-inducible protein GILZ. *The Journal of biological chemistry* **2001,** *276* (31), 29603-10.
334. Kriechbaum, K.; Prager, S.; Mylonas, G.; Scholda, C.; Rainer, G.; Funk, M.; Kundi, M.; Schmidt-Erfurth, U.; Diabetic Retinopathy Research, G., Intravitreal bevacizumab (Avastin) versus triamcinolone (Volon A) for treatment of diabetic macular edema: one-year results. *Eye* **2014,** *28* (1), 9-15; quiz 16.
335. Dincer, S.; Ozdurmus, S., Mathematical model for enteric film coating of tablets. *Journal of pharmaceutical sciences* **1977,** *66* (8), 1070-3.

VITA

Hoang My Trinh (Holly) was born on 20th November 1984, in Ho Chi Minh City, Viet Nam. She completed her Bachelor of Pharmacy from Ho Chi Minh City University of Medicine and Pharmacy in 2008. After completion of her B. Pharm. degree, she worked for Pfizer and worked as Lecturer at Quang Trung College, Viet Nam until July 2010. She joined the Interdisciplinary Ph.D. program at UMKC in October 2012 to pursue a Ph.D. degree in Pharmaceutical Science and Chemistry. She is an active member of American Association of Pharmaceutical Scientists (AAPS), Association of Research in Vision and Ophthalmology (ARVO), Rho Chi Society, and Pharmaceutical Sciences Graduate Student Association (PSGSA). She served as the Treasurer of PSGSA student chapter, UMKC, in 2013 and vice president of PSGSA in 2014. She also served as student representative of Graduate Program Committee (GPC), executive board member of IDSC and Editor Member of Journal of Interdisciplinary Research (JIDR) in 2015. She served as treasurer of control release society (CRS) in 2016. She has received UMKC School of Graduate Studies Research Grant Program in 2016, Pharmacy Foundation Judith Hemberger Graduate Scholarship 2015, 2016 and a regular recipient of Graduate Assistance Funds (GAF) from UMKC Women's Council since 2014.

She completed her doctoral studies in May 2018 under the guidance of Dr. Ashim K. Mitra. She has authored/co-authored several peer reviewed publications and book chapters and has presented her work in a number of international and national conferences such as AAPS, OMICS, ARVO and PGSRM.